CATALYTIC BEHAVIOUR OF METALLOPHTHALOCYANINES

TOWARDS THE DETECTION OF NITRIC OXIDE.

THESIS

Submitted to
Rhodes University
in fullfilment of the requirements for the degree of

DOCTOR OF PHILOSOPHY

by

LEA SIBULELO VILAKAZI

March 2001

Department of Chemistry
Rhodes University
Grahamstown

TO MY PARENTS

Thabo and Gladys

ACKNOWLEDGEMENTS

I would like to express my sincere gratitude to my supervisor, **Prof. T. Nyokong** for giving me an opportunity, support and an atmosphere that allowed me to grow beyond my cognition. **Prof.**, it has been a pleasure and a learning experience to work under your supervision.

I would also like to thank the following:

- My research colleagues, for their support in different ways during the preparation of this manuscript and for having made the laboratory a home away from home.
- **Kenneth Oezoeman, Joshua Oni, Changwe Nchinda**, my daughter **Nomfundo** and **Dr. Janice Limson** for proof reading parts of this manuscript.
- My friends **Mvusy**, **Mantoa** and **Jacky**, girls, I owe my sanity to you.
- **NRF** for financial support.

Finally, I would like to thank my family for their continued support.

Abstract

Electrocatalytic reduction and oxidation of nitric oxide (NO) using cobalt phthalocyanine complexes have been studied and compared to vitamin B_{12} and other metallophthalocyanine (MPc) complexes. Modifying a glassy carbon electrode with these complexes resulted in improved sensitivity of the electrode allowing detection of NO to 10^{-9} mol dm^{-3}. The mechanisms of catalysis were studied. Electrocatalysis of NO involves coordination of NO to the MPc complex. Hence catalytic activity is affected by the nature of the metal center. However coordination of NO to the MPc complex has to be reversible to eliminate poisoning of the electrode. Though FePc gave the best sensitivity and lowered the reduction potential more than CoPc, the strong Fe-NO bond resulted in the poisoning of the electrode hence, rendering the electrode unstable.

Rate constants for NO coordination to the MPc complexes were studied. These rates were smaller than the studied NO porphyrin coordination rates. Electrocatalytic reduction of NO using MPc complexes involves a transfer of an electron from the metal center to the NO ligand. Hence, substitution of electron-donating groups on the cobalt pthalocyanine complex resulted in improved sensitivity and catalytic activity.

A CoPc modified microelectrode (11μm) was used to monitor NO in human blood components and to detect NO in a rat brain. Detections of NO were also done in aqueous solutions in the presence of interfering species such as dopamine and serotonin. An interaction between NO and serotonin was observed.

TABLE OF CONTENTS

LIST OF ABBREVIATIONS

Cat	=	catalase
Cbl	=	cobalamin
CPu	=	caudate putamen
Cyt	=	cytochrome c
CV	=	cyclic voltammetry
CT	=	charge transfer
DA	=	dopamine
DMA	=	dimethylamine
DMF	=	N,N-dimethyl formamide
DMSO	=	dimethylsulphoxide
DPV	=	differential pulse voltammetry
ESR	=	electron spin resonance
FTIR	=	Fourier Transform Infrared
GCE	=	glass carbon electrode
HOMO	=	highest occupied Molecular orbital
Hb^{III}	=	methemoglobin
IR	=	infra red
LUMO	=	lowest occupied Molecular orbital
LMCT	=	ligand to metal charge transfer
MLCT	=	metal to ligand charge transfer

MPc	=	metallophthalocyanine
MP	=	metalloporphyrin
Mb^{III}	=	metmyoglobin
NO	=	nitric oxide
NOS	=	nitric oxide synthase
OEP	=	octaethylporphyrinato dianion
OSW	=	square wave voltammetry
OTTLE	=	optically transparent thin layer electrochemical cell
PDT	=	Photodynamic therapy
Pc	=	phthalocyaninato dianion
PE	=	polymerised eugenol
sGC	=	soluble guanylyl cyclase
SCE	=	saturated calomel electrode
THMPP	=	tetrakis (4-hydroxy-3-methoxyphenyl) porphyrinato dianion
TMPS	=	tetrakis sulfonatomesityl porphyrinato dianion
TmTP	=	tetra-m-tolyporphyrinato dianion
TPPS	=	tetrakis sulfonatophenyl porphyrinato dianion
TPP	=	tetraphenylpophyrinato dianion
TSPc	=	tetrasulfonated phthalocyaninato dianion
TEAP	=	tetraethyl ammonium perchlorate
UV	=	ultra violet
Vis	=	visible
$VitB_{12}$	=	cyanocobalamin

$VitB_{12a}$	=	Co(III) aquacobalamin
$VitB_{12r}$	=	Co(II) aquacobalamin
$VitB_{12s}$	=	Co(I) aquacobalamin

LIST OF SYMBOLS

σ	=	sigma
π	=	pi
ΔH	=	enthalpy change
ΔS	=	entropy change
ΔV	=	volume change
ν	=	stretching frequency
i_p	=	peak current
i_{pa}	=	anodic peak current
i_{pc}	=	cathodic peak current
n	=	number of moles of electrons transferred
A	=	electrode area
C	=	concentration
D	=	diffusion ceficient
v	=	scan rate
ΔE	=	separation between peak potentials
$E^{1/2}$	=	half wave potential
E^0	=	formal reduction potential
E_p	=	peak potential
E_{pa}	=	anodic peak potential
E_{pc}	=	cathodic peak potential
F	=	Faradays constant
α	=	transfer coefficient

Γ	=	surface coverage
ε	=	extinction coefficient
R	=	gas constant
T	=	temperature in Kelvin
k^0	=	standard rate constant
Q	=	charge
$W_{1/2}$	=	peak at ½ height
t	=	electrolysis time
r	=	electrode radius

LIST OF FIGURES

LIST OF SCHEMES

LIST OF TABLES

1. INTRODUCTION

Nitric oxide (NO) is a small, potentially toxic diatomic free radical, that is stable in the absence of air but relatively unstable in air. The industrial importance of NO in the manufacturing of nitric acid and its pervasive role in the chemistry of the atmosphere has resulted in extensive literature of fundamental and applied research on its chemistry. NO is one of the major pollutants produced during fuel combustion and consequently there is considerable interest in the conversion of NO to less harmful products such as nitrogen gas, hydrazine and ammonia.

Recent discoveries of the multiple roles of NO in human physiology have led to an outburst of research on this molecule. In mammals NO is produced by three enzymes known as nitric oxide synthase, (NOS). The three NOS isoforms are, NOS-I, NOS-II and NOS-III.[1] The exact nature of the enzyme depends on the tissue from which it is obtained. NOS-I and NOS-III are found in neurons and endothelial cells. They are constitutive i.e. they respond rapidly to activation. NOS-II is permanently active, producing large amounts of NO for sustained periods of time. NOS-II is associated with pathological conditions such as Alzheimer's disease.[2] However, its localization in the developing brain suggests a potential role in the regulation of blood flow, angiogenesis and vascular permeabilty.[1]

NO has a number of roles in mammalian physiology. It has been found to act as a regulator of blood pressure. NO synthesized by the endothelial cells diffuse out in all directions and on reaching the smooth muscle, it induces a relaxation effect. This allows the vessels to dilate and in turn lower the blood pressure. Recently, direct administration of NO has been attempted in the treatment of vasoconstriction that is confined to the

lungs.[3] Infants with persistent pulmonary hypertension of the newborn and older patients with adult respiratory distress syndrome, have been given low concentrations of NO through respiratory ventilators.[3] This has worked well due to NO's short physiological half-life. The procedure does not cause unwanted drop in blood pressure in other parts of the body.

Nitric oxide also acts against blood clotting. When a blood vessel is damaged, excessive bleeding is prevented by platelet aggregation, forming a plug which adheres to the wall of the blood vessel. Aggregation also occurs in blood coagulation, forming a clot which acts against bleeding after an injury. However, in patients with high cholesterol levels, a heart attack may be caused by abnormal clotting of the blood in a coronary vessel. NO inhibits both platelet aggregation and adhesion. The role of NO in this regard is to counteract the aggregation and adhesion effects of substances that are produced by the body after an injury.

The body's reaction to foreign, living or non-living matter is through its immune response. A key part of this response is from cells known as the macrophages. These cells are found in all organs and tissues. Their structure varies depending upon the location. Macrophages can kill invading microbes and it is in the killing process that NO seems to be involved. NO is toxic to invading bacteria and unhealthy host cells. It is part of the body's natural defense against the malaria parasite.[4]

NO produced by macrophages for fighting infections may bring about massive hypotension, a condition known as septic shock which can be fatal. Also, though it is cytotoxic towards early tumour cells, it can also act as a carcinogen i.e. a cancer causing agent. NO is present at quite high concentrations in cigarette smoke and so could

contribute to dangerous effects of passive smoking. High levels of NO in the brain may lead to degenerative conditions such as senile dementia.

NO also acts as a neurotransmitter. However, the precise physiological role of neuronal NO is not yet fully known. NO has been implicated as a mediator of certain neurons that do not respond to the neurotransmitters acetylcholine or norepinephrine. NO sensitive neurons of this type have been found in several peripheral tissues including the cardiovascular, urogenital, respiratory and digestive systems. Non-invasive means of applying NO releasing substances to the penis have been suggested as a novel way to treat impotence[3].

These biological and medical roles of NO indicate the importance of understanding the fundamental chemistry of NO under conditions relevant to its biological formation and decay. A lot of research has been done but a number of challenges still remain. One of the challenges is how to modify NO such that it is action specific. NO binds to a number of metals and so there may be possibilities for inorganic drugs containing NO as a ligand. The other challenge is to be able to manage, monitor and control levels of NO present in biological systems.

AIMS OF THE PROJECT

- The aim is to study the interactions of NO with metallophthalocyanine (MPc) complexes as possible scavengers of the nitric oxide.
- To study the catalytic behaviour of MPc complexes towards oxidation and reduction of NO.
- To apply MPc modified electrodes in the electrochemical determination of nitric oxide in biological systems.

1.1 Chemistry of nitric oxide.

NO is a colorless gas at room temperature with a boiling point of –151.8 °C and a melting point of –163.6 °C. The liquid and gas are colorless when pure. The solubility in water at 25 °C and 1atm is 2.2×10^{-3} mol dm^{-3}.[5] For its physiological purposes, NO is always present as an aqueous solution.[4] NO was first characterized in 1772 by Joseph Priestley.[6] He prepared the gas by reacting nitric acid (HNO_3) with a metal, e.g. copper, equation 1.1.

$$3Cu + 8H^+ + 2NO_3^- \longrightarrow 3Cu^{2+} + 2NO + 4H_2O \quad \text{.....1.1}$$

The gas was collected over water. Since then there has been a number of methods used to prepare NO, one of which is a simple reaction of sodium nitrite with sulfuric acid. Industrially the gas is prepared by the catalytic oxidation of ammonia, equation 1.2

$$4NH_3 + 5O_2 \xrightarrow{\text{Pt-Rh}} 4NO + 6H_2O \quad \text{.....1.2}$$

The arrangement of the eleven valence shell electrons in NO is best represented by a simplified molecular orbital diagram, Figure 1.1.[7] The single 2s and three 2p atomic orbitals of nitrogen and oxygen combine to form eight molecular orbitals. Four of these are bonding, ($\sigma 2s$, $\sigma 2p_x$, $\pi 2p_y$, $\pi 2p_z$) and four are antibonding, ($\sigma^* 2s$, $\pi^* 2p_y$, $\pi^* 2p_z$, $\sigma^* 2p_x$). The bonding and the antibonding 2s orbitals cancel and a sigma (σ) bond is formed by the filled $\sigma 2p^2_x$ orbital. A pi (π) bond is formed by the filled $\pi 2p^2 z$ orbital. The half-filled $\pi^* 2p^1 y$ half cancels the filled $\pi 2p^2 y$ orbital, thus giving half a bond. The bond order is thus two and a half. This is consistent with the NO bond length of 1.150Å, which is intermediate between a triple and a double bond distance.

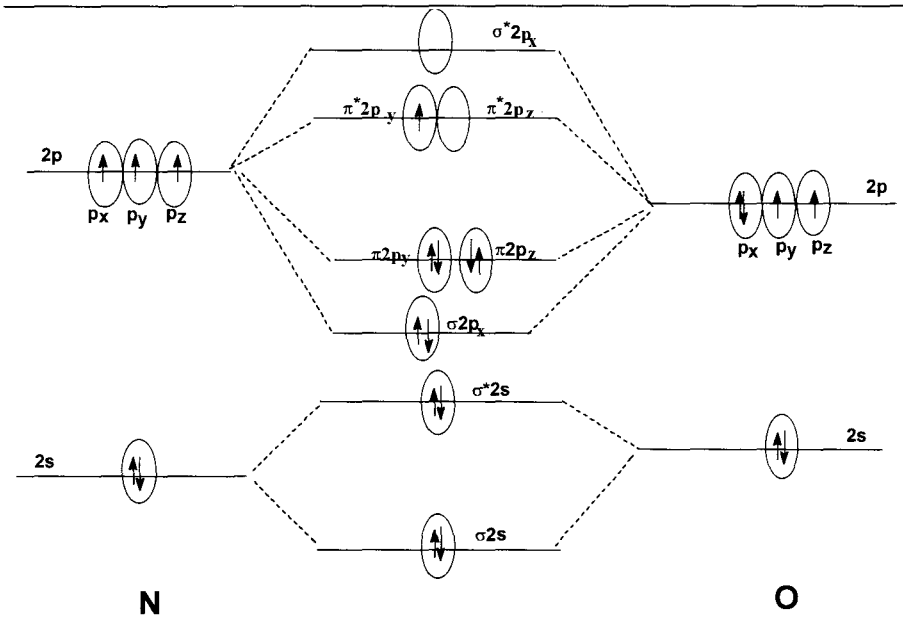

FIGURE 1.1 Molecular orbital diagram of NO

NO does not exhibit a strong tendency to dimerize. It does not undergo any hydrolysis in aqueous media.[8] There is no exchange of oxygen atoms between NO and H_2O at 25 °C. This implies that NO in aqueous solution exists essentially in an unaltered molecular form and it is not an anhydride of $H_2N_2O_3$. The complete lack of interaction between NO and H_2O, i.e. its hydrophobic property, is central to its physiological function. NO can pass freely across cell walls.

The reaction of NO with oxygen complicates the study of NO in aqueous solutions, equations 1.3 to 1.5.[6]

$2NO + O_2 \longrightarrow 2NO_2$ 1.3

$NO + NO_2 \longrightarrow N_2O_3$ 1.4

$4NO + O_2 + 2H_2O \longrightarrow 4\,HNO_2$ 1.5

NO_2, N_2O_3 and NO_2^- can result in a variety of side reactions, some of which are catalytic. To eliminate O_2, aqueous solutions have to be deoxygenated by passing high purity nitrogen or argon gas through the solution. In biological systems NO has been shown to react with a super oxide anion, O_2^- to form peroxynitrite, equation 1.6.[9]

$NO + O_2^- \longrightarrow {}^-OONO$ 1.6

At physiological pH range, ^-OONO is protonated and it disappears rapidly in solution as a result of the rearrangement to form a nitrate, NO_3^-. The nitrate is formed via the formation and recombination of the radicals, $^{\cdot}OH$ and $^{\cdot}NO_2$.

The chemistry of NO is basically determined by the relative ease of the removal of the single antibonding electron and the resulting stability of the nitrosonium, NO^+ ion. The removal of the antibonding electron in NO results in a stronger bond in NO^+ than in NO. The bond length decreases by 0.09Å and the vibration frequency rises from 1840 cm^{-1} in NO to between 2150 and 2400 cm^{-1} in NO^+, depending on the environment.[10]

NO can be reduced by a wide variety of reagents. The extent of reduction depends on the reducing agent employed, the reaction stoichiometry and other conditions e.g. whether a catalyst was employed or not. Porphyrins and in recent years phthalocyanines have been used as catalysts in the reduction and oxidation reactions of NO.

1.2 Background on metallophthalocyanine complexes.

NO easily form complexes with transition metal ions, including those found in metalloproteins. Studies of NO interaction with metalloporphyrins (MP) have increased the understanding of the interaction of NO with heme containing biomolecules such as hemoglobin and myoglobin. Metallophthalocyanine (MPc) complexes have a similar structure to the metalloporphyrins and have been used to mimic the properties of the naturally occurring MP. MPc complexes have an added advantage in that they are more stable to degradation than MP.

MPc complexes are porphyrin derivatives. They are blue to green pigments which have a wide variety of uses including printing inks, surface coatings, paper and clothing dyes.[11] In recent years, MPc complexes have found application in medicine as photosensitizers in the treatment of some cancer tumours using photodynamic therapy (PDT).[12] There has been a growing interest in the reactions of MPc complexes with NO owing to the similarity of the former to natural occurring metalloporphyrin and their added advantage of stability.

The structure of MPc, Figure 1.2, resembles that of porphyrin except that the porphyrin ring system is made up of pyrrole units instead of the isoindole units found in phthalocyanines.[13] The pyrrole units in porphyrins are linked by carbon atoms whilst the isoindole units in phthalocyanine are linked by nitrogen atoms.

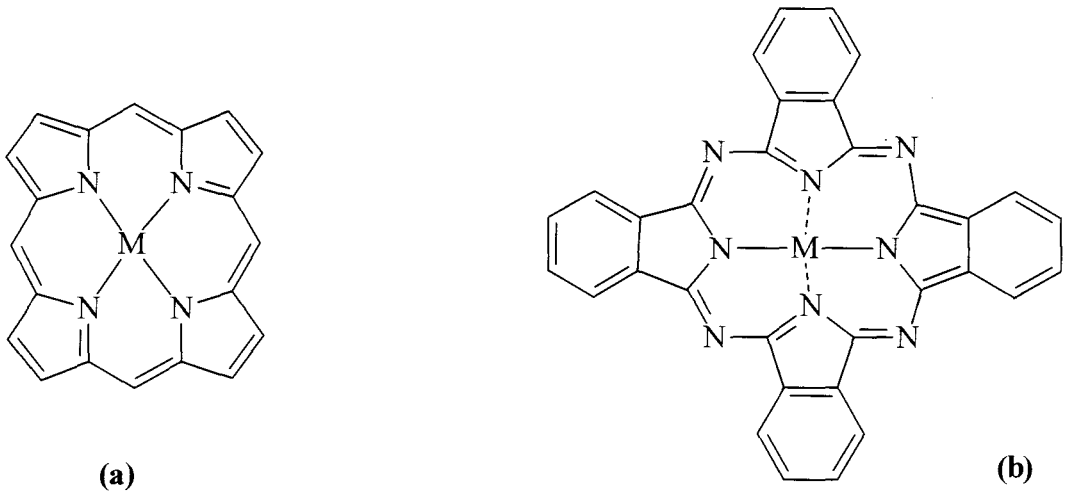

FIGURE 1. 2 Molecular structures of (a) metalloporphyrin and (b) metallophthalocyanine.

1.2.1 Electronic structure of metallophthalocyanine.

According to Gouterman's four orbital theory the highest occupied molecular orbitals (HOMO) of the MPc ring are the $a_{1u}(\pi)$ and $a_{2u}(\pi)$, the lowest unoccupied orbital (LUMO) of the MPc ring is the $e_g(\pi)$, Figure 1.3.[14]

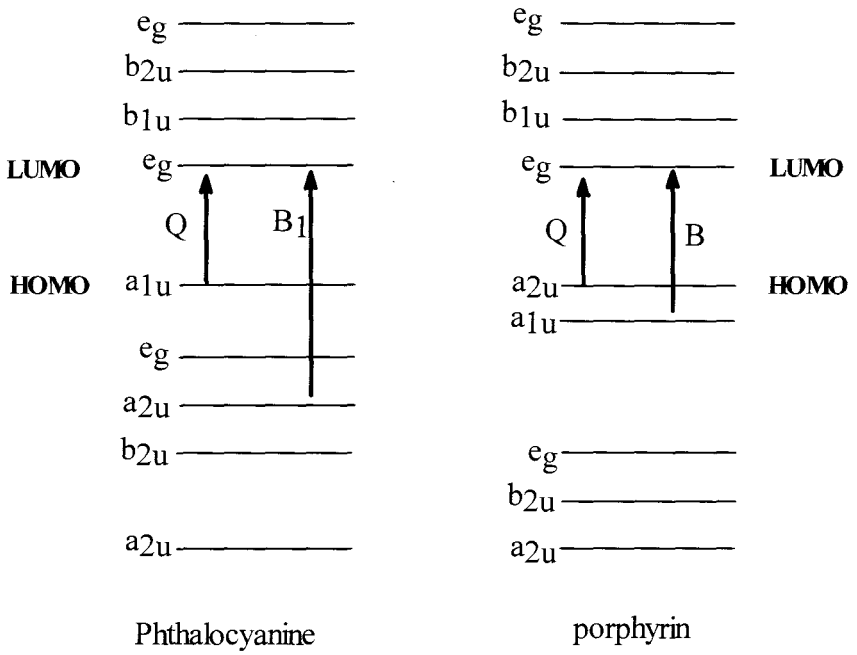

FIGURE 1.3 Simplified energy level diagram for metalloporphyrin and metallophthalocyanine.

In porphyrins a_{2u} and a_{1u} are close together, while for phthalocyanine, the two HOMO orbitals (a_{1u} and a_{2u}) are quite far apart.

The first two allowed $\pi-\pi^*$ bands (Q and B bands) arise from transitions from a_{1u} and a_{2u} into the e_g orbital. For MPc, a_{1u} lies well above a_{2u}, but for porphyrins a_{2u} lies above a_{1u} and are close together resulting in extensive configuration interaction. Thus the spectra for porphyrins shows a weak Q band and a very intense B (or Soret) band whilst for MPc the Q band is very intense, Figure 1.4.

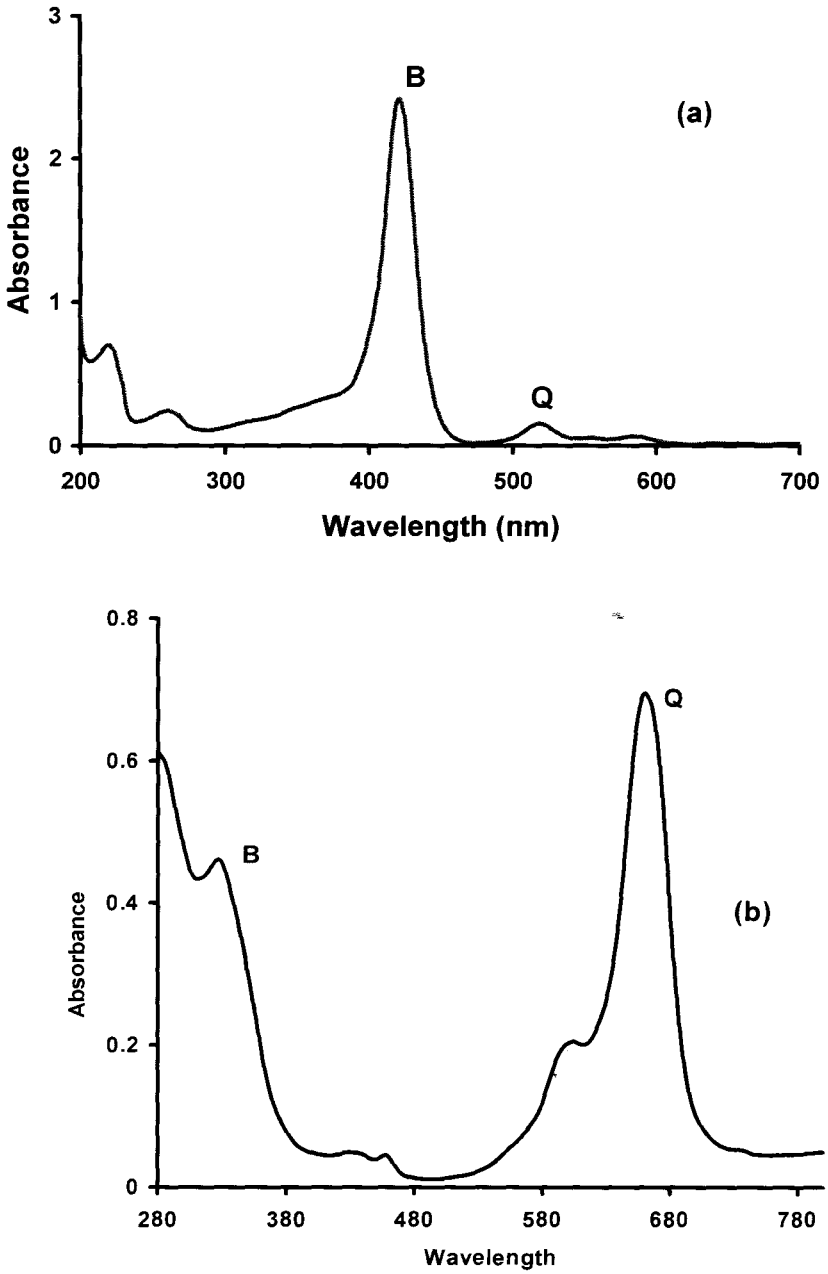

FIGURE 1.4 Absorption Spectra of a typical, (a) metalloporphyrin and (b) metallophthalocyanine complex.

If the central metal in the MPc complex has d-orbitals that lie in between the HOMO – LUMO gap of the ligand (MPc ring), there is a possibility of an electron transfer from the occupied ring orbital to an unfilled metal orbital resulting in metal to ligand charge transfer (LMCT). Electron transfer can also occur from the occupied metal d orbital to the unfilled orbital of the ligand resulting in metal to ligand charge transfer (MLCT), Figure 1.5.

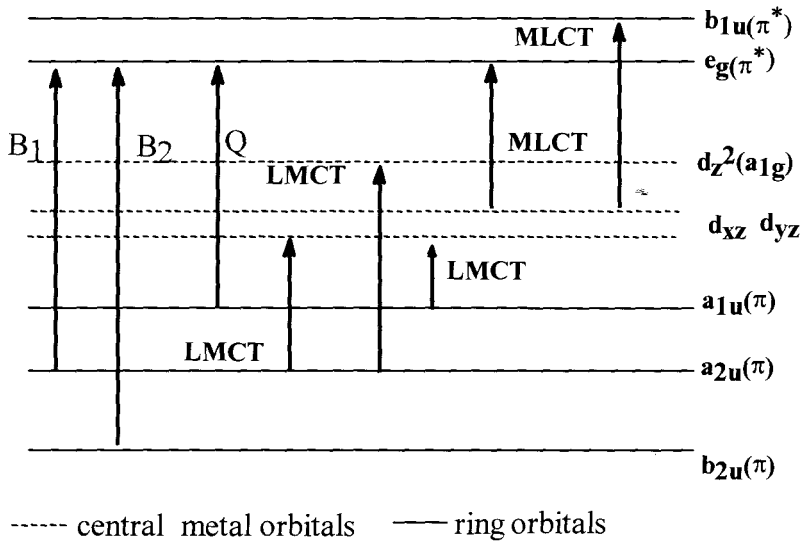

FIGURE 1. 5 A simplified energy level diagram of a metallopthalocyanine complex showing typical charge transfer transitions.

Charge transfer (CT), transitions are characterized by weak absorption bands on both sides of the Q band, i.e. near the infrared region and in the 500 nm region.

1.2.2 Absorption spectra of porphyrins and phthalocyanines.

Porphyrins have an intense absorption band between 390 nm and 425 nm, the B or Soret band, with two to four much weaker bands, Q bands, situated between 480 nm and 700 nm, Figure 1.4. The number and intensity of these bands can give clues to the substitution pattern of the porphyrin. It can also give a clue as to whether the porphyrin is metallated or not. MPc complexes have an intense absorption band in the 600-700 nm region (the Q band) and a weak band, B band in the 350 nm region.

The distinction between the spectra of different peripherally substituted phthalocyanines is not as pronounced as that between different porphyrins. For MPcs, the intensity of the Q band is reasonably constant from complex to complex. In part this arises because the Q band in phthalocyanine is essentially an allowed transition, which is not so dependent on the intensity of gaining mechanisms that are required by the Q band in porphyrins.[14]

Gouterman's[14] orbital theory predicts that perturbations to the energies of the HOMO (a_{1u} and a_{2u} symmetry) and LUMO (e_g) caused by replacing the porphyrin meso carbons with nitrogen atoms and fusing the benzene rings onto the pyrrole, vastly increases the probability of forbidden transitions between these orbitals. The net effect is to increase the intensity of the visible bands at the expense of the near ultra violet (UV) band. As a result the MPc appear blue to green depending on the position of the visible absorption bands. Most of the applications of MPc complexes result from their absorption spectra in the visible region.

Oxidation and reduction in MPc complexes

Oxidation and reduction in MPc can occur at the central metal or on the ring. The ring in neutral MPc complexes carries a –2 charge hence, MPc complexes are represented as MPc(-2). Oxidation on the ring [MPc(-2)] occurs by successive removal of each electron from the HOMO resulting in the formation of $[MPc(-1)]^{+}$ and $[MPc(0)]^{2+}$ cation radicals, Figure 1.6.

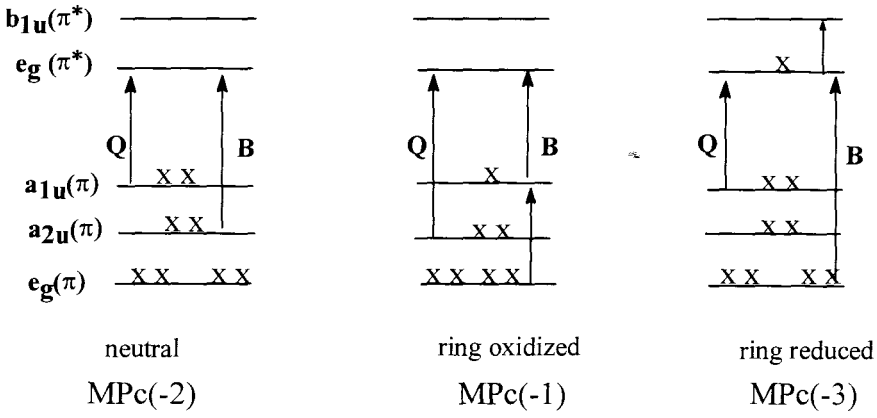

FIGURE 1. 6 A simplified energy level diagram for oxidized and reduced MPc species.

The formation of $[MPc(-1)]^{+}$ radical results in a partially filled HOMO. The presence of a hole in $a_{1u}(\pi)$ permits an allowed transition from $e_g(\pi)$ levels lying below the $a_{1u}(\pi)$. The formation of the $[MPc(-1)]^{+}$ species is characterized by the loss of intensity of the Q band, the formation of weak bands in the 700 and 825 nm regions, and a broad band centered near 500 nm. The ease of oxidation of the MPc ring is

significantly greater than that of the corresponding porphyrin complexes. This is due to the enhanced delocalization in the MPc macrocycle

Ring reduction corresponds to successive addition of up to four electrons to the LUMO resulting in the formation of $[MPc(3-)]^{-1}$, $[MPc(4-)]^{-2}$, $[MPc(5-)]^{-3}$, $[MPc(6-)]^{-4}$ species, Figure 1.6.[15] Addition of the electrons to the LUMO permits the $\pi^* - \pi^*$ transitions to occur from the e_g π^* to the higher energy π^* molecular orbital of the ring. However the resulting bands are very weak since the MPc ring is perturbed.[16] For those metals which do not have their d- orbitals between the HOMO-LUMO gap of the ring, oxidation and reduction occurs exclusively on the Pc ring, e.g. the main group metal MPc.

Metal oxidation and reduction is characterized by a shift in the Q band position without much change in the intensity. Whether the redox process occurs on the ring or on the central metal depends on the metal, the axial ligand, solvent and ring substituents.

1.2.3 Electrochemical properties of MPc complexes.

In general oxidation and reduction in MPc are expected at the central metal and /or at the Pc ring. In each case one or more electron transfer processes may be observed. Usually two successive ring oxidations and up to four ring reductions may occur on a platinum electrode.[17] Ring reductions are generally electrochemically reversible but ring oxidations often, are not reversible. Identification of the nature of a given redox product is usually based on electronic spectroscopy sometimes on the electron spin resonance spectroscopy (ESR). It is generally possible to identify where reduction or oxidation

occurred, i.e. at the metal center or on the Pc ring[18,19] using UV/Visible spectroscopy (see Section 1.2.2).

The presence of a transition metal in the center of the Pc ring affects the redox processes that occur at the phthalocyanine unit. One or more redox processes may occur at the central metal, at potentials that are between ring oxidation and reduction. If the solvent, supporting electrolyte or an added ligand can bind to the axial position of the metal ion in one or more of its oxidation states, the observed redox potential will depend on the choice of the solvent, the electrolyte or the added ligand.

ESR spectroscopy data has shown that Ni(II), Cu(II) and Zn(II) phthalocyanine species do not undergo metal redox processes, at potentials that are between ring reduction and ring oxidation.[17] However with Fe and Co which can be in the M(I), M(II) and M(III) oxidation states, in most cases the oxidation of the phthalocyanine (Pc) ring only occurs after the metal has been oxidized to its M(III) state. In most cases reduction of the phthalocyanine ring only occurs after the metal has been reduced to its M(I) state. The ability to reduce an MPc complex increases, i.e. the potential becomes less negative as the oxidation state of the central metal ion increases. As stated above, most oxidations of the ring in transition metal Pcs are electrochemically irreversible.

Solvent effects on the redox potentials of the Pc ring are small, however they are more significant on metal redox processes. In strong binding solvents, metal oxidation in cobalt phthalocyanine complexes occurs before ring oxidations. Since Co(III) has the ability to coordinate two ligands, the oxidation potential is solvent dependent. In non coordinating solvents such as dichlorobenzene, Co(III) species do not form. Under these conditions the Co(III)/Co(II) couple is shifted to high positive potentials and is not

observed. However, if pyridine is added to such a solution Co(III) species are formed.[17,20,21,22] In strongly binding solvents, the d^7 electron configuration of Co(II) is destabilized and the potentials shift negatively with increasing donor strength of the solvent. The donor strength of the solvents follow the order; DMA = DMF<DMSO<pyridine, where DMA, DMF and DMSO represent dimethylamine, dimethylformamide and dimethylsulfoxide respectively. In this work electrochemical properties of CoPc and other MPc complexes are explored for their use as electrocatalysts.

1.3 Interaction of NO with metalloporphyrins and metallophthalocyanines.

During the past decade, considerable attention has turned to the reactions of metalloporphyrins with NO, owing to the various biological functions that have been attributed to NO. Many responses in mammals emanate from the interaction of NO with the ferrous heme.[23] Ferric nitrosyl heme proteins have been found to be involved in fungal and bacterial denitrification processes, especially in the enzyme nitritereductase.[24] Also, ferric heme proteins in the salivary glands of a blood sucking insect, *Rhodnius prolixus*, have been found to be capable of reversibly binding NO.[25] This helps the insect to feed on blood. The principal targets for NO under bioregulatory conditions are metal centers, primarily iron. The ferroheme enzyme soluble guanylyl cyclase (sGC) is the best characterized example of such targets.[26] Studies into the binding of NO with MPs have aided the understanding of how NO interacts with hemoglobin, myoglobin and sGC. Studies into the interaction of NO with iron porphyrins have been extended to other MPs such as Co, Ru, Os and others.

1.3.1 Interactions with porphyrins.

Metalloporphyrin nitrosyl complexes are formed as a result of axial ligation of NO to the central metal. Thus the classification thereof is based on the interaction of NO with the central metal. Metalloporphyrin nitrosyl complexes mainly occur in two classes. The character of the NO group determines the geometry of the complex. NO can exist as a nitrosyl cation, NO^+, when electrons are donated to the metal from the NO group. This will result in a linear nitrosyl complex with M-NO bond of 180°.[27] If NO exists as NO^-,

where electron donation is from the metal to the NO ligand, the complex will be bent at an angle of about 120°.[27]

180° 120°

Scheme 1. 1 Geometries of nitrosyl complexes.

However, attempts to correlate structures, physical properties and reactivity of metal nitrosyl complexes using the formal oxidation state of the nitrosyl group has not been successful. It has been demonstrated that transition metal nitrosyls are highly covalent. Hence, Enemark and Feltham[28] have made use of the molecular orbital correlation method in describing bonding in the metal nitrosyl complexes. Properties of the metalloporphyrin nitrosyl complexes are determined primarily by the nature of the highest occupied molecular orbital (HOMO). The value *n,* that defines the geometry, is the number of metal d electrons plus the electron in the π* orbital of NO. The notation $\{MNO\}^n$ is used.

In metalloporphyrin nitrosyl complexes with square-pyramidal and pseudo octahedral geometries for five and six trans coordinate derivatives respectively, the important values of *n* are 6,7,8. For the first row transition metal porphyrins, the geometry is linear (MNO angle = 180^0) for n = 6 and bent for n=8 with MNO angle of 120^0. MNO complexes with n=7 have an intermediate geometry between linear and bent with a MNO angle of 145°.[29] The three geometries are apparent in the analysis of the

meso-tetraphenylporphyrin (TPP) complexes of Mn^{2+}, Fe^{2+} and Co^{2+}. The following bond angles were observed,[30,31,32] $Mn^{II}TPP$ = 176.2°, $Fe^{II}TPP$ = 142° $Co^{II}TPP$ = 128.5°. The Mn and the Co complexes are consistent with the $\{MNO\}^6$ and $\{MNO\}^8$ geometries, i.e. linear and bent, respectively. The Fe complex exhibits an intermediary geometry between linear and bent. The axial $M\text{-}N_{NO}$ bond distance in the complexes is in the order Mn<Fe<Co (1.644<1.743<1.833 Å), indicating a decrease in π interaction in the bonding systems.

The effect of changing the environment of the Co(II) nitrosyl porphyrin by changing peripheral groups of the porphyrin ring has been reported.[33] It was observed that changing the basicity of the complex did not change the geometry of the NO-Co(II) porphyrin complex. Similar behaviour has been reported for cobalt nitrosyl porphyrins.[34]

The kinetics of the nitrosylation of various heme proteins as well as for a number of model compounds have been reported. Photodissociation of NO from nitrosyl metalloporphyrins is usually reversible, hence these have been used to investigate the kinetics of the nitrosylation reactions. In such reactions, flash photolysis is used to labilize NO from the (NO)MP precursor and relaxation of the non steady state system back to equilibrium is monitored spectroscopically, equation 1.7.[35]

$$\mathbf{MP + NO} \underset{k_{off}}{\overset{k_{on}}{\rightleftharpoons}} \mathbf{(NO)MP} \quad \text{.....1.7}$$

Under excess NO conditions, the spectra decays exponentially according to the following reaction, equation 1.8:

$$\mathbf{k_{obs} = k_{on}\,[NO] + k_{off}} \quad \text{.....1.8}$$

The plot of k_{obs} versus [NO] is linear with a slope, k_{on} and intercept k_{off}. The ratio of the rate constants, k_{on} / k_{off} = K, gives the equilibrium constant for the formation of the nitrosyl complex under these conditions. For many systems especially those of ferroheme complexes or proteins, the reverse reaction is exceedingly slow.

Laverman *et al.*[36] reported on the dissociative mechanism for the reactions of NO with water soluble iron(III) porphyrins, tetrakis(4-sulfonatophenyl) iron(III) porphyrin, ($Fe^{III}(TPPS)(H_2O)_2^{3-}$), and tetrakis(sulfonatomesityl) iron(III) porphyrin, ($Fe^{III}(TMPS)(H_2O)_2^{n-}$). Laser flash photolysis of aqueous solutions of these complexes under defined NO pressure gave transient spectra which was consistent with the spectral difference between $Fe^{III}(por)(H_2O)(NO)^{n-}$ and $Fe^{III}(por)(H_2O)_2^{n-}$. The transients decayed exponentially to regenerate the equilibrium mixture of solvated and nitrosyl complexes. No permanent photoproducts were observed hence the decay represented the relaxation of the Fe^{III}(por)/NO system (where por = TPPS or TMPS), according to equation 1. 9.

Fe(por) + NO $\rightleftharpoons$ **Fe(por)(NO)**.....1.9

The plot of k_{obs} versus [NO] was linear with a slope, k_{on} of 3.0 x 10^6 dm^3 mol^{-1} s^{-1} and intercept, k_{off} of 7.3 x 10^2 s^{-1} , for por = TMPS giving k_{on} / k_{off} ratio of 4.1 x 10^3 mol dm^{-3}.

In order to understand the mechanism of the reaction of NO with porphyrin, measurements of k_{on} and k_{off} were performed as a function of temperature and hydrostatic pressure to determine the change in enthalpy, ΔH, entropy, ΔS and volume, ΔV.[36] Temperature and hydrostatic pressure experiments, gave sizable ΔH, and very positive ΔS values for k_{on} and k_{off}. The calculated ΔV_{on} and ΔV_{off} values were substantially positive. The large and positive ΔS, and ΔV values for k_{on} and k_{off} represent a substitution

mechanism which is dominated by ligand dissociation as indicated by equations 1.10, and 1.11.[35]

$$Fe^{III}(por)(H_2O)_2 \underset{k\text{-}1}{\overset{k_1}{\rightleftharpoons}} Fe^{III}(por)(H_2O) + H_2O \quad \text{.....1.10}$$

$$Fe^{III}(por)(H_2O) + NO \underset{k\text{-}2}{\overset{k_2}{\rightleftharpoons}} Fe^{III}(por)(H_2O)NO \quad \text{.....1.11}$$

As reported by Ostrich *et al.*,[37] water exchange between the solvent (equation 1.10) and $Fe^{III}(TPPS)(H_2O)_2^{n-}$ occurs at a first order rate k_{ex} = 1.4 x 10^7 s^{-1} at 25 °C, which far exceeds the k_{obs} determined for [NO]. If the steady state approximation were taken with regard to the intermediate, $Fe^{III}(por)(H_2O)$, the k_{obs} of the non equilibrium mixture generated by flash photolysis would be, equation 1.12,[35]

$$k_{obs} = \frac{k_1 k_2[NO] + (k_{-1})(k_{-2})[H_2O]}{k_{-1}[H_2O] + k_2[NO]} \quad \text{.....1.12}$$

Under the experimental conditions, the authors concluded that $k_{-1}[H_2O] >> k_2[NO]$ since both steps involve diffusion limited competition for the unsaturated metal center and $[H_2O] >> [NO]$. Accordingly, $k_{on} = k_1k_2/k_{-1}[H_2O]$ and $k_{off} = k_{-2}$. Since k_2 and the k_{-1} steps represent similar reactions of the unsaturated intermediates, $[Fe^{III}(por)(H_2O)]$ with an incoming ligand, NO and water respectively, the differences in their activation

parameters should be small. Furthermore, the values of ΔH, and ΔS for water exchange on $[Fe^{III}(TPPS)(H_2O)_2]^{3-}$ were very similar to the respective k_{on} activation parameters. Thus the factors that determine H_2O exchange kinetics for the di-aquo species also dominate the kinetics of the k_{on} step of NO, for the same species. Hence, the reaction parameters of $Fe^{III}(TPPS)(H_2O)_2^{3-}$ and $Fe^{III}(TMPS)(H_2O)_2^{n-}$ are largely defined by a dissociative mechanism.[36]

In contrast to the Fe(III) porphyrins, the ΔS and ΔV values for the "on" reaction determined for tetrakis(4-sulfonatophenyl) iron(II) porphyrin, $Fe^{II}(TPPS)$, and tetrakis(sulfonatomesityl) iron(II) porphyrin, $Fe^{II}(TMPS)$, were much smaller and the corresponding k_{on} values were three orders of magnitude faster. The kinetics of ligand binding in ferrohemes led to a proposed mechanism in which an encounter pair, {Fe(por)||L}, is formed before bond formation, equation 1.13.[38]

$$Fe^{II}(por) + L \underset{k_{-d}}{\overset{k_d}{\rightleftharpoons}} \{ Fe^{II}(por) \| L \} \xrightarrow{k_a} Fe^{II}(por)(L) \quad \text{.....1.13}$$

In this model, k_d is the rate constant for formation of the counter pair by diffusion, k_{-d} is the rate constant for the diffusion of the reactants apart, and k_a represent the rate constant for the formation of the Fe-L bond. If the steady state approximation is made with respect to the encounter pair {Fe(por)||L}, then equation 1.14 holds.[38]

$$k_{on} = (k_d\, k_a) / (k_{-d} + k_a) \quad \text{.....1.14}$$

The two limiting cases are, either one in which ligand binding is activation controlled or where the reaction is diffusion controlled. In the former $k_d >> k_a$. In the case of Fe^{II}(TPPS) and Fe^{II}(TMPS), the ΔV_{on} values measured were larger than those expected for a diffusion limited rate in water but much smaller than those found for ferriheme analogs.[36] This suggest that k_{on} in equation 1.14, is largely dominated by the diffusional terms. The rates for the reaction of NO with Fe^{II}(TPPS) and Fe^{II}(TMPS) were found to be within one order of magnitude from that of the diffusion limit in water. The behaviour of Co^{II}(TPPS) with NO to give Co^{II}(TPPS)(NO) was found to be quite similar to that of the Fe^{II} analogs with $k_{on} = 2.3 \pm 0.1 \times 10^9$ $dm^3mol^{-1}s^{-1}$ at 298K.[38] Therefore it can be concluded that the kinetics of the "on" reaction for Co^{II}(TPPS) are dominated by diffusion processes.

The formation of the nitrosyl complex from Fe(III) pophyrin complexes, is accompanied by a charge transfer to give $Fe^{II}(NO^+)$.[39] The absorption spectrum of Fe^{III}TPPS in aqueous solutions exhibited a peak at 393 nm in the Soret band region . The peak is red shifted to 420 nm when the nitric oxide adduct is formed.[40] The red shift is explained in terms of a charge transfer interaction from NO to the metal center, forming $(NO^+)Fe^{II}$TPPS. The iron is no longer high spin Fe(III) but low spin Fe(II). The formation of the Fe(II) nitrosyl complex is further accompanied by entropy and volume changes. These changes are due to the solvation changes as charge redistributes from the Fe(III) state to the Fe(II) state accompanied by a spin change from high spin to low spin. However, the formation of Fe(II) nitrosyl complex from Fe(II) porphyrin is accompanied by a blue shift in the spectrum. The absorption peak of Fe^{II}TPPS at 425 nm is blue shifted to 412 nm by forming $(NO)Fe^{II}$TPPS.[40] Analogous shifts of Soret bands were

observed for manganese(II) tetraphenylporphyrin, $Mn^{II}TPP$,[41] Fe(II) and Fe(III) hemoproteins on exposure to NO. However, when the solution of cobalt tetrakis(N-methyl-2-pyridyl) porphine, $[Co^{III}(2\text{-tmpyp})]^{5+}$ was purged with NO in pH 4 buffer, there was a blue shift of the Soret band, from 426 to 412 nm instead of the expected red shift.[42] The final spectra resembled that of $[Co^{II}(2\text{-tmpyp})(NO)]^{4+}$ confirming reductive nitrosylation. The absorption spectra of cobalt(II) octaethyl porphyrin, Co(II)OEP and Co(II)TPP, NO adducts in 2-methyltetrahydrofuran, MTHF, were red shifted, from 515 nm, to 523 nm and from 526 nm to 537 nm respectively.[43] Reductive nitrosylation has also been reported for FeTPPCl and MnTPPCl nitrosyl complexes.[44,45]

Studies of the reaction mechanism for reductive nitrosylation of ferrihemoproteins, ferricytochrome c (cyt^{III}), metmyoglobin (Mb^{III}), methemoglobin (Hb^{III}), in buffer solutions, have been reported.[39] The rate of nitrosylation was found to be pH dependent. For cyt^{III} and Hb^{III} the reductive process was much faster at pH>7.0 than at pH<7.0. For the formation of Mb^{III}-NO, the equilibrium constants, K values are much smaller at pH $\geq$ 8.2 than those at pH $\leq$ 7.2. The difference in the K values, is attributed to the possible changes in the conformation of the protein with changes in the pH. Hoshino *et al.*[40] have summarized rates of nitrosylation for a number of Fe(II) and Fe(III) heme proteins (see Table1.1). These rates are in part a function of protein structure. For both Fe(II) and Fe(III) cytochrome c, the rates of nitrosylation are very slow. The protein limits the access of NO to the metal cite. The equilibrium constants for NO coordination are in the order, $Cat^{III} > Cyt^{III} \sim Mb^{III} > Fe^{III}TPPS$ (see Table 1.1).

Table1. 1 Rate constants for some nitrosylation reactions of porphyrins and hemoproteins

Reaction	k_f / $dm^3mol^{-1}s^1$	k_r / s^{-1}	Equilibrium const. K / $dm^3\ mol^{-1}$	References
$Fe^{II}TPPS + NO \underset{k_r}{\overset{k_f}{\rightleftharpoons}} (NO)Fe^{II}TPPS$	1.8×10^9	~0	-	40
$Mn^{II}TPP + NO \underset{k_r}{\overset{k_f}{\rightleftharpoons}} (NO)Mn^{II}TPP$	5.3×10^8	-	-	41
$Cat^{III} + NO \underset{k_r}{\overset{k_f}{\rightleftharpoons}} (NO)Cat^{III}$	3.0×10^7	1.7×10^{-2}	1.8×10^5	40
$Mb^{II} + NO \underset{k_r}{\overset{k_f}{\rightleftharpoons}} (NO)Mb^{II}$	1.7×10^7	1.2×10^{-4}	-	40
$Fe^{III}TPPS + NO \underset{k_r}{\overset{k_f}{\rightleftharpoons}} (NO)Fe^{III}TPPS$	7.2×10^5	6.8×10^{-2}	1.1×10^3	40
$Mb^{III} + NO \underset{k_r}{\overset{k_f}{\rightleftharpoons}} (NO)Mb^{III}$	1.9×10^5	13.6	1.4×10^4	40
$Cyt^{III} + NO \underset{k_r}{\overset{k_f}{\rightleftharpoons}} (NO)Cyt^{III}$	7.2×10^2	4.4×10^{-2}	1.6×10^4	40
$Cyt^{II} + NO \underset{k_r}{\overset{k_f}{\rightleftharpoons}} (NO)Cyt^{II}$	8.3	2.87×10^{-5}	-	40

TPP = Tetraphenyl porphyrin, Cat = Catalase, Mb = Metmyoglobin, Cyt =Cytochrome c

The equilibrium constants of Cat^{III}, Cyt^{III}, Mb^{III} are an order of magnitude larger than that of $Fe^{III}TPPS$. This suggests that the surrounding proteins have an effect on both the rate of association and of dissociation process of NO from the heme. The rate constants, k_f, for nitrosylation follow the order $Cat^{III} >> Fe^{III}TPPS > Mb^{III} >> Cyt^{III}$.

Nitrosyl nitro complexes of ruthenium have been reported.[46,47] These were synthesized by reacting ruthenium porphyrin carbonyl, Ru(P)(CO), with NO [where P= octaethylporphyrin (OEP) or tetra-m-tolyporphine (TmTP)]. The reaction proceeds via the formation of an intermediate, $Ru(P)(NO)_2$, equation 1.15.[46]

$$\mathbf{Ru(P)(CO) + 2NO \rightleftharpoons Ru(P)(NO)_2 + CO} \quad \text{.....1.15}$$

Under conditions of excess NO, the formation of $Ru(P)(NO)_2$ is irreversible and is first order with respect to [NO]. The second slower stage is the conversion of the intermediate which is accompanied by reduction of NO to N_2O. The rate is second order with respect to [NO], equation 1.16.[46]

$$\mathbf{Ru(p)(NO)_2 + 2NO \leftrightarrow Ru(P)(NO)(ONO) + N_2O} \quad \text{.....1.16}$$

It has been reported that the nitrosyl nitro complexes of ruthenium, Ru(P), (where P = tetraphenyl porphyrin, TPP), undergo irreversible reduction at the metal center. This is accompanied by dissociation of the axial ligand trans to NO, resulting in a mononitrosyl porphyrin complex, (NO)Ru(TPP).[47]

1.3.2 Interaction of NO with metallophthalocyanines.

Axial ligation of NO to FePc, CoPc, MnPc and Ni(II)TSPc (TSPc = tetrasulfonate phthalocyanine) has been reported.[48, 49, 50] It has been reported that when NO reacts with Fe(II)Pc, the resulting complex is Fe(III)Pc(NO). There is an electron transfer from the Fe metal ion to the NO ligand during the formation of the Fe nitrosyl phthalocyanine

complex.[48] Similar behaviour was observed for Co(II)Pc.[49] However, for (NO)Mn(II)Pc, electron transfer is from the NO ligand to the metal such that the nitrosyl is coordinated to the Pc as NO^{+}.[48] Axial bonds in the MPc complex are generally equal or slightly shorter in the MPc than in the porphyrin complex.

As with porphyrins, the number of d-type electrons in the MNO complex is related to the geometry and the electronic structure of the complex.[48] For divalent Mn, Fe and Co complexes, the configuration $\{MNO\}^{6}$, $\{MNO\}^{7}$, $\{MNO\}^{8}$, (where the superscript refers to the n values) holds.[48] The NO, IR stretching frequencies for MPc complexes closely resembles those of the corresponding MP complexes, (see Table 1.2). Coordination properties of MPc and MP differ in degree and not in kind and there are many parallels in their structural characteristics. However, the coordination characteristics of the individual metals are an important determining factor.

Table 1. 2 Table of NO stretching frequencies comparing MTPP and MPc, NO.

MPc	νNO / cm^{-1}	Reference	MTPP	νNO / cm^{-1}	Reference
Mn	1737	48	Mn	1735	51
Fe	1689	48	Fe	1670	52
Co	1698	48	Co	1689	31

For pentacoordinated nitrosyl complexes, the energy level of the π^* orbital of the NO ligand is very close to that of the metal d-orbital.[53] This affects the distribution of the electron density in the M-NO bond. The electron density on the NO^+ group is as a result not necessarily smaller than that on the NO^- group.[54] Electron density of NO in metal nitrosyl complexes is very sensitive to the metal and other ligands in the complex. This affects the νNO and it renders the IR technique unreliable as a tool to determine the geometry of the nitrosyl complexes.[55] However, in general linear nitrosyl porphyrin and phthalocyanine complexes have νNO greater than 1700 cm^{-1} and bent geometries frequently have νNO less than 1700 cm^{-1}.[50]

Ascenzi and co-workers have reported on the kinetic studies of the reaction of NO with iron phthalocyanine, FePc.[49] Like iron porphyrin, FePc forms a mononitrosyl derivative, (NO)FePc. The reaction in DMSO, where the axial and free solvent molecules are omitted, may be written as equation 1.17

$$FePc + NO \underset{k_r}{\overset{k_f}{\rightleftharpoons}} (NO)FePc \quad \text{.....1.17}$$

The equilibrium constant for NO ligation to FePc in DMSO was found to be 1.1×10^6 $dm^3\ mol^{-1}$. The second order rate constant for nitrosylation, k_f was $(2.2 \pm 0.4) \times 10^4$ $dm^3\ mol^{-1}\ s^{-1}$ and the rate constant for dissociation, k_r, $(2.0 \pm 0.4) \times 10^{-2}$ s^{-1}. The overall second order dependence of the rate of nitrosylation of FePc is not inconsistent with the dissociation mechanism as in the porphyrins.

To the author's knowledge there are no other reports on the kinetics of the interaction of NO with other MPc complexes, hence it is the aim of this project to study further the mechanisms and the kinetics of NO binding to MPc complexes. NO adducts of cobalt substituted myoglobin and hemoglobin have been reported,[56] hence the substitution, of iron by cobalt in synthetic porphyrins has gained considerable attention. In this work the aim is to study the interaction of NO with cobalt phthalocyanine, CoPc and cobalt tetrasulfophthalocyanine, $[CoTSPc]^{4-}$ and vitamin B_{12}. The reactivity of these cobalt complexes will be compared with other MPc complexes.

1.4 Spectra and electrochemical properties of cyanocobalamin ($VitB_{12}$).

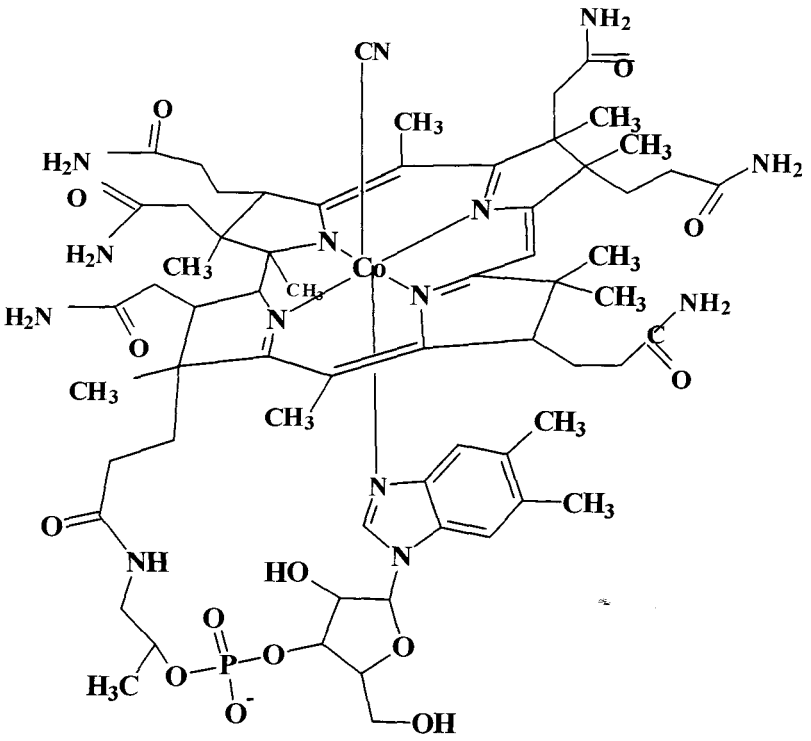

FIGURE 1. 7 Molecular structure of cyanocobalamin.

Cyanocobalamin, ($VitB_{12}$), is composed of two principal parts, the highly substituted, reduced porphyrin-like macro ring, and the nucleotide which contains a sugar residue, Figure 1.7. The macro ring contains cobalt(III) chelated to the 4 nitrogen atoms of the ring, to one N atom of the benzimidazole group below the ring, and to a cyanide ion. The entire structure, except the CN group, is referred to as cobalamin (Cbl(III)) hence vitamin B_{12}, ($VitB_{12}$) is frequently termed cyanocobalamin.

Vitamin B_{12} and its derivatives, the corphyrins have a number of features in common with phthalocyanines, in particular their structure and absorption spectra.[57,58] Cyanocobalamin is the most common form of cobalamins extracted from living organisms and dispensed in medical treatments. It is also present in mammalian tissue and fluids. The other common form of cobalamin is the Co(III), aquacobalamin ($VitB_{12a}$) where the cyanide ligand is substituted by the water molecule. In the Co(II) state, the aquacobalamin is known as $VitB_{12r}$ and in the Co(I) state it is known as $VitB_{12s}$.

There have been conflicting reports about the interaction of cobalamins with nitric oxide. When NO was passed through a solution of a Co(II) complex of aquacobalamin, ($VitB_{12r}$), there were no changes observed in the UV/Visible spectra except for traces of $VitB_{12a}$.[59] No changes were observed either when NO was passed through a solution of $VitB_{12a}$ for 3 hr. Wolak *et al.*,[60] used spectrophotometric and electrochemical techniques to investigate the interaction of NO with $VitB_{12a}$. No direct substitution between the water molecule of $VitB_{12a}$ and NO was observed. They found that the spectra resulting from the reaction of $VitB_{12a}$ and NO was identical to that observed when $VitB_{12a}$ was reacted with NO_2^-. The kinetics of the reaction of $VitB_{12a}$ with NO saturated solutions containing nitrite impurities, did not give first order kinetics although an appropriate excess NO was used, whilst under the same experimental conditions but substituting nitrite for NO, the kinetics gave good first order behaviour. They concluded that it is nitrite and not NO that reacts with $VitB_{12a}$, since it is difficult to obtain NO without NO_2^- impurities.

However experiments with the Co(II) aquacobalamin ($VitB_{12r}$) indicated significant spectral and kinetic differences between nitrite and NO reactions.[60] Nitrite

reactions with $VitB_{12r}$ were slow and the final UV/Visible spectra resembled that of a mixture of $VitB_{12a}$-NO_2^- and $VitB_{12r}$-NO. The reaction of $VitB_{12r}$ with NO was fast and in oxygen free conditions, a characteristic UV/Visible spectrum was observed. This implies that $VitB_{12r}$ does bind NO.

There has been a report of Cbl(III)NO that was detected by EPR when hydroxocobalamin acetate (Cbl(III)OH), methylcobalamin (MeCbl) and adenosylcobalamin (AdoCbl) respectively were reacted with NO.[61] However, further investigations using Fourier transform infrared spectroscopy (FTIR) to detect the N-O stretching frequency of bound NO to either Cbl(III) or Cbl(II), were not successful. This implies that neither Cbl(II) nor Cbl(III) forms a stable complex with NO. When NO was added to Cbl(II), mass spectroscopy results revealed the presence of NO_2^-. This implied that Cbl(II) which is present in aerated Cbl(III) solutions, reduces NO to NO_2^-. This reaction is however not fast enough to account for the interference of Cbl(III) with biological NO.

It has been reported that in aerated solutions of Cbl(III), superoxocobalamin, $Cbl(III)O_2^-$, is also present.[61] It is also reported that NO reacts rapidly and irreversibly with $Cbl(III)O_2^-$.[61] Thus, it is believed that the latter reaction accounts for the observed biological interference of Cbl(III) with NO. $Cbl(III)O_2^-$ is spontaneously generated from Cbl(II) and oxygen in aerated solutions. This may result in a cyclic mechanism for the rapid elimination, through oxidation, of NO. In this work, reaction of NO with $VitB_{12}$, under nitrogen saturated conditions using electrochemical and UV/Visible spectroscopy will be investigated. Findings thereof will be discussed in chapter 4.

The electrochemistry of cobalamins is well known. Lexa and co-workers,[62,63,64] have reported on the effect of pH on the electrochemistry of aquacobalamin. They found that beyond pH 7.8 the tendency of $VitB_{12r}$ to disproportionate to $VitB_{12s}$ increases, hence the Co^{III}/Co^{II} and Co^{II}/Co^{I} couples tend to merge. It has been reported[65] that with regard to the conversion of Co(III) to Co(II) in cobalamins, there is a correlation between the rate of electron transfer and the strength of the axial ligand-cobalt bond. The stronger the bond, the slower and more difficult is the electron transfer.[65] Hence, electron transfer is slower for hydroxocobalamin than it is for aquacobalamin due to the greater affinity of OH^- for Co(III), compared to that of the H_2O molecule. Similar behaviour is observed in the case of the reduction of Co(II) to Co(I). Strong coordinating solvents render reduction slower than less coordinating solvents, hence Co(II) to Co(I) is slower in DMSO than in water. For both Co(III)/Co(II) and Co(II)/Co(I) systems, the conversion does not only involve electron transfer but there is at the same time the loss of one ligand. The loss of a ligand occurs because the most stable forms of the Co(III), Co(II) and Co(I) cobalamins are six, five and four coordinated complexes, respectively.[65]

Under the influence of cyanide, the Co(III) form of cyanocobalamin is more stable than the Co(II) form. The standard potential of the Co(III)/Co(II) redox couple is close to or even negative to that of Co(II)/Co(I) couple.[66] This causes the two couples to merge, resulting in a two electron process i.e. Co(III)/Co(I) couple.

The cyclic voltammetry of $VitB_{12}$ shows a delayed rise in current and fails to produce a well defined cathodic peak. This indicates that this reaction is both slow and irreversible. The cathodic, Co(III)/Co(I) couple occurs at –1.03 V versus saturated calomel electrode (SCE) and the anodic peak, attributed to a Co(I)/Co(II) couple, occurs at potentials of –

0.9 V *vs* SCE.[67] The separation of the cathodic and anodic wave is much greater than the 0.028 V expected for a reversible process.

1.5 Methods of NO detection.

As indicated earlier (Section 1), it is important to be able to measure and monitor NO in biological systems. In that view, several researchers have employed a number of techniques in an attempt to achieve this. NO has been determined by monitoring the chemiluminescence reactions of NO with ozone or with luminol and hydrogen peroxide.[68,69,70] Electron spin resonance and spectroscopic methods have also been employed in studying NO.[71,72,73,74,75] Physiologically important NO bound compounds such as nitroprusside, heme iron and copper in proteins and nitrosothiols have been studied using these techniques.[76] However these techniques suffer from being *ex situ* detection techniques which rely on the measurement of secondary products of NO. Electrochemical methods for NO detection offer features that are not available with other methods. In electrochemistry microelectrodes can be placed in a single cell or tissue at the proximity of the NO source, making *in situ* detection of NO possible.

Electrochemical methods currently available for NO detection are based on the electrochemical oxidation of NO on solid electrodes. NO oxidation occurs much easier than reduction because of the unpaired electron in the HOMO of NO (see Figure 1.1). If the current generated during NO oxidation is linearly proportional to the NO concentration, the oxidation current is used as an analytic signal. This current can be measured in amperometric or voltammetric mode. In the amperometric mode, the potential at which NO is oxidized is kept constant. In the voltammetric mode, the current is measured while the potential is linearly scanned across a region that includes NO oxidation. Both methods of measurement provide a quantitative signal. Whilst the amperometric method is faster than the voltammetric method, the latter provides

additional qualitative information, specifically, that the current being measured results from NO oxidation. Oxidation of NO on a solid electrode proceeds via two steps; an electrochemical reaction followed by a chemical reaction.[77] The first step is a one electron transfer from NO to the electrode, equation 1.18,

$$NO \rightarrow NO^+ + e^- \quad \text{.....1.18}$$

NO^+ is a relatively strong lewis acid and in the presence of OH^-, it is converted to nitrite, equation 1.19,

$$NO^+ + OH^- \rightarrow HNO_2 \quad \text{.....1.19}$$

NO is reduced at potentials that are more negative than the reduction potential of oxygen. It is thus difficult to measure NO under aerobic conditions. Catalysts have been immobilized on the electrode to improve the efficiency of the electrode and to lower the reduction potential of NO.

Understanding of biological roles of NO requires detailed studies of its production and transportation which in turn require, its measurement *in situ* and in real-time. Measurement of NO in biological systems is complicated by the fact that NO has a very short half-life of approximately six seconds,[78] and that it occurs at very low concentrations. NO is readily oxidized by oxygen to nitrite, NO_2^- and nitrate, NO_3^-. Most methods of NO measurement have thus relied on the measurement of secondary products such as the nitrite and nitrate.[79] There has been a growing interest in the direct and *in vivo* determination of NO. Methods for direct NO measurement have to be fast, show good sensitivity and selectivity. The desire to measure small amounts of NO for

both *in vivo* and *in vitro* studies, has led to an active area of research involving designing of microelectrodes or microsensors.

Microelectrode design and fabrication has recently been central to NO research and it has thus reached very high levels of sophistication. Microelectrodes of appropriate dimensions have been fabricated and inserted into single cells or microslices of tissue.[80,81] Some microsensors are now commercially available.[82] Microelectrodes have other advantages over the conventional electrodes. They offer high sensitivity, which allows for very low NO concentration determination. Response is very fast such that measurements can be done at micro and even smaller time frames. Currents are very low such that there is little or no solution resistance permitting the non usage of an electrolyte. This makes the use of microelectrodes ideal for biological *in vivo* determinations. Carbon fiber microelectrodes have already been employed for the measurement of several neurotransmitters in the brain.

The rich redox chemistry of NO allows for its determination by either oxidation or reduction. However in biological systems analysis by oxidation is preferred over reduction because of the presence of dissolved oxygen which can be reduced before NO. The oxygen reduction signal could mask the NO signal. Most studies of NO measurement in biological media are based on the measurement of the oxidation currents of NO. Nitrite, ascorbate, cathecolamines and other species can seriously interfere during the detection, however nitrite is the most problematic of them all.[83] For selectivity of NO, chloropene,[84] Nafion®,[85] cellulose acetate,[86] nitrocellulose and silicone membranes have been used directly on carbon, platinum and gold electrodes.[82] Nafion® offers an

electrostatic barrier against anionic interferents such as nitrite whilst cellulose acetate prevents the effect of protein adsorption.[87]

Studies into the possible interferences from some neurotransmitters have been reported.[88] Fast cyclic voltammetry was used to measure NO and dopamine (DA), simultaneously in rat caudate putamen (CPu) slices. Analysis of the electrochemical signals obtained from the mixture of DA and NO showed that subtraction of either DA or NO component, revealed the contribution of the other component. Hence, the signal was a summation of both DA and NO. Pressure ejection of NO into CPu slices resulted in a dose and site dependent DA release. More DA was released in the dorsolateral than in the dorsomedial CPu. However, pressure ejection of DA did not generate NO. Authors concluded that electrically stimulated DA release was not mediated by a prior release of NO. In this thesis, further investigation into the possibility of the interference of DA and serotonin in NO detections is carried out.

Nitrite is an oxidation product of NO, and it gets oxidized at potentials that are only 60 to 80 mV more positive than NO oxidation.[80,89,90] This presents a problem since the electrode fails to discriminate between the two, i.e. the signals may overlap resulting in broad peaks. Nafion®, Figure 1.8, is a negative polymer which tends to stabilize the formation of the NO^+ ion, hence inhibiting the formation of the nitrite (equation 1.18 and 1.19). In this way nitrite is prevented access to the electrode and other common biological anions are repelled away from the electrode surface. However, coating the electrode with Nafion® causes NO currents to decrease. Therefore, Nafion® film thickness should be optimized in order to achieve the best possible detection limit. In order to test the integrity of the Nafion® film, Malinski *et al.*[89] have measured the current

due to the conversion of nickel(II)porphyrin to nickel(III)porphyrin, Ni^{II}/Ni^{III} after each coating of the electrode with Nafion®. Authors assert that the oxidation of Ni^{II} to Ni^{III} occurs only if a diffusion of the hydroxyl ion (OH^-) into the film is possible. A Nafion® film with sufficient thickness will prevent any anionic species penetration, hence the OH^- ion, resulting in the disappearance of the Ni^{II} / Ni^{III} peak in the voltammogram.

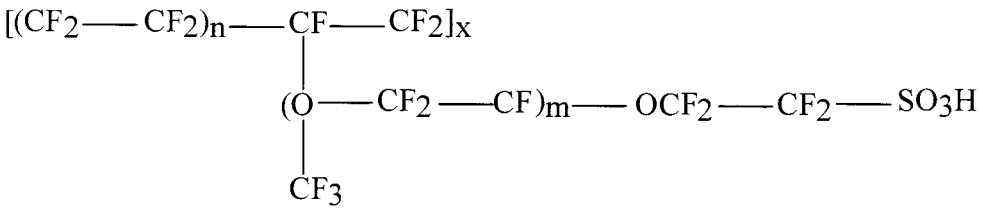

FIGURE 1. 8 Molecular structure of Nafion®

Recently there has been a report of a Nafion®-free bipolymetric sensor for selective and sensitive NO detection.[91] The sensor is a glassy carbon electrode modified by polymerized nickel(II) tetrakis (4-hydroxy-3-methoxyphenyl) porphyrin (NiTHMPP) covered with polymerised eugenol (4-allyl-2-methoxyphenol) abbreviated as PE. The sensor showed sensitivity of up to 85 x 10^{-9} mol dm^{-3} and selectivity against negative species and in addition it was selective against the positively charged species: DA, and epinephrine.

1.5.1 Porphyrin based electrodes.

A variety of materials have been used as catalysts to improve the sensitivity of the microelectrode. Use of thin polymer membranes have been reported.[92,93] However, these

suffered a drawback in application due to the instability of these electrodes to prolonged NO exposure. Metalloporphyrins have been used extensively as catalysts in the detection of NO by electrochemical methods.[80,89,94,95] It has been shown that pyrrole based polymers containing porphyrin complexes are good catalysts for electrocatalytic reduction of NO.[96] In general, porphyrin modified electrodes have given higher sensitivity than unmodified electrodes. However Bedioui and coworkers,[85] have reported that the nickel porphyrin, NiP, immobilized on a gold microdisc or microfiber electrode did not give expected improvements of the detection limit. The lowest [NO] detected was in the region of 10 μm. The implication is that the porphyrin film inhibited NO diffusion. It thus appears that it may be necessary to optimize the immobilization of the porphyrin complex onto the electrode. The porphyrin modified electrodes are stable for the detection of NO. The catalytic activity of several iron porphyrins have been reported.[97,98,99]

During electrocatalysis, there is however a reversible interaction of NO with the porphyrin but the electrode still remains stable.[98] This interaction is characterised by the disappearance of the metal center redox peak, Fe(III)/Fe(II) at –0.3 V, when Fe(III)porphyrin was used as a catalyst, and the appearance of the new NO catalytic peak at –0.6 V.[98] There was a regeneration of the porphyrin metal redox couple in buffer in the absence of NO after the catalytic reaction. Reversibility of the NO-protein complex on the protein modified electrodes was found to be pH dependent.[100]

It has been reported that changing the peripheral ligands on the porphyrin, changes the rate of NO coordination.[101] Stronger electron withdrawing groups on the peripheral positions of the Mn(II)P, resulted in a slow reaction of the MP with NO. This

is to be expected since there is a decrease in the MPc π electron delocalization into the dz^2 metal orbital.

The sensitivity and selectivity of the porphyrinic sensor depends not only on the potential at which NO oxidizes, but also on the catalytic process of NO oxidation. Surface effects, axial ligation to the central metal, gas permeability through sensor layers and fast removal of NO^+ (the oxidation product of NO) by Nafion® are important in promoting fast and selective oxidation of NO.[77] Current density for NO oxidation on the porphyrin sensor depends on the film quality and high quality films will show better detection limits. Most of the molecules which undergo fast random polymerization on the electrode surface such as tetraphenylporphyrins with amino or pyrole substituents on the phenyl ring, will form films with a well developed surface but poor catalytic properties for NO oxidation.[77]

Using a computer controlled micropositioner, the microsensor can be implanted into a single cell or placed on the surface of the cell membrane or at a controlled distance from the cell membrane. Malinski and co-workers[89] have used a porphyrin modified sensor to monitor NO in endothelial cells. Tetrakis(3-methoxy-4-hydroxyphenyl)-nickel(II) porphyrin (NiTMHPP) was electrodeposited on a 0.5 - 0.8 μm carbon fiber followed by a coat of Nafion®. The microsensor was placed on the surface of endothelial cell membrane. After injection of Bradykinin (an NO inducing agent) into the medium near the endothelium cell, release of NO was observed using an amperometric method. A maximum NO concentration of 490 ± 30 nmol dm^{-3} was observed after about 30 sec. This surface concentration is in the same region as that observed on endothelial cell membrane from porcine aorta using a similar microsensor.[80] Using this microsensor, NO

could be detected in amounts of 10^{-20}mol in a cell.[102] Differential pulse voltammetry (DPV) recorded in whole blood samples 20 seconds after the samples were obtained from healthy volunteers, showed a small peak at 0.63 V. This potential is characteristic of NO oxidation on the NiTMHPP microsensor.[80] Thus trace amounts of NO were still present in the blood 20 seconds later. Further measurements of collagen induced NO in washed blood platelets using the NiTMHPP microsensor, indicated that NO is inactivated more rapidly by chemical reactions in the blood than in platelets.

Investigations into the lifetime of NO in human blood components have been reported.[89] NO solution of known concentration was added to the whole blood, blood serum and blood plasma and its decay was monitored with DPV. A decrease of current with time was attributed to two processes: diffusion of NO to the bulk solution and the chemical reaction of NO with blood components. Both processes were slow in blood serum and fast in whole blood. Detection of NO in vascular smooth muscle of normotensive and hypertensive rats using NiTMHPP have been reported.[103]

Rivot *et al.*[104] have reported on the use of a nickel porphyrin microsensor in *in vivo* monitoring of NO within the dorsal horn of the lumbar spinal cord of decerebrated spinal rats. A characteristic NO peak was observed at 0.65 V *vs* Ag|AgCl. The peak remained stable for 3 hours, which indicated that significant amounts of NO are produced continuously. *In vivo* detection of NO release in penile corpora cavernosa in a rat model erection has been reported.[105] The microsensor was made up of a 30 μm (diameter) carbon fiber covered with NiTMHPP, and Nafion®. Following the insertion of the microelectrode in the corpus cavernosum, a small oxidation current signal was detected at

about 0.65 V (*vs* Ag|AgCl). For most studies there is a general consistency in oxidation potential of NO when NiTMHPP modified electrode was used.

Calibration data of the NiP microsensor, for the selective detection of NO by differential normal pulse at 0.75 V (SCE), with a concentration ranging from 1.5 nmol dm^{-3} to 40 μm, has been reported.[106] From the data, it appears that nickel porphyrin coated carbon fibers are suitable for detections in the nanomolar concentration range. A sensitivity value of 40 nmol dm^{-3} has been reported for NO detection with a NiP modified microsensor.[107] However, the catalytic mechanism of these nickel porphyrin film micro electrodes is not fully understood. The manner in which the NiP film electrode interacts with NO is not obvious. Trevin and coworkers,[108] investigated the possibility of NO ligation to the NiP. There were no significant changes on the spectra when NO was added to the nickel porphyrin, whilst changes were observed in the case of iron and manganese porphyrins.[98,101] These results suggest that the role played by the porphyrin may be that of a simple organic layer modifying the electrode surface without any specific chemical interaction with NO.[95]

It has been reported that NiTMHPP at pH 7.4 actually exists as a demetallated H_2TMHPP species.[109] The interaction between NO and the NiTMHPP modified electrode at this pH is thus not related to the well known axial complexation of the central metal cation of the porphyrin complex with small molecules such as NO. Also, the peak currents due to electro-oxidation of NO do not depend on the nature of the film (poly-NiTMHPP or poly-H_2TMHPP). In both cases the currents were the same. It is believed that the Ni(II) plays a role in the electro-oxidation of NiTMHPP in alkaline media. The attachment of NiTMHPP to the electrode surface is connected with the oxidation of OH^-

anions. Electrodeposition of the NiTMHPP complex between 0.0 and +0.7 V (*vs* SCE), where the formation of OH^- radicals does not occur, was not possible.[109] It thus appears that poly-NiTMHPP coated carbon electrodes reported as excellent electrocatalytic mediators for NO detections are in fact sensors with demetallated films. These observations indicate that electro-oxidation of NO can be done using modified electrodes without any metal redox couple in their structure.

1.5.2 Metallophthalocyanine based electrodes.

MPc complexes constitute a class of catalysts with some advantages over metal and metal oxides in terms of cost. In addition, the catalytic processes for MPc complexes as well as those of MP complexes can be described in terms of definite parameters such as chemical structure, chemical and physical properties. Their reactive centers can be identified and consequently can be varied or optimized.[110] The site of oxidation or reduction is an important factor in the electrocatalytic activity of MPc complexes. Redox properties are expected at the central metal in MnPc, FePc and CoPc, whilst ring-based processes occur in ZnPc, NiPc and CuPc.[111] MPc complexes with metal based oxidation process are expected to show better electrocatalytic activity than ring-based MPc complexes. There has been conflicting reports about NiPc, with some authors asserting metal based activity and some, ring-based activity.[111,112]

The catalytic activity of MPc complexes is partly due to their ability to bind ligands axially. The electronic structure of the metal center is related to the redox potential of the MPc and serves to explain the activity of differently metallated MPcs. The catalytic activity is related to the relative energies between the d orbitals of the metal

in the Pc and the analyte.[113] Metals having the d orbitals which are very different in energy from that of the axial ligand (analyte) will show lower activity than those lying at energies similar to the HOMO of the ligand. Consequently, if the electronic levels of a bare electrode i.e. without modification, and those of the analyte are too far apart, electron transfer is difficult. Hence the MPc catalyst acts as a mediator by supplying intermediate electronic levels and increasing the probability of electron transfer.[114] MPc complexes have been used successfully as electrocatalysts for many reactions.[110, 115,116,117,118,119,120,121]

Electrochemical oxidation of mercaptoethanol, cysteine and glutathione using MPc complexes, have been reported.[110] Zagal and coworkers have reported on the catalytic electro-oxidation of hydrazine on Fe, Co, Cu and Ni phthalocyanines.[122] Their findings indicate that the catalytic activity is in the order, FePc>CoPc >CuPc~NiPc. This trend is similar to that observed for catalytic reduction of oxygen.[110] It is not suprizing that Fe and Co give better catalytic activity than Cu and Ni, since the redox processes of the latter involve the ring instead of the metal. Reduction of nitrite and nitrate using MPc modified glassy carbon electrodes, GCE has been reported.[123] The reduction potentials of nitrite and/or nitrate, on MPc-GCE shifted to positive potentials depending on the MPc complex in the order: CuPc>FePc>NiPc>CoPc>MnPc>ZnPc>GCE. CuPc does not show metal based redox activity in solution, hence the mechanism for the reduction of NO_2^- and NO_3^- on MPc modified electrodes must be different from that of oxygen reduction and hydrazine oxidation. It has been reported that MPc complexes that can bind both the reactant and the product reversibly are expected to show high catalytic activity for the formation of the relevant products.[124] Hence, the strong catalytic activity of CuPc in this

case was attributed to the possibility of strong binding of the reduction products, ammonia, and reactants to CuPc.

Cobalt phthalocyanines have been used as catalysts in a number of reactions. Baldwin *et al.*[125] has reported on the use of CoPc-containing carbon paste electrode in the determination of glutathione and cysteine in blood plasma. There was a significant lowering of the oxidation potential and the electrode was sufficiently stable and reproducible. The ease and reproducibility with which fresh carbon paste chemically modified surfaces can be generated make the approach attractive with blood and plasma matrices, which are prone to fouling and deactivating the electrode. The electrode exhibited high sensitivity, (see Table 1.3) and selectivity compared to conventional carbon electrodes.

Table1. 3 Catalytic activity of CoPc modified electrodes.

MPc - catalyst	modification mode	analyte	detection limit (mol dm^{-3})	reference
CoPc	carbon paste	cycsteine	2.7×10^{-12}	125
CoPc	carbon paste	thiopurines	8×10^{-12}	128
CoPc	carbon paste	hydrazine	10^{-8}	126
CoPc	carbon paste	sulfhydryl	2.7×10^{-12}	127
CoTAPc	electrodeposition	NO	1.2×10^{-7}	130
CoTAPc	electrodeposition	NO	1.0×10^{-8}	131

A CoPc carbon paste electrode was used to detect thiopurines in blood plasma.[128] The CoPc carbon paste electrode showed higher catalytic activity and stability compared to a carbon and an unmodified carbon paste electrodes.

Electroreduction of NO using a CoPc-GCE has been reported.[129] Selective conversion of NO to ammonia was obtained with a maximum efficiency of 92.3% on a CoPc-GCE. Similar results were obtained with a H_2Pc coated electrode, but the yield of ammonia was not as high. The coordination of Co atom to the phthalocyanine ring promotes a partial electron transfer from the metal d_z^2 orbital to NO, hence, the production of ammonia. In acidic media, pH 2, the CoPc modified electrode gave the best separation of the waves due to NO reduction and hydrogen evolution, respectively. It was further observed that the catalytic activity of CoPc was directly proportional to the thickness of the film on the electrode. In contrast, catalytic currents decreased with an increase in the Pc layer when H_2Pc was used. Simultaneous detection of NO and NO_2^- on a ring disc electrode modified with electropolymerized film of cobalt(II) tetraaminophthalocyanine (polyCoTAPc) has been reported.[130] A detection limit of 1.2 x 10^{-7} mol dm^{-3} was obtained for NO. Jin *et al.*[131] reported on the determination of NO using electropolymerised films of CoTAPc, CuTAPc and NiTAPc. The detection limits (Table 1.3) of the three MPc complexes, were in the order: CuTAPc>CoTAPc =NiTAPc.

Coordination of NO to MPc complexes of Fe, Co an Mn is accompanied by chemical shifts of electron binding energies of the central metal atoms, which indicates appreciable electron transfer between the central metal and NO.[110] The reported studies on the catalytic reduction and oxidation of NO using CoPc as a catalyst do not give a

mechanism for catalysis. In this work the mechanisms of electrocatalysis of NO using a CoPc, $[CoTSPc]^{4-}$ and $VitB_{12}$ are studied.

1.6 Electrochemical techniques.

In voltammetric techniques, information about the analyte is obtained from monitoring current as a function of applied potential. For purposes of this thesis, voltammetric techniques *viz.*. cyclic, differential pulse and square wave voltammetric techniques are discussed. Bulk electrolysis will also be discussed.

1.6.1 Cyclic voltammetry.

Cyclic voltammetry (CV), is the most effective analytical technique available for the study of redox systems. In CV the potential is scanned linearly from the initial value E_i to a second value E_f, irrespective of the direction , and then back to the starting potential E_i, hence the term cyclic. CV allows the electrode potential to be scanned rapidly in search of redox couples. Once the couple is located, it is characterized from peak potentials on the voltammogram, Figure 1.9.

From Figure 1.9, it is apparent that CV is capable of rapidly generating a new species during the forward scan and monitors its fate on the reverse scan. To obtain a cyclic voltammogram, the current at the working electrode, in an unstirred solution is measured during the potential scan. The important parameters of a CV are the magnitudes of the anodic (i_{pa}) and cathodic (i_{pc}) peak currents, the anodic (E_{pa}) and cathodic (E_{pc}) peak potentials. Cyclic voltammetric processes are either reversible, quasi-reversible or irreversible depending on the nature of the reaction.

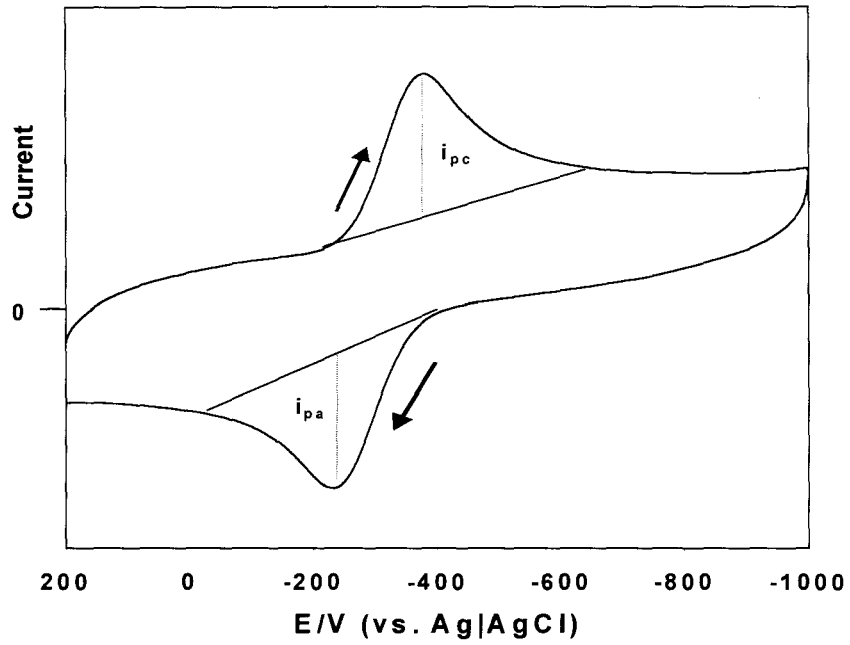

FIGURE 1. 9 Diagram showing a typical cyclic voltammogram of a quasi-reversible reaction.

Reversible process

The system is said to be reversible when the species oxidized or reduced during the forward scan are reduced or oxidized respectively during the reverse scan. At 25^0C the peak current, i_p, for a reversible couple is given by the Randles-Sevcik equation, see equation 1. 20.[132]

$$i_p = (2.69 \text{ X } 10^5)n^{3/2}ACD^{1/2}v^{1/2} \quad \text{.....1.20}$$

Where i_p is the peak current,

n - number of moles of electrons transferred,

A - the electrode area in cm^2,

C- the concentration of the species to be oxidized or reduced in the bulk solution (mol cm^{-2})

D- the diffusion coefficient (cm^2 s^{-1})

v - the scan rate. (V s^{-1})

From equation 1.20, the peak current is directly proportional to concentration C, and it increases with an increase in the square root of the scan rate $v^{1/2}$. For reversible systems, the magnitude of i_{pa} is equal to that of i_{pc}, i.e. i_{pa}/i_{pc} is unity. The potential difference ΔE between the two peak potentials, E_{pa} and E_{pc}, is constant irrespective of the scan rate, for reversible systems, equation 1. 21.

$$\Delta \mathbf{E} = \frac{\mathbf{RT}}{\mathbf{nF}} = \mathbf{E}_{p_a} - \mathbf{E}_{p_c} \qquad \text{.....1.21}$$

At 25° C, equation 1. 22

$$\Delta \mathbf{E}_p = \mathbf{E}_{pa} - \mathbf{E}_{pc} = \mathbf{0.059}/n \qquad \text{.....1.22}$$

The potential midway between the two peak potentials, $E^{1/2}$, is the formal reduction potential (corrected to the reference electrode used) of the couple, equation 1. 23.

$$\mathbf{E}^0 = \mathbf{E}^{1/2} = \frac{(\mathbf{E}_{pa} + \mathbf{E}_{pc})}{\mathbf{2}} \qquad \text{.....1.23}$$

Irreversible process.

Electrochemical irreversibility is caused by a slow electron exchange of the redox species with the working electrode. Individual peaks are reduced in size and widely separated. Often there is a single oxidation or reduction peak and no reverse wave. Totally irreversible systems are characterized by a shift of the peak potential, E_p with the scan rate. Irreversible systems are described by equation 1. 24.[132]

$$\mathbf{E_p = E^0 - (RT/\alpha nF)\,[0.78 - \ln (k^0 / D^{1/2}) + \ln (\alpha nFv/RT)^{1/2}]} \quad \text{.....1.24}$$

α is the transfer coefficient

F is the Faraday constant

R is the gas constant

T is temperature in kelvin

k° is standard rate constant.

All other symbols are as described under equation 1.20.

Thus from equation 1.24, it is apparent that E_p occurs at potentials higher than E^0 with the overpotential related to the standard rate constant, k^0, and the transfer coefficient, α. Independent of the value of k^0, such peak displacement can be compensated by an appropriate change in scan rate. The peak potential and the half peak potential at 25 ^{0}C will differ by $48/\alpha n$ mV. Hence the voltammogram becomes more drawn out as αn decreases.

The peak current for irreversible systems is given by equation 1. 25.

$$\mathbf{i_p = (2.99 \times 10^5) n(\alpha n)^{1/2} A C D^{1/2} v^{1/2}} \quad \text{.....1.25}$$

i_p is proportional to the bulk concentration but will be lower in height.

For an irreversible and diffusion controlled process, the slope of the plot of i_p versus $v^{1/2}$ is related to the moles of electrons transferred by equation 1. 26. [132]

$$\mathbf{Slope/Q = nF/4RT} \quad \text{.....1.26}$$

Where Q, the charge under the peak, is given by equation 1. 27.[133]

$$\mathbf{Q = nFA\Gamma} \quad \text{.....1.27}$$

Where Γ is the surface coverage and all other symbols are as described above.

Quasi – reversible process

Quasi – reversible systems with k^0 in the $10^{-1} > k^0 > 10^{-5}$ cm s^{-1} the current is controlled by both the charge transfer and mass transport. Quasi – reversible voltammograms are more drawn out and exhibit a larger separation in peak potentials compared to a reversible system. For quasi reversible systems the peak current is not proportional to the square root of the scan rate.

1.6.2 Differential Pulse Voltammetry.

Pulse voltammetric techniques are aimed at increasing the sensitivity by lowering the detection limits of voltammetric measurements. This is achieved by substantially increasing the ratio between the faradaic and the non faradaic currents . Detection limits can be lowered down to 10^{-8} concentration levels. Pulse techniques are all based on a sampled current as the potential steps. A sequence of such potential steps, each with duration of about 50 ms, is applied on a working electrode. After the potential is stepped, the charging current decays exponentially to a negligible value, while the faradaic current decays more slowly. Consequently, sampling the current late in the pulse life allows for discrimination against the charging current.

Differential – pulse voltammetry (DPV), is an extremely useful technique in analyzing trace amounts of organic and inorganic species. In DPV potential is increased in small increments and potential pulses of fixed magnitude are superimposed on a linear potential ramp. The current is sampled twice, i.e. just before the application of the pulse (i_1) and again late in the pulse life (i_2), when the charging current has decayed. Instrumentally, the first current is subtracted from the second and the current difference is plotted against the applied potential. The resulting voltammogram consist of current / potential peak, the height of which is directly proportional to the concentration of the analyte.

The differential pulse operation is very effective in correcting for the background current. The charging current contribution to the differential current is negligible.[132] The peak shaped response of DPV measurements improves resolution between species with similar redox potentials. In some cases DPV is able to discriminate between peaks that

are about 50 mV apart. The peak at half height, $W_{1/2}$, is related to the electron stoichiometry by the equation 1. 28.[132]

$$W_{1/2} = \frac{3.52RT}{nF} \quad \text{.....1.28}$$

Thus for n = 1 $W_{1/2}$ is 90.4 mV and for n=2 $W_{1/2}$ is 45.2 mV at 25^0C.

The selection of the pulse amplitude and scan rate requires a trade off among sensitivity, resolution and speed. Larger pulse amplitudes result in larger and broader peaks. Irreversible systems result in lower and broader peaks, i.e. sensitivity and resolution is compromised. DPV is however much slower than CV and is not appropriate for species that are not highly stable.

1.6.3 Osteryoung quare – Wave Voltammetry.

Osteryoung square wave voltammetry (OSWV), is a large amplitude differential technique. In OSWV a wave form made up of a symmetrical square wave is superimposed on a base staircase potential.[134] Current is sampled twice during each square wave cycle, at the end of the forward pulse and at the end of the reverse pulse. The difference between the two measurements is plotted against the staircase potential. The resulting peak-shaped voltammogram is symmetrical about the half-wave potential and the peak current is proportional to the concentration. Like the DPV, OSWV discriminates well against the charging background current and it is able to perform detections up to 10^{-8} mol dm^{-3}. The major advantage of OSWV when compared to DPV is its speed hence, the analysis time is drastically reduced.

1.6.4 Controlled potential electrolysis / Bulk electrolysis.

In controlled potential electrolysis, the potential of the working electrode is held at a fixed potential that is slightly higher than the peak potential of the voltammogram, and the electroactive species is oxidized or reduced completely. Both the working and the auxiliary electrodes have to be of a large surface area and the solution must be stirred well. It is important to work in a three electrode cell since the currents passing through the solution can be quite large. With aqueous reactions, a platinum plate is convenient as an auxiliary electrode. Controlled potential electrolysis is used to generate products (oxidation or reduction) for further analysis using spectral and other techniques. When electrolysis is complete the total charge, Q, passed during the electrolysis is obtained by integrating the current as a function of time, equation 1. 29.

$$\mathbf{Q = it} \quad \text{.....1.29}$$

Q – charge in coulombs

i – current in amps

t – time in seconds

According to Faraday's law the amount of charge passed during electrolysis, is as shown by equation 1. 30.

$$\mathbf{Q = nFvC} \quad \text{.....1.30}$$

Where **n** - is number of electrons,

F - faraday constant ($C\ mol^{-1}$)

v- volume of material electrolysed in the cell (ml)

C - concentration of material electrolysed (mol dm^{-3})

1.7 Microelectrodes.

Microelectrodes offer analytical advantages including detections in microflow systems and analysis of very small (microlitre) samples. Because of very small total currents at microelectrodes, it is possible to work at highly resistive solutions that would develop large ohmic (iR) drops with conventional electrodes. The total diffusion controlled current is composed of the planar flux and the radial flux diffusion components, equation 1.31.[132]

$$i_{total} = i_{planar} + i_{radial} \quad \text{.....1.31}$$

For disk, spherical and hemispherical geometries of the microelectrode, the general expression for the radial component in equation 1.31 above is given by equation 1.32.[132]

$$i_{radial} = \mathbf{arnFDC} \quad \text{.....1.32}$$

where **r** is the electrode radius

a is a function of the electrode geometry

n is the number of electrons transferred

F is the Faraday constant

D is the diffusion coefficient

C is the concentration

The extent by which the planar or radial component dominates depends on the relative dimensions of the electrode and the diffusion layer. This is expressed by the dimensionless parameter, Dt/r_0^2, where t is the electrolysis time and r_0 is the smallest

dimension of the electrode.[132] For large values (>1) of Dt/r_0^2 , the current approaches steady state and sigmoidal voltammograms are observed. For small Dt/r_0^2 values, peak shaped voltammograms are observed and planar diffusion dominates in this case. The shape of the voltammogram thus depends on the scan rate of the experiment.

1.8 Electrocatalysis.

Redox reactions of some electroactive species depend on the nature of the medium. For example, reduction of nitrites and nitrates occur easily in acid media i.e. at more positive potentials than in basic media.[123] To achieve reduction in a basic media at reasonably low potentials, catalysts are employed. The role of a catalyst is to provide an alternative reaction route which avoids the slow step and allows the reaction to occur at an increased current density close to the reversible potential. A catalyst does not take part in a reaction, it may undergo transformation during the reaction but it is regenerated at the end of the reaction.

For homogeneous catalysis, the catalyst and the substrate are in a single phase, in solution. The catalyst and the substrate interact forming an adduct which is transported to the electrode by diffusion, where electron transfer occurs. The catalyst is then regenerated as the adduct is spontaneously broken up. For heterogeneous catalysis, the catalyst is immobilized on to the electrode and acts as a mediator through which charge transfer occurs. Such an electrode would be referred to as a modified electrode. The electrocatalyst stimulates the charge transfer between the electrode and the substrate in solution.[129] In this way an electrocatalyst is not only capable of lowering redox potential but improves sensitivity an selectivity. In CV, electrocatalysis is observed by either the absence of the reverse peak, or the enhancement in current of the forward peak, or both of them, Figure 1.10. Electrocatalysis is also characterized by a shift in potential to more favourable (lower) values.

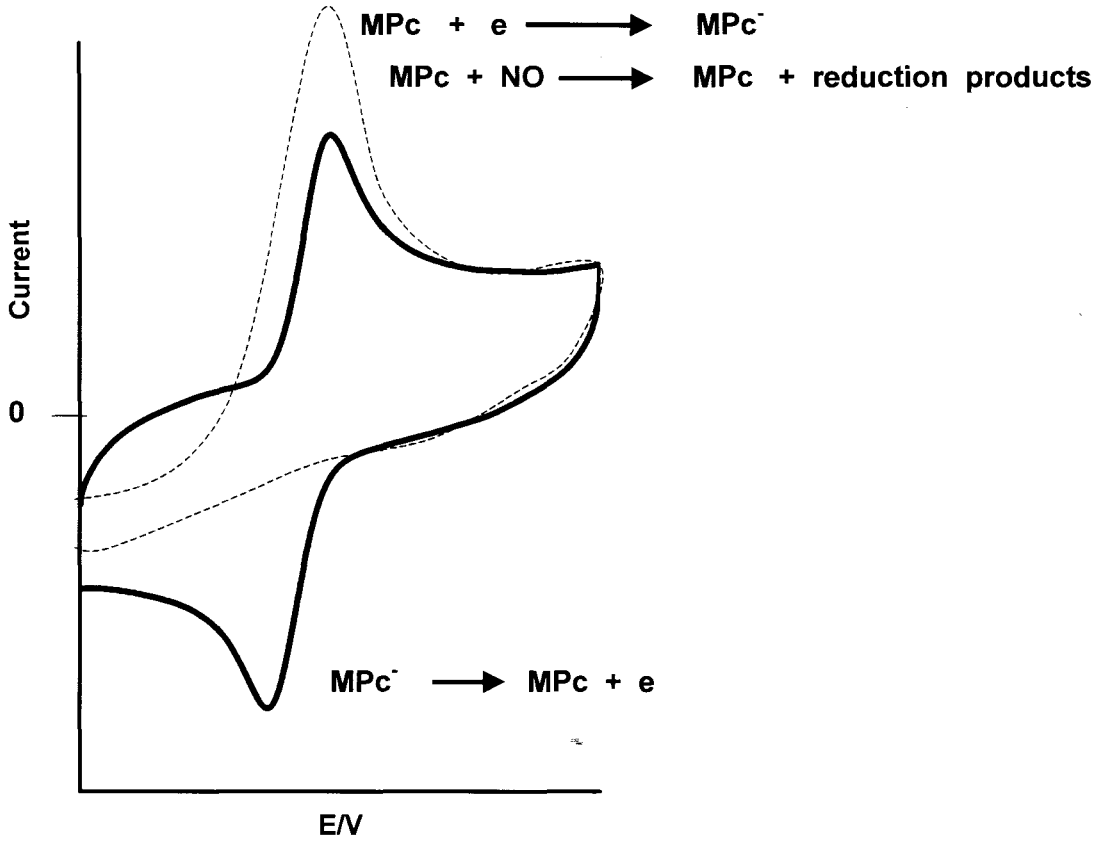

FIGURE 1.10 Diagram showing typical electrocatalytic behaviour.

1.8.1 Methods of modifying electrodes for heterogeneous catalysis.

The well known methods of modifying electrodes are; (i) the drop dry method or dip dry (ii) electrochemical deposition (iii) vacuum deposition and (iv) carbon paste electrode. For the purpose of this thesis only the first two methods are discussed.

Drop dry or dip dry method.

A concentrated solution of the catalyst is prepared by dissolving the catalyst in a solvent where maximum solubility can be achieved. In the dip dry method, an electrode

that had been thoroughly cleaned is dipped into the solution and is immediately removed and allowed to dry. The solvent evaporates leaving a thin uniform layer on the electrode surface. The problem with this method is that reproducibility is difficult since the amount of the material immobilized on the electrode is not controlled. Alternatively, a known volume of the catalyst is transferred onto the electrode using a pipette, in the drop dry method. The method is easy and varying the number of depositions can vary the thickness of the catalyst layer. However, the layer formed may crack and some of the catalyst may fall off the electrode, especially if the layer is too thick.

Electrochemical deposition.

Electrodeposition is achieved by repetitive voltammetric scanning of the catalyst in solution within a chosen potential range. This procedure relies on the variation of the catalyst solubility with the oxidation state, such that film formation will occur irreversibly when the catalyst is oxidized or reduced to its less soluble state. Varying the number of scans within the chosen potential range can vary the thickness of the film. Polymer films that have been deposited this way have been found to be completely insoluble in the analyte solution irrespective of the solvents used.

CHAPTER TWO: EXPERIMENTAL

2.1 Reagents

2.2 Synthesis

2.3 Methods

2.4 Instrumentation

2. EXPERIMENTAL

2.1 Reagents.

Sodium nitrite was purchased from BDH. Cobalt(II) sulfate, cobalt acetate, ammonium molybdate, monosodium salt of 4- sulfophthalic acid, ammonium chloride, aluminium chloride, urea, nitrobenzene, sodium chloride, sodium hydroxide, 2,3-pyridine dicarboxylic acid and silver nitrate were all purchased from SAARCHEM. Nafion® (5% aqueous solution) was purchased from Aldrich.

All purchased reagents and catalysts were either of reagent or analytical grade, and were used without further purification. Pyridine, dimethylsulfoxide (DMSO) and dimethylformamide (DMF) were freshly distilled. Tetraethylammonium perchlorate, (TEAP) and sodium sulfate were recrystallized from ethanol before use as electrolytes. TEAP was synthesized as described below.

Preparation of tetraethylammonium perchlorate (TEAP).

TEAP was prepared by mixing equal volumes of hot solutions of 1.0 mol dm^{-3} sodium perchlorate and 1.0 mol dm^{-3} tetraethylammonium chloride. The mixture was cooled in ice cold water. The precipitate formed was then filtered and washed with ice cold ethanol and later recrystallised from hot absolute ethanol, giving white crystals.

2.2.1 Synthesis of phthalocyanine complexes.

Phthalocyanine complexes of iron (FePc), copper (CuPc), nickel (NiPc), manganese (MnPc), zinc (ZnPc) and cobalt (CoPc) were purchased from Aldrich. Cyanocobalamin ($VitB_{12}$) was purchased from Sigma. Cobalt(II) tetrasulfophthalocyanine, $Na_4[Co^{II}TSPc].2H_2O$, chloro Al(III) tetrasulfophthalocyanine, $Na_4[ClAl(III)TSPc].2H_2O$ were synthesized and purified as reported by Weber (see Section 2.2.1 and 2.2.2).[135] Tetrakis (1-methyl-4-pyridyl) porphine was purchased from Aldrich and was metallated with cobalt, as described in Section 2.2.3. Cobalt(II)-2,9,16,23-tetranitrophthalocyanine (CoTNPc), cobalt(II)-2,9,16,23-tetraaminophthalocyanine-2-hydrate (CoTAPc), cobalt(II)-2,9,16,23-tetracarboxyphthalocyanine (CoTCPc) were synthesized as described in Sections 2.2.4 to 2.2.6.

2.2.2 Synthesis of tetrasodium salt of cobalt(II) 4,4',4'',4'''-tetrasulfophthalocyanine (2) Na_4[CoTSPc], Scheme 2.1.

The sodium salt of cobalt(II) tetrasulfonated phthalocyanine was prepared according to the procedure adapted from that reported by Weber and Busch.[135] Monosodium salt of 4-sulfophthalic acid **(1)** (6.48 g, 0.0243 mole), ammonium chloride (0.71 g, 0.0136 mole), urea (8.71 g, 0.146 mole), ammonium molybdate (0.11 g, 0.0001 mole) and cobalt(II) sulphate-7-hydrate, (2.04 g, 0.0072 mole) were grounded together until a homogeneous mixture was obtained. Nitrobenzene (40 ml) was added to a 250 ml round bottom flask fitted with a thermometer, a condenser and a stopper and was heated to 180 °C. The grounded solid reagents were slowly added to nitrobenzene with stirring. The temperature was maintained between 160 °C and 190 °C. The heterogeneous

mixture was heated for 6 hrs keeping the temperature at 190 °C. The crude product was crushed and washed with methanol until the smell of nitrobenzene could no longer be detected. The remaining solid was washed with 1000 ml of a 1.0 mol dm^{-3} hydrochloric acid saturated with sodium chloride. The solution was briefly heated to boiling, allowed to cool down to room temperature and then filtered. The resulting solid was dissolved in 300 ml of 0.1 mol dm^{-3} sodium hydroxide. The solution was then heated to 80 °C and filtered while still hot, NaCl (40.5 g) was then added to the filtrate. The slurry was stirred and heated to 80 °C until ammonia evolution stopped. The product was washed with 80% aqueous ethanol until the filtrate was chloride free (tested with 1 mol dm^{-3} silver nitrate). The product was refluxed for 4 hrs in 100 ml absolute ethanol, allowed to cool down to room temperature. A blue product, Na_4[CoTSPc] **(2)** was obtained after filtration and was dried in *vacuo* over silica gel. Yield = 80%. Elemental analysis: Calculated for $Na_4CoS_4C_{32}O_{12}H_{12}N_8 .2H_2O$; C, 37.84%; H, 1.6%; N, 11.0% . Found C, 38.0%; H, 1.6%; N, 11.0%. IR spectra (KBr discs, cm^{-1}) 2370w, 1622m, 1379m,1256s, 1098m, 1029vs, 805s, 697s, 632w, 381m.

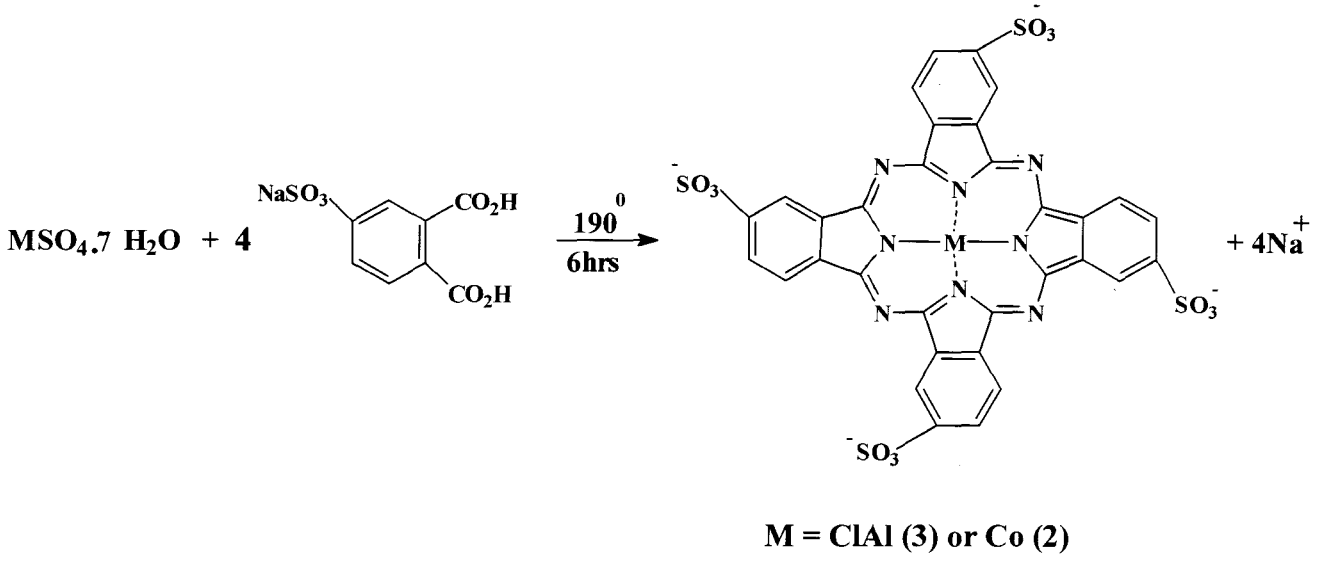

Scheme 2. 1 Simplified synthetic route of $[CoTSPc]^{4-}$ and $[ClAlTSPc]^{4-}$

2.2.3 *Preparation of tetrasodium salt of aluminium(III) 4,4',4'',4'''-tetrasulfophthalocyanine (3), Na_4[ClAl(III)TSPc], Scheme 2.1.*

Chloro aluminium tetrasalfophthalocyanine complex, $[ClAlTSPc]^{4-}$, was prepared using the procedure adapted from that of Weber and Busch.[135] Synthetic route for $[ClAlTSPc]^{4-}$ is the same as that of $[CoTSPc]^{4-}$, Scheme 2.1 except that $AlCl_3$ was used instead of cobalt sulfate. Yield = 45%. IR spectra (KBr discs, cm^{-1}) 1626w, 1398w, 1340m, 1192s, 1143m, 1105m, 1028vs, 918m, 834m, 754m, 697m, 640m, 598m.

2.2.4 *Preparation of tetrakis(I-methyl-4pyridyl) Co(II) porphyrin (5), CoTMP[136], Scheme 2.2.*

Following literature methods for metallation of porphyne,[136] a solution of tetrakis(1-methyl-4-pyridyl)porphyne **(4)** (0.005g, 3.67 $x10^{-6}$ mole) and cobalt acetate (0.000914g, 3.67 x 10^{-6} mole) in DMF was refluxed for 1 hr. The reaction was monitored

with UV/Visible spectroscopy. The resulting solution was allowed to cool and the solvent was evaporated to dryness. Yield = 60%. IR spectra (KBr discs, cm^{-1}) 1634vs, 1455m, 1188m, 998m, 796s.

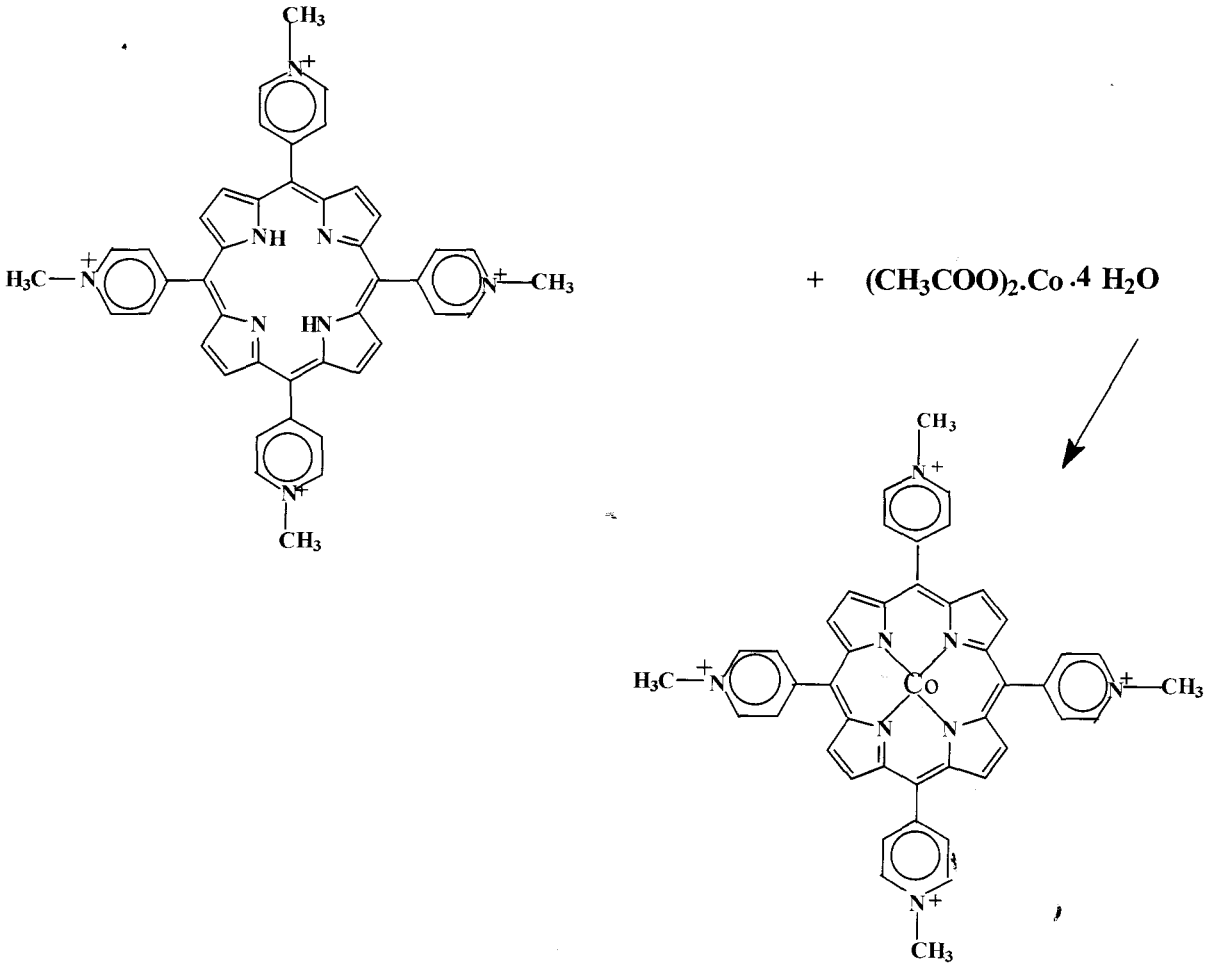

Scheme 2. 2 Simplified synthetic route for tetrakis (1-methyl-4pyridyl)Co(II)porphyrin.

2.2.4 Preparation of cobalt(II)-2,9,16,23-tetranitrophthalocyanine 2-hydrate (7), CoTNPc,[137] Scheme 2.3.

This complex was synthesized according to literature methods.[137] 4-Nitrophthalimide **(6)** (1.921 g, 0.01mol), cobalt chloride (0.594 g, 0.0025 mol), ammonium chloride (0.267 g, 0.0049 mol), ammonium molybdate (0.04 g, 0.00004 mol)

and excess of urea, (3 g, 0.05 mol) were grounded together and added to nitrobenzene (10 ml) and refluxed for 5 hrs at 185 °C. The solid product was filtered and Soxhlet extracted overnight with methanol to remove remaining nitrobenzene. The deep green solid was added to 1mol dm^{-3} hydrochloric acid (30 ml) saturated with sodium chloride. The suspension was boiled for 5minutes and filtered after cooling. After adding the solid to 1 mol dm^{-3} sodium hydroxide (30 ml) containing sodium chloride (11 g) the solution was heated at 90 °C for 30 minutes. The solid was separated by centrifuge and treatment with 1 mol dm^{-3} HCl and 1 mol dm^{-3} NaOH was repeated twice. The green compound **(7),** was washed with water (100 ml) and dried overnight at 100 °C. Yield = 75%. IR (KBr discs, cm^{-1}) 1538s, 1350s. UV/Visible (λmax, nm (logε)) 724 (3.93), 651 (3.55), 366 (3.70)

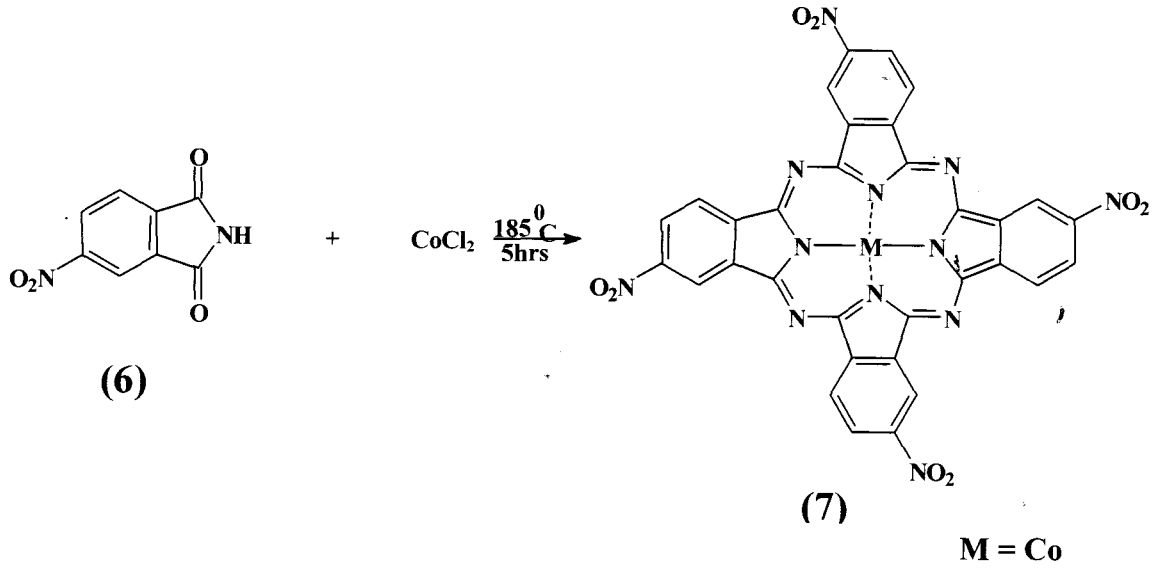

Scheme 2. 3 Simplified synthetic route of CoTNPc

2.2.5 *Preparation of cobalt(II)-2,9,16,23-tetraaminophthalocyanine (8) CoTAPc,[137] Scheme 2.4.*

Following literature methods,[137] finely grounded cobalt(II)-2,9,16,23-tetranitro-phthalocyanine **(7),** (1.4 g, 0.00186 mol) was suspended in water (60 ml) and sodium sulfide nonahydrate (11.1 g, 0.045 mol) was added, the mixture was then stirred at 50 °C for 5 hrs. The green product was separated by centrifuge and treated with 1 mol dm^{-3} HCl, (180 ml). The solid was then stirred in 1 mol dm^{-3} NaOH (120 ml) for 1 hr and was centrifuged again. The product **(8)**, was washed with water and dried overnight at 100 °C. Yield = 90%. IR (KBr discs, cm^{-1}): 3330s, 1610s. UV/Visible (λmax, nm (logε)) 714 (4.44), 367 (4.35), 292 (4.44).

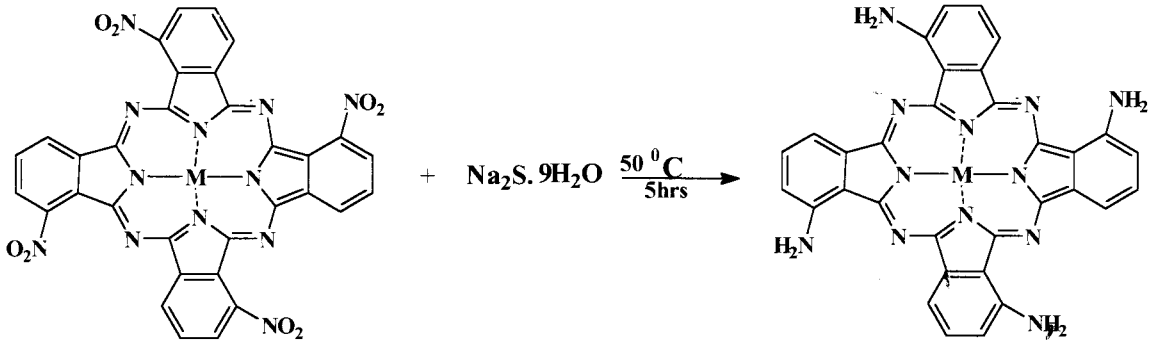

(7) **(8)**

Scheme 2. 4 Simplified synthetic route of CoTAPc. **M = Co**

2.2.6 *Preparation of cobalt(II)-2,9,16,23-tetracarboxyphthalocyanine (10), CoTCPc,[138] Scheme 2.5.*

Following literature methods,[138] a finely grounded mixture of trimeliticanhydride **(9)**, (5 g, 0.025 mol), urea (15 g, 0.025 mol), cobalt chloride (3.57 g, 0.015 mol) and ammonium molybdate (0.5 g, 0.0005 mol) was added to nitrobenzene (75 ml) and refluxed at 165 °C for 3 hrs. The dark blue-green solid was filtered off and Soxhlet extracted overnight with methanol to remove any nitrobenzene left. The solid **(10)**, was dried overnight at 100 °C. Yield = 30%. IR (KBr discs, cm^{-1}): 3350s, 1700m. UV/Visible (λmax, nm (logε)): 678 (3.94), 611 (3.31), 339 (3.45).

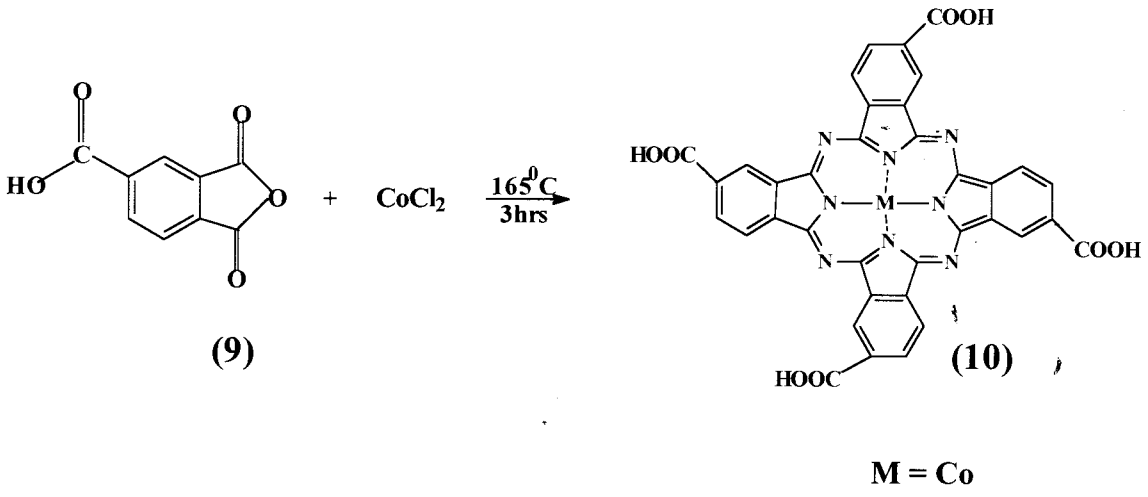

Scheme 2. 5 Simplified synthetic route of $[CoTCPc]^{4-}$

2.3 Preparation of nitric oxide solutions.

NO was prepared by adding saturated sodium nitrite to a 0.2 mol dm^{-3} solution of sulfuric acid under nitrogen atmosphere. The NO produced was passed through a column containing solid potassium hydroxide to remove higher oxides of NO. It was then bubbled into nitrogen saturated deionized water or DMSO. For the preparation of DMSO solutions, in addition to KOH in the column, a drying agent was added. NO solutions in either water or DMSO were freshly prepared before use and kept in glass flasks fitted with a rubber septum. The concentration of NO was determined by the method proposed by Ascenzi *et al.*[5] The method is based on the reversible reaction, equation 2.1.

$$\mathbf{NO + FePc(DMSO)_2 \leftrightarrow FePc(NO)(DMSO) + DMSO} \quad \text{.....2.1}$$

A small amount of FePc was dissolved in DMSO under nitrogen and the solution was filtered anaerobically. The concentration of this solution was accurately determined by measuring its extinction coefficient at 651 nm (ε_{651}= 7.49 x 10^4 dm^3 $cm^{-1}mol^{-1}$). The solution was diluted under nitrogen to obtain an iron phthalocyanine complex concentration that is one hundred-fold lower than that of the nitric oxide solution, so as to keep the added volumes of NO negligible with respect to the starting volume. A spectrophotometric cell with a stopper was filled with a known volume of FePc / DMSO solution. After each addition of NO solution in either water or DMSO to the FePc / DMSO solution, the difference spectrum of FePc with respect to the NO free solution was recorded between 620 and 700 nm. The differences in molar absorbance at 651 and 669 nm (absorbance maxima of FePc(DMSO)(NO) species) were used to calculate the fraction of the reaction Y defined as, equation 2.2.[5]

$$Y = \frac{[FePc(NO)(DMSO)]}{[FePc(DMSO)_2] + [FePc(NO)(DMSO)]} = \frac{\Delta\varepsilon}{\Delta\varepsilon_\tau} \quad \text{.....2.2}$$

Where $\Delta\varepsilon$ is the absorptivity change measured at a given concentration of added NO. $\Delta\varepsilon_t$ is the value for saturation (-1.58×10^4 and 2.05×10^4 dm^3 mol^{-1} cm^{-1} at 651 and 669 nm, respectively). For a 1:1 reaction (equation 2.1), with Y defined as in equation 2.2 above, equation 2.3 holds:

$$\frac{[NO]_\tau}{[FePc]_\tau} = Y + \frac{1}{K.[FePc]_\tau}.\left(\frac{Y}{1-Y}\right) \quad \text{.....2.3}$$

Molar concentrations are the total NO and FePc amounts present and K is the equilibrium constant for equation 2.1. If C_{NO} is the NO concentration of the solution and V_{NO} is the added volume, and if the total volume is considered constant then, equation 2.4 holds.

$$[NO]_\tau / [FePc]_\tau = (C_{NO} / [FePc]_\tau)(V_{NO} / V_\tau) \quad \text{.....2.4}$$

Substituting equation 2.4 into equation 2.3 gives,

$$\frac{C_{NO}.V_{NO}}{[FePc]_\tau.V_\tau} = Y + \frac{1}{K[FePc]_\tau}\left(\frac{Y}{1-Y}\right) \quad \text{.....2.5}$$

When the right hand member of equation 2.5 is plotted against V_{NO} a straight line is obtained, the slope of which is C_{NO} / $[FePc]_t$ (V_t) from which C_{NO} was calculated. NO concentration in water was also calculated using the reported solubility[5] of 2.2×10^{-3} mol dm^{-3}. NO could also be obtained by using NO_2^-. It has been reported that at low pH, nitrite disproportionates significantly to nitric oxide, as shown by equation 2. 5.[101]

$$2NO_{(aq)} + NO_3^- + 2OH^- \leftrightarrow 3NO_2^- + H_2O \quad \text{.....2.6}$$

The equilibrium constant for the above reaction , K = 1.1 x 10^{20} M^{-2}.

At pH 4, 43% of the nitrite disproportionates to NO. In some of the studies NO has been generated from nitrite in pH 4 buffer.

2.4 Methods

2.4.1 Kinetics and equilibria.

Kinetics and equilibria studies were monitored at constant temperature with a Cary IE UV-Visible spectrophotometer. A known volume of MPc solution was added to a spectrophotometric cell of 1 cm path length and the absorption spectrum of the solution was recorded. A known volume of a deaerated solution of NO was then added to the cell and the spectra was monitored with time. Bubbling of nitrogen was continued while NO was being added to the cell. The cell was fitted with a stopper to avoid oxygen affecting the reaction. Concentrations of the MPc were kept constant (10^{-5} to 10^{-6} mol dm^{-3}) whereas NO concentrations were varied. NO concentrations were kept larger by at least a factor of 10, thereby maintaining pseudo-first order conditions.

2.4.2 Electrochemical methods.

2.4.2.1 Voltammetry.

Voltammetric measurements were done in a conventional three electrode system, Figure 2.1. Data was collected with the Bio-Analytical system (BAS) model CV-50W or CV-100W, voltammetric analyzer. For cyclic voltammetry of NO in solution or for characterisation of MPc complexes, a glassy carbon electrode (GCE; 3.0 mm diameter) was used as a working electrode and a platinum wire as an auxiliary electrode. The reference electrode was the Ag|AgCl (3 mol dm^{-3} KCl) for aqueous solutions. For non-aqueous solutions, either a silver wire pseudo reference or a BAS non-aqueous reference electrode were employed. The non-aqueous reference electrode was a silver wire/silver ion electrode [($Ag|Ag^{+}$ (0.1 mol dm^{-3})], containing a silver wire immersed in 0.1 mol dm^{-3}

^{3} $AgNO_3$ and 0.1 mol dm^{-3} TEAP/DMSO. For aqueous solutions sodium sulfate was used as an electrolyte whilst for non-aqueous solutions TEAP was used. For electrochemical characterisation of the MPc or MP, and for their electrodeposition and drop dry preparation, the concentrations were in the range 10^{-4} to 10^{-3} mol dm^{-3}. For detections in biological systems, differential pulse, square wave or cyclic voltammetry, were recorded using a BAS carbon fiber microelectrode (11 μm diameter) as a working electrode and a platinum wire as an auxiliary electrode. The reference electrode was the Ag | AgCl (3 mol dm^{-3} KCl). The DPV settings were: scan rate = 20 mV s^{-1}; pulse amplitude = 50 mV; pulse width = 50 msec. An atmosphere of nitrogen was maintained throughout the voltammetry scans. However, certain experiments for biological studies were performed without bubbling nitrogen.

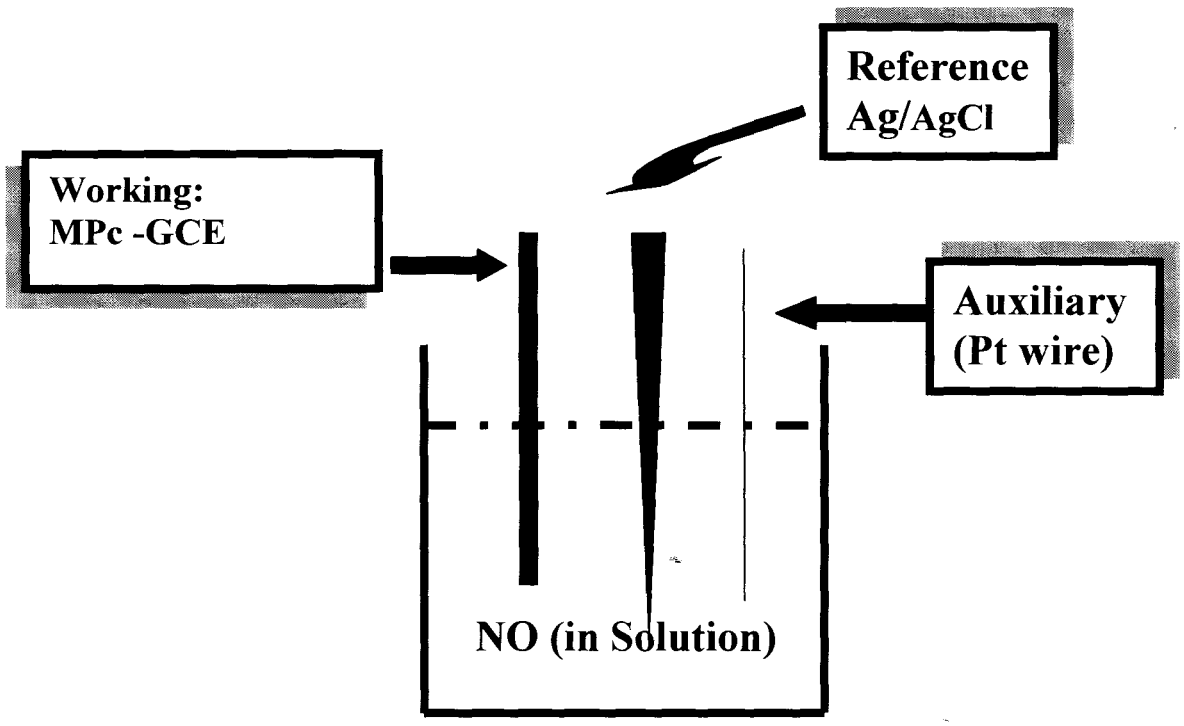

Figure 2. 1 A three electrode system, showing heterogeneous catalysis of NO on a modified GCE.

For homogeneous electrocatalytic reactions, the catalyst, MPc or MP complex and NO were in solution. The catalyst concentration was kept constant whilst the NO concentration was varied. For heterogeneous electrocatalysis, a glassy carbon electrode, modified with MPc (MPc- GCE) was employed as a working electrode. The glassy carbon electrode was modified with a MPc or MP complex by electrodeposition, or by the drop dry method. For NO detections in biological media, the microelectrode was modified with CoPc or other MPc complexes by electrodeposition, scanning from -1000 mV to 1000 mV at a scan rate of 500 mV s^{-1}. Prior to coating, the GCE or the

microelectrode was polished with alumina on a Buehler felt pad, followed by soaking in dilute nitric acid and rinsing in water, acetone and the solvent of interest.

2.4.2.2 Bulk electrolysis.

To investigate the possible reduction products of NO, bulk electrolysis experiments were performed. For bulk electrolysis, a two compartment cell was employed, with a platinum plate of area 2.2 cm^2 as a counter electrode and a Ag | AgCl (3 mol dm^{-3} KCl) reference electrode. The GCE electrode modified by electrodeposition or a carbon rod modified by drop dry method, were used as a working electrode for bulk electrolysis. The counter electrode was separated from the compartment housing the working and the reference electrodes to prevent reduction products from being oxidized at the counter electrode. A nitrogen atmosphere was maintained for all bulk electrolysis experiments.

Ammonia determination.

Yields of ammonia obtained from bulk electrolysis were determined by the Nessler method and by monitoring the absorbance at 400 nm.[139] The Nessler reagent was prepared by dissolving 35 g of potassium iodide in 100 ml water. Mercury chloride solution (4%) was added with stirring until a slight red precipitate was formed. Sodium hydroxide (120 g) in 250 ml water was added with stirring. The solution was made up to a litre with distilled water. Small amounts of mercury (II) chloride were added until the solution was permanently turbid. The solution was kept in a dark bottle overnight. A series of ammonia standards were prepared containing 1.0 ml to 6 ml of ammonium chloride diluted to 50 ml. 1 ml of Nessler reagent was added to each standard. The

solutions were allowed to stand for 10 minutes and then compared with the unknown. Absorbances of the solutions including the unknown were read at 400 to 425 nm.

Hydroxylamine.

Hydroxylamine was determined spectroscopically using the specific test described in the literature.[42] 0.2 ml of the electrolysis solution, 3 ml potassium hypophosphate (KHP) and 1 ml of 0.01 mol dm^{-3} ferrozine were mixed and diluted to 8 ml with deionized water. After addition of 2 ml of a 0.01 mol dm^{-3} $FeCl_3$ solution, the reaction was allowed to proceed for 7 minutes and the absorbance was then recorded at 564 nm. The hydroxylamine concentration was calculated from a calibration curve.

2.4.2.3 Spectroelectrochemical methods.

Spectro electrochemical techniques were used to characterize the interaction of $VitB_{12}$ with NO. An optically transparent thin-layer electrochemical (OTTLE) cell constructed as described by Hart *et al.*[140] was employed. The working and the counter electrodes were Pt grits and a silver wire was employed as the pseudo reference electrode. Solutions of sodium nitrite and $VitB_{12}$ were prepared in pH 4 buffer. $VitB_{12}$ solution was introduced into the OTTLE cell, and electrolysis was performed at potentials more negative than the reduction peak of $VitB_{12}$ (-1.1 V). Changes were monitored with UV/Visible spectrometer. Then a known concentration of sodium nitrite solution in pH 4 buffer (hence, containing NO, Section 2.3) was added to $VitB_{12}$ of the same concentration as before and the reaction was monitored with a UV/Visible spectrometer.

2.5 Instrumentation.

Electrochemical data was collected with the Bio Analytical system (BAS) model CV-50 or BAS model CV-100 Voltammetric Analyzer. All electrochemical measurements were carried out under a nitrogen atmosphere unless otherwise stated. Nitrogen was supplied by MG Fed gas and was purified by passing through a Drierite self indicating mesh 8 (unhydrous $CaSO_4$) from SAAR chemicals. Fourier transform infrared (FTIR) spectra were collected with a Perkin Elmer Spectrum 2000 IR spectrometer using a potassium bromide disks for solid products, or cesium iodide (CsI) salt windows for liquid solutions. Electronic absorption spectra were recorded with a Cary IE UV-Visible or a Cary 500 UV/NIR spectrophotometer. Bulk electrolysis was performed using a BAS CV 27 voltammograph analyzer.

2.6 Preparation of biological material for analysis.

2.6.1 Human blood.

Blood was collected from healthy individuals into glass tubes containing ethylenediaminetetraacetic acid (EDTA). A portion was centrifuged to provide plasma and serum. The samples were stored in the fridge at 0 °C for a maximum of 1 week. Some experiments were performed on the same day of blood collection and some a week later. There were no differences in the results.

2.6.2 Rat brain.

Inbred rats of the Wistar strain were used. Rats were allowed access to a standard diet and water. They were sacrificed by neck fracture and then decapitated. Rat brain was removed and sliced immediately. The brain slices were each placed in a petri dish with a culture medium. The culture medium used was a Fitton-Jackson, BGJB. Bradykinin (sigma) was used to induce NO. Analysis was performed within an hour after the rat was sacrificed after which the brain slices did not respond to Bradykinin and the NO signal was no longer observed.

RESULTS AND DISCUSSION

CHAPTER THREE: DETECTION OF NITRIC OXIDE USING COBALT PHTHALOCYANINE COMPLEXES.

3.1 Spectroscopic studies

3.2 Kinetics and equilibria studies

3.3 Voltammetric characterisation

3.4 Homogeneous catalysis

3.5 Heterogeneous catalysis

3.6 Analysis of reduction products

3. DETECTION OF NO USING COBALT PHTHALOCYANINE COMPLEXES*

3.1 Spectral characterisation of NO interaction with phthalocyanine complexes.

3.1.1 Interaction of NO with cobalt phthalocyanine (CoPc).

The UV/Visible absorption spectra of Co(II)Pc in DMSO has an intense Q band at 660 nm. A less intense absorption peak is observed at a lower wavelength (600 nm) and is assigned to a vibronic transition, Figure 3.1(a). In DMSO solutions, CoPc is known to be a six co-ordinate complex, hence the starting complex for these studies is expected to be the $(DMSO)_2CoPc$ species.[14] The spectra with a Q band at 660 nm is thus due to the $(DMSO)_2CoPc$ species. Fig 3.1 shows the absorption spectral changes observed when a DMSO solution of NO (1.1×10^{-4} mol dm^{-3}) was added to a solution of $(DMSO)_2CoPc$. On addition of NO, the Q band of the $(DMSO)_2CoPc$ species shifts isosbestically from 660 to 666 nm. An isosbestic point was observed at 657 nm. The presence of an isosbestic point is a clear indication that only two absorbing species are present in solution. X-ray photoelectron spectroscopy studies have shown that electron transfer from the metal to NO occurs following coordination of NO to CoPc.[48] On the other hand, reductive nitrosylation has been reported for the coordination of NO to Co^{II} porphyrin complexes.[42]

The possibility of the oxidation of $Co^{II}Pc$ to the $Co^{III}Pc$ species following addition of NO to $(DMSO)_2CoPc$ in solution was investigated. When NO was added to solutions

* The following papers have resulted from the research work presented in this chapter and are not referenced further in this thesis: S. Vilakazi and T. Nyokong, Polyhedron, **17**, 1998, 4415, AND: S. Vilakazi and T. Nyokong, Polyhedron, **19**, 2000, 229.

of chemically generated $Co^{III}Pc$ species in DMSO, the Q band of the resulting complex was observed at 665 nm, a wavelength very close to that obtained in Fig 3.1(b) following addition of NO to $Co^{II}Pc$. Based on the absorption spectral data and on the X-ray photoelectron spectroscopic data reported before,[43] the complex formed following coordination of NO to $Co^{II}Pc$ has been represented as the $Co^{III}Pc(NO^{-})$ species.

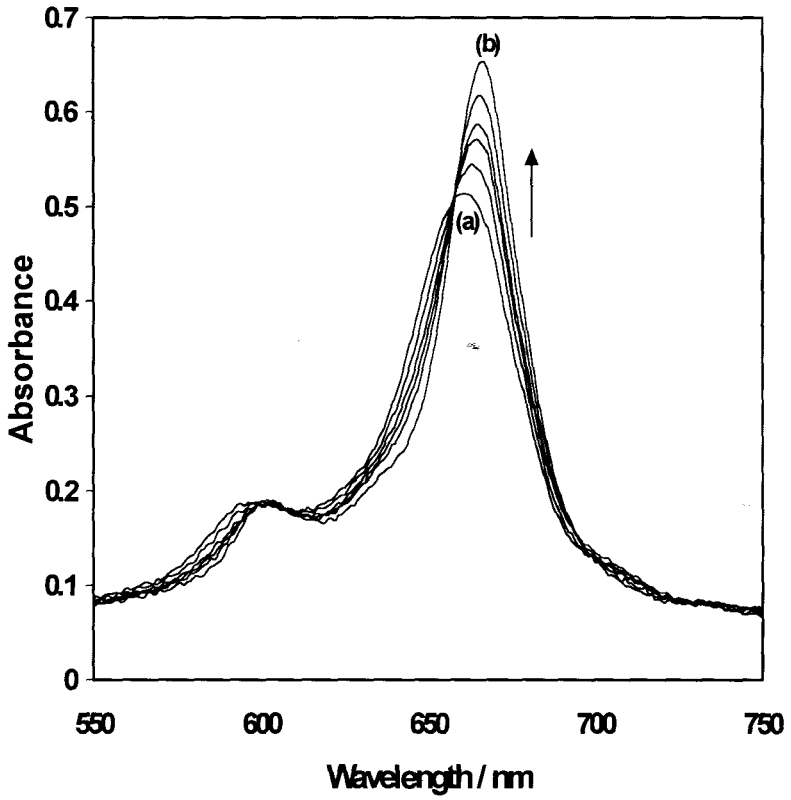

FIGURE 3.1 Absorption spectral changes observed on addition of NO (1.1×10^{-4}mol dm^{-3}) to CoPc in DMSO. (a) Before NO addition (b) 18 min after NO addition.

To further characterise the interaction between NO and $Co^{II}Pc$, IR spectroscopy was employed. For IR studies, dichloromethane and not DMSO was employed as a solvent due to the strong IR vibrations of the latter in the region of NO vibrations. The IR spectra of $Co^{II}Pc$ in CH_2Cl_2 in the presence of NO, showed a new IR band at 1680 cm^{-1}, Figure 3.2. The IR spectrum of free NO was observed at 1847 cm^{-1}. The IR spectra of cobalt(II) porphyrins in CH_2Cl_2 and in the presence of NO, showed the ν_{NO} in the 1681 - 1695 cm^{-1} region.[33] Thus, the IR band observed at 1680 cm^{-1} is assigned to bound NO. Vibrational frequencies of NO greater than 1700 cm^{-1} have been associated with the electron transfer from NO to the central metal and have a linear geometry. NO vibration frequencies that are less than 1700 cm^{-1}, have been associated with a metal to NO electron transfer and exhibit a bent geometry.[50] Thus, the observation of an NO frequency lower than 1700 cm^{-1} for the complex formed when NO is added to $Co^{II}Pc$, supports the formation of the $(NO^-)Co^{III}Pc$ species as a result of electron transfer from the central metal to NO and suggests a bent geometry. Attempts to synthesise solid (NO)CoPc species by bubbling NO through solutions of CoPc in dimethylformamide, and then evaporating the solvent, resulted in the formation of a complex that was more soluble in organic solvents than the original species. Absorption spectral studies of the solid formed showed the presence of a $Co^{III}Pc$ species, as judged by the absorption at 666 nm.

3.1.2 Interaction of NO with cobalt tetrasulfophthalocyanine $[CoTSPc]^{4-}$.

Introduction of the negatively charged sulfonate groups onto the CoPc renders the latter to be water soluble. The study of the interaction of NO with $[CoTSPc]^{4-}$ species

was undertaken in order to compare the aqueous studies with the non aqueous studies presented above for CoPc. Like other tetrasulfonated phthalocyanines, $[CoTSPc]^{4-}$ species forms aggregates in aqueous solution.[141] The electronic absorption spectrum is explained in terms of the monomer/dimer equilibrium.

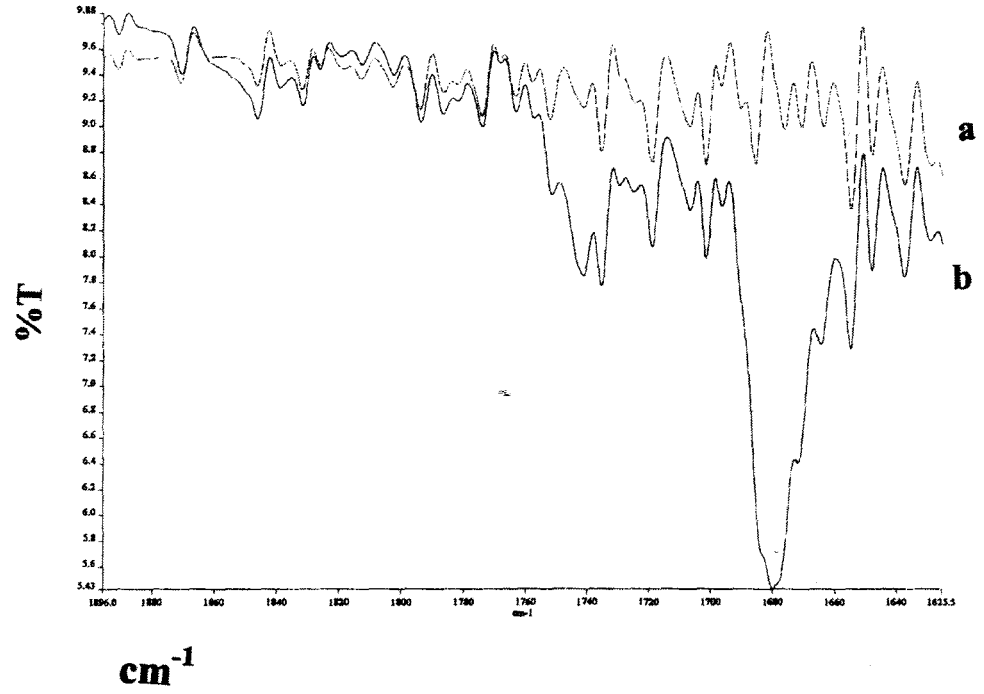

FIGURE 3.2 IR spectra of (a) CoPc in CH_2Cl_2 (b) CoPc in CH_2Cl_2 after bubbling NO gas.

The lower energy band near 670 nm has been attributed to the monomeric species and the higher energy band near 620 to the dimeric species.[142] Aggregation as indicated by the predominance of the 620 nm band over the 665 nm band, is more prominent in acidic media than in basic media.[141] It has also been reported that aggregation increases

with an increase in ionic strength.[142] In water in the absence of added electrolytes there is a predominance of the monomeric form over the dimeric form, Figure 3.3(a).

It has also been reported that $[CoTSPc]^{4-}$ reversibly binds oxygen.[142] However, in neutral solutions, the formation of the $[CoTSPc]^{4-}$ oxygen adduct was found to be negligible even after prolonged periods of oxygen bubbling. In these studies, oxygen was carefully excluded by bubbling nitrogen to both NO and $[CoTSPc]^{4-}$ solutions and no spectral changes were observed in $[CoTSPc]^{4-}$ in the absence of NO.

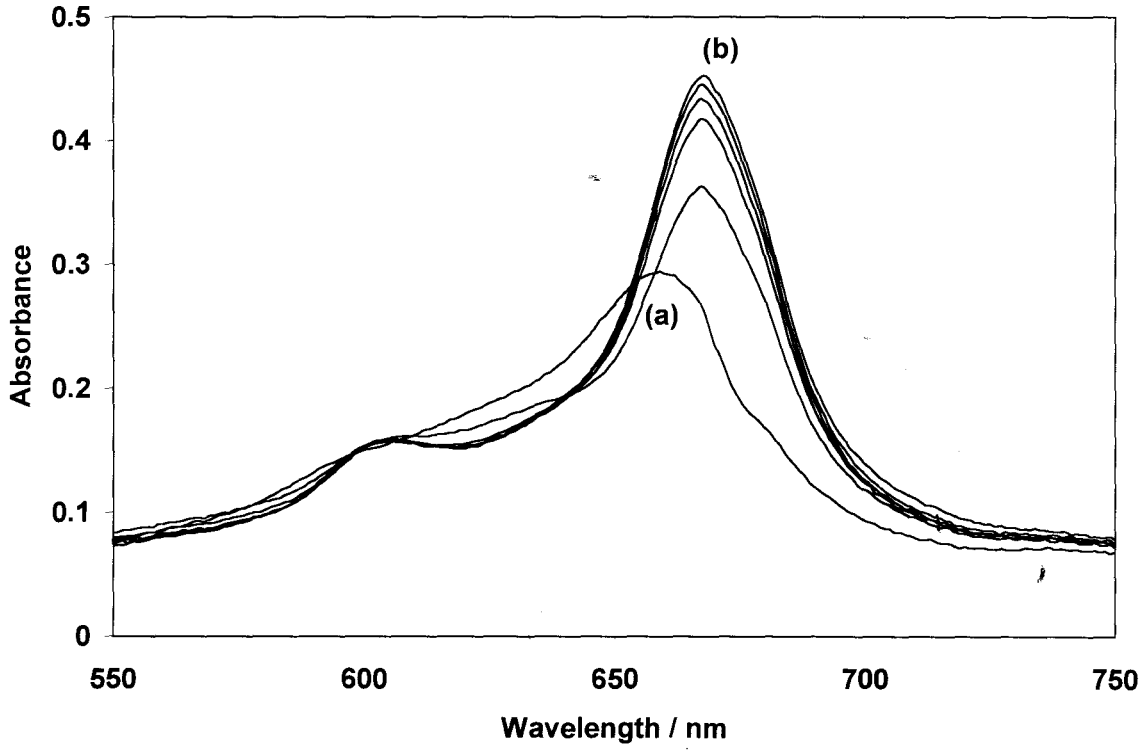

FIGURE 3. 3 Absorption spectra of $[CoTSPc]^{4-}$ in water. (a) before NO addition (b) 18 min after addition of NO (3.5×10^{-5} mol dm^{-3}).

On coordination of molecules such as nitrite and histidine to $[CoTSPc]^{4-}$, the peak due to the monomer increases in intensity and shifts to longer wavelengths, while the peak due to the dimeric species decreases in intensity.[123,143] Figure 3.3 shows spectral changes which were observed when NO was added to solutions of $[Co(II)TSPc]^{4-}$. The monomeric peak of $[CoTSPc]^{4-}$ was observed at 659 nm before addition of NO, Figure 3.3(a). As indicated above, the spectra is typical for $[CoTSPc]^{4-}$ in water, at low electrolyte concentrations, with the peak due to the monomer dominating under these conditions. On addition of NO to $[Co(II)TSPc]^{4-}$, a shift in the peak due to the monomer, from 659 to 667 nm, was observed, Figure 3.3(b). The intensity of the peak at 667 nm increased isosbestically with time, Figure 3.3(b), however, the isosbestic point does not include the initial spectrum. This shift in the spectrum is associated with the coordination of NO to the $[CoTSPc]^{4-}$ species. A shift and increase in the monomeric peak of the $[CoTSPc]^{4-}$ species on coordination of histidine and nitrite has been reported.[123,143] An increase and shifting in the monomer peak in $[CoTSPc]^{4-}$ was also observed on formation of an adduct between this species and oxygen. Since oxygen was carefully excluded from the solutions containing NO and $[CoTSPc]^{4-}$, the spectral changes shown in Figure 3.3 are associated with the formation of an adduct between NO and $[CoTSPc]^{4-}$.

As indicated above, X-ray photoelectron spectroscopy studies have indicated oxidation of the central metal in FePc and CoPc when the complexes are exposed to NO.[49] Electron transfer from Ni(II) to NO has also been implicated on coordination of NO to $[Ni(II)TSPc]^{4-}$, resulting in the formation of the $[(NO^{-})Ni(III)TSPc]^{4-}$ species.[50] It is suggested that oxidation of the central metal also occurs on coordination of NO to the $[CoTSPc]^{4-}$ species, forming a Co(III)TSPc-NO complex, as was the case with CoPc

discussed above. Oxidation of $[CoTSPc]^{4-}$ using chemical oxidants (e.g. bromine) resulted in the spectra similar to that shown in Figure 3.3(b). As the reaction proceeds, there is a possibility of traces of the dimeric species that are being converted to the monomeric species. This conversion contributes to a lack of a clear isosbestic point between the spectra of the starting complex, $[CoTSPc]^{4-}$ and that of the new complex, $[(NO)CoTSPc]^{4-}$.

In nitrosyl complexes, ν(NO) ranges from 1500 to 1900 cm^{-1}. ν(NO) for cobalt tetrakis(*N*-methyl-2-pyridyl)porphine (Co(2-TMpyP) was observed at 1722 cm^{-1},[42] and for CoPc(NO), discussed above, at 1680 cm^{-1}. IR spectra of the solid formed by reacting $[Co(II)TSPc]^{4-}$ with NO showed a new band at 1730 cm^{-1}, in the range for coordinated NO. This value is higher than those reported for NO coordinated to cobalt porphyrins (e.g 1722 cm^{-1}). Generally, oxidized cobalt porphyrin complexes show ν(NO) at higher frequencies than neutral complexes.[33] Thus, the higher ν(NO) values for the $[(NO)CoTSPc]^{4-}$ complex could be a consequence of the oxidation of $[Co(II)TSPc]^{4-}$ to $[Co(III)TSPc]^{3-}$ following coordination of NO. However, a frequency higher than 1700 cm^{-1} was not observed for CoPc(NO), as discussed above. As mentioned above, oxidation of $[Ni(II)TSPc]^{4-}$ to $[Ni(III)TSPc]^{3-}$ following coordination of NO has been observed. The IR spectra of the $[Ni(III)TSPc(NO^{-})]^{4-}$ complex showed ν(NO) at 1660 cm^{-1},[5] much lower than the value reported here for the $[Co(III)TSPc(NO)]^{4-}$ complex. Vibrational frequencies of NO greater than 1700 cm^{-1} have been associated with linear geometry of the M-N=O complexes and those of lower frequency to a bent geometry.[50] The high vibrational frequency (> 1700 cm^{-1}) reported here for $[CoTSPc]^{4-}$ suggests a linear geometry, and NO to metal electron transfer. However, spectroscopic proof is

given above for the oxidation of $[CoTSPc]^{4-}$ on addition of NO. For CoPc the NO vibrational frequencies were observed at 1680 cm^{-1}. The difference in the stretching frequencies of (NO)CoPc and $[(NO)CoTSPc]^{4-}$ could be due to the environmental effects. It has been reported that in five coordinated nitrosyl complexes, stretching frequencies show some sensitivity to the environmental effects.[29] Solution of $[Co(III)TSPc(NO^-)]^{4-}$ obtained by bubbling NO into $[CoTSPc]^{4-}$ aqueous solution, showed a weak band at 1707 cm^{-1} and the band at 1730 cm^{-1} observed from the solid $[Co(III)TSPc(NO^-)]^{4-}$ was not observed. This shows that the IR technique is unreliable for structural determinations. Oxidation of NO to NO_2^- is likely following its coordination to $[CoTSPc]^{4-}$. NO_2^- stretching frequencies were observed at 1401, 1306, 830 cm^{-1} in Co(III)(2-TMpyP(NO).[42] New IR bands were not observed in this region for the [CoTSPc(NO)] complex.

3.1.3 Interaction of NO with aluminium tetrasulfophthalocyanine $[ClAlTSPc]^{4-}$.

$[ClAlTSPc]^{4-}$ is not aggregated in solution. This is due to the presence of the axial ligand, which prevents stacking that is observed with $[CoTSPc]^{4-}$. $[ClAlTSPc]^{4-}$ is thus monomeric in aqueous solution. Studies on its interaction with NO were thus undertaken in order to compare with the normally aggregated $[CoTSPc]^{4-}$. In water, the spectra of $[ClAlTSPc]^{4-}$ exhibits a strong band at 676 nm which is assigned to the monomeric species, Figure 3.4(a).

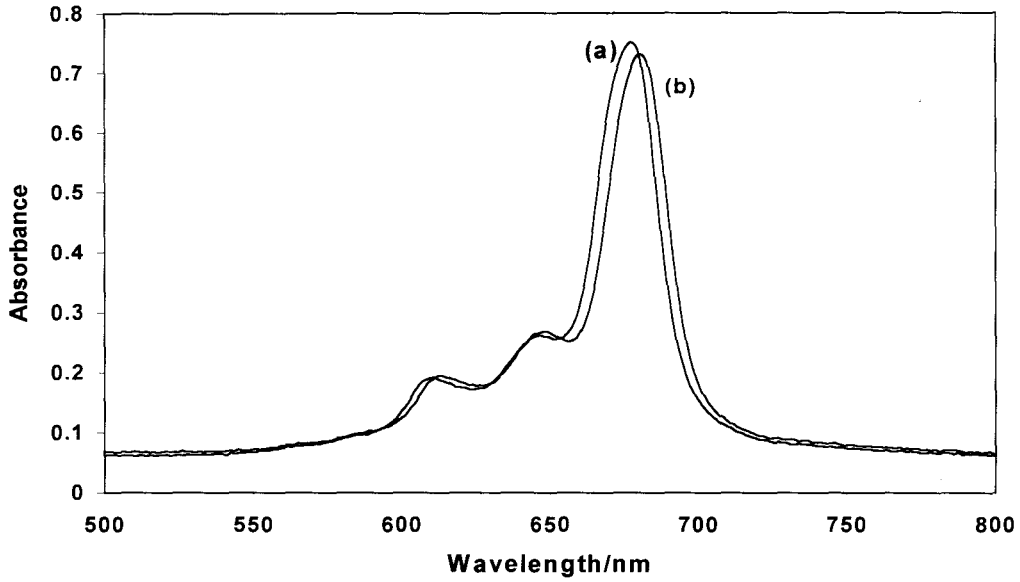

FIGURE 3. 4 Absorption spectra of $[ClAlTSPc]^{4-}$ in water (a) before NO addition (b) after NO addition.

When NO was added to an aqueous solution of $[ClAlTSPc]^{4-}$, Figure 3.4(b), the reaction happened instantaneously such that it was not possible to follow the kinetics of the reaction using the techniques discussed in this work. However, spectral changes observed were typical of axial ligand exchange.[14] Central metal redox processes also show a shift in the Q band, but for $[ClAlTSPc]^{4-}$ no metal redox processes are expected. Thus, the spectral changes could only be due to axial ligand exchange, probably from Cl^- to NO.

3.2 Kinetic and equilibrium studies of the interaction of NO with phthalocyanine complexes.

3.2.1 Interaction of NO with cobalt phthalocyanine (CoPc).

Kinetic and equilibrium data for the coordination of NO to CoPc were determined by monitoring the formation of the (NO)CoPc species. The increase in the Q band of this species at 666 nm (Figure 3.1) was monitored and recorded at regular intervals. The concentrations of NO ranged from 6 $x10^{-5}$ to 1.2 x 10^{-4} mol dm^{-3}. The concentration of CoPc was kept constant at 4.5 x 10^{-6} mol dm^{-3}. Since excess NO concentrations were used, pseudo first order conditions were assumed for kinetic studies.

Plots of $\ln(A_\infty - A_t)$ against time, (where A_∞ is the absorbance at the end of the reaction, A_t, is the absorbance at time t), were linear for the formation of the (NO)CoPc species, Figure 3.5. The linearity of the plots confirms that the reaction between CoPc and NO is first order with respect to the former.

The observed rate constant (k_{obs}) is given by the slope of the plot of $\ln(A_\infty - A_t)$ against time. The observed rate constant was obtained for various concentrations of NO. Plots of the observed rate constant, k_{obs}, versus the concentration of NO were linear, Figure 3.6. This shows that the coordination is first order in NO.

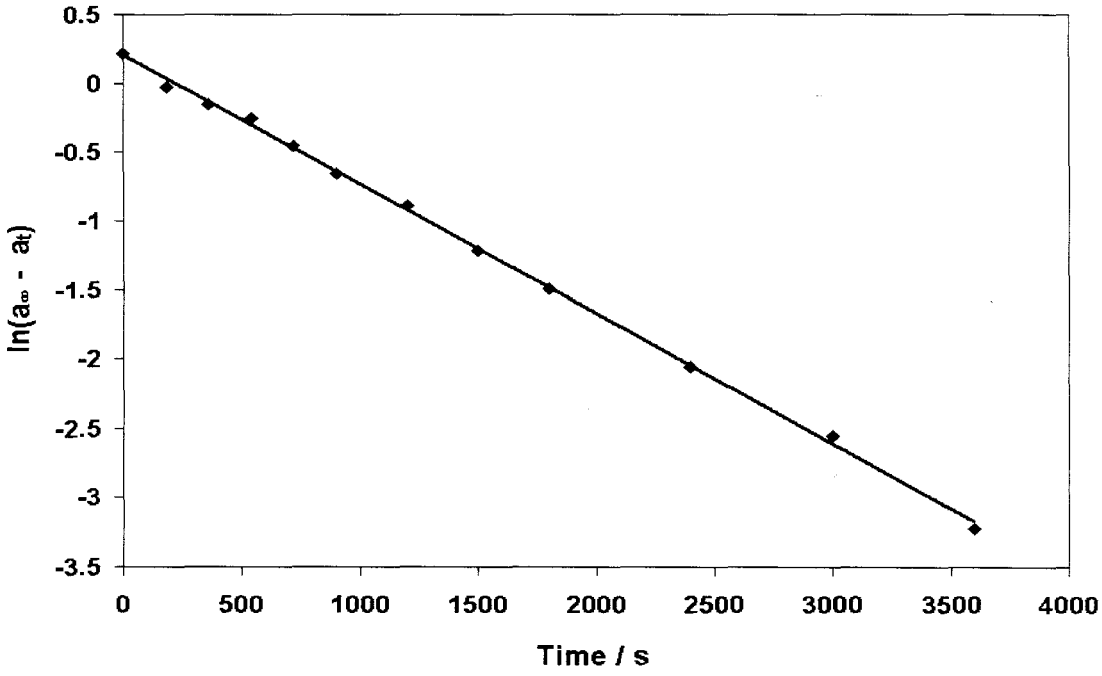

FIGURE 3. 5 Plot of $\ln(A_\infty - A_t)$ *vs* time, for the reaction of NO (1.1×10^{-4} mol dm^{-3}) with CoPc (4.5×10^{-6} mol dm^{-3}).

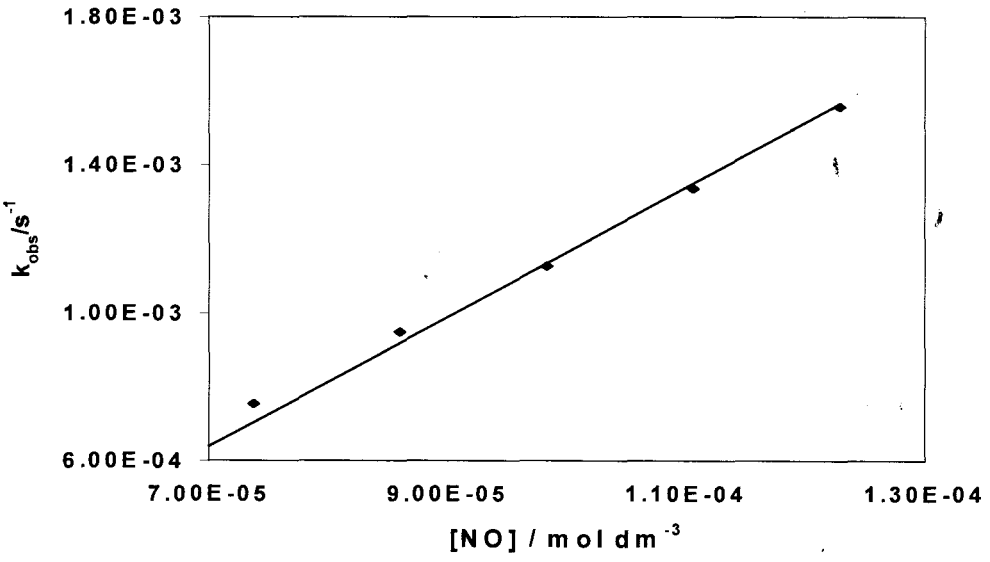

FIGURE 3. 6 Plot of the observed rate constant, k_{obs}, *vs* the concentration of NO for the formation of the (NO)CoPc species.

Axial ligand substitution reactions in metallophthalocyanines are dissociative with the formation of a highly reactive five-co-ordinate intermediate.[144,145] As discussed above, in DMSO solution CoPc is coordinated to DMSO and is represented as $CoPc(DMSO)_2$. The axial ligand substitution in $(DMSO)_2CoPc$ may thus be represented by equation 3.1 and 3.2.

$$(DMSO)_2Co(II)Pc \underset{k_{-1}}{\overset{k_1}{\rightleftharpoons}} (DMSO)Co(II)Pc + DMSO \quad \text{.....3.1}$$

$$NO + (DMSO)CoPc \underset{k_{-2}}{\overset{k_2}{\rightleftharpoons}} [(DMSO)(NO)CoPc \quad \text{.....3.2}$$

The rate law for axial ligand exchange reactions in MPc complexes shown by equations 3.1 and 3.2 is generally given by the equation similar to equation 1.13, except that DMSO replaces water, equation 3. 3

$$k_{obs} = \frac{k_1 k_2 [NO] + k_{-1} k_{-2} [DMSO]}{k_{-1} [DMSO] + k_2 [NO]} \quad \text{.....3.3}$$

Since DMSO is a solvent its concentration is large, hence $k_{-1}[DMSO] >> k_2[NO]$ and equation 3.3 becomes equation 3. 4.

$$k_{obs} = \frac{k_1 k_2 [\mathbf{NO}] + k_{-1} k_2 [\mathbf{DMSO}]}{k_{-1} [\mathbf{DMSO}]} \quad \text{.....3.4}$$

which can be expressed as equation 3. 5:

$$k_{obs} = \frac{k_1 k_2 [\mathbf{NO}]}{k_{-1} [\mathbf{DMSO}]} + k_{-2} \quad \text{.....3.5}$$

representing $\frac{k_1 k_2}{k_{-1}[\mathbf{DMSO}]}$ as k_f and $k_r = k_{-2}$, equation 3.5 can be written as equation 3.6:

$$\boldsymbol{k_{obs} = k_f[NO] + k_r} \quad \text{.....3.6}$$

Where k_f is the rate constant for the forward reaction and k_r is the rate constant for the reverse reaction.

Least square analysis of the data presented in Figure 3.6 gave k_f = 15.0 ± 0.3 dm^3 mol^{-1} s^{-1} from the slope and from the intercept, k_r = 3.1 ± 0.1 x 10^{-4} s^{-1} was obtained. Using these values of rate constants, the value of the equilibrium constant (K_{eq}) for NO coordination to CoPc was estimated to be K_{eq} = 4.8 x 10^4 dm^3 mol^{-1} from the relationship, $K_{eq} = k_f/k_r$.

Equilibrium data were determined by standard spectroscopic techniques using equation 3.7:

$$\mathbf{Log[(A_{eq} - A_0)/(A_\infty - A_{eq})] = LogK_{eq} + n\ Log[NO]} \quad \text{.....3.7}$$

In equation 3.7, A_{eq} is the equilibrium absorbance at 666 nm, A_0 is the absorbance before addition of NO and A_∞ is the absorbance after the complete formation of the (NO)CoPc complex, as determined from the final absorbance at 666 nm, Figure 3.1(b). Figure 3.7 shows a plot of $\log[(A_{eq} - A_0)/(A_\infty - A_{eq})]$ versus log[NO]. A linear plot with a slope near unity ($n = 0.9 \pm 0.1$) was obtained, showing that only one mole of NO is co-ordinated to the CoPc species. The linearity of the plot confirms the coordination of NO to the CoPc complex.

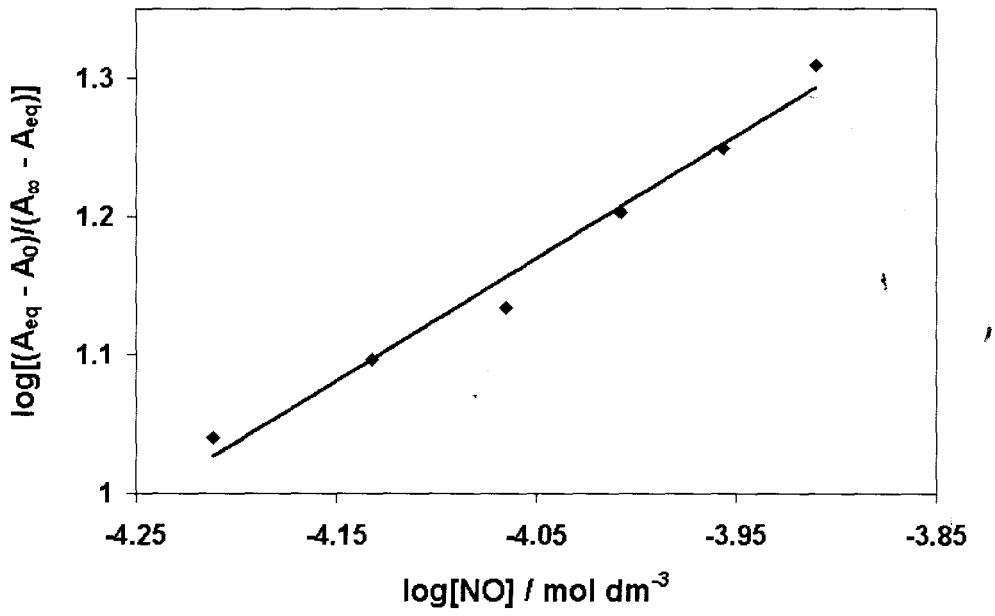

FIGURE 3. 7 Plot of log $[(A_{eq} - A_0)/(A_\infty - A_{eq})]$ *vs* log[NO] for the formation of the (NO)CoPc species.

Least square analysis gave an equilibrium constant of K_{eq} = 5.4 ± 0.4 x 10^4 dm^3 mol^{-1} which is in agreement, within experimental error, with the value determined above from the k_f / k_r ratio.

For the coordination of NO to $(DMSO)_2FePc$, Ascenzi *et al.*[145] obtained an equilibrium constant of 1.1 x 10^6 dm^3 mol^{-1}, and k_f = 2.2 x 10^4 dm^3 mol^{-1} s^{-1} . These values are much larger than the values obtained in this work for the coordination of NO to $(DMSO)_2CoPc$. The coordination of pyridine to $(DMSO)_2FePc$ also occurred with much larger equilibrium and rate constants than the coordination of pyridine to $(DMSO)_2CoPc$.[146] This implies that the five co-ordinate (DMSO)FePc species is more reactive than the corresponding (DMSO)CoPc. The equilibrium constants observed for coordination of NO to CoPc are of the same order of magnitude as the equilibrium constants reported for the coordination of NO to cytochrome C and metmyoglobin.[40] The rate constant for the coordination of NO to CoPc is similar to the rate constants reported for the coordination of NO to Mn porphyrin complexes.[101]

3.2.2 Interaction of NO with cobalt tetrasulfophthalocyanine, $[CoTSPc]^{4-}$.

In order to study the kinetics of the reaction of NO with $[Co(II)TSPc]^{4-}$, the formation of the $[Co(III)TSPc(NO)]^{4-}$ complex was followed at 667nm by recording absorbance at regular intervals, Figure 3.3. Plots of $\ln(A_\infty - A_t)$ versus time, where A_∞ is the absorbance at the end of the reaction and A_t is the absorbance at time t, were linear, Figure 3.8. Since the concentrations of NO were at least ten fold higher than that of $[CoTSPc]^{4-}$, pseudo first order conditions were assumed. The linearity of the plot implies that the reaction was first order with respect to $[CoTSPc]^{4-}$.

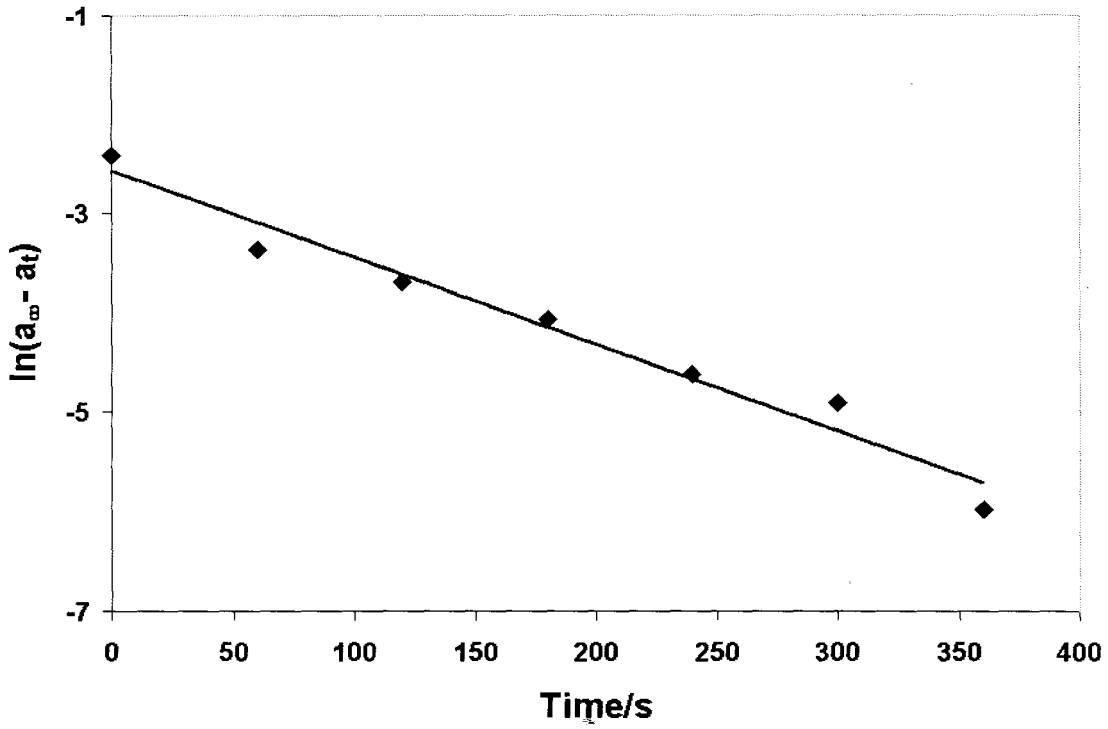

FIGURE 3. 8 Plot of $\ln(A_\infty - A_t)$ *vs* time for the reaction of NO (6.75×10^{-5} mol dm^{-3}) with $[CoTSPc]^{4-}$ (5.0×10^{-6} mol dm^{-3}).

The coordination of NO to $[Co(II)TSPc]^{4-}$ may be represented by equations similar to equation 3.3 to 3.6. From the plots shown in Figure 3.8, the observed rate constants, k_{obs}, were obtained from the slope of each graph at different NO concentrations.

Plots of k_{obs} versus the concentration of NO were also linear, Figure 3.9, showing that the coordination is first order in NO and obeys the rate law as expressed by equation 3.6. Least square analysis of the data presented in Figure 3.9 gave $k_f = 142 \pm 7$ dm^3 mol^{-1} s^{-1} from the slope and $k_r = 5.4 \pm 0.8 \times 10^{-4}$ s^{-1} was obtained from the intercept. Using these values of rate constants, the value of the equilibrium constant for NO

coordination to $[Co(II)TSPc]^{4-}$ was estimated to be $K_{eq} = 2.6 \times 10^5$ dm^3 mol^{-1} from the relationship, $K_{eq} = k_f/k_r$.

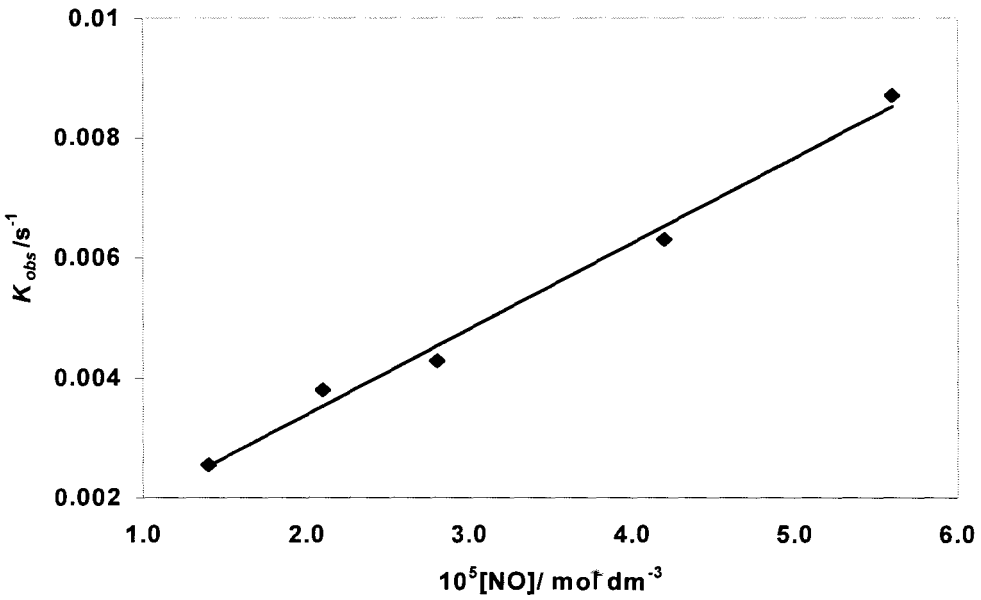

FIGURE 3. 9 Plot of the observed rate constant (k_{obs}) *vs* the concentration of NO, for the formation of $[(NO)(CoTSPc]^{4-}$ species.

The number of NO molecules coordinated to the $[Co(II)TSPc]^{4-}$ species were determined using equation 3.7, as discussed above. A_{eq} is the equilibrium absorbance at 667 nm, A_0 is the absorbance before addition of NO and A_∞, the absorbance after the complete formation of the $[(NO^-)Co(III)TSPc]^{4-}$ complex, determined from the final absorbance at 667 nm. Figure 3.10 shows a plot of $\log[(A_{eq} - A_0)/(A_\infty - A_{eq})]$ versus log[NO]. A linear plot with a slope n = 0.97 ± 0.07 was obtained, showing that only one molecule of NO is coordinated. The equilibrium constant K_{eq} was determined from the intercept to be 3.0 ± 0.5 x 10^5 dm^3 mol^{-1}. This value is in good agreement, within

experimental error with the equilibrium constant calculated above from the k_f and k_r values.

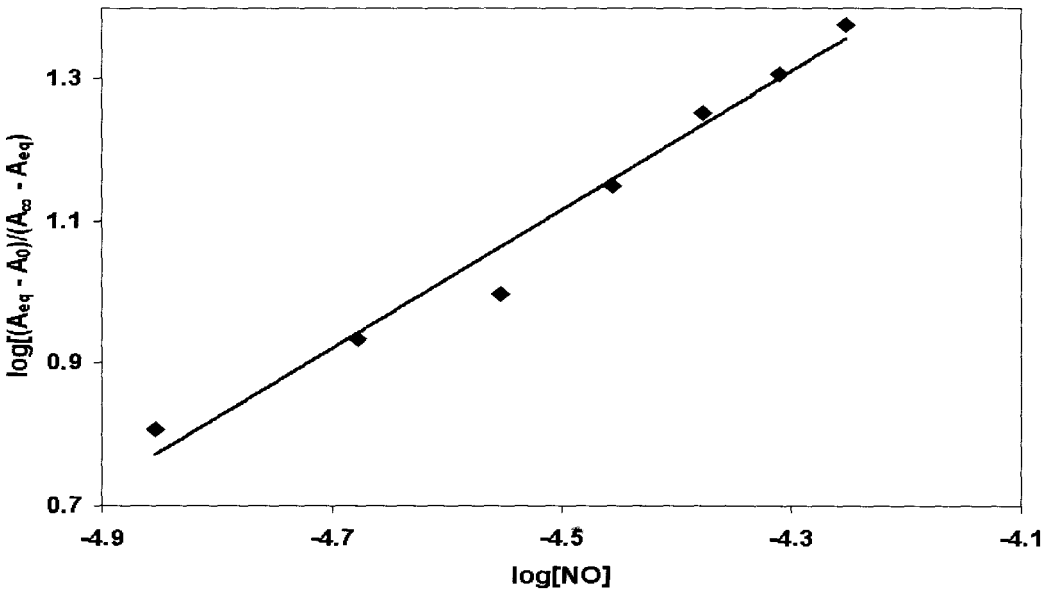

FIGURE 3. 10 Plot of $\log[(A_{eq} - A_0) / (A_\infty - A_{eq})]$ *vs* log[NO], for the formation of $[(NO)CoTSPc]^{4-}$.

The ligation of sulfonate groups to the Pc ring in CoPc renders the central metal, Co, more electron rich in $[CoTSPc]^{4-}$ than in CoPc. Since the coordination of NO to either CoPc or $[CoTSPc]^{4-}$ is accompanied by an electron transfer from the cobalt metal to NO, the rate of the forward reaction and hence, the equilibrium constant, are larger for the $[CoTSPc]^{4-}$ reaction with NO than for the CoPc reaction with NO (see Table 3.1).

Table 3.1 compares the values of the rate constant for the coordination of NO to $[Co(II)TSPc]^{4-}$ and CoPc with the values for its coordination to iron(II) porphyrin, metmyoglobin and hemoglobin. The k_f values for the coordination of NO to the latter three molecules is much higher than the value for the coordination to $[Co(II)TSPc]^{4-}$ or

CoPc. A low rate constant was also reported for the coordination of NO to manganese porphyrin complexes.[101] Axial ligand exchange reactions occur more slowly for CoPc than for FePc complexes.[146] The equilibrium constants for the coordination of NO to $[Co(II)TSPc]^{4-}$ and CoPc were however larger than for coordination of NO to the Fe(II) porphyrin, metmyoglobin and hemoglobin complexes, Table 3.1.

TABLE 3. 1 Equilibrium and rate constants for coordination of NO to phthalocyanines and some porphyrins.

Complex	K / dm^3 mol^{-1}	k_f / dm^3 mol^{-1} s^{-1}	Reference
Fe(III) porphyrin	1.1×10^3	7.2×10^5	40
Metmyoglobin	1.4×10^4	1.9×10^5	40
Hemoglobin		2.5×10^7	40
MnTMPyP		21	101
CoPc	5.4×10^4	15	this work
CoTSPc	3.0×10^5	142	this work
FePc	1.1×10^6	2.2×10^4	49

TMPyP = tetramethyl pyridyl porphyrin

3.3 Voltammetric Characterization of MPc complexes.

3.3.1 Cobalt phthalocyanine (CoPc).

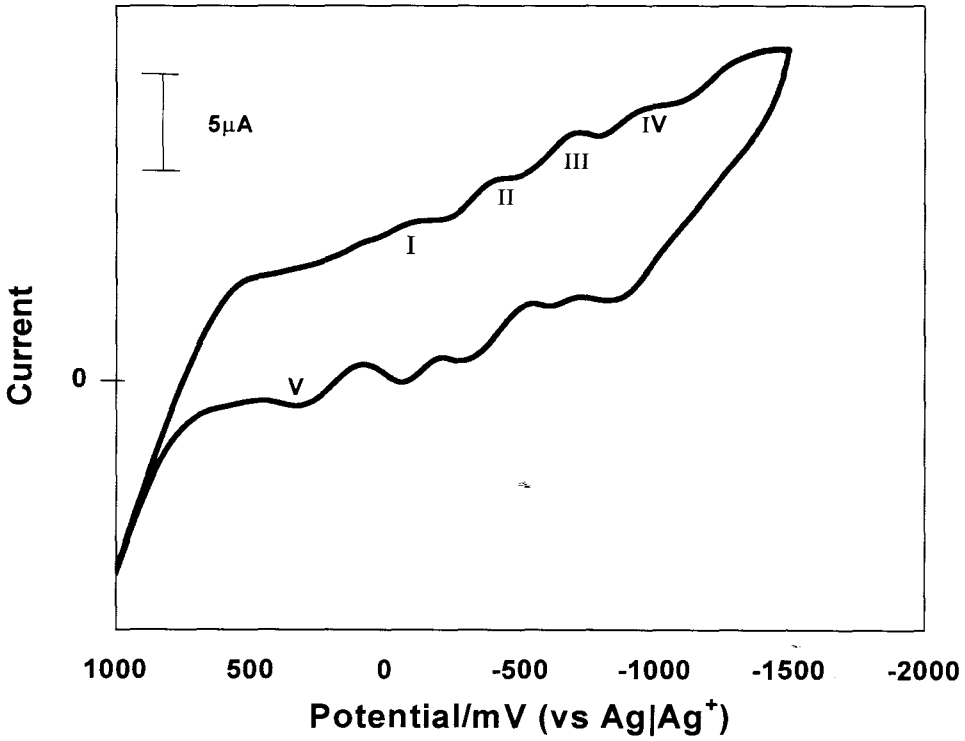

FIGURE 3. 11 Cyclic voltammogram of CoPc in DMSO. Electrolyte is 0.1 mol dm^{-3} TEAP and the scan rate = 100mV s^{-1}.

Cyclic voltammetry of CoPc in donor solvents such as DMSO is well documented.[147] Figure 3.11 shows the cyclic voltammogram of CoPc in DMSO in the absence of NO. The first reduction in CoPc is known to occur at the central Co^{II} metal to form the $Co^{I}Pc$ species.[147] Subsequent reductions occur at the phthalocyanine ring. Thus, the reduction labelled I in Figure 3.11 is assigned to $Co^{II}Pc(-2)/Co^{I}$ Pc(-2). The metal

reduction in $Co^{II}Pc$ in dimethylacetamide was observed at -0.2 V versus saturated calomel electrode.[147] The rest of the reductions are then due to ring-based processes. The half-wave potentials ($E^{1/2}$) for couples I, II, III and V were respectively found to be -0.08, -0.36, -0.66 and -0.93 V *vs* $Ag|Ag^+$, Table 3.2.

TABLE 3. 2 Potential assignments of Co(II)Pc reduction processes in DMSO containing TEAP *vs* Ag/Ag^+. Ag/Ag^+ = non aqueous reference electrode described in Section 2.4.2.1. ΔE = separation between cathodic and anodic potentials.

Process	$E^{1/2}$/V (*vs* $Ag\|Ag^+$)	Assignment	ΔE/mV
I	-0.08	$Co^{II}Pc(-2)/Co^{I}Pc(-2)$	60
II	-0.36	$Co^{I}Pc(-2)/Co^{I}Pc(-3)$	60
III	-0.66	$Co^{I}Pc(-3)/Co^{I}Pc(-4)$	70
IV	-0.93	$Co^{I}Pc(-4)/Co^{I}Pc(-5)$	60

All couples were reversible one electron processes according to equation 1.22.

3.3.2 Cobalt tetrasulfophthalocyanine, $[CoTSPc]^{4-}$.

Typical cyclic voltammograms of $[CoTSPc]^{4-}$ in water are shown in Figure 3.12. As in CoPc above, the first reduction is known to occur at the central metal, followed by reduction of the phthalocyanine ring.[148]

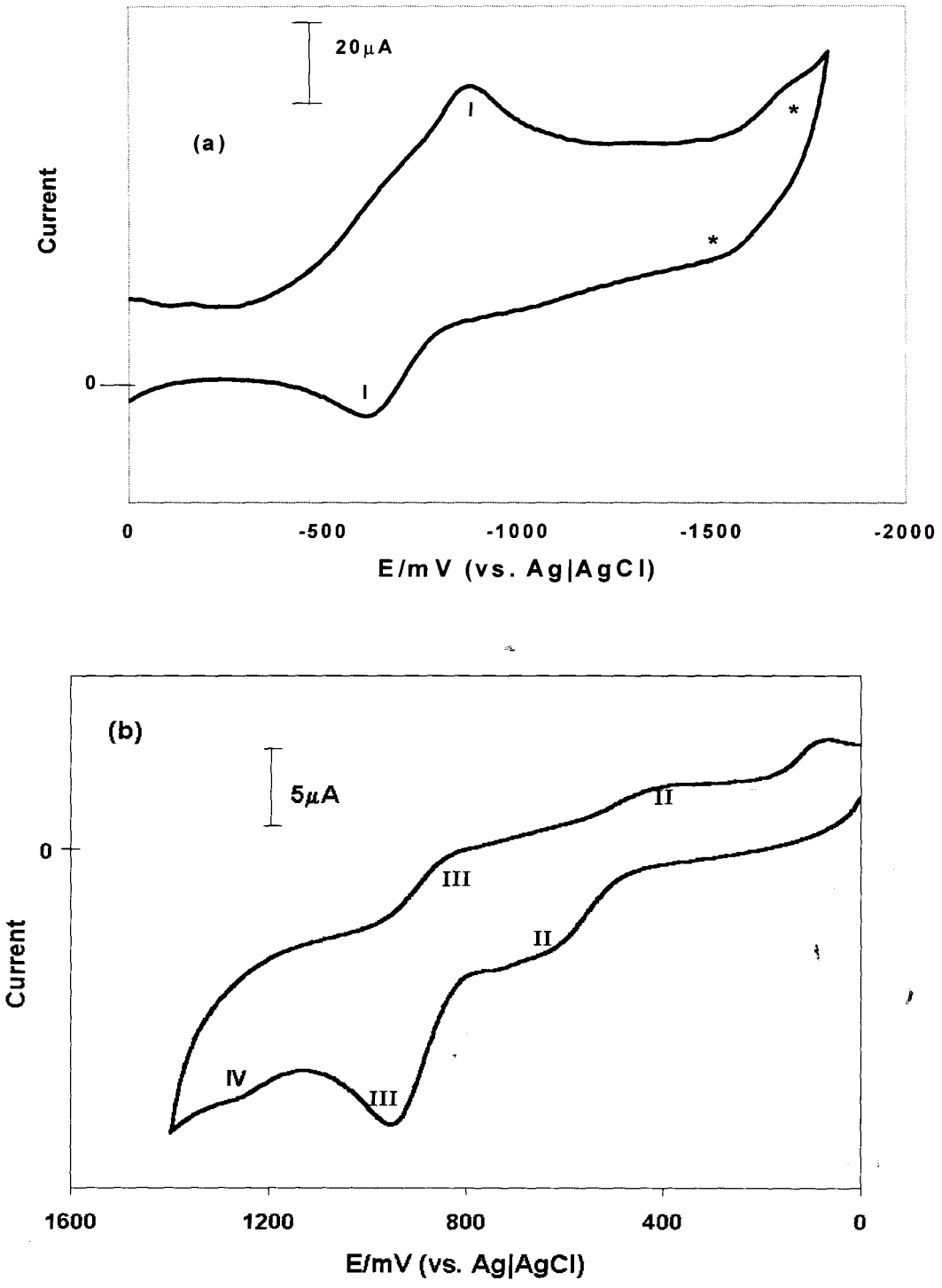

FIGURE 3. 12 Cyclic voltammogram of $[COTSPc]^{4-}$ in water. Electrolyte Na_2SO_4. (a) reduction scan (b) oxidation scan. Scan rate = 100 mV s^{-1}.

A quasi reversible reduction couple at –0.76 V, labelled (I) in Figure 3.12(a), is assigned to metal reduction, $[Co(II)TSPc(-2)]^{4-}$ to $[Co(I)TSPc(-2)]^{5-}$. ΔE for this couple is 300 mV. A second weak reduction couple was observed near -1.5 V (labelled with *) and is tentatively assigned to ring reduction. This couple is in the range of ring reduction in the CoPc complex. ΔE for the ferrocenium/ferrocene (fc^{+}/fc) couple was found to be 60 mV under the same experimental conditions. In comparison with literature, the couple labelled (II) at 0.52 V, Figure 3.12(b), arises from the stabilization of mixed valence intermediates from the reaction presented as $[Co(II)TSPc(-2)]_2^{8-}$ + $[Co(III)TSPc(-2)]_2^{6-}$ → $2[Co(II)TSPc(-2) \cdot Co(III)TSPc(-2)]^{7-}$ since $[CoTSPc]^{4-}$ is known to form dimers.[147] The couple labelled (III) is in the range of metal oxidation in $[CoTSPc]^{4-}$ species and is thus assigned to $[Co(II)TSPc(-2)]^{4-}$ to $[Co(III)TSPc(-2)]^{3-}$. This couple was quasi reversible in that the forward peak was more intense than the reverse peak. The peak labelled IV is typical of ring oxidation in $[CoTSPc]^{4-}$ species in water and is hence assigned to $[Co(III)TSPc(-2)]^{3-}$ to $[Co(III)TSPc(-1)]^{2-}$.[147] Table 3.3 gives the $E^{1/2}$ and the ΔE values for some of the assigned couples.

TABLE 3. 3 Potential assignments of $[CoTSPc]^{4-}$ in water containing Na_2SO_4.

Process	$E^{1/2}$/V(*vs* Ag|AgCl)	Assignment	ΔE/mV
I	-0.76	$[Co^{II}TSPc(-2)]^{4-}/[Co^{I}TSPc(-2)]^{5-}$	300
III	0.89	$[Co^{III}TSPc(-2)]^{3-}/[Co^{II}TSPc(-2)]^{4-}$	107
IV	1.3*	$[Co^{III}TSPc(-1)]^{2-}/[Co^{III}TSPc(-2)]^{3-}$	-

* irreversible

3.3.3 Aluminium tetrasulfophthalocyanine, [ClAlTSPc]$^{4-}$

A cyclic voltammogram of $[ClAlTSPc]^{4-}$ in water and in the presence of Na_2SO_4 electrolyte, exhibited two very weak reduction couples labelled (I) and (II). The reduction couples showed very weak return peaks. Since no reduction is expected at the Al metal, the peaks can only be assigned to the ring reduction from $[ClAl(III)TSPc(-2)]^{4-}$ to $[ClAl(III)TSPc(-3)]^{5-}$ couple (I) and $[ClAl(III)TSPc(-3)]^{5-}$ to $[ClAl(III)TSPc(-4)]^{6-}$ couple (II), Figure 3.13. An irreversible very weak oxidation peak was observed at 1.1 V (III) and is assigned to the ring oxidation, $[ClAl(III)TSPc(-2)]^{4-}$ to $[ClAl(III)TSPc(-1)]^{3-}$. The half wave potentials $E^{1/2}$ for couples I and II were found to be, –0.55 V and –0.89 V respectively.

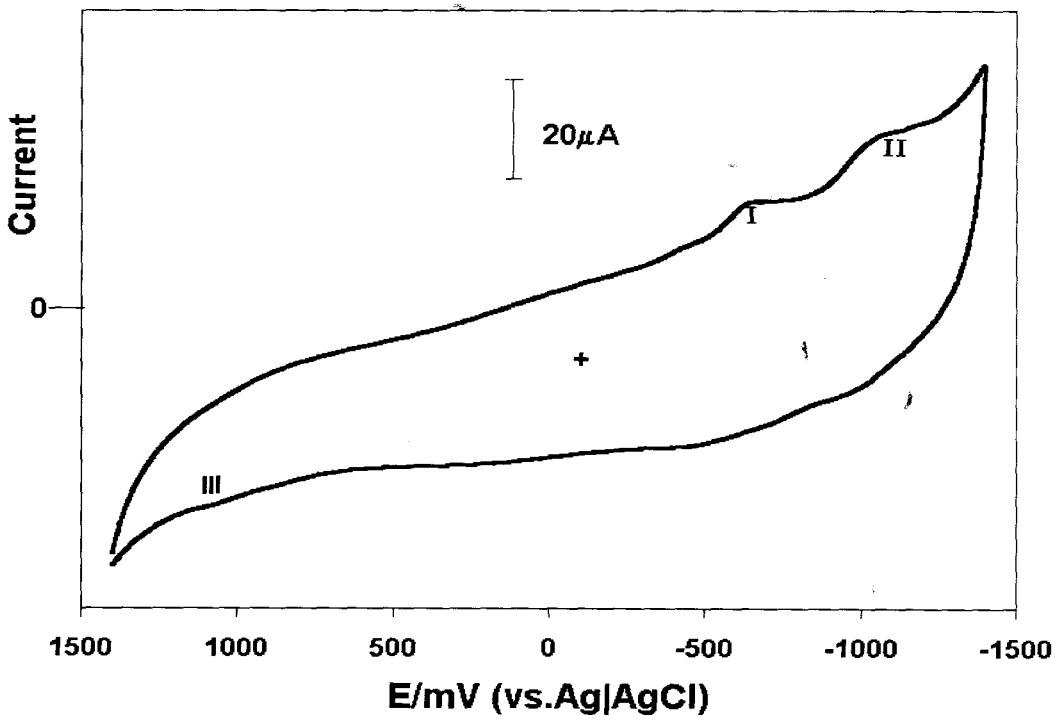

FIGURE 3. 13 Cyclic voltammogram of $[ClAlTSPc]^{4-}$ in water and Na_2SO_4 electrolyte.

Scan rate = 100 mV s^{-1}.

TABLE 3. 4 Potential assignments for $[ClAlTSPc]^{4-}$ in water containing Na_2SO_4.

Process	$E^{1/2}$/ V (*vs* Ag|AgCl)	Assignment	ΔE /mV
I	-0.55	$[ClAl(III)TSPc(-2)]^{4-}/[ClAl(III)TSPc(-3)]^{5-}$	176
II	-0.89	$[ClAl(III)TSPc(-3)]^{5-}/[ClAl(III)TSPc(-4)]^{6-}$	314

3.4 Homogeneous catalysis of NO.

3.4.1 Cobalt phthalocyanine as a catalyst.

Figure 3.14 shows the cyclic voltammograms of CoPc in DMSO before and after the addition of NO. On addition of NO (prepared by bubbling NO gas through DMSO) to solutions of CoPc in DMSO, the cyclic voltammogram shown in Fig. 3.14(b) was obtained. Following the discussion in Section 3.1.1, the coordination of NO to CoPc involves an internal electron transfer, hence the cyclic voltammogram in Fig. 3.14(b) should be due to the $(NO)Co^{III}Pc$ species in DMSO. Three quasi-reversible reduction couples were obtained. The current response of the reduction couples were enhanced relative to the current response of the reduction couples for CoPc in the absence of NO. In addition, the reduction couples in Fig. 3.14(b) are observed at slightly different potentials than the potentials for the reduction of $(DMSO)_2Co^{II}$ Pc. A considerable enhancement in the cathodic currents was observed for the fourth reduction, labelled IV on addition of NO to $(DMSO)_2CoPc$. There was no corresponding return peak for IV following addition of high concentrations of NO. The large increase in cathodic current relative to the anodic currents is typical behaviour for catalytic reduction. The catalytic peak was observed at -0.93 V *vs* $Ag|Ag^+$ (non aqueous), Figure 3.14(b).

The potential of the catalytic peak shifted to more negative values with increase in NO concentrations. The catalytic currents for the reduction of NO increased with increase in NO concentration as shown in Figure 3.15, clearly showing that peak IV is due to the reduction of NO. Figure 3.16(a) shows a plot of the variation of the catalytic currents with increase in NO concentration. The catalytic peak currents also increased linearly

with increase in the square root of scan rate, Figure 3.16(b) for scan rates ranging from 50 to 500 mV s^{-1}, confirming a diffusion controlled process for the reduction of NO.

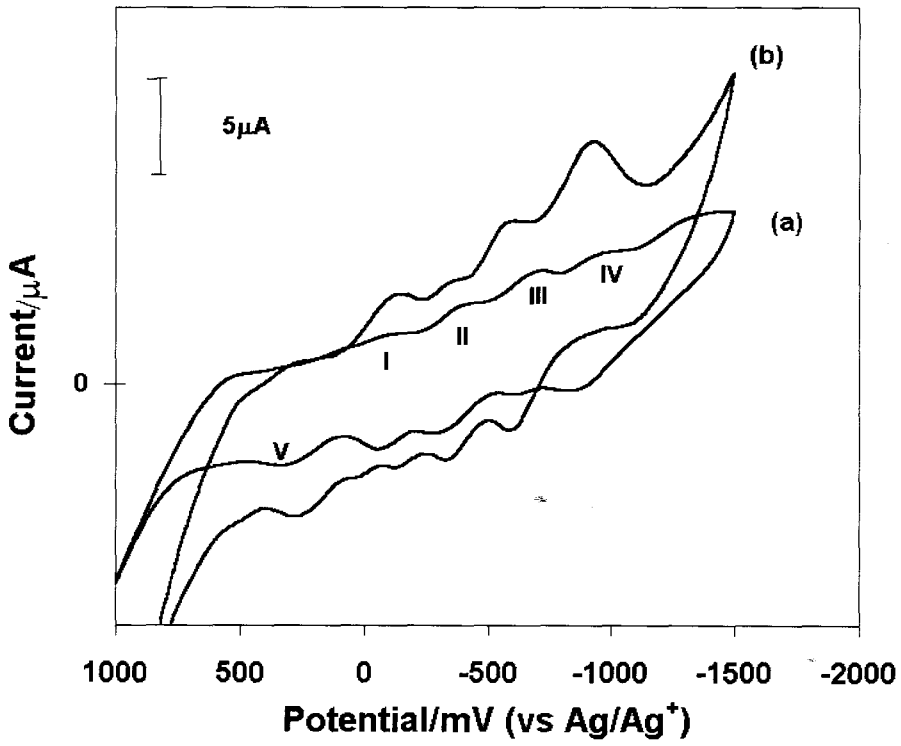

FIGURE 3. 14 Cyclic voltammogram of CoPc in DMSO (a) before (b) after addition of NO (1.1×10^{-4} mol dm^{-3}). Electrolyte is 0.1 mol dm^{-3} TEAP and the scan rate = 100mV s^{-1}.

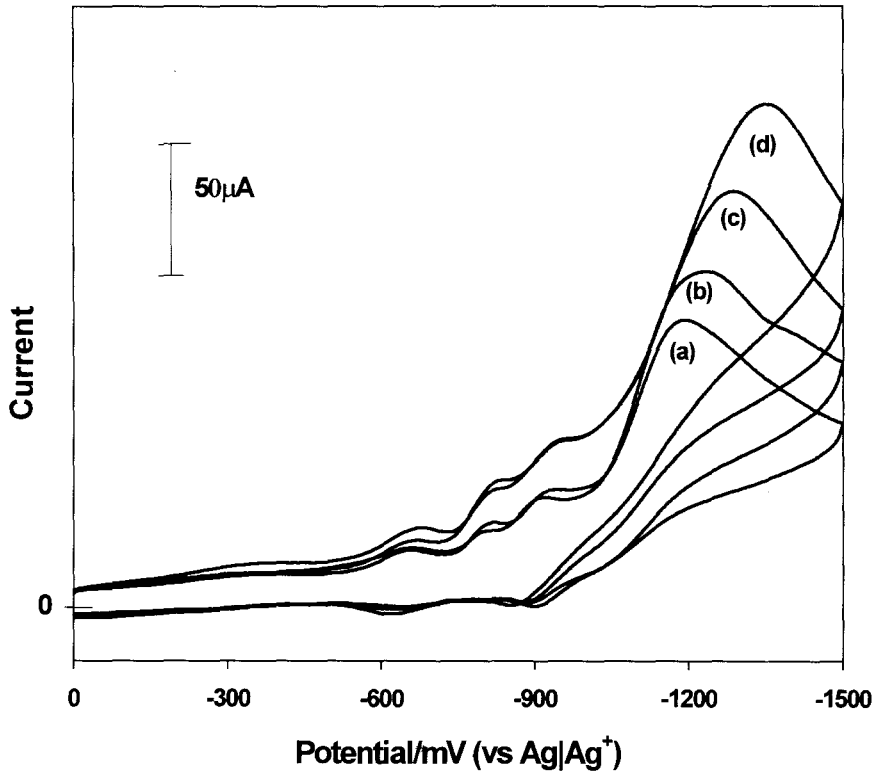

FIGURE 3. 15 Cyclic voltammograms of CoPc in DMSO in the presence of increasing concentrations of NO: (a) 4.6×10^{-4} (b) 5.7×10^{-4} (c) 6.7×10^{-4} (d) 8.3×10^{-3} mol dm^{-3}. Electrolyte is 0.1 mol dm^{-3} TEAP. Scan rate = 100 mV s^{-1}.

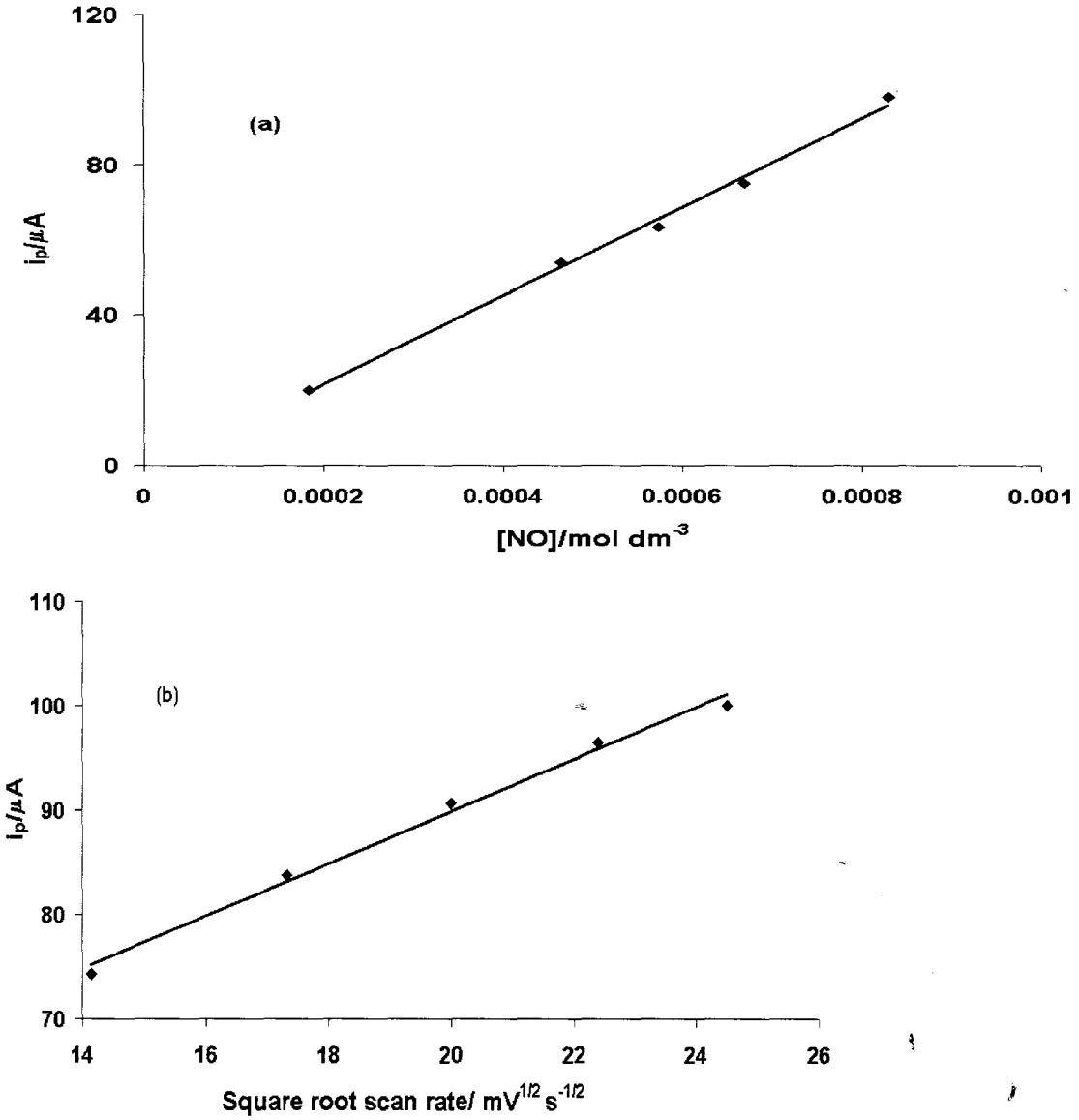

FIGURE 3. 16 Plots of the variation of the catalytic currents with (a) increase in NO concentration and

(b) square root of scan rate *vs* current. Catalyst = CoPc.

As discussed in Section 3.3.1 above, reduction in CoPc occurs first at the central metal to give a $Co^{I}Pc$ species. Subsequent reductions are expected to occur at the phthalocyanine ring, as assigned in Table 3.2. The reduction labelled IV is at the potentials reported for ring reductions of the CoPc species.[147] The fact that an enhancement in the cathodic currents of the peaks associated with phthalocyanine ring-based reductions is observed on addition of NO to CoPc, suggests that it is these reductions that are involved in catalysing the reduction of NO. In many reductions involving CoPc as a catalyst, metal-based reduction processes have been suggested as playing a major role.[110] This work however, shows that ring-based processes may be involved in the catalytic reduction of NO using CoPc. The following mechanism is thus proposed for the reduction of NO using CoPc in solution:

$$\mathbf{Co^{II}Pc(-2) + NO \rightarrow (NO)Co^{III}Pc(-2)} \quad \text{.....3.5}$$

$$\mathbf{(NO)Co^{III}Pc(-2) + e^{-} \rightarrow (NO)Co^{II}Pc(-2)} \quad \text{.....3.6}$$

$$\mathbf{(NO)Co^{II}Pc(-2) + e^{-} \rightarrow (NO)Co^{I}Pc(-2)} \quad \text{.....3.7}$$

$$\mathbf{(NO)Co^{I}Pc(-2) + e^{-} \rightarrow (NO)Co^{I}Pc(-3)} \quad \text{.....3.8}$$

$$\mathbf{(NO)Co^{I}Pc(-3) + ne^{-} \rightarrow NH_3 \text{ and other products}} \quad \text{.....3.9}$$

The DMSO solvent and the overall charge have been left out of the above equations for clarity. Following the formation of the reduction products it is expected that the $Co^{II}Pc$ species would be regenerated.

3.4.2 Cobalt tetrasulfophthalocyanine as a catalyst.

Figure 3.17 shows the cyclic voltammograms for the reduction of $[CoTSPc]^{4-}$ in water before and after the addition of NO. The concentration of $[CoTSPc]^{4-}$ used in Figure 3.12(a) was much higher than that used in Figure 3.17(b). When NO (prepared by bubbling NO gas in water) was added to aqueous solution of $[CoTSPc]^{4-}$, the cyclic voltammogram in Figure 3.17(b) was obtained. From spectroscopic characterisation of the interaction of NO with $[CoTSPc]^{4-}$, Section 3.1.2, the cyclic voltammetry in Figure 3.17 (b) is due to the $[(NO^{-})Co(III)TSPc]^{4-}$ species. On addition of NO to $[CoTSPc]^{4-}$ there is enhancement of the cathodic peak due to Co(II)/Co(I) species labelled peak I near -0.8 V but the most dramatic enhancement is observed at –1.1 V, peak II. The peak labelled II increases with increase in NO concentration as shown in Figure 3.17. This suggests that it is not the Co(II)/Co(I) species that catalyse the reduction of NO. The enhancement of currents at potentials more negative than that of the Co(II)/Co(I) couple shows that it is the ring-based processes that are involved in the catalysis of NO. The NO reduction peak in water and Na_2SO_4 electrolyte on a GCE, in the absence of $[CoTSPc]^{4-}$ was observed at –1.2 V. Thus in addition to enhancement of the currents, lowering of the reduction potential from –1.2 V in the absence of $[CoTSPc]^{4-}$ to –1.1 V in presence of $[CoTSPc]^{4-}$ occurs, as is expected for a catalytic process. Thus for both CoPc and $[CoTSPc]^{4-}$ in solution, NO catalysis is by ring-based processes.

The potential for the catalytic peak did not vary appreciably with increase in NO concentration. The catalytic currents for the reduction of NO increased with increase in NO concentration, Figure 3.17(b), (c), (d), clearly showing that peak (II) is due to NO reduction.

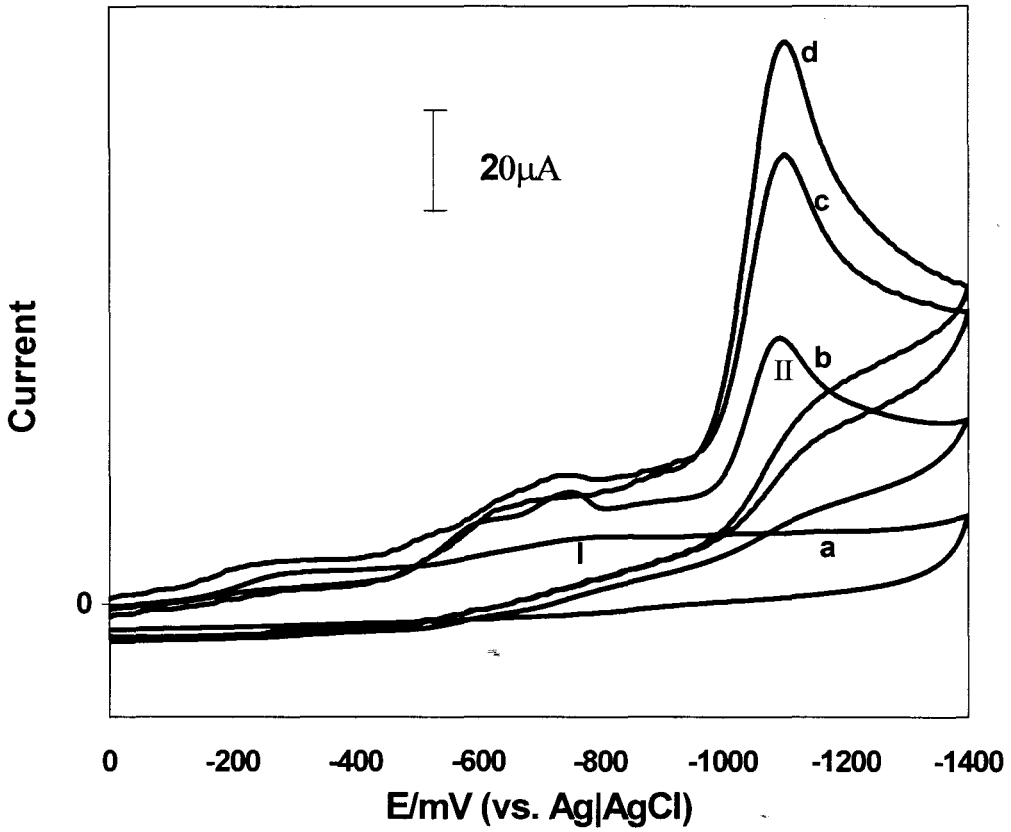

FIGURE 3. 17 Cyclic voltammetry of $[CoTSPc]^{4-}$ in water with Na_2SO_4 as an electrolyte in the presence of (a) 0, (b) 1.88×10^{-4}, (c) 2.5×10^{-4}, (d) 3.14×10^{-4} mol dm^{-3} NO. Scan rate = 100 mV s^{-1}.

Figure 3.18(a) shows a plot of the variation of NO catalytic currents with increase in NO concentration for $[CoTSPc]^{4-}$. The catalytic currents also increased linearly with increase in the square root of scan rate ranging from 50 to 500 mV s^{-1}, indicating a diffusion controlled process within this scan rate range, Figure 3.18(b).

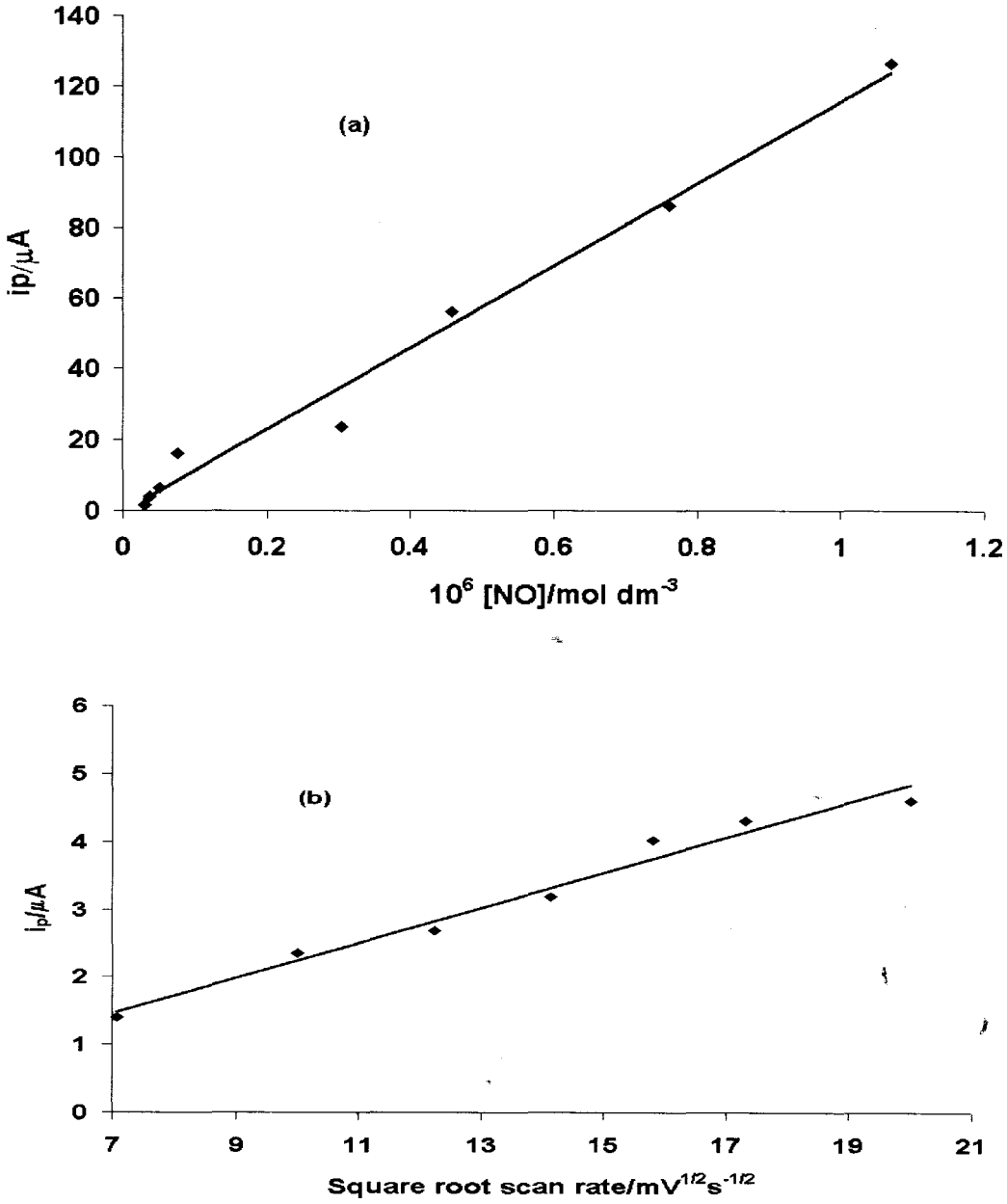

FIGURE 3. 18 Plots of the variation of the catalytic currents with (a) NO concentration and (b) square root of scan rate. Catalyst = $[CoTSPc]^{4-}$.

As was observed for CoPc, it is the ring-based processes that are involved in the catalytic reduction of NO. The following mechanism is proposed for NO reduction in the presence of $[CoTSPc]^{4-}$.

Co(II)TSPc(2-) → (NO)Co(III)TSPc(2-) 3.10

(NO)Co(III)TSPc(2-) + e^- → (NO)Co(II)TSPc(2-) 3.11

(NO)Co(II)TSPc(2-) + e^- → (NO)Co(I)TSPc(2-) 3.12

(NO)Co(I)TSPc(2-) + e^- → (NO) Co(I)TSPc(3-) 3.13

(NO) Co(I)TSPc(3-) + ne^- → reduction products 3.14

The axial water ligand and the overall charge have been left out for clarity. Equation 3.10 is a result of NO coordination in water which was confirmed spectroscopically, before in Figure 3.3.

Figure 3.19 shows the cyclic voltammogram for the oxidation of $[CoTSPc]^{4-}$ in water in the presence and absence of NO. On addition of NO to aqueous solution of $[CoTSPc]^{4-}$, an enhancement of the peak at 1.3 V labelled IV was observed, Figure 3.19(b). As discussed in Section 3.3.2 above, this peak is assigned to the ring oxidation, again suggesting the involvement of ring-based processes in the catalysis of NO by $[CoTSPc]^{4-}$ in solution. The currents for peak IV increased linearly with increase in NO concentration showing that peak IV is due to NO oxidation, Figure 3.20.

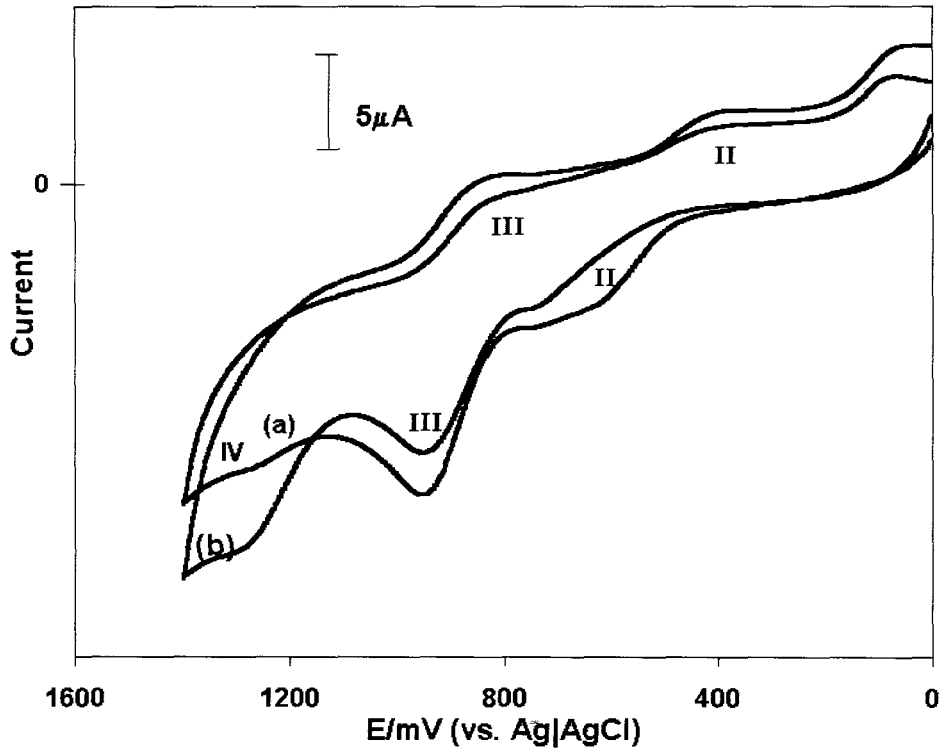

FIGURE 3. 19 Cyclic voltammogram of $[CoTSPc]^{4-}$ in water in the presence of Na_2SO_4 (a) before (b) after addition of NO (7.8×10^{-5} mol dm^{-3}). Scan rate = 100 mV s^{-1}.

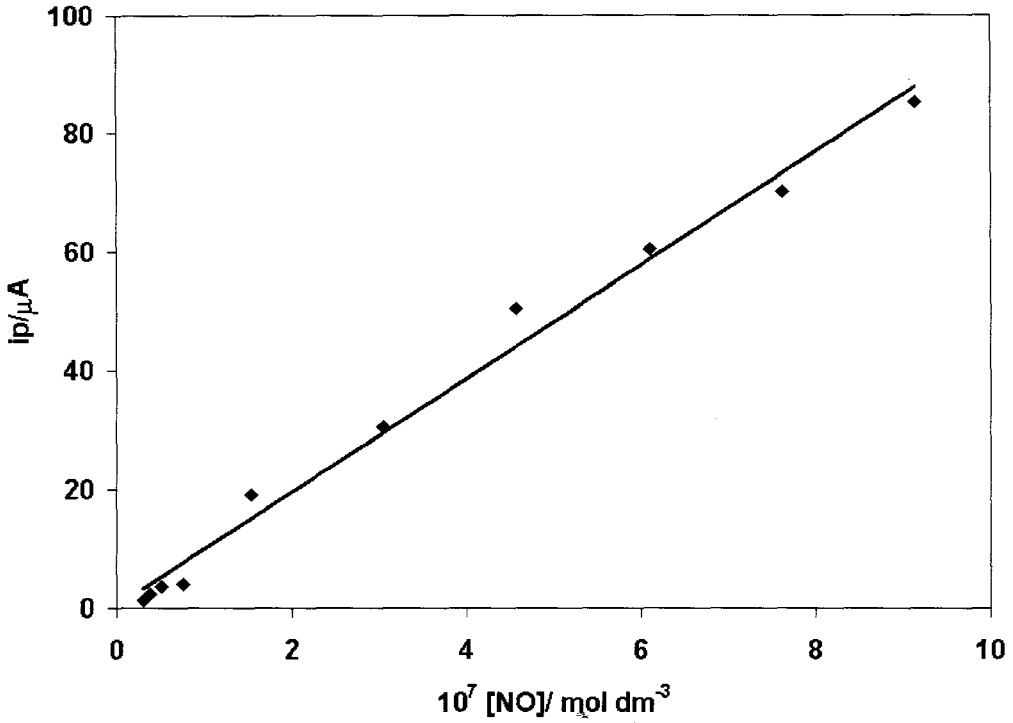

FIGURE 3. 20 Plot of the variation in oxidation currents with increase in NO concentration.

Catalyst = $[CoTSPc]^{4-}$.

3.4.3 Aluminium tetrasulfophthalocyanine as a catalyst.

Figure 3.21 shows a cyclic voltammogram for the oxidation and reduction of NO in a solution of $[ClAlTSPc]^{4-}$ in water and using Na_2SO_4 as an electrolyte. Reduction of NO by $[ClAlTSPc]^{4-}$ in solution showed small enhancement in currents which did not increase with increase in NO concentration, Figure 3.21(b). More definite changes were observed on the oxidation side. In the absence of NO the cyclic voltammogram of $[ClAlTSPc]^{4-}$ showed a weak oxidation peak at 1.1 V, peak III, which is due to the ring oxidation as discussed above (Section 3.3.3), Figure 3.21(a). In the presence of NO this

peak labelled III*, shifted and was observed at 0.9 V *vs* Ag|AgCl, Figure 3.21(b). This indicates the presence of a new complex which is probably due to the exchange in the axial ligands as discussed in Section 3.1.3.

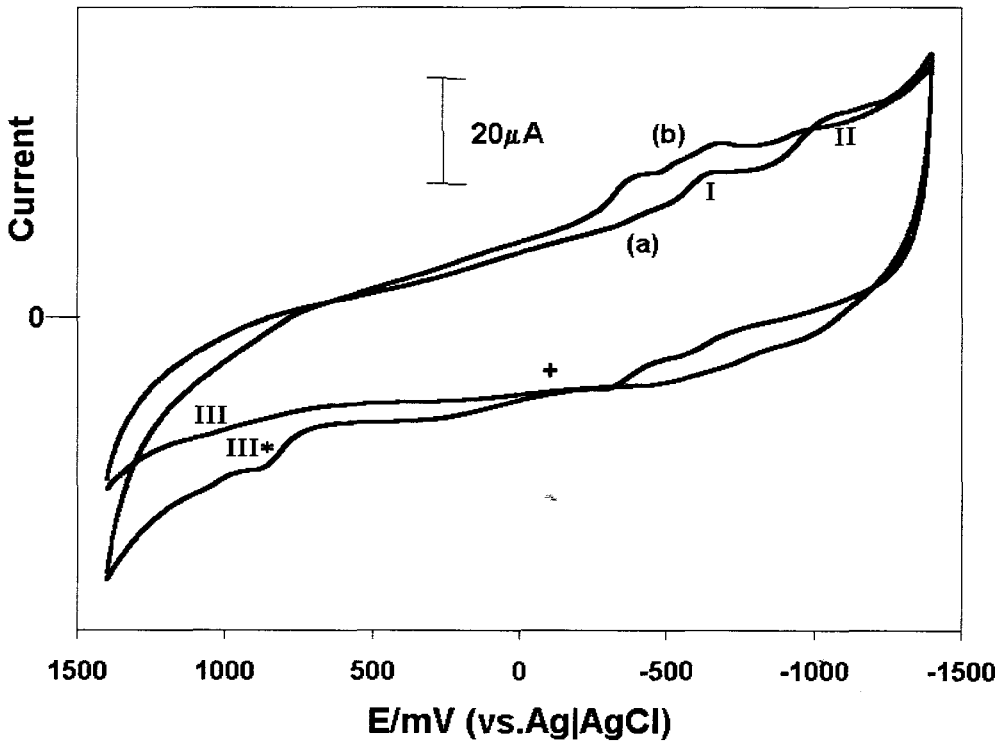

FIGURE 3. 21 Cyclic voltammogram of $[ClAlTSPc]^{4-}$ in water and Na_2SO_4 electrolyte (a) before (b) after NO addition (1.0×10^{-5} mol dm^{-3}). Scan rate = 100 mV s^{-1}.

The NO oxidation peak in the absence of $[ClAlTSPc]^{4-}$, in water and Na_2SO_4 electrolyte, was observed at 1.0 V. The lowering of potential and the increase in current are diagnostic of catalytic behaviour. The NO oxidation peak increased with an increase in NO concentration, indicating that $[ClAlTSPc]^{4-}$ catalyses the oxidation of NO, Figure 3.22. The catalytic peaks shifted to more positive potentials with an increase in NO concentration, Figure 3.22.

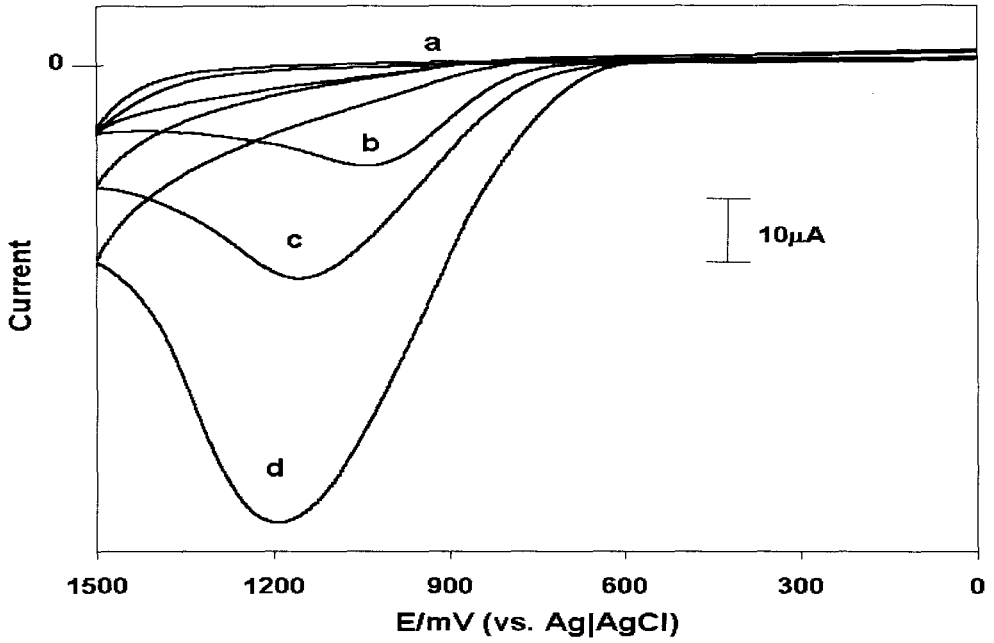

FIGURE 3. 22 Cyclic voltammograms of $[ClAlTSPc]^{4-}$ in water containing Na_2SO_4, in the presence of increasing concentrations of NO: (a) 0, (b) 7.16×10^{-3}, (c) 1.42×10^{-3}, (d) 2.68×10^{-3} mol dm^{-3}. Scan rate = 100 mV s^{-1}.

The catalytic peaks shown above (Figure 3.22) are observed for higher concentrations of NO than in Figure 3.21, hence, the peaks are shifted to more positive potentials than 0.9 V. A plot of the square root of scan rate versus catalytic currents, was linear for scan rates up to 200 mV s^{-1}. This confirms a diffusion-controlled movement of the species to the electrode at these scan rates. Under pH 4 buffer solution conditions, $[ClAlTSPc]^{4-}$ did not catalyze the oxidation of NO.

Since oxidation occurs at the ring in $[ClAlTSPc]^{4-}$, ring-based oxidative catalysis is suggested, equation 3.15 to 3.17.

[ClAl(III)TSPc(2-)] + NO → **[(NO)Al(III)TSPc(2-)]** 3.15

[(NO)Al(III)TSPc(2-)] → **[(NO)Al(III)TSPc(1-)** + **e**$^-$

.....3.16

[(NO)Al(III)TSPc(1-)] → **[ClAl(III)TSPc(2-)]** + oxidation products 3.17

Equation 3.15 is a result of the spectroscopic evidence for the possible coordination of NO to $[ClAlTSPc]^{4-}$, Figure 3.4. Equation 3.17 is a result of internal electron transfer and the oxidation of NO, hence the enhancement in currents.

3.5 Heterogeneous catalysis.

3.5.1 Cobalt phthalocyanine as a catalyst.

For heterogeneous catalysis, the glassy carbon electrode (GCE) was modified by a drop dry method. A saturated solution of CoPc in pyridine (~ 10^{-3}) was prepared and a drop thereof was placed on the electrode surface and allowed to dry in air. The cyclic voltammetry of NO on GCE modified with CoPc (CoPc-GCE) was determined in pH 4 phosphate buffer solution. Figure 3.23 shows the cyclic voltammogram of a CoPc-GCE in pH 4 buffer. In the absence of NO the reduction couple due to adsorbed CoPc is observed near - 0.15 V *vs* Ag|AgCl.

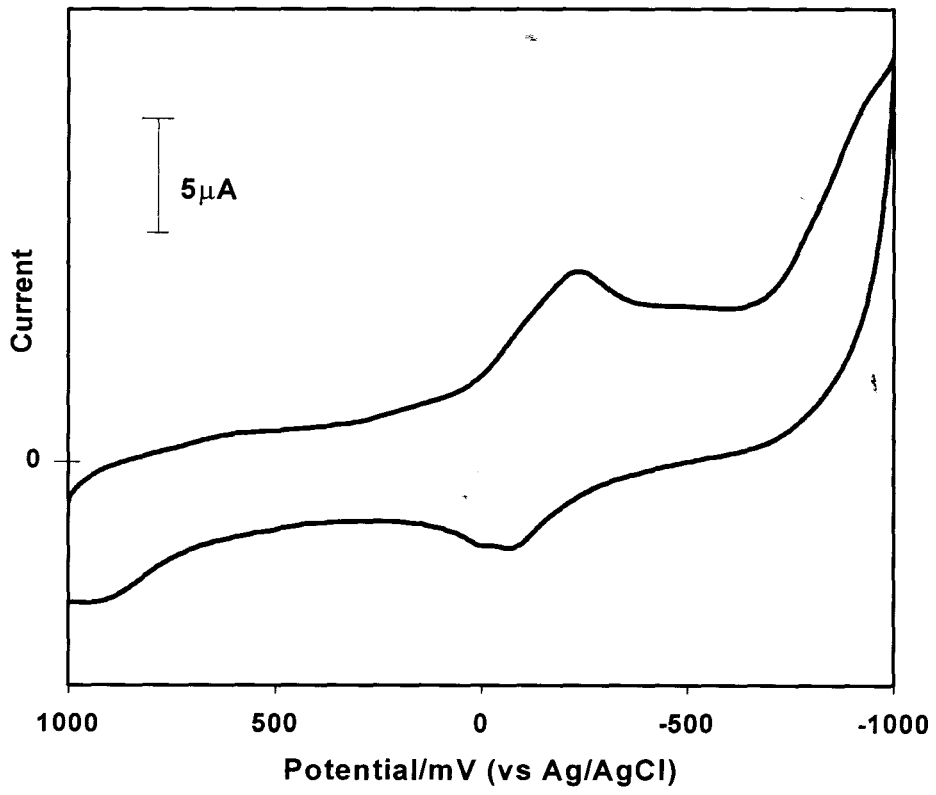

FIGURE 3. 23 Cyclic voltammogram of CoPc-GCE in pH4 buffer. Scan rate = 100 mV s^{-1}

Reduction peaks observed for adsorbed CoPc have been assigned to Co^{III}/Co^{II} and Co^{II}/Co^{I}.[110]

On addition of 7.0×10^{-4} mol dm^{-3} NO solution to the buffer solution, there was a significant increase in the CoPc reduction peak current due to reduction of NO. When an unmodified GCE was used under pH 4 buffer conditions, a very small NO reduction peak was observed at about –0.6 V, Figure 3.24(a). On a CoPc modified electrode, catalytic NO reduction current rose sharply from about -0.6 V and showed a reduction peak at -0.93 V. The catalytic currents observed in Figure 3.24(b), for NO on CoPc-GCE, were much higher than the reduction currents observed for NO of the same concentration, on an unmodified glassy carbon electrode, Figure 3.24(a). This large increase in the CoPc reduction currents is diagnostic of catalytic reduction of NO, even though the reduction potential for NO occurs at more negative values on CoPc-GCE. However the rise in currents start at –0.6 V.

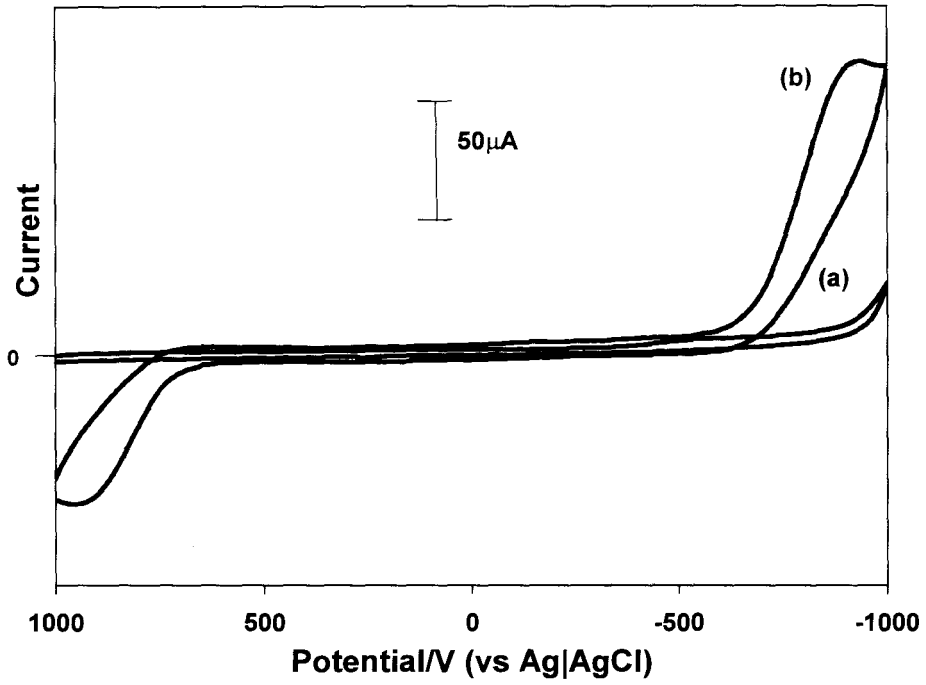

FIGURE 3.24 Cyclic voltammograms of NO (7.0×10^{-4} mol dm^{-3}) on (a)unmodified glassy carbon electrode and (b) on CoPc modified glassy carbon electrode in pH 4 buffer. Scan rate = 100 mV s^{-1}.

The reduction currents at -0.93 V increased linearly with increase in the concentration of NO, Figure 3.25(a). The plot of square root of scan rate versus catalytic currents was also linear confirming a diffusion controlled process, Figure 3.25 (b). The NO reduction peak on a glassy carbon electrode modified with CoPc has been reported at - 0.8 V in a citric acid-hydrochloric acid solution,[129] which is less negative than was observed under the conditions employed in this work. The catalytic currents did not decrease significantly with subsequent scan on the same CoPc-GCE, indicating that the electrode was not deactivated by the adsorption of the reduction products.

Catalytic currents were also observed for the oxidation of NO on CoPc-GCE, with a peak at 0.94 V *vs* Ag/AgCl. The catalytic currents increased with increase in NO concentration. The NO oxidation was observed as a weak and broad peak at 1.1 V on an unmodified electrode in pH 4 buffer. The lowering of the NO oxidation potential and the enhancement in currents are a clear indication of the catalytic oxidation of NO.

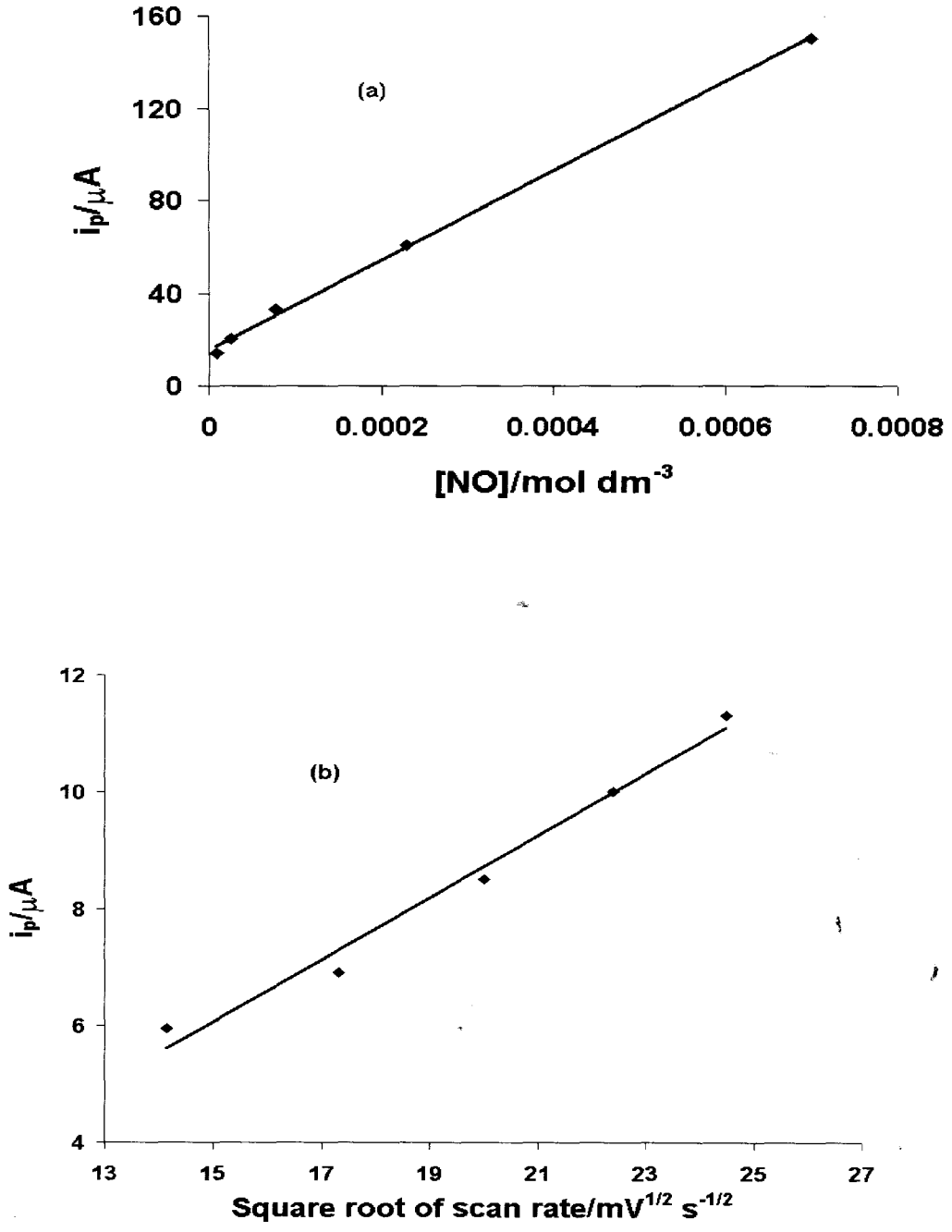

FIGURE 3.25 (a) Plot of [NO] *vs* catalytic currents for the reduction of NO on CoPc-GCE. Electrolyte = pH 4 buffer and the scan rate = 100 mV s^{-1} (b) Plot of square root of scan rate *vs* catalytic reduction currents.

3.5.2 Cobalt tetrasulfophthalocyanine as a catalyst.

For electrocatalytic reactions, a glassy carbon electrode modified with $[Co(II)TSPc]^{4-}$, represented as (CoTSPc- GCE) was employed as a working electrode. The glassy carbon electrode was modified by anodic electrodeposition from a 1 x 10^{-3} mol dm^{-3} solution of $[CoTSPc]^{4-}$ in DMF containing 0.1 mol dm^{-3} TEAP as an electrolyte, as reported before.[148] The deposition was carried out by scanning repetitively at 100 mV s^{-1} between –1.2 V and 1.4 V *vs* $Ag|Ag^{+}$ (non-aqueous) Figure 3.26. However on transferring the modified electrode to a pH 4 buffer solution, the reduction currents of adsorbed $[CoTSPc]^{4-}$ were very weak and did not contribute significantly to the peak currents in Figure 3.27(b).

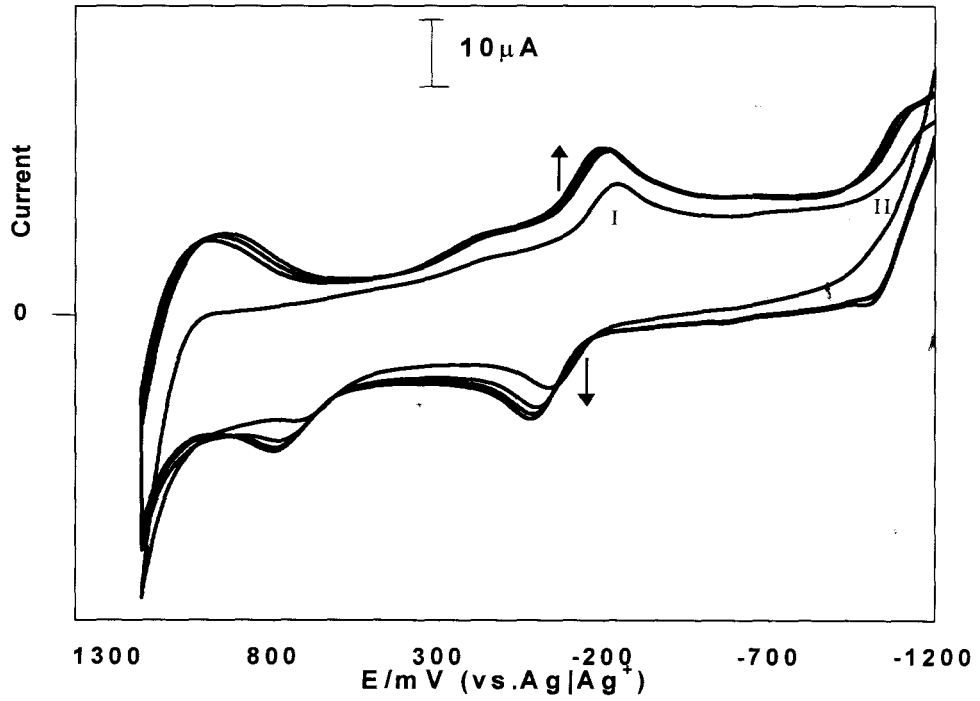

FIGURE 3. 26 Cyclic voltammogram of $[CoTSPc]^{4-}$ in DMF and TEAP electrolyte, showing repetitive scanning for electrodeposition onto a GCE. Scan rate = 100 mV s^{-1}.

The couples labelled I and II are assigned to metal and ring reduction in $[Co(II)TSPc]^{4-}$ with the formation of $[Co(I)TSPc(-2)]^{5-}$ and $[Co(I)TSPc(-3)]^{6-}$ respectively. These reductions were observed at more negative potentials in water containing Na_2SO_4, Figure 3.12(a).

Typical cyclic voltammograms for the reduction of NO on an unmodified GCE and on a GCE modified with $[Co(II)TSPc]^{4-}$ in pH 4 buffer solution are shown in Figure 3.27. On CoTSPc-GCE, a catalytic peak was observed at -0.96 V *vs* Ag | AgCl for the reduction of NO, Figure 3.27(b). The voltammogram for the reduction of NO on unmodified GCE is shown in Figure 3.27(a), a broad peak was observed at –0.6 V as discussed in Section 3.5.1.

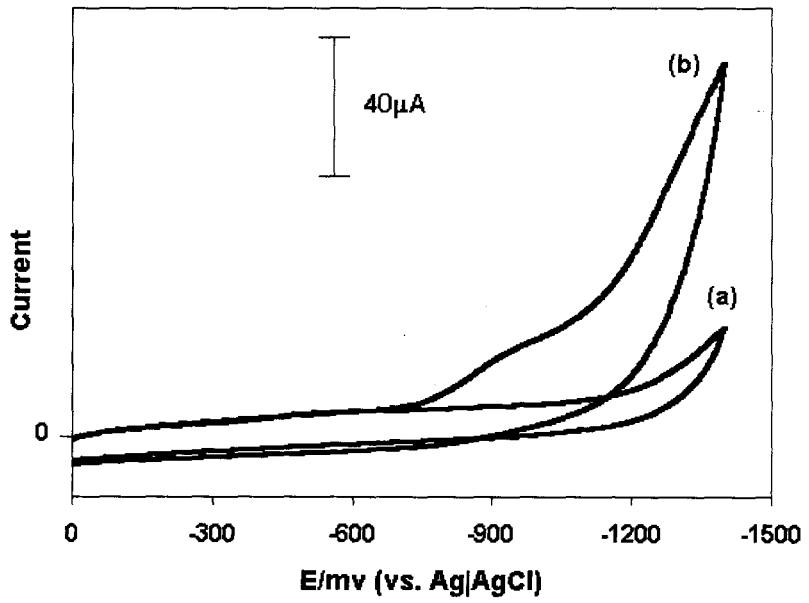

FIGURE 3. 27 Cyclic voltammogram for the reduction of 1.0 x 10^{-5} mol dm^{-3} NO on (a) unmodified GCE and (b) CoTSPc-GCE. Scan rate = 100 mV s^{-1} in pH 4 buffer.

The reduction currents for NO observed on GCE modified with $[Co(II)TSPc]^{4-}$ are much higher than the currents observed for the reduction of the same concentration of NO on an unmodified GCE. The peak currents for the reduction of NO on GCE modified with $[Co(II)TSPc]^{4-}$ increased with an increase in NO concentration as shown in Figure 3.28(a). A plot of the square root of scan rate versus catalytic currents was linear implicating a diffusion controlled process, Figure 3.28(b). The modified electrode showed stability towards the reduction of NO in that the currents did not decrease appreciably with scan number. The peak at - 0.96 V *vs* Ag | AgCl as shown in Figure 3.27 is almost at the same potential as that observed for reduction of NO (- 0.93 V) on CoPc modified glassy carbon electrode in pH 4, as discussed above (Section 3.5.1). The observation of the enhancement in currents of the NO reduction peak when CoTSPc-GCE is used, is a clear indication of catalytic behaviour of $[CoTSPc]^{4-}$.

The pH of the media plays an important role in the catalytic reduction or oxidation of NO. The peak for the catalytic reduction of NO on a GCE varied with pH; in pH 4 buffer NO reduction was observed at –0.6 V; in water containing sodium sulfate it was observed at - 1.2 V; and in pH 7 at -1.1 V *vs* Ag | AgCl.

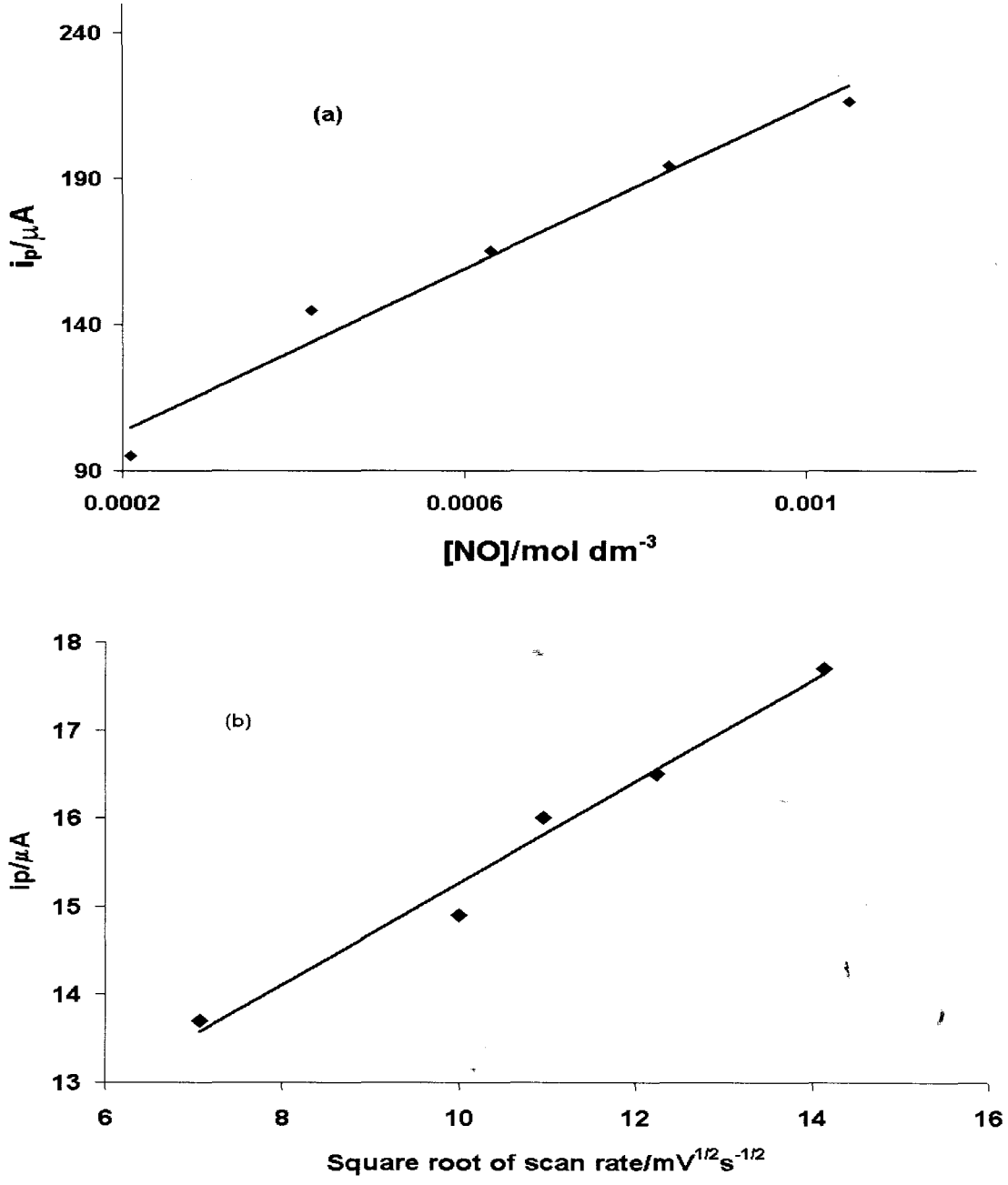

FIGURE 3.28 (a) Plot of variation of the catalytic currents for reduction of NO on CoTSPc – GCE *vs* [NO], scan rate = 100 mV s^{-1}. (b) Square root of scan rate *vs* catalytic currents for reduction of NO in pH 4 buffer.

The cyclic voltammograms for the oxidation of NO in pH4 buffer, on an unmodified GCE and on GCE modified with $[CoTSPc]^{4-}$ are shown in Figure 3.29. There is a considerable enhancement in the oxidation currents of NO when GCE is modified with $[Co(II)TSPc]^{4-}$ compared with unmodified GCE. A weak broad peak at pH 4 is observed for NO on unmodified GCE near 1.1 V as noted above (Section 3.5.1). On CoTSPc-GCE, the oxidation peak for NO is well resolved and observed at 1.08 V. The enhancement in oxidation currents when CoTSPc-GCE is employed shows that the $[Co(II)TSPc]^{4-}$ species acts as a catalyst for the oxidation of NO. The currents for the oxidation of NO on CoTSPc-GCE increased with increase in NO concentration as shown in Figure 3.30. The lowest concentration of NO that could be determined using either the oxidation or reduction of NO on CoTSPc-GCE was of the order of 10^{-9} mol dm^{-3}.

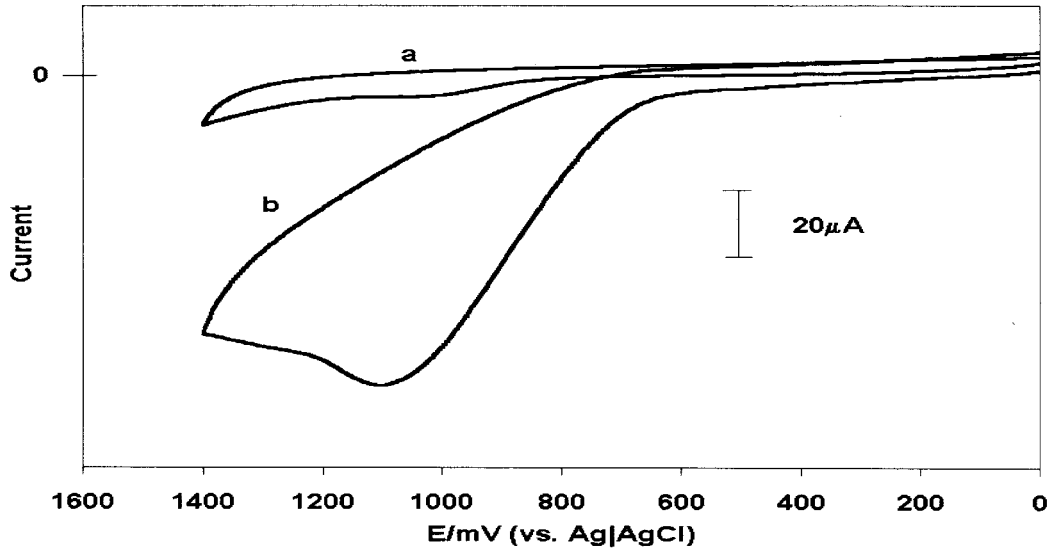

FIGURE 3. 29 Cyclic voltammogram for the oxidation of 2.1 x 10^{-4} mol dm^{-3} NO on unmodified GCE and (b) CoTSPc-GCE. Scan rate = 100 mV s^{-1}. pH 4 buffer.

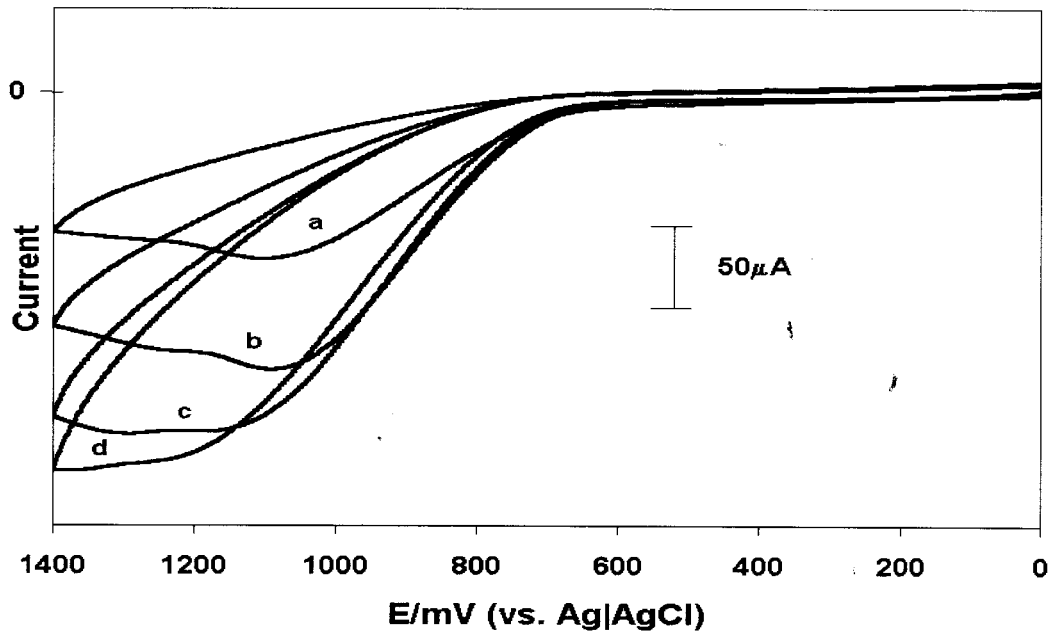

FIGURE 3. 30 Cyclic voltammograms of CoTsPc – GCE in the presence of increasing concentrations of NO (a) 2.1 x 10^{-4} mol dm^{-3} (b) 4.2 x 10^{-4} mol dm^{-3} (c) 6.3 x 10^{-4} mol dm^{-3} (d) 8.4 x 10^{-4} mol dm^{-3}. pH 4 buffer. Scan rate = 100 mV s^{-1}.

3.5.3 Aluminium tetrasulfophthalocyanine as a catalyst.

The GCE was modified with $[ClAlTSPc]^{4-}$ by electrodeposition from a 1 x 10^{-3} mol dm^{-3} solution in water containing sodium sulfate as an electrolyte.[148] The deposition was done by repetitive scanning at 100 mV s^{-1} between –1.4 V and 0.1 V *vs* Ag|AgCl, in a similar manner to $[CoTSPc]^{4-}$, Figure 3.26 above. For reproducibility, 30 scans were recorded, however it was observed that after 25scans, there was no further change in the amplitude of the peaks.

The cyclic voltammogram for the oxidation of NO on an unmodified GCE and on a GCE modified with $[ClAlTSPc]^{4-}$, (AlTSPC-GCE) are shown in Figure 3.31. When AlTSPc-GCE is used, there is an increase of the oxidation current compared to that observed on an unmodified GCE, Figure 3.31(a). On an unmodified electrode, a broad peak of NO oxidation was observed at 1.0 V (Section 3.4.3) in water and Na_2SO_4 electrolyte whilst, with AlTSPc-GCE the catalytic peak is observed at 0.96 V. The modified MPc electrode slightly reduces the oxidation potential whilst it enhances the oxidation current. As in solution catalysis, there was a linear increase of the catalytic oxidation current with an increase in the concentration of NO, Figure 3.32(a). The lowest concentration of NO that could be determined was of the order of 10^{-9} mol dm^{-3}. The system is diffusion controlled as indicated by the linearity of the square root of the scan rate plot versus catalytic currents, Figure 3.32(b). There was no significant enhancement in currents that were observed for the reduction of NO on AlTSPc-GCE. Reactions in pH 4 buffer solutions did not show any catalysis.

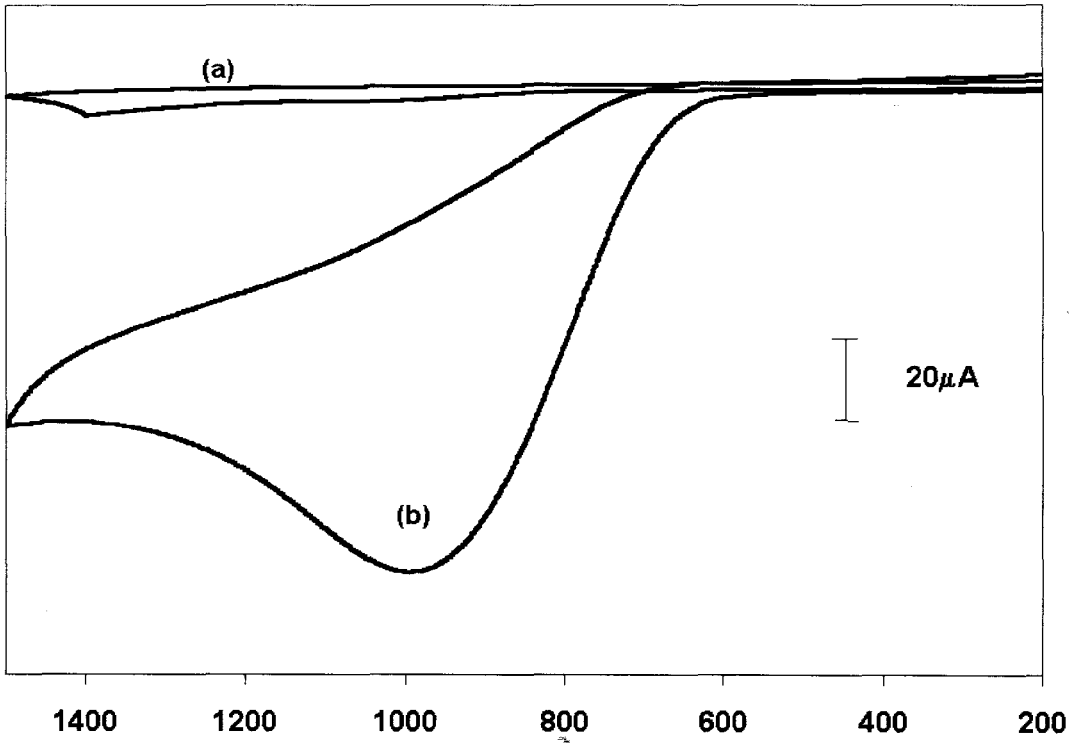

FIGURE 3. 31 Cyclic voltammogram of the oxidation of 7.5 x 10^{-2} mol dm^{-3} NO on (a) unmodified GCE and (b) on AlTSPc-GCE in water and Na_2SO_4. Scan rate = 100mV s^{-1}.

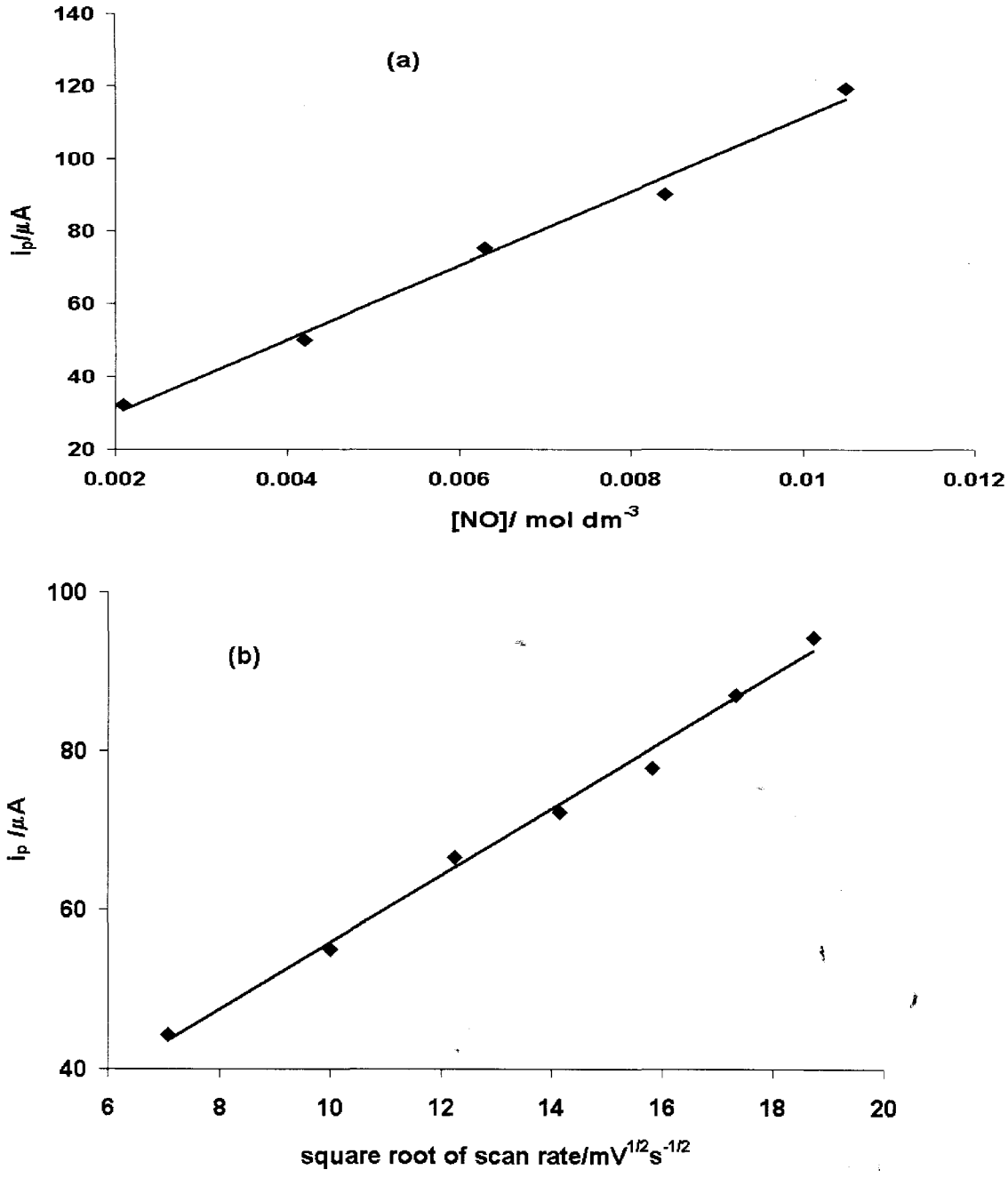

FIGURE 3. 32 Plot of (a) concentration of NO *vs* oxidation catalytic currents on AlTSPc- GCE, (b) square root of scan rate *vs* catalytic currents. Electrolyte = Na_2SO_4.

3.6 Analysis of reduction products.

A solution of NO (2.1 x 10^{-3} mol dm^{-3}) in pH 4 buffer was electrolysed at the catalytic reduction potential, -0.95V for CoPc and –0.96 V for $[CoTSPc]^{4-}$. For CoPc, a carbon rod (0.2 cm^2) modified by drop dry method, from a pyridine solution of CoPc was used as a working electrode (CoPc-GCE). For $[CoTSPc]^{4-}$, a GCE was modified by electrodeposition in DMF solution of $[CoTSPc]^{4-}$as explained in Section 3.5.2 and was employed as a working electrode. Electrolysis on CoPc-GCE was carried out in two hours, whilst for CoTSPc-GCE, six hours was required since the electrode surface was smaller. At the end of electrolysis, the charge Q was noted, the solution was sampled and tested for ammonia and hydroxylamine as described in Section 2.4.2.2. The current decreased exponentially with time. From equation 1.30, (Q = nFvC) n, the number of moles of electrons involved in the reduction process, was calculated and found to be 5. Since reduction of NO to ammonia requires five electrons, the value of n =5 confirmed that NH_3 was one of the reduction products of NO. For CoPc, analysis of the solution (see Section 2.3.2) following bulk electrolysis gave a 35% yield of ammonia (with respect to NO) after two hours of electrolysis of 10 cm^3 solution. Trace amounts of hydroxylamine were also detected. For $[CoTSPc]^{4-}$, analysis of the solution obtained following bulk electrolysis confirmed the presence of ammonia with yields of about 25%. The current efficiency for ammonia production was determined to be 89%. As in CoPc, traces of hydroxylamine were also found.

CHAPTER FOUR: DETECTION OF NO USING CYANOCOBALAMIN

4.1 Homogeneous catalytic studies

4.2 Spectroelectrochemical studies

4.3 Heterogeneous catalytic studies

4.4 Product analysis

4. DETECTION OF NO USING CYANOCOBALAMIN.*

Vitamin B_{12} derivatives have been shown to have similar catalytic activity as cobalt (II) tetrasulfophthalocyanine.[57] Many reactions that are catalysed by $[CoTSPc]^{4-}$ are also catalysed by vitamin B_{12} derivatives. These reactions include the oxidation of hydrazine,[58,149] alkyl halides, [150,151,152,153] dioxygen[154] and cysteine.[155] Hence, in this work catalytic behaviour of cyanocobalamin ($VitB_{12}$) towards the detection of NO is studied.

4.1. Homogeneous catalytic studies.

For homogeneous studies, cyanocobalamin was dissolved in buffer (pH 4 or pH 9) and solutions of known concentration of NO in the appropriate buffer were added. The electrochemistry of cyanocobalamin is well known.[66] As mentioned earlier (Section 1.4) it has been reported that there is a correlation between the rate of electron transfer for the conversion of Co(III) to Co(II) of the cobalamins and the strength of the axial ligand-cobalt bond. Electron transfer is more difficult for strong coordinating ligands.[65] The presence of strong axial ligands such as CN^-, has been shown to induce large negative shifts of the Co^{III}/Co^{II} reduction in cyanocobalamin, resulting in the merger of Co^{III}/Co^{II} and Co^{II}/Co^{I} reduction couples and hence, in a direct two-electron reduction of Co^{III} to Co^{I}.[66] In other forms of cobalamins with weaker coordinating ligands, such as aquacobalamin, the two reduction waves are well separated.[150]

* The work presented in this chapter has been published in the following journal and it is not referenced in this thesis; S.L. Vilakazi and T.N. Nyokong, Electrochim. Acta., **46**, 2000, 453.

pH 9 Studies.

For these studies, NO solutions were prepared from NO gas as described in Section 2.3.

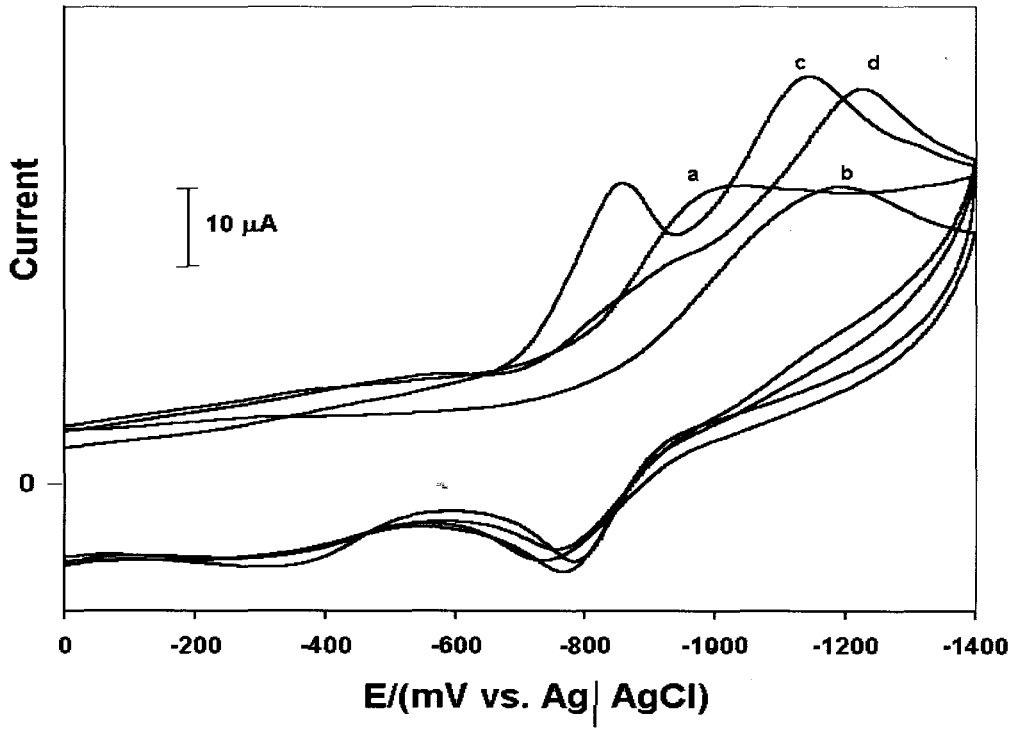

Figure 4. 1 Cyclic voltammogram of $VitB_{12}$ at pH 9 buffer; (a) in the absence of NO; (b) in the presence of 6.0 x 10^{-4} mol dm^{-3} NO; (c) in the presence of 8.0 x 10^{-4} mol dm^{-3} NO; (d) in the presence of 1.7 x 10^{-3} mol dm^{-3} NO. Scan rate = 100 mV s^{-1}.

Figure 4.1(a) shows the cyclic voltammogram of $VitB_{12}$ in pH 9 buffer. A reduction peak is observed at - 1.00 V *vs* Ag | AgCl. The corresponding anodic peak is much smaller than the forward (cathodic) peak. The reduction is associated with the one-step two-electron reduction of the Co^{III} center to Co^{I}.[66] Addition of NO to solutions containing $VitB_{12}$ results first in a shift of the cathodic peak due to the reduction of

$VitB_{12}$, from -1.00 V to -1.20 V, without significant changes in the magnitudes of the reduction currents, Figure 4.1(b). This suggests that the number of electrons involved in the reduction of $VitB_{12}$ in the presence of NO is similar to that for $VitB_{12}$ alone. The absence of a significant increase in the magnitudes of the peak currents on addition of NO shows the lack of catalytic activity at this stage. There is only a small shift in the potential in the return peak following addition of NO to $VitB_{12}$. The observation of a shift in the reduction peak of $VitB_{12}$ on addition of NO, suggests that the complex being reduced is an adduct between NO and $VitB_{12}$, which is represented here as $VitB_{12}(NO)$.

As indicated in the introduction, there have been conflicting reports concerning the coordination of NO to aquacobalamin ($VitB_{12a}$). Some studies have reported the formation of a $VitB_{12r}$ (NO) complex, whereas some reports have suggested that NO does not coordinate to cobalamin (Cbl) but that it reacts with the superoxo complex of Cbl, which is always present in aerated solutions of Cbl.[61] However, solutions employed for cyclic voltammetry in this work were de-aerated with nitrogen prior to use and an atmosphere of nitrogen was maintained throughout the cyclic voltammetry scans. The shift in the reduction peak observed for $VitB_{12}$ in the presence of NO, Figure 4.1(b), shows that a new complex is being reduced, this complex is most likely an adduct between NO and $VitB_{12}$.

An increase in the concentration of NO over that employed in Figure 4.1(b), resulted in the observation of a new reduction peak at - 0.86 V and the shifting of the peak at - 1.20 V to -1.15 V *vs* Ag | AgCl, Figure 4.1(c). This splitting of the reduction peak was observed when concentrations of NO were greater or equal to 8×10^{-4} mol dm^{-3} for $VitB_{12}$ concentrations of 1.4×10^{-4} mol dm^{-3}. The reduction peak for NO in the

absence of $VitB_{12}$ catalyst was observed at - 0.97 V in pH 9 buffer. The same peak was observed at –0.6 V (Section 3.5.1) at pH 4, hence there is a shift to more negative values at pH 9. The splitting in the reduction peaks of $VitB_{12}$ in the presence of NO and the fact that the currents of the split peaks are more enhanced than for the reduction of $VitB_{12}$ in the absence of NO (and after the initial addition of NO), suggests that catalytic reduction of NO by $VitB_{12}$ occurs at this stage. A splitting in the reduction peaks of $VitB_{12}$ in the presence of oxygen was also attributed to the catalytic behaviour of $VitB_{12}$ towards electroreduction of O_2.[154]

Addition of large amounts of NO (>1.3 x 10^{-3} mol dm^{-3}) resulted in the disappearance of the less negative peak at - 0.86 V and the shifting of the second peak to - 1.23 V, without much reduction in intensity, Figure 4.1(d). Similar changes in the cyclic voltammograms were observed on addition of varying amounts of cyanide to $VitB_{12}$.[66] These authors showed that on addition of small amounts of cyanide, there was a splitting of the reduction peak and the shifting to more negative potentials. This splitting into two one-electron reduction waves on addition of cyanide to cyanocobalamin was described as a stepwise reduction of the central Co^{III} to Co^{II} and finally to Co^{I}. It is suggested here that the split peaks observed on addition of increasing amounts of NO, Figure 4.1(c), are a result of a stepwise reduction of Co^{III}. Figure 4.1(d) shows that the currents for the less negative reduction peak (at -0.86 V) decreased with increase in NO concentrations. There were no significant enhancements in the return peak as the NO concentration increased. It has been reported before that the shape and location of the reduction peaks of $VitB_{12}$ may depend on the history of the glassy carbon electrode.[66] The cyclic voltammograms shown in Figure 4.1 were however found to be reproducible. Based on the above

observations, the following mechanism is suggested for the catalytic reduction of NO, Scheme 4.1.

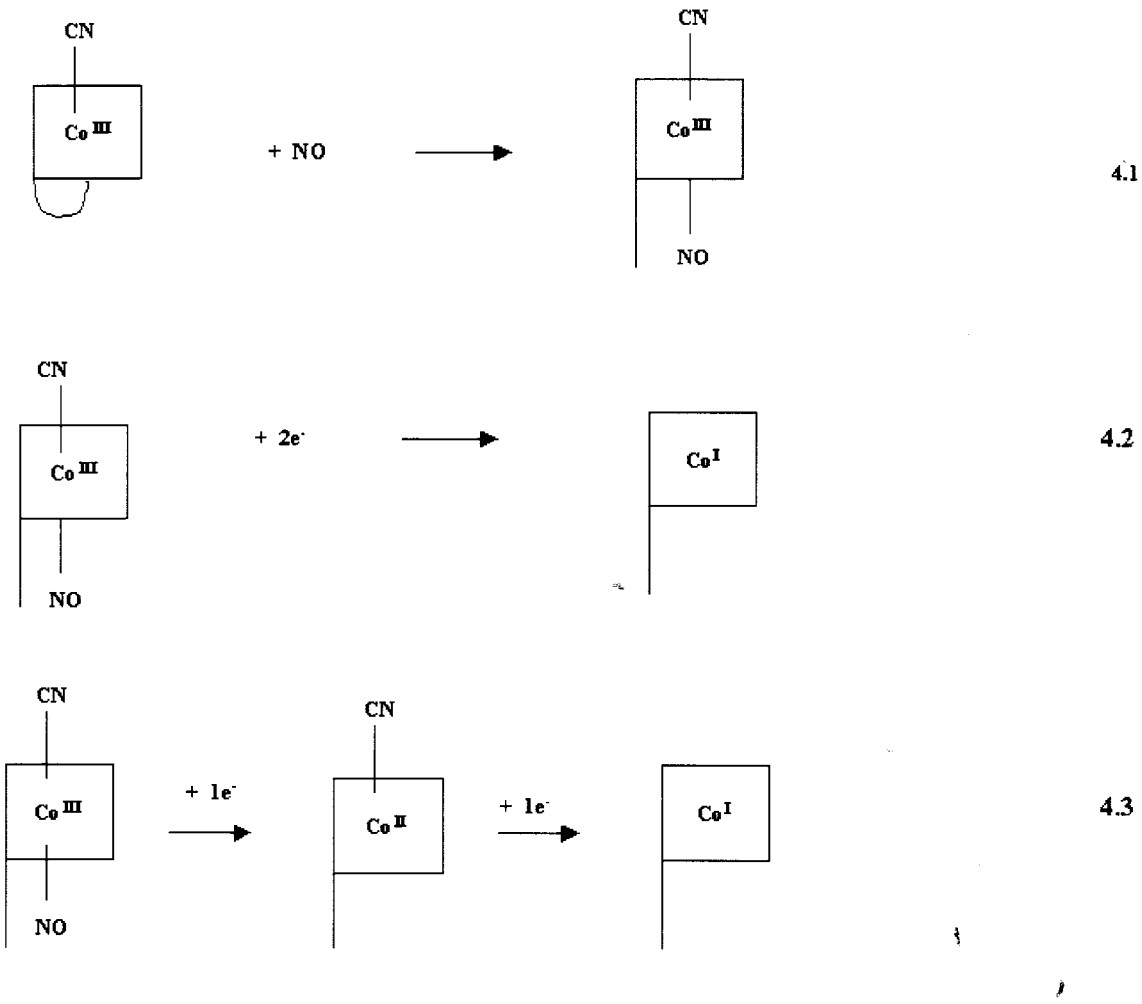

Scheme 4. 1 Proposed mechanism for the interaction of NO with $VitB_{12}$.

The first step in the proposed mechanism is the cleavage of the 5,6 - dimethylbenzimidazole-Co^{III} bond, followed by the possible coordination of NO to $VitB_{12}$ forming a $VitB_{12}(NO)$ adduct, according to equation 4.1. This would account for the initial shift in the cyclic voltammogram on addition of small amounts of NO.

However, no significant spectroscopic changes on addition of NO to $VitB_{12}$ solutions were observed, suggesting that the adduct between NO and $VitB_{12}$ is only stable on the cyclic voltammetry time scale. Cleavage of the 5,6-dimethylbenzimidazole ligand from the axial position normally occurs on coordination of axial ligands to Co^{III} cobalamins.[66] The complex formed in equation 4.1 is then reduced by direct one step two-electron transfer (equation 4.2) at more negative potentials than for $VitB_{12}$ in the absence of NO, Figure 4.1(b). It is important to note that the most stable form of Co^{I} cobalamins is four-coordinate,[65] hence it is likely that the axial ligands are lost upon reduction, as shown in equation 4.2. The splitting of the reduction peaks on further addition of NO is attributed to the consecutive one-electron reduction of Co^{III} to Co^{II} and then to Co^{I}, according to equation 4.3. Co^{II} cobalamins favour a five-coordinate environment hence, it is expected that one of the axial ligands will be lost on reduction. Earlier studies have shown that the axial ligands may be replaced by the solvent.[66] It is thus likely that the shift in the reduction peak to more negative reduction potentials as shown in Figure 4.1(d) reflects changes in the axial ligand. At pH 9, the hydroxide ion rather than the solvent, is most likely to coordinate to the axial position. Both the Co^{I} and Co^{II} complexes formed by equation 4.3 then catalyse the reduction of NO with the formation of products such as ammonia, as will be demonstrated below. The decrease in the currents of the first reduction peak and increase in the second, more negative reduction peak on addition of large concentrations of NO reflects the better catalytic activity of Co^{I} versus the Co^{II} complex.

pH 4 studies using NO_2^- as a source of NO.

As indicated in Section 2.3 it is known that nitrite disproportionates to form nitric oxide and nitrate. At pH 4, about 43% of NO_2^- disproportionates into NO, providing an adequate amounts of NO for electrocatalytic studies.[101] For studies at pH 4, a solution of 0.05 mol dm^{-3} $NaNO_2$ was employed as a source of NO. Cyclic voltammograms of $VitB_{12}$ at pH 4 in the absence and presence of NO_2^- (1.0×10^{-2} mol dm^{-3}) are shown in Figure 4.2. Figure 4.2(b) shows the cyclic voltammogram of NO (from NO_2^-) in pH 4 buffer in the absence of $VitB_{12}$. A broad peak is observed near - 1.20 V. As discussed in Chapter 3 (Section 3.5.2), the peak for the reduction of NO on GCE depends on the medium. In pH 4 and pH 9 solutions, using dissolved NO gas, this peak was observed at –0.60 V and –0.97 V, respectively. The observation of this peak at –1.20 V when nitrite is used as a source of NO, represents a significant shift. This shift is probably due to the medium but could also be attributed to the history of the electrode. The cyclic voltammogram of $VitB_{12}$ in the absence of NO_2^- is shown in Figure 4.2(a). The two-electron broad reduction peak is observed near -1.00 V for $VitB_{12}$. Figure 4.2(c) shows the cyclic voltammogram of $VitB_{12}$ in the presence of NO_2^-. A catalytic peak is observed at -1.22 V. Even though the catalytic peak is observed at approximately the same potentials in the presence and in the absence of $VitB_{12}$, the large enhancement in currents indicates catalytic behaviour.

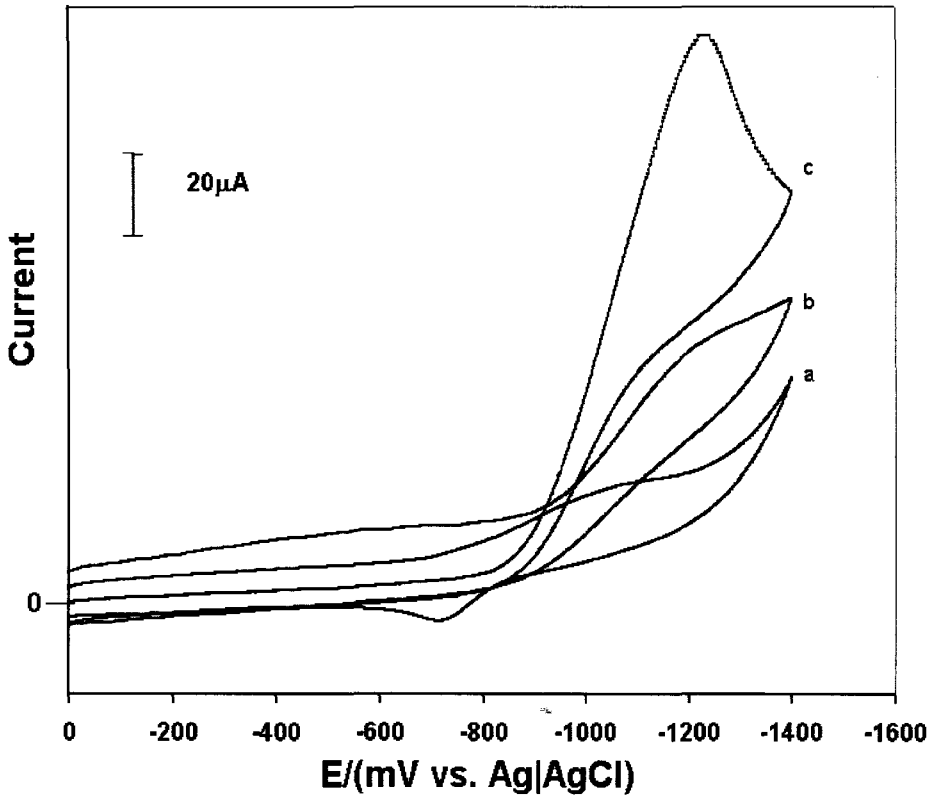

Figure 4. 2 Cyclic voltammogram of (a) $VitB_{12}$ in pH 4 buffer in the absence of NO_2^-; (b) NO_2^- in the absence of $VitB_{12}$; (c) NO_2^- following addition of $VitB_{12}$. Scan rate = 100 mV s^{-1} $[NO_2^-] = 6.0 \times 10^{-4}$ mol dm^{-3}; $[VitB_{12}] = 1.4 \times 10^{-4}$ mol dm^{-3}.

The splitting and shifting in potential of the reduction peaks observed above for pH 9 using NO solutions prepared from NO gas were not observed at pH 4 when NO_2^- was used as a source of NO. However, the splitting was observed at pH 4 when NO solutions were prepared from the NO gas instead of using NO_2^- as a source of NO. The catalytic peak for the reduction of NO (from NO_2^-) at pH 4 was observed at the same potential when NO solutions prepared from NO gas were used instead of using NO_2^- as a source of NO. This observation confirms that it is the catalytic reduction of NO, and not

the other ions in solution, that is observed in Figure 4.2. As mentioned above the presence of strong axial ligands induce large negative shifts of the Co^{III}/Co^{II} reduction potential, causing the merging of Co^{III}/Co^{II} and Co^{II}/Co^{I} couples which gives a direct two-electron reduction in cobalamins. The absence of splitting of the reduction waves when NO_2^- is used as a source of NO suggests that the ions present in solution, NO_2^-, NO and NO_3^-, shift the Co^{III}/Co^{II} reduction couple to negative potentials. This shifting is to such an extent that the individual Co^{II}/Co^{I} and Co^{III}/Co^{II} couples are not observed. Only the direct two-electron reduction is observed under these conditions. The splitting in the reduction peaks was not observed even for very low concentrations of NO_2^- ($<1.0 \times 10^{-4}$ mol dm^{-3}). The fact that the splitting of the peaks that was observed when NO solutions prepared from NO gas (instead of NO from NO_2^-) were used at pH 4, confirms that the presence of other ions (NO_2^-, NO_3^-) in solution affect the direct two-electron reduction of $VitB_{12}$. The currents for the catalytic peak increased linearly with the square root of the scan rate (for scan rates ranging from 50 mV s^{-1} to 200 mV s^{-1}) showing that the catalytic reduction of NO is a diffusion controlled process at these scan rates. The catalytic peak increased linearly with NO_2^- concentration, as shown in Figure 4.3.

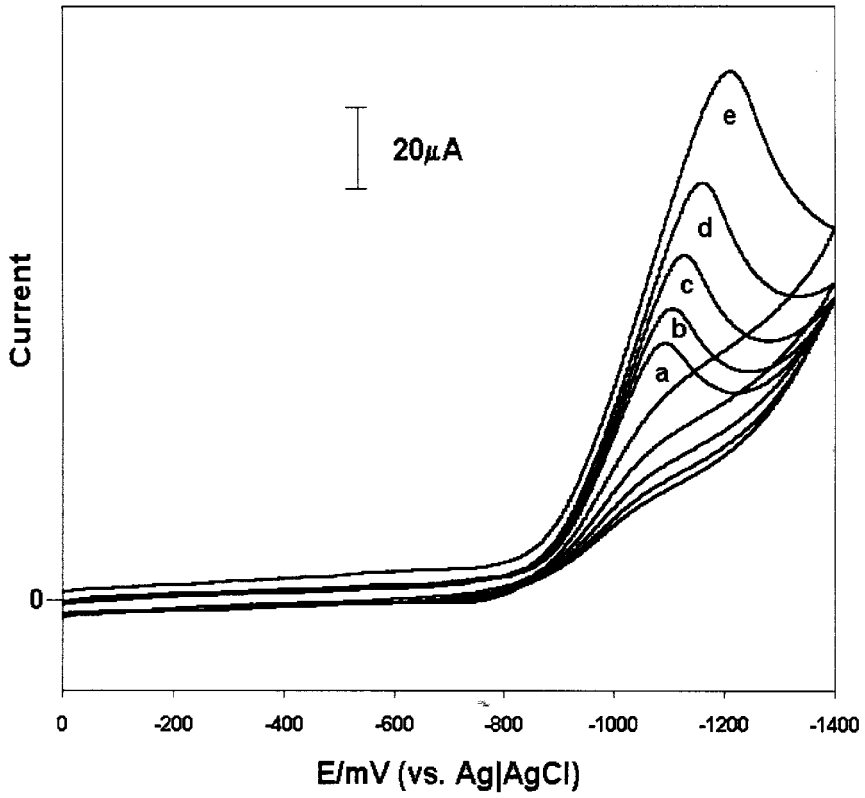

Figure 4. 3 Cyclic voltammograms of NO_2^- in the presence of $VitB_{12}$. $[NO_2^-]$ = (a) 1.5×10^{-4} (b) 2.5×10^{-4} (c) 3.5×10^{-4} (d) 4.5×10^{-4} (e) 6×10^{-4} mol dm^{-3}. Scan rate = 100 mV s^{-1}. pH 4 buffer.

4.2 Spectroelectrochemical Studies.

The spectral changes observed on electrochemical reduction of cyanocobalamin and other cobalamines have been described.[66,150] The electronic absorption peaks for Co^{III} cyanocobalamin were observed at 368 and 580 nm, following the addition of cyanide and in the presence of Na_2SO_4.[66] The Co^{II} and Co^{I} complexes are characterized by peaks at 473 nm and 390 nm, respectively, in aquacobalamin.[150] Spectro-electrochemistry of $VitB_{12}$ in pH 4 buffer and using the OTTLE cell, at potentials slightly more negative than the reduction peak (-1.2 V) of $VitB_{12}$ gave spectral changes shown in Figure 4.4. The absorption spectral peaks due to the Co^{III} cyanocobalamin species were observed at 550 and 361 nm before electrolysis. Following electrolysis in the OTTLE cell for 20 minutes the peaks due to the Co^{III} cyanocobalamin species decreased in intensity, a new peak developed at 482 nm, and the resolution of the peak at 307 nm improved.

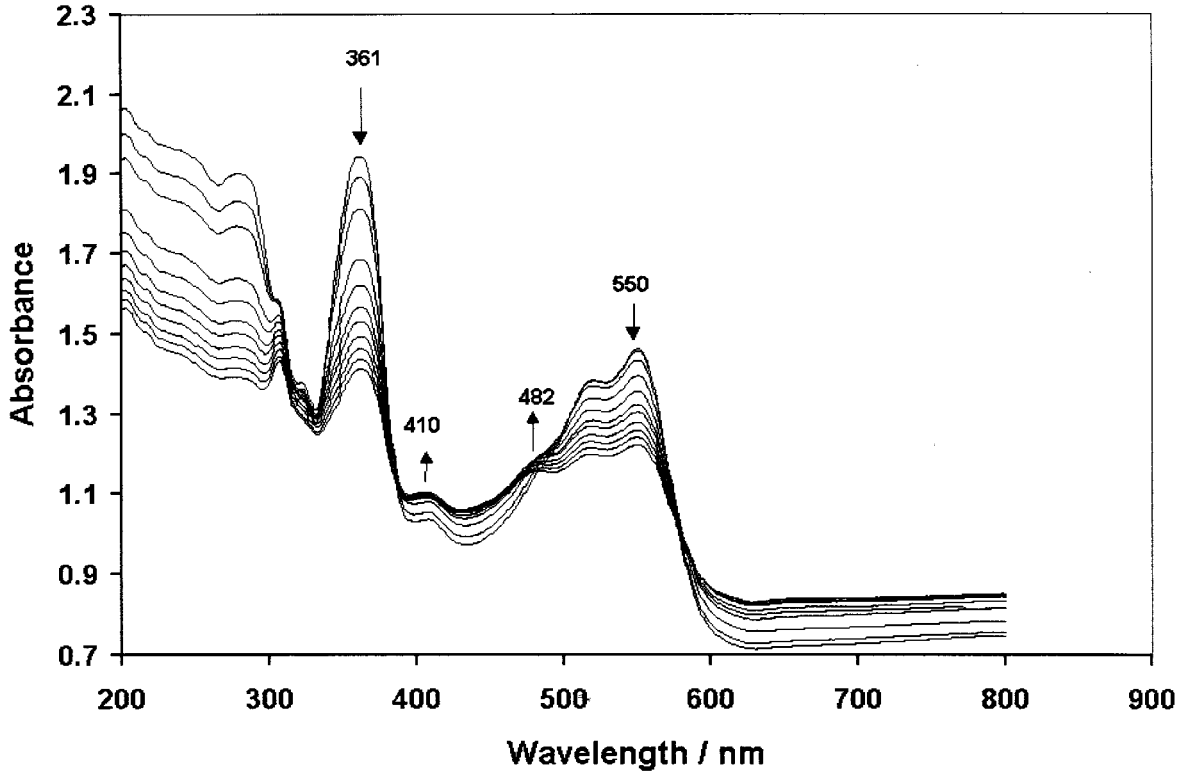

Figure 4. 4 Electronic absorption spectral changes observed on electrolysis of $VitB_{12}$ in pH 4 buffer at the potential of the reduction peak (-1.2 V *vs* Ag|AgCl).

In comparison with the literature, these spectral changes are associated with the formation of the Co^{II} complex. An enhancement in the shoulder near 410 nm is indicative of a transition from protonated base-off to unprotonated base-on in Co^{II} cyanocobalamin complexes.[66] The peak associated with the formation of Co^{I} species (near 387 nm) was not observed. The number of moles of electrons was calculated to be n = 1.1 ± 0.1, showing that one mole of electrons was transferred during the electrolysis. Thus one-electron reduction was observed following electrolysis under thin layer conditions,

whereas in cyclic voltammetry, a direct two-electron reduction was observed. There have been contradictory reports on the mode of reduction of $VitB_{12}$ on various electrodes. There have been reports of the reduction of $VitB_{12}$ by two one-electron reduction steps from Co^{III} to Co^{II} to Co^{I} on a GCE,[154] while as mentioned above, direct two-electron reduction of Co^{III} to Co^{I} on a GCE has been reported by some authors,[66] however, different electrolytes were used. The use of different types of electrodes has also been shown to influence the observation of a direct two-electron reduction of $VitB_{12}$ as opposed to two one-electron reduction steps.[66,151,156] Thus, the observation of a direct two-electron reduction of $VitB_{12}$ is dependent on the experimental conditions. The cyclic voltammetry studies reported in Figure 4.1 were recorded on a GCE whereas, the OTTLE studies were carried out using a platinum grit working electrode. The observed differences in the number of electrons transferred when the OTTLE was used and when cyclic voltammetry on a GCE was employed, could be a result of the differences in the cell conditions.

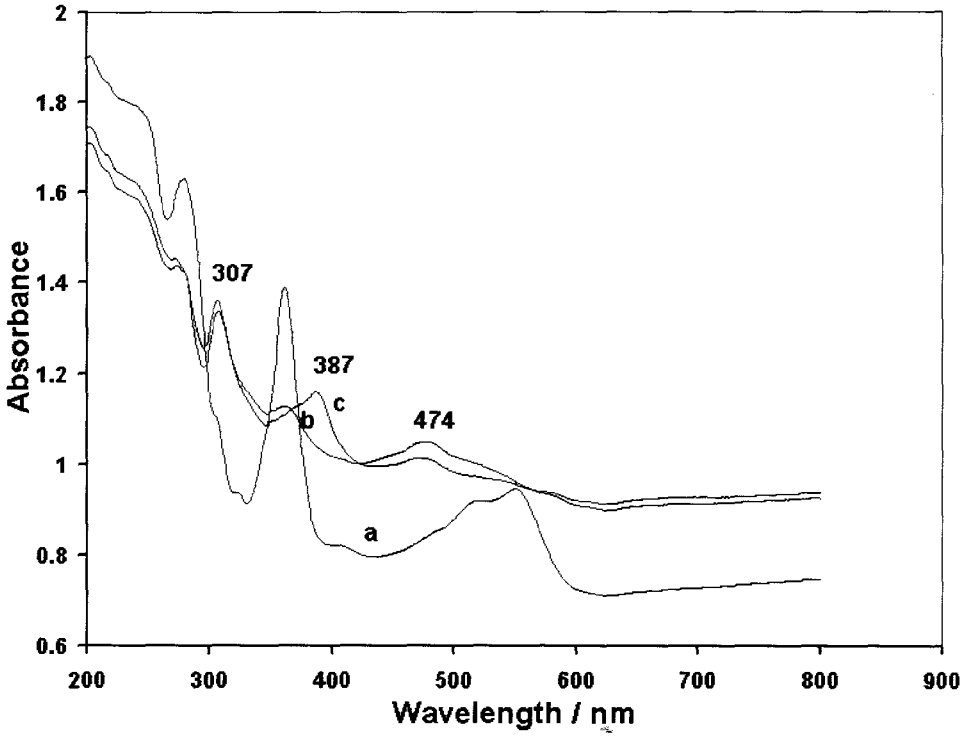

Figure 4. 5 Spectral changes observed during electrolysis (at - 1.2 V *vs* Ag | AgCl) of $VitB_{12}$ in the presence of NO_2^- and in pH 4 buffer (0.05 mol dm^{-3}) at potentials of the reduction peak (-1.2 V *vs* Ag|AgCl). [$VitB_{12}$] = 1.4 x 10^{-4} mol dm^{-3}. Spectra (a) before; (b) after 5 min; (c) after 20 min of electrolysis

Figure 4.5 shows spectral changes observed during electrolysis (at –1.2 V *vs* Ag|AgCl) of $VitB_{12}$ in the presence of NO_2^- and in pH 4 buffer. There was a general increase in the background on addition of NO. The absorption bands observed at 550 and 361 nm for $VitB_{12}$ before electrolysis, decreased in intensity and new bands were observed at 474 and 307 nm after five minutes of electrolysis. These bands are

characteristic of the Co^{II} cyanocobalamin complex and were observed for the electrolysis in the absence of NO_2^- as discussed above (Figure 4.4). The band at 474 nm was however observed at 482 nm in the absence of NO_2^-, suggesting an axial ligand exchange or loss in the presence of NO_2^-, and hence, resulting in a shift in the absorption peak. Since Co^{II} complexes are five-coordinate, a loss of the CN from Co^{III} (Scheme 4.1) would occur.

Comparison of the IR spectra before and after electrolysis to the point of formation of mainly the Co^{II} species (as depicted by spectral changes shown in Figure 4.5(b)) showed that the vibration peak due to bound CN^-, observed at 2370 cm^{-1} before electrolysis, was still present following the formation of the Co^{II} species. This suggests that it is not the CN ligand that is lost upon formation of the Co^{II} species, leaving the possibility of the loss of NO. The 387 nm peak observed after a longer electrolysis time [Figure 4.5(c)] is characteristic of the Co^{I} species. The number of moles of electrons transferred following electrolysis of $VitB_{12}$ in the presence of NO_2^- was n = 4, implying catalytic reduction of NO in addition to reduction of $VitB_{12}$.

4.3 Heterogeneous catalytic studies.

For heterogeneous electrocatalytic reactions, a glassy carbon electrode (GCE) modified with cyanocobalamin (represented as GCE-VitB_{12}) was employed as a working electrode. The GCE was modified with VitB_{12} by the electrodeposition method as discussed for $[CoTSPc]^{4-}$ electrodeposition, Section 3.5.2. The deposition was carried out by scanning a solution containing VitB_{12} in pH 9 buffer repetitively from -1.4 to -0.2 V *vs* Ag | AgCl at a scan rate of 100 mV s^{-1}. For reproducibility, 25 scans were used for each coating of the electrode. The surface coverage was calculated to be $\Gamma = 1.7 \times 10^{-12}$ mol cm^{-2} from the charge under the cathodic curve. The electrode coated in this manner was found to be highly effective for the catalytic oxidation or reduction of NO. Prior to coating with the VitB_{12} complex, the GCE was polished with alumina (<10 μm) on a Buehler felt pad, followed by soaking in dilute nitric acid and rinsing in water.

When the GCE modified with VitB_{12} by electrodeposition was used for the cyclic voltammetry of NO_2^- at pH 4, there was considerable enhancement in the reduction currents of NO when compared to the reduction of the same NO concentration on unmodified GCE, Figure 4.6. This shows that VitB_{12} catalyses the reduction of NO. As mentioned above, at low pH, NO is formed as a result of the disproportionation of NO_2^-. The catalytic reduction peak was observed at - 1.19 V. The cyclic voltammetry of the GCE modified with VitB_{12} in pH 4 buffer gave a very weak peak near - 1.0 V, the currents thereof have an insignificant contribution to the currents in Figure 4.6(b). The cyclic voltammetry of the GCE in buffer only did not show any significant background currents.

The catalytic currents for reduction of NO on GCE-$VitB_{12}$ decreased with repetitive scanning, but the decrease was much slower than that observed when unmodified GCE was employed for NO detection. Currents on unmodified electrode were less than 0.1 μA after 3 scans, compared to 5 μA observed after 20 scans on GCE modified with $VitB_{12}$, for the same concentration of NO_2^-. This shows that coating the GCE with $VitB_{12}$ improved its stability. Higher catalytic currents were observed when $VitB_{12}$ was employed as a homogeneous catalyst than when adsorbed (for the same concentration), suggesting that $VitB_{12}$ is a more efficient as a homogeneous catalyst.

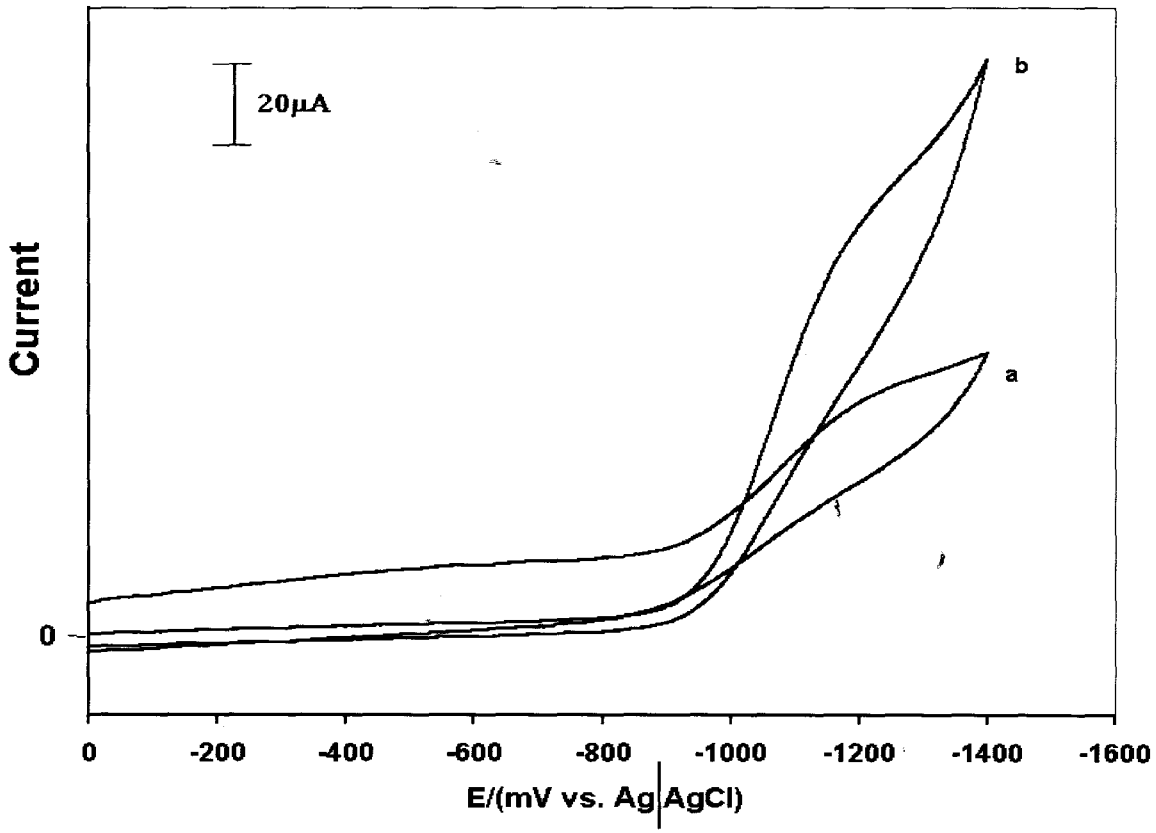

Figure 4.6 Cyclic voltammetry for the reduction of 2.5 x 10^{-2} mol dm^{-3} NO_2^- in pH 4 buffer on (a) unmodified GCE (b) GCE modified with $VitB_{12}$. Scan rate = 100 mV s^{-1}.

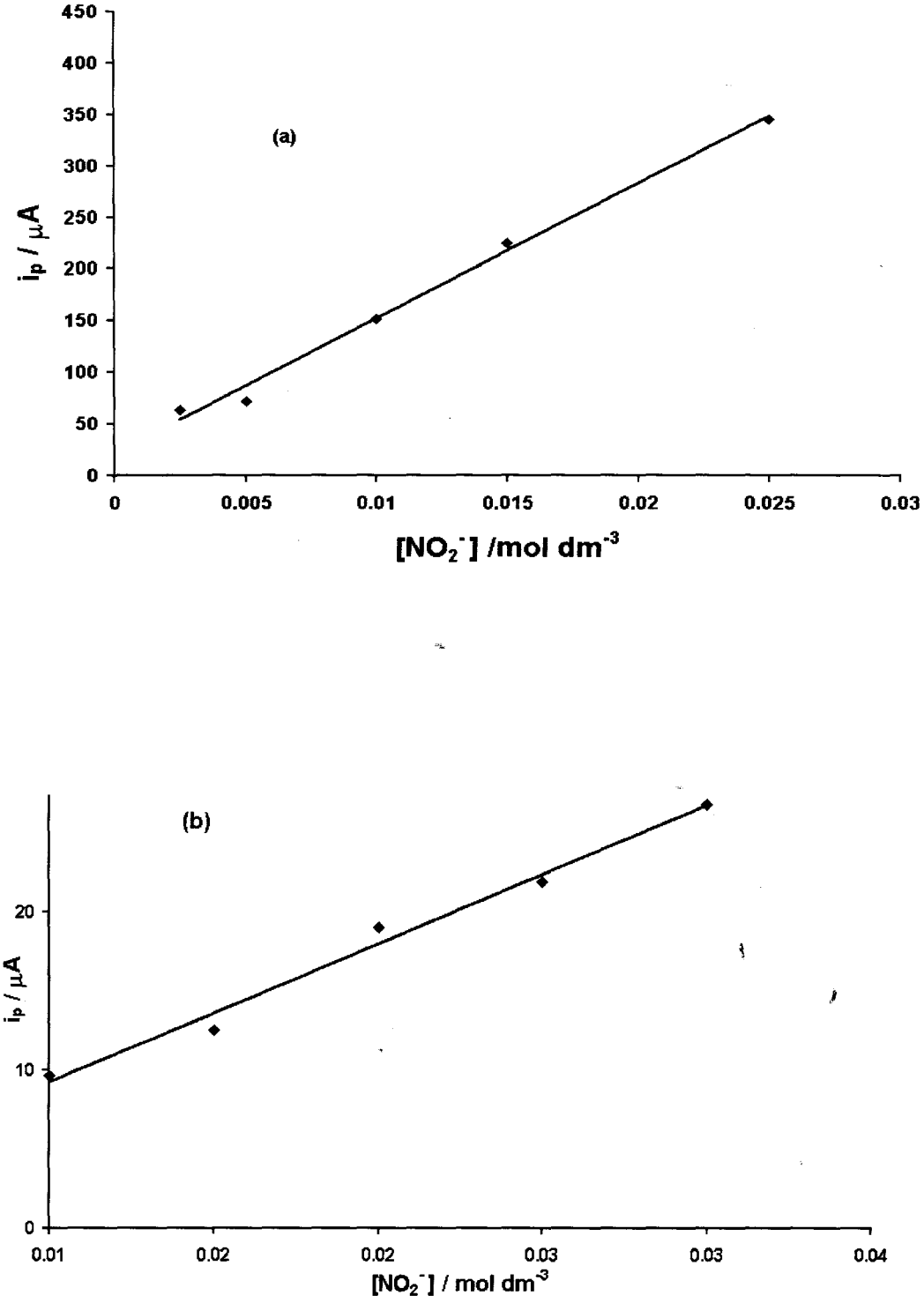

Figure 4. 7 The variation of the currents *vs* $[NO_2^-]$ for (a) reduction; (b) oxidation, in pH 4 buffer. Scan rate = 100 mV s^{-1} on $VitB_{12}$ – GCE.

The catalytic currents increased with increase in NO concentration as shown in Figure 4.7(a). At pH 7 the catalytic currents for reduction of NO on GCE-$VitB_{12}$ were observed at - 0.98 V, and also increased linearly with increase in NO concentration. On an unmodified GCE at pH 7, the NO reduction peak was observed at –1.1 V (Section 3.5.2). This shows that, $VitB_{12}$ results in both the enhancement in current and the shifting of potentials to a less negative value, both requirements for a good catalytic behaviour.

Oxidation of NO (prepared from NO gas) at pH 7 on GCE-$VitB_{12}$ occurred at 1.11 V. Oxidation catalytic currents increased with the increase in NO concentration, Figure 4.8. At pH 7 the NO oxidation peak was not observed on an unmodified GCE.

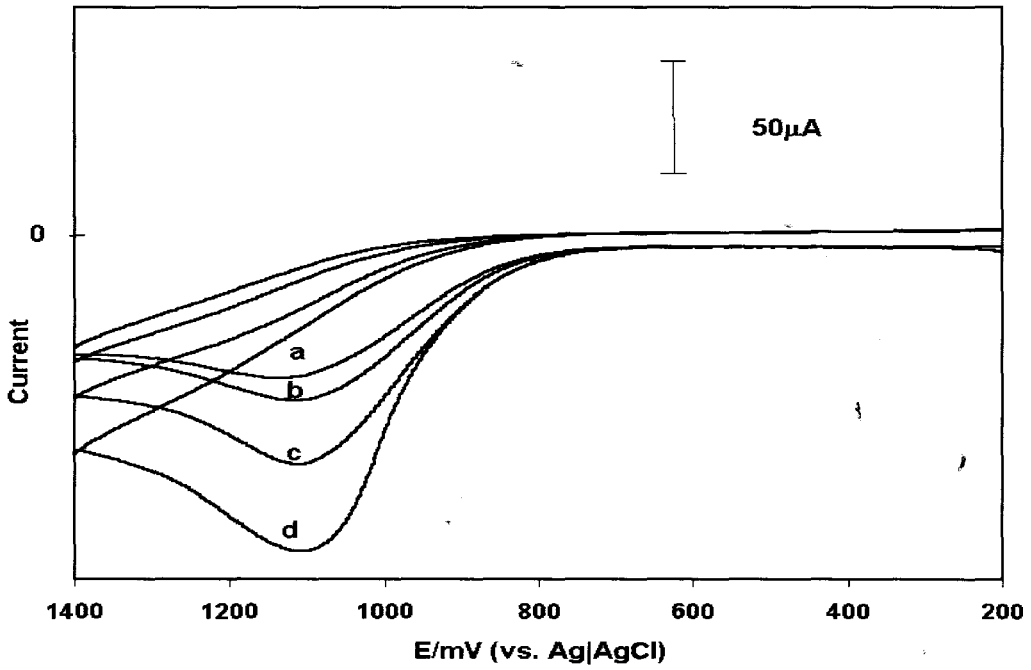

Figure 4. 8 The variation of oxidation catalytic currents with increase in NO concentrations at pH 7, on $VitB_{12}$-GCE. [NO] = (a) 6.3×10^{-4} (b) 8.4×10^{-4} (c) 1.26×10^{-3} (d) 1.47×10^{-3} mol dm^{-3}. Scan rate=100mV s^{-1}.

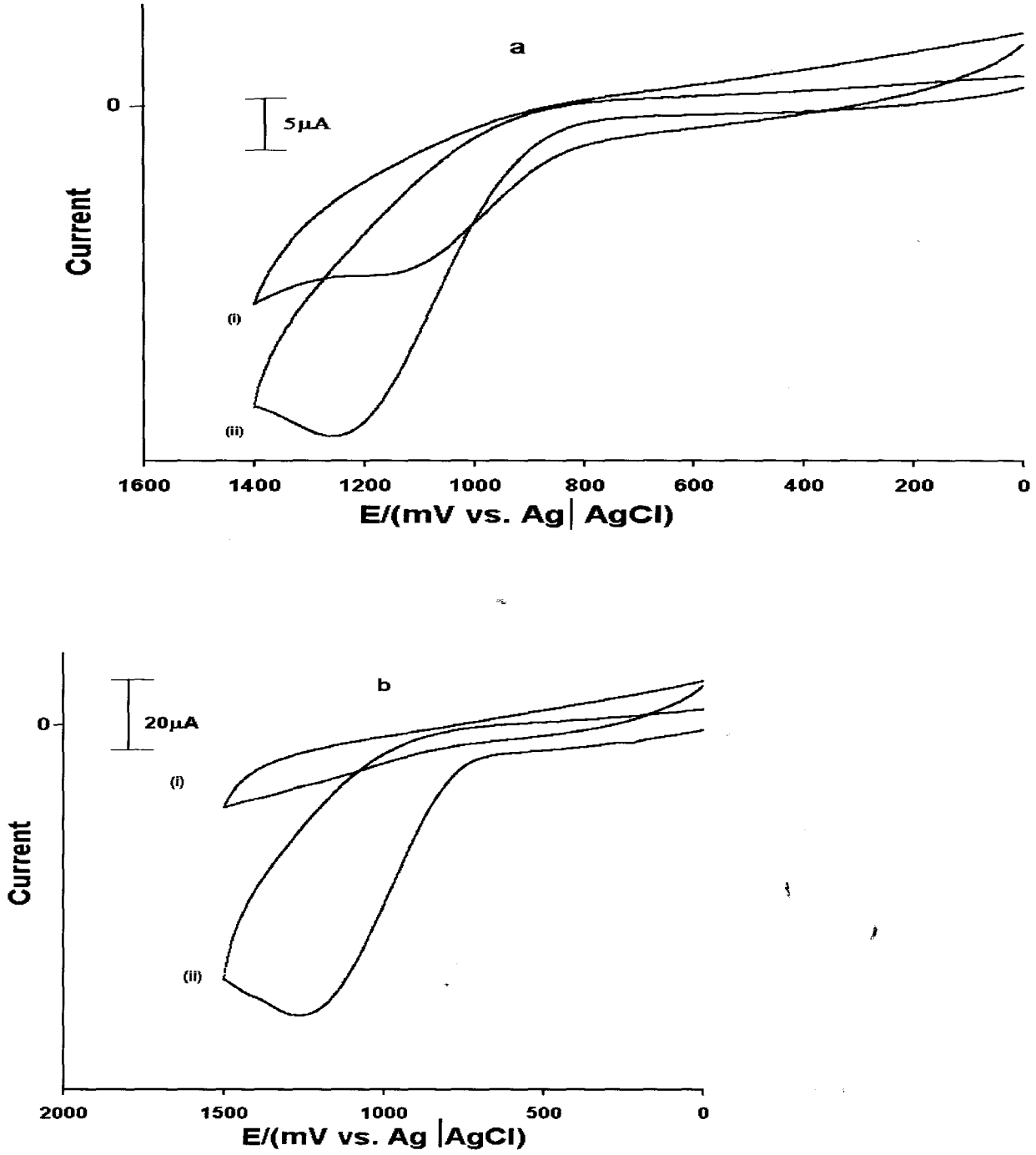

Figure 4. 9 Cyclic voltammetry for oxidation of NO on GCE – $VitB_{12}$. (a) 4.2 x 10^{-4} mol dm^{-3} NO in pH 9 buffer, (b) 2.5 x 10^{-4} mol dm^{-3} NO_2^- in pH 4 buffer. Cyclic voltammetry of NO on (i) unmodified GCE and (ii) GCE – $VitB_{12}$. Scan rate = 100 mV s^{-1}.

Oxidation of NO on GCE-$VitB_{12}$ at pH 9 or pH 4 occurred with catalytic peaks at 1.21 V and 1.35 V, respectively, Figure 4.9. The peak for oxidation of NO on unmodified GCE was observed 1.10 V at pH 9 and as a broad feature near 1.1 V at pH 4, Figure 4.9. Even though there was no improvement in terms of the lowering of the oxidation potential, the enhancement of the oxidation currents at pH 4, and 9 respectively, confirm that $VitB_{12}$ catalyses the oxidation of NO. As in reduction, catalytic currents for solution studies were higher than those for adsorbed $VitB_{12}$. The oxidation currents increased linearly with the concentration of NO_2^- (hence NO) as shown in Figure 4.7(b), for studies at pH 4.

Since $VitB_{12}$ cannot be oxidized at the metal, the catalytic oxidation mechanism may involve oxidation of the ring followed by an electron transfer from NO to the ring of $VitB_{12}$. However, no cyclic voltammogram peaks were observed for the oxidation of $VitB_{12}$ within the potential range of Figure 4.8 and 4.9. It is likely that $VitB_{12}$ only improves the surface of the GCE without being involved in the electron transfer process.

4.4 Product analysis for the catalytic reduction of NO.

For bulk electrolysis, a two compartment cell was employed. We used the GCE electrode coated with $VitB_{12}$ as described above as the working electrode for bulk electrolysis. The counter electrode was a platinum plate of area 2.2 cm^2, and a Ag | AgCl (3 mol dm^{-3} KCl) reference electrode was employed as explained in the Experimental Section. Phosphate buffer at pH 4 and pH 9 were employed for all electrochemical studies.

Controlled potential electrolysis of solutions containing NO at potentials of the catalytic reduction peak for NO on $VitB_{12}$ modified GCE, -1.2 V *vs* Ag | AgCl gave ammonia as the main product of the reduction. For these studies, NO solutions prepared from NO gas, Section 2.3, was employed, for both pHs. The number of moles of electrons transferred were found to be pH dependent. At pH 4, six electrons were obtained and at pH 9, five electrons were obtained. In both cases ammonia and hydroxylamine were found to be present as products. The product distribution was also dependent on the pH value, with less ammonia (25%) being produced at pH 9 due to deficiency of protons, as compared to 38% at pH 4. The amount of hydroxylamine produced at both pH 4 and 9 was very small (2% and 3%, respectively). This may be due to the fact that hydoxylamine is converted to ammonia during the electrolysis.

CHAPTER FIVE: CoPc MODIFIED MICROELECTRODE FOR DETERMINATION OF NO IN BIOLOGICAL SYSTEMS.

5.1 Heterogeneous catalysis using CoPc-ME

5.2 Detection of NO in the presence of interfering species

5.3 Comparative study of some MPc complexes towards NO detection

5.4 Monitoring NO in biological media

5. CoPc MODIFIED MICROELECTRODE FOR DETERMINATION OF NO IN BIOLOGICAL SYSTEMS.*

As indicated in the Introduction, nitric oxide (NO) plays a number of roles in mammalian physiological processes. It is responsible for smooth muscle relaxation, anticoagulation of blood platelets and neurotransmission. Direct detection of NO *in vivo* is a necessity for studying its role in these physiological processes. Since NO is unstable with a short half- life of about 6 seconds, methods for direct determination of NO must be fast, must show good selectivity and sensitivity. The desire to measure small amounts of NO, both *in vivo* and *in vitro*, has led to an active area of research which involves the designing of microsensors. The main challenge is to develop microsensors for *in vivo* real-time NO detection in the presence of interfering ions such as NO_2^- and neurotransmitters. Simultaneous measurement of NO in the presence of possible interfering species requires the electrodes to be capable of separating the potentials of these species significantly enough to allow for accurate determination.

Catalysts such as metalloporphyrin and metallophthalocyanine have been used to improve the sensitivity hence, the NO detection limits of the electrode. To eliminate interference from nitrite, electrodes have been further coated with Nafion®.[87,95] Cobalt (CoTAPc), nickel (NiTAPc) and copper (CuTAPc) tetraaminophthalocyanine complexes were employed by Jin and co-workers[131] for the detection of NO in the presence of interfering molecules such as cathecolamines, ascorbic acid, uric acid and nitrites. In this work a carbon fiber microelectrode modified with CoPc is employed for the detection of

* Work presented in this chapter is in press in the J. Electroanal. Chem. 2001.

NO in aqueous solutions, in the presence of the neurotransmitters serotonin and dopamine.

5.1 Heterogeneous catalysis of NO using CoPc modified microelectrode.

The microelectrode was modified by electrodeposition of CoPc complex and the modified microelectrode is represented as, CoPc-ME. The deposition was carried out by repetitive scanning of a CoPc solution from 1.0 to - 1.0 V, at a scan rate of 500 mV s^{-1} using cyclic voltammetry. CoPc solutions were prepared in dimethylformamide (DMF) or pyridine without addition of an electrolyte. A silver wire pseudo reference and ferrocenium/ferrocene (fc^{+}/fc) couple used as an internal standard were employed. The fc^{+}/fc couple was determined to be 0.41 V *vs* Ag|AgCl (3 mol dm^{-3} KCl). For reproducibility, a fixed number of scans (100) were used for each coating of the electrode. A differential pulse voltammetry (DPV) of the coated electrode in buffer solution was recorded and an anodic curve was observed. The surface coverage (Γ) calculated from the charge under this anodic curve was 2 x 10^{-10} mol cm^{-2}.

Approaches to electrochemical analysis of NO are based on catalytic oxidation or reduction of this species. As indicated in the Introduction, NO detection based on oxidation, eliminates the interference of oxygen for detections in aerobic conditions. NO oxidation on CoPc -ME gave the best results, hence the results for the oxidation of NO are reported in this work.

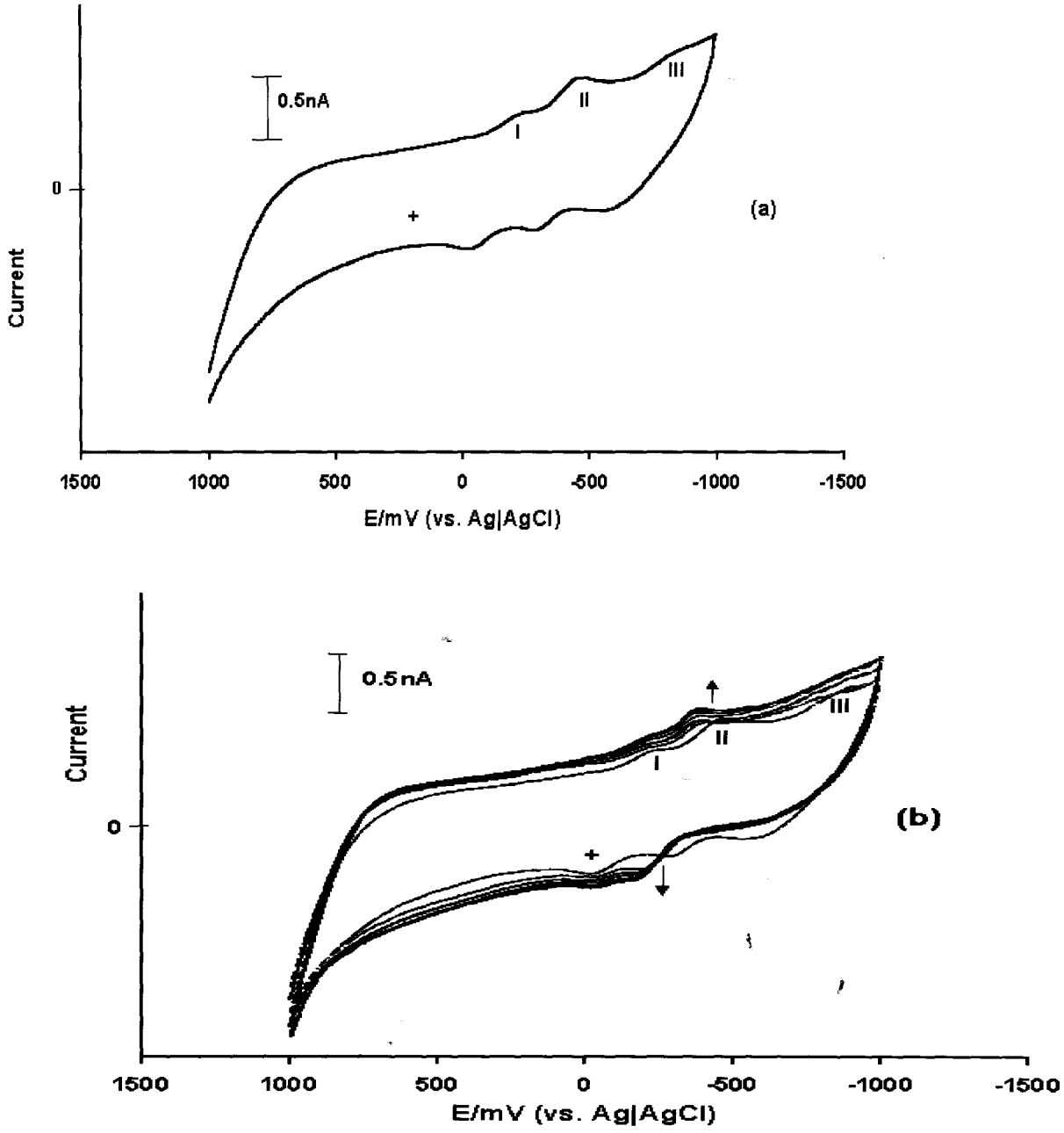

Figure 5. 1 (a) Cyclic voltammogram, of CoPc in DMF on a carbon microelectrode, in the absence of an electrolyte. (b) Continuous cyclic voltammetry scanning of CoPc in DMF on a carbon microelectrode in the absence of an electrolyte.
Scan rate =500 mV s^{-1}.

Figure 5.1(a) shows the cyclic voltammogram of CoPc in DMF, in the absence of an added electrolyte. Repetitive scanning in the potential range + 1.0 to - 1.0 V, resulted in the evolution of the cyclic voltammogram shown in Figure 5.1(b). As explained in Chapter 3 (Section 3.3.1) the first reduction in $Co^{II}Pc$ complexes is known to occur at the central metal with the formation of a $Co^{I}Pc$.[147]

Thus couple I in Figure 5.1 is due to the central metal reduction in $Co^{II}Pc$ with the formation of the $Co^{I}Pc$ species, and couples II and III are then associated with the subsequent reduction of the phthalocyanine ring and the formation of $Co^{I}Pc(-3)$ and $Co^{I}Pc(-4)$ species, respectively. No oxidation processes were observed within the potential range used for Figure 5.1. The Co^{III}/Co^{II} couple is known to be involved in oxidation reactions catalysed by CoPc complexes. However, the potential for this couple is very sensitive to the nature of the solvent and ions present in solution which may take part in axial ligation.[157] Under the conditions used for Figure 5.1, such as the absence of an added electrolyte, the Co^{III}/Co^{II} couple was not observed, probably because it was shifted to more positive potentials, outside the potential range of Figure 5.1.

The growth pattern observed in Figure 5.1(b) indicates film formation on the surface of the microelectrode as a result of electrodeposition of CoPc onto the electrode. In Figure 5.1(b), the return peak for couple II shifted to less negative potentials and couple III become less defined on the second and subsequent scans. In situations where the first scan differs from subsequent scans in peak positions, polymerization and adsorption of the species onto the electrode is implied.[42] In this work pH 7.4 has been chosen because it is within the range of the human physiological pH. When the coated electrode was transferred to the blank solution (pH 7.4 buffer only) and using a Ag | AgCl

reference, a very weak broad peak was observed near 0.84 V. This peak is due to adsorbed CoPc and is in the range for the Co^{III}/Co^{II} couple in this complex.[147] DPV peak for the oxidation of NO on unmodified microelectrode was observed at 0.74 V, Figure 5.2(a). When CoPc-ME was employed for the analysis of NO, large oxidation currents were observed, Figure 5.2(b). A large enhancement in currents[155] and/or a shift in potential to lower values[127] are indicative of catalytic activity. Even though the potential for NO oxidation shifted to slightly more positive values on CoPc-ME when compared to unmodified electrode, the large increase (approximately eight-fold) in current observed in Figure 5.2(b) is a clear indication of the catalytic activity of the CoPc modified electrode. Thus, CoPc catalyses the oxidation of NO. The catalytic peak for NO oxidation was observed at 0.80 V.

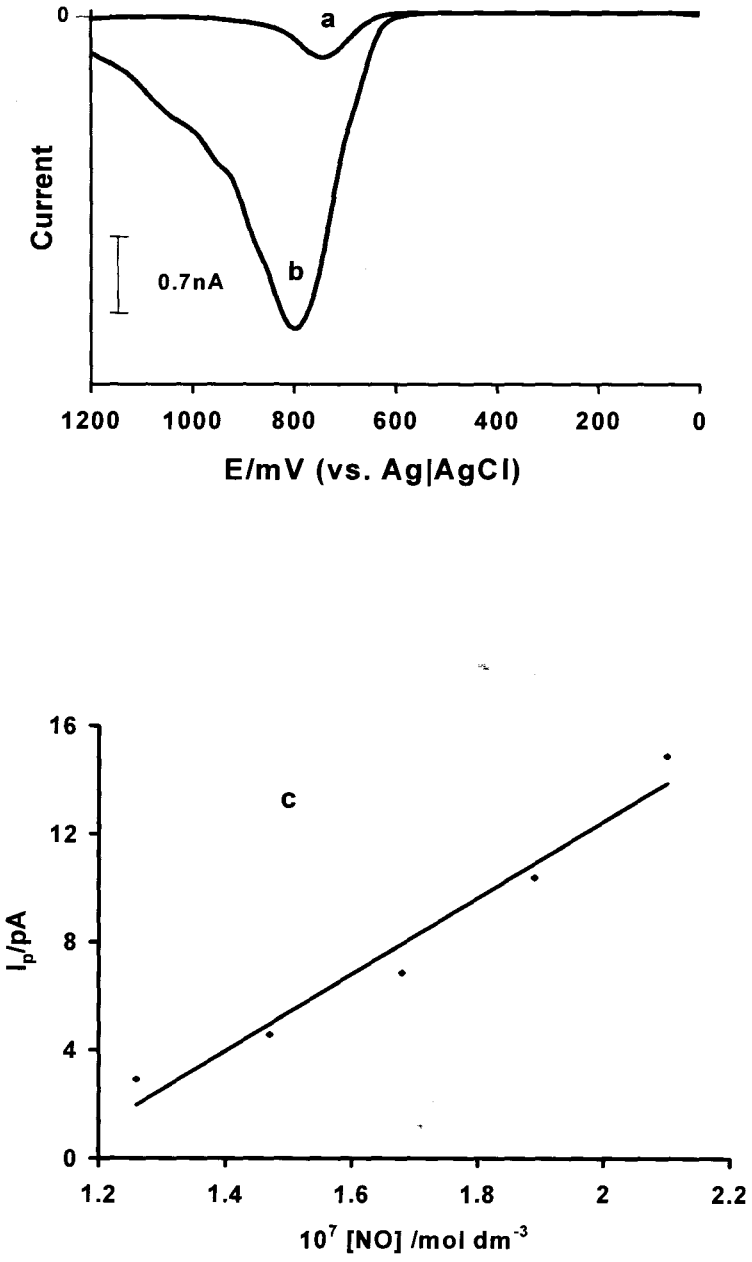

Figure 5. 2 DPV of (a) NO on unmodified microelectrode, (b) NO on CoPc-ME. [NO] = 1.0×10^{-4} mol dm^{-3}. (c) Variation of DPV currents with NO concentration for the catalytic oxidation of NO on CoPc-ME. Electrolyte pH 7.4 buffer.

The CoPc-ME was found to be stable towards the determination of NO at pH 7.4 since there was no significant decrease in anodic currents on consecutive scanning (20 scans) of the CoPc-ME in NO solution. Also, plots of the peak currents versus the square root of scan rate were linear for scan rates of up to 500 mV s^{-1}, showing that the oxidation of NO was a diffusion controlled process on the CoPc-ME under these conditions. The anodic currents for NO oxidation on CoPc-ME varied linearly with the concentration of NO for concentrations ranging from 2.1 x 10^{-4} to 2.1 x 10^{-10} mol dm^{-3}. Figure 5.2(c) shows the linear plot in the 10^{-7} mol dm^{-3} range, a correlation coefficient of 0.979 was obtained for this plot. The relative standard deviation for the lowest detection limit, 2.0 x 10^{-10} mol dm^{-3}, was 3% for 20 DPV scans. The detection limit of 2.0 x 10^{-10} mol dm^{-3} is better than that obtained using metal tetraaminophthalocyanine modified microelectrodes[131] and is in the same range as that reported for the porphyrin based microsensor reported by Malinski et al,[80] for analysis of NO in single cells. The stability of the CoPc-ME and the low detection limit makes this electrode a good candidate for NO analysis.

It is expected that the first step in the catalytic process of NO on CoPc adsorbed carbon electrodes, is the oxidation of the $Co^{II}Pc$ to the $Co^{III}Pc$ species at the electrodes.[127] In homogeneous CoPc catalysis of NO, ring-based processes were observed, Chapter 3 (Section 3.4). However, complexes behave differently in different states (i.e. in solution or in the solid state). Thus, the catalytic behaviour involving metal oxidation proposed by Baldwin[127] is likely in this case. The increase in sensitivity of the CoPc modified electrode may then be attributed to the diffusion of NO to the electrode, followed by reduction of the $Co^{III}Pc$ at the electrode to $Co^{II}Pc$ as follows: -

$Co^{II}Pc \rightarrow Co^{III}Pc + e^-$ 6.1

$Co^{III}Pc + NO \rightarrow$ **$Co^{II}Pc$ + oxidation products of NO (e.g. nitrite)**.....6.2

Coordination of NO to the CoPc adsorbed on the surface of the electrode is likely to occur.

5.2 Detection of NO on CoPc-ME in the presence of interferents.

5.2.1 Determination of NO in the presence of nitrite.

Since the ultimate aim in constructing microsensors for NO detection is for *in vivo* studies, it is important to test the modified electrode for the effects of possible biological interferences. Nitrite is one of the major interfering ions for NO detection. As was indicated in the introduction, the oxidation potentials of NO and nitrite are close to one another and hence the electrode is not able to discriminate between the two species. Figure 5.3(a) shows the DPV scan of a mixture of NO and NO_2^-. An oxidation peak was observed at 0.9 V on a CoPc – ME. This potential is more positive than that observed for NO (0.8 V) on CoPc-ME in the absence of nitrite. This peak is broad indicating the overlapping of the two potentials. The concentration of nitrite is a one hundred-fold higher than that of NO. After the CoPc – ME was coated with Nafion® the peak potentials of NO, Figure 5.3(c) and that of the mixture (nitrite and NO) solutions were observed at the same potential, 0.80 V, Figure 5.3(b). This shows that the electrode successfully discriminated between the two species, i.e. only NO is determined.

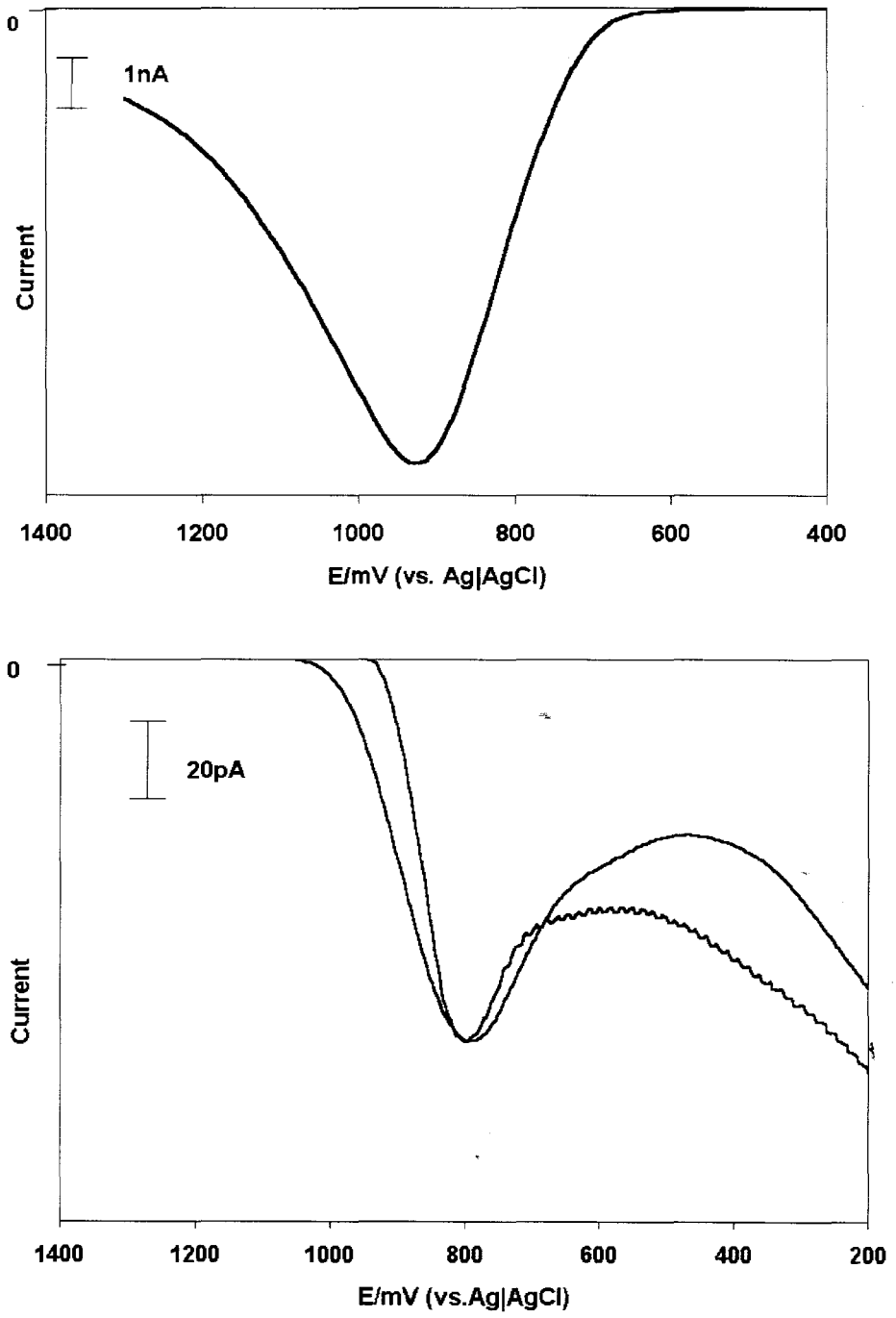

Figure 5. 3 DPV of a mixture of NO (2.1×10^{-4} mol dm^{-3}) and NO_2^- (1.0×10^{-2} mol dm^{-3}) on

(a) CoPc – ME and (b) CoPc – ME coated with Nafion®.

(c) DPV of NO (2.1×10^{-4} mol dm^{-3}) on CoPc – ME coated with Nafion®.

However, the short fall of Nafion® is that it reduces the sensitivity of the electrode, hence there is a need to optimize the coating of the electrode with Nafion®. For this work, optimum coverage was attained by dipping the modified microelectrode for 10 seconds in a 5% aqueous alcohol based solution of Nafion®. However, $[CoTSPc]^{4-}$ without a coating of Nafion® showed some discrimination between NO and nitrite, Figure 5.4 below. This implies that the negative charge on the $[CoTSPc]^{4-}$ tends to repel any anions in the vicinity of the electrode surface. However, unlike using Nafion® where nitrite is not detected at all, when using $[CoTSPc]^{4-}$ some nitrite is able to reach the electrode surface, but is detected at potentials more positive than NO, Figure 5.4 (b). Also, though the potential of the NO and nitrite mixture, Figure 5.4(c) was the same as that of NO alone, Figure 5.4(a) the mixture showed higher currents implicating that the signal is a summation of both NO and NO_2^-.

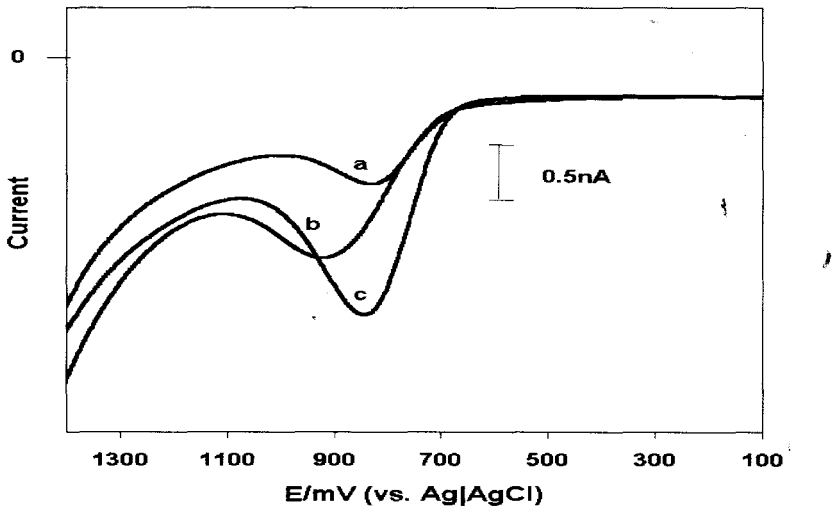

Figure 5. 4 DPV of: (a) NO, (b) NO_2^- and (c) NO and NO_2^-, on CoTSPc – ME.

$[NO_2^-] = 1.0 \times 10^{-2}$ mol dm^{-3} $[NO] = 2.1 \times 10^{-4}$ mol dm^{-3}

5.2.2 Effect of oxygen on NO detections.

The effects of oxygen were investigated since oxygen is expected to be present in biological systems. For all DPV experiments, a nitrogen atmosphere, was maintained. However, when no nitrogen was bubbled during the studies, the peak currents and potentials were the same as those obtained for nitrogen bubbled solutions. This confirms that oxygen present in solution does not interfere with the catalytic oxidation of NO, whilst oxygen presents problems for NO reduction since it gets reduced before NO. However, bubbling of oxygen to NO solutions resulted in an irreversible shifting of potentials to more positive values. This implies a formation of higher oxides of NO which are oxidized at more positive potentials.

5.2.3 Detection of NO in the presence of ascorbic acid.

Ascorbic acid also occurs in biological systems. It has been previously found to contribute high current backgrounds. Figure 5.5 shows a DPV of a mixture of NO (2.1 x 10^{-4} mol dm^{-3}) and ascorbic acid (1.0 x 10^{-1} mol dm^{-3}) on CoPc – ME. The concentration of ascorbic acid is 1000 times more than NO. Two well-separated peaks were observed and there was not a significant increase in the background current compared to when NO was alone in solution. NO currents increased linearly with increase in NO concentration in the presence of ascorbic acid and the magnitudes of NO currents did not change in the presence of ascorbic acid. Hence, determinations of NO would be possible in the presence of ascorbic acid.

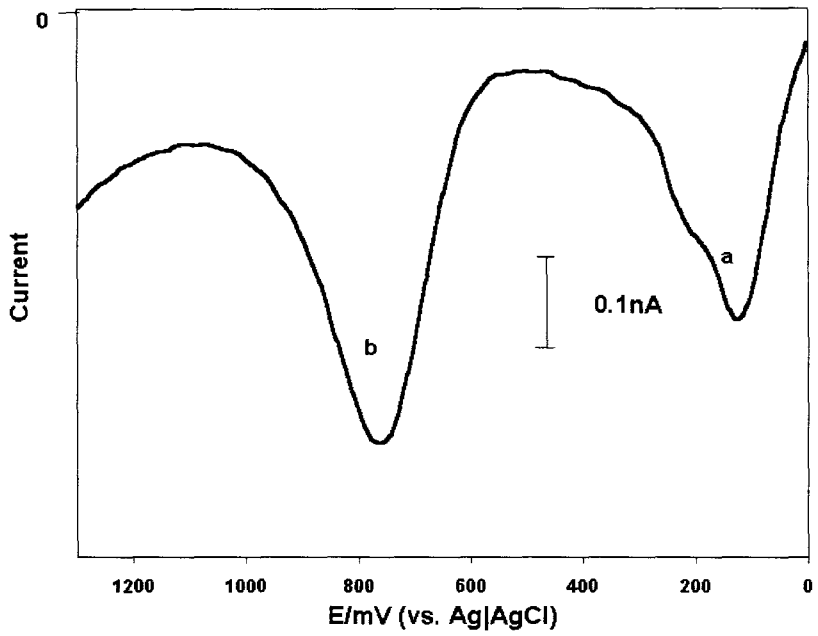

Figure 5. 5 DPV of a mixture of ascorbic acid (1.0×10^{-1}mol dm^{-3}) and NO (2.1×10^{-4} mol dm^{-3}). (a) Peak due to ascorbic acid, (b) peak due to NO.

5.2.4 Detection of NO in the presence of dopamine and serotonin.

Nitric oxide is also found in the brain and it has been found to be a carrier of some neurotransmitters. Its possible interference with some neurotransmitters, dopamine and serotonin was investigated. Studies into the possible interference between NO and dopamine have been reported.[88] Figure 5.6(a) shows the DPV of NO on CoPc-ME in the presence of approximately two fold excess of serotonin and dopamine. Well separated anodic peaks were observed for serotonin, dopamine and NO, showing that these species can be obtained simultaneously under these conditions. Increasing the concentration of NO in the presence of excess but constant and equal amounts of dopamine and serotonin

resulted in the increase in the DPV currents for NO and dopamine but a decrease in the oxidation currents of serotonin. These changes in oxidation currents were observed when the concentration of serotonin was larger than that of NO. The observed decrease in the oxidation currents of serotonin on increasing NO concentration, suggests that there is some interaction between NO and serotonin. The serotonin peak eventually disappeared as the concentration of NO was increased. There was no significant shift in the oxidation potential of NO in the presence of dopamine and serotonin, when compared to the potential of NO alone on CoPc-ME.

As noted in the Introduction, its been reported that simultaneous fast cyclic voltammetry of NO and dopamine on rat brain slices, using carbon fiber working electrode revealed that the electrochemical signals were a summation of both dopamine and NO oxidation signals.[88] However, in this work separate peaks for NO and dopamine were observed. The calibration curve obtained for NO in the presence of excess but constant amounts of dopamine and serotonin was linear, Figure 5.7, however, the oxidation currents of NO were lower than that of NO alone (i.e. in the absence of dopamine and serotonin).

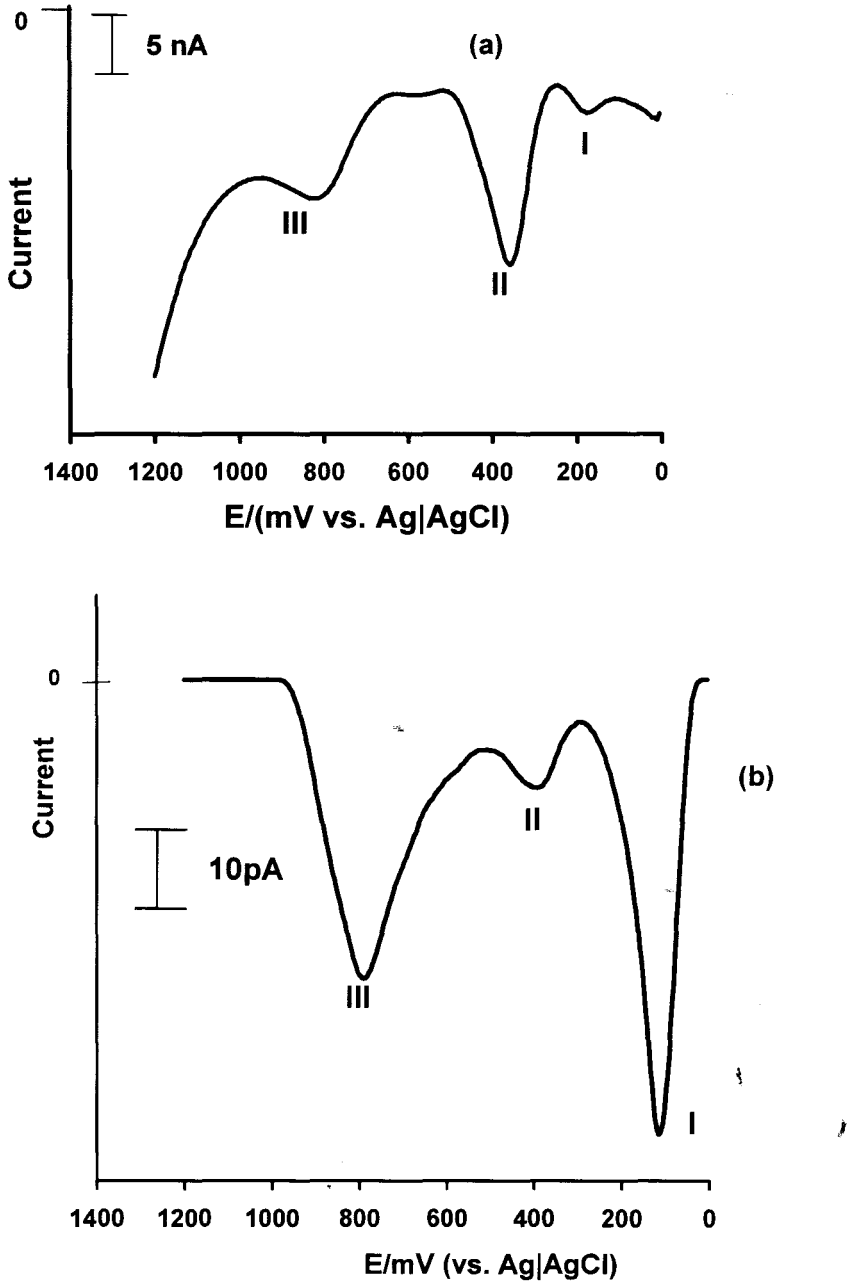

Figure 5. 6 (a) Differential pulse voltammogram of NO (2.1×10^{-4} mol dm^{-3}) in the presence of dopamine (3.7×10^{-4} mol dm^{-3}) and serotonin (3.6×10^{-4} mol dm^{-3}). pH 7.4 buffer (**I**) dopamine, (**II**) serotonin and (**III**) NO.

(b) Differential pulse voltammogram of NO (2.1×10^{-4} mol dm^{-3}) in the presence of serotonin (7.7×10^{-3} mol dm^{-3}). pH 7.4 buffer (**I**) product of interaction between NO and serotonin, (**II**) serotonin and (**III**) NO.

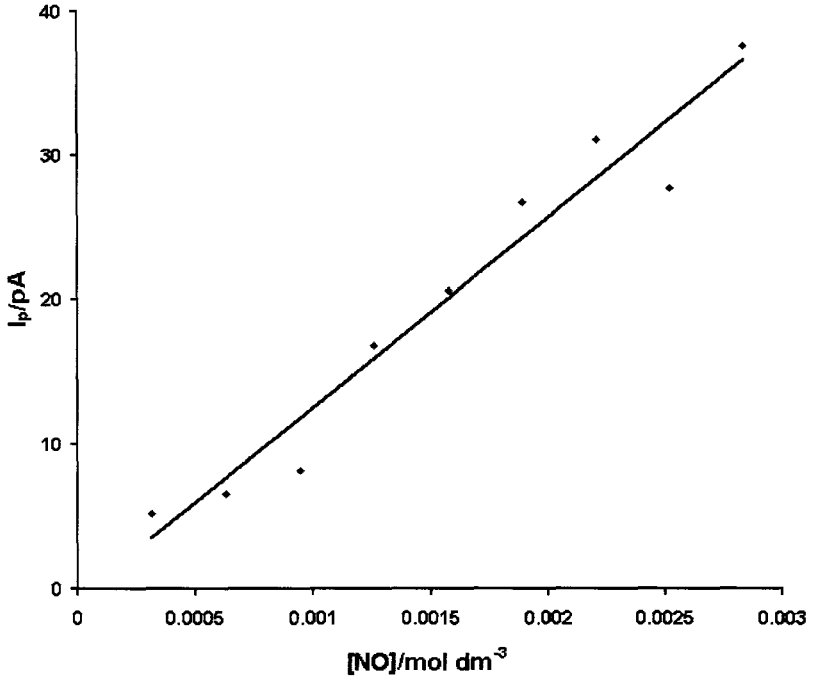

Figure 5. 7 Variation of DPV currents with NO concentration for the catalytic oxidation of NO on CoPc-ME in the presence of dopamine and serotonin (each at 1.0×10^{-2} mol dm^{-3}). pH 7.4 buffer conditions.

NO is known to act as an agent for the deamination of some natural amines during its (NO) cancer-inducing process.[4] This could explain the disappearance of the serotonin oxidation peak with increase in the concentration of NO. A peak at 0.11 V (labelled I) was observed when NO and serotonin were determined simultaneously, in the absence of dopamine, Figure 5.6(b). This peak was not present when NO or serotonin were determined separately. The increase in the dopamine oxidation currents with increase in NO concentration, reported above, did not occur in the absence of serotonin. This suggests that the increase in dopamine currents with increase in NO concentration is a result of the combination of the currents for the oxidation of the deamination products of

serotonin and the oxidation currents of dopamine. The currents for the oxidation of dopamine did not change with increase in NO concentration in the absence of serotonin. This implies no interaction between dopamine and NO.

5.3 A comparative study of some MPc complexes towards NO detection.

Figure 5.8 compares the anodic currents and potentials obtained from DPV studies for the oxidation of NO on CoPc-ME with those obtained from MnPc-ME, FePc-ME, NiPc-ME, CuPc-ME and ZnPc-ME, for the same concentration of NO. The same number of cyclic voltammetry scans for electrodeposition of the MPc onto the microelectrode were employed. The magnitudes of the catalytic currents for the oxidation of NO on MPc modified microelectrode varied with the MPc complexes as follows: CuPc < ZnPc < MnPc < CoPc ~ NiPc < FePc. The scale in Figure 5.8 has been expanded and the potentials used are expressed to three decimal places hence, the peak for CoPc-ME is at 796 mV whilst its been rounded off to 0.80 V in Section 5.1.

The potential for the oxidation of NO was found to be less positive for FePc-ME and became more positive following the sequence above. FePc gave the largest currents and also gave the least positive oxidation potential for NO, which are both desired conditions for electrocatalysis. Thus FePc was found to be the best electrocatalyst for the detection of NO with CuPc showing the poorest catalytic activity. As discussed earlier, (Section 3.4), CoPc forms a (NO)CoPc complex on interaction with NO. FePc is also known[5] to form an (NO)FePc complex. The rate and equilibrium constants for the formation (NO)FePc[5] were found to be respectively, three and two orders of magnitude higher than the values determined in this work for the formation of (NO)CoPc. Thus the high catalytic activity of the FePc species could be related to the high rate constant for the formation of the (NO)FePc species. However, FePc-ME did not have a good stability for NO detection when compared to CoPc-ME, in that some fouling of the electrode was observed on repetitive scanning. This may be due to the fact that FePc forms stronger

bonds with NO than CoPc hence, affecting the regeneration of the electrode. The electrode is hence poisoned and unstable for NO determination.

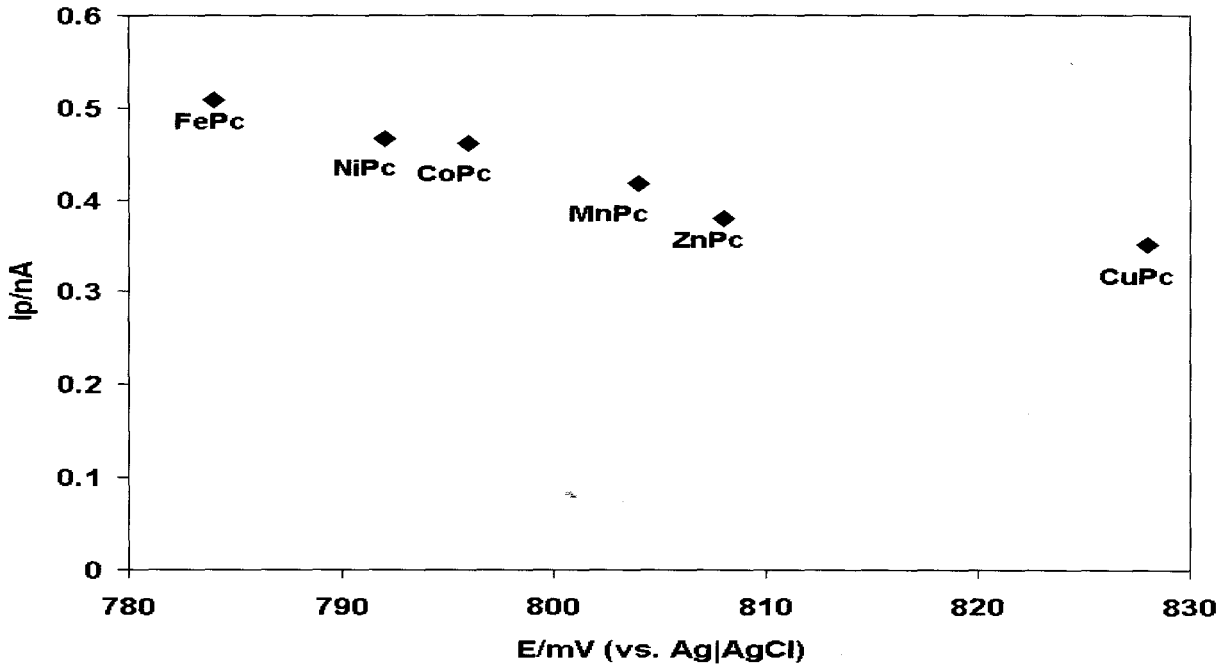

Figure 5. 8 Comparison between NO oxidation currents and potentials on the various MPc-ME. [NO] = 2.1 x 10^{-4} mol dm^{-3} in pH 7.4 buffer.

The site of oxidation or reduction is an important factor in the catalytic activity of MPc complexes. Oxidation and reduction processes are expected at the central metal in FePc, MnPc and CoPc,[111] whereas ring-based processes occur in ZnPc, NiPc and CuPc. MPc complexes with metal-based oxidation processes are expected to show better catalytic activity towards the oxidation of analytes. The observation of good catalytic

activity for CoPc, FePc and MnPc towards the oxidation of NO is thus in accordance with the general catalytic behaviour of MPc complexes. FePc and CoPc are known to be the best catalysts for oxygen reduction.[110] The observation that NiPc is in the same category as CoPc as an electrocatalyst is surprising since oxidation in NiPc is known to occur at the ring, with the metal showing no catalytic activity,[111] though there has been some controversy with some reports suggesting that metal oxidation occurs in NiPc.[112] When unmetallated Pc (H_2Pc) was employed as a catalyst, the catalytic currents for the oxidation of NO were much lower (than those observed for the other MPc complexes) hence suggesting that the central metal plays an important role in the catalysis process.

Detection of NO using $[CoTSPc]^{4-}$, $VitB_{12}$, tetrakis(1-methyl-4 pyridyl) cobalt (II) porphyrin (CoP) and CoPc, modified microelectrodes, coated with Nafion® as described earlier were compared, Figure 5.9. The currents for $VitB_{12}$-GCE and CoTSPc-GCE are too small to observe on the scale of Figure 5.9, due to the much larger currents for CoPc-ME. The order of catalysis as measured by current enhancement was as follows; $CoPc>>VitB_{12}>CoP>[CoTSPc]^{4-}$.

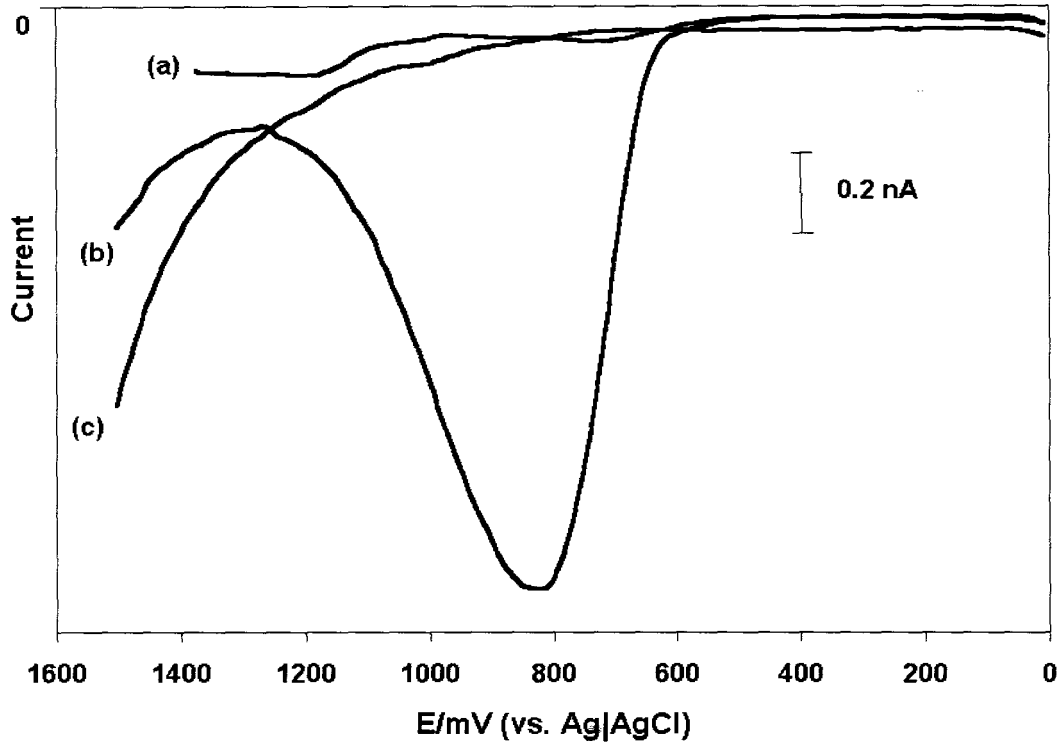

Figure 5. 9 DPV scans of NO oxidation on (a) $VitB_{12}$ -ME (b) CoPc-ME (c) CoTSPc-ME, [NO] = 0.5 x 10^{-4} mol dm^{-3}.

Since CoPc was the best catalyst, the effect of changing peripheral substituents was investigated. The effect of substituting either an electron withdrawing or an electron donating group on the catalytic activity for, the detection of NO was studied using a 11 μm carbon fiber. The following complexes were electrodeposited on the microelectrode; cobalt(II) tetraaminophthalocyanine (CoTAPc), cobalt(II) tetranitrophthalocyanine (CoTNPc), cobalt(II) tetracarboxyphthalocyanine (CoTCPc). For reproducibility each complex was immobilized on the electrode by scanning the solution of the complex in DMF between –0.4 V and 1.0 V. It has been reported that repetitive scanning of a solution of CoTAPc in DMF from 0 to 1.0 V results in a gradual increase in the oxidation

currents due to the polymerization of this complex.[158,159] DPV scan of each complex was recorded at constant NO concentration. The following order of catalytic activity as judged by the magnitude of currents was observed: CoTAPc>CoPc>CoTCPc>CoTNPc. The peak potentials did not vary much, and were within a 0.03 V range. It is not suprising that CoTAPc exhibited better catalytic activity than CoPc. Electron donating groups attached to the Pc ring make the oxidation of the complex easier. The mechanism of NO oxidation is believed to proceed via the oxidation of the cobalt metal.[127] However, CoPc-ME was more stable than the CoTAPc-ME in that the catalytic currents decreased more rapidly with scan number for the latter, whilst no significant decrease was observed for CoPc-ME.

5.4 Monitoring NO in biological media.

5.4.1 Monitoring of NO in human blood.

In order to characterize the decay of NO in human blood and its components, NO was introduced to whole blood, to blood plasma and blood serum. The lifetime of NO was determined by recording the differential pulse voltammograms (on CoPc-ME coated with Nafion®) with time following the injection of NO (2.1×10^{-4} mol dm^3) to 1 ml of whole blood, blood plasma or serum. NO was injected as close to the microelectrode as possible. Figure 5.10 and Figure 5.11 show the decrease in the catalytic currents, with time, for NO oxidation in blood serum and whole blood, respectively, following the injection. Similar changes were observed for blood plasma. Changes shown in Figure 5.10 and 5.11 were observed even when there was no attempt to exclude oxygen. The decrease in current with time (observed in Figure 5.10 and 5.11) can be attributed to the diffusion of NO into the bulk solution and to its chemical reaction with blood components. Complete exclusion of oxygen may not have been achieved even in cases where nitrogen was bubbled through the blood or its components, hence reactions of NO with traces of oxygen would occur in Figure 5.10 and 5.11. The peak for oxidation of NO, on CoPc-ME coated with Nafion®, was observed at 0.70 V in blood plasma and at 0.71 and 0.74 V in blood serum and whole blood, respectively. The oxidation currents for the NO oxidation decreased without a significant shift in potential.

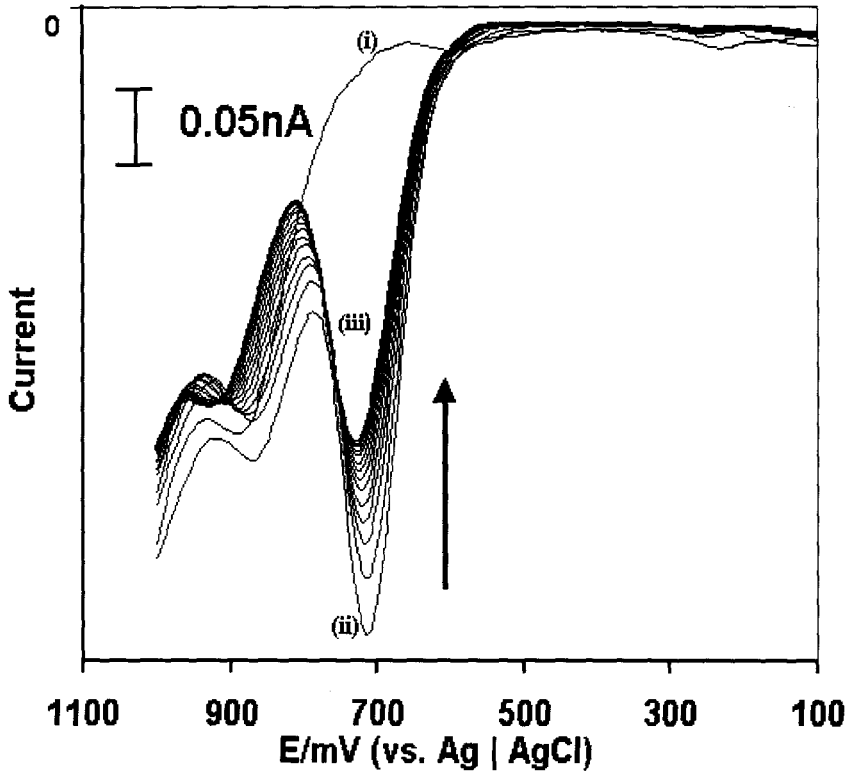

Figure 5. 10 Differential pulse voltammograms for the oxidation of NO (on CoPc-ME) following injection of 2.1 x 10^{-4} mol dm^{-3} NO into blood serum. (i) before NO injection (ii) immediately after NO injection (iii) 30 min after injection.

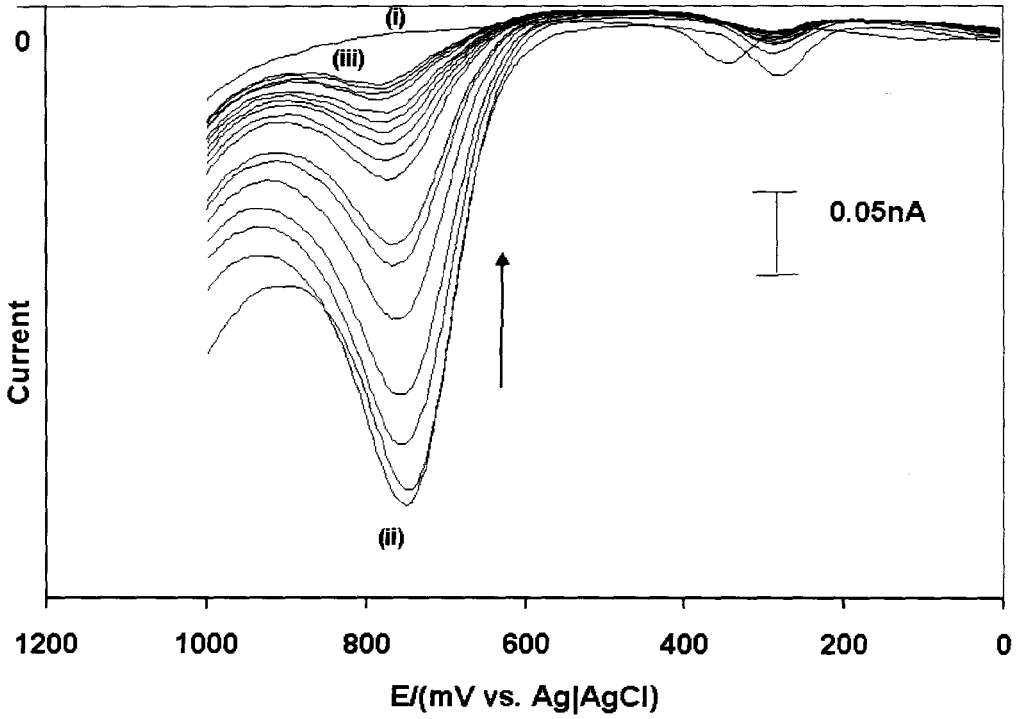

Figure 5. 11 Differential pulse voltammograms for the oxidation of NO (on CoPc-ME) following injection of 2.1 x 10^{-4} mol dm^{-3} NO into whole blood. (i) before NO injection (ii) immediately after injection and (iii) 30 min after injection.

However, a shift in the peaks to more positive potentials was observed after the first scan when Nafion® was not employed to coat the CoPc-ME electrode, Figure 5.12. This shift could be due to the interference of the anions such as nitrite on the electrode. The CoPc-ME electrode coated with Nafion® was found to be stable to NO detection in blood or blood components, in that for the same concentration of injected NO, similar currents were obtained for a fresh solution of blood, without having to re-coat the electrode.

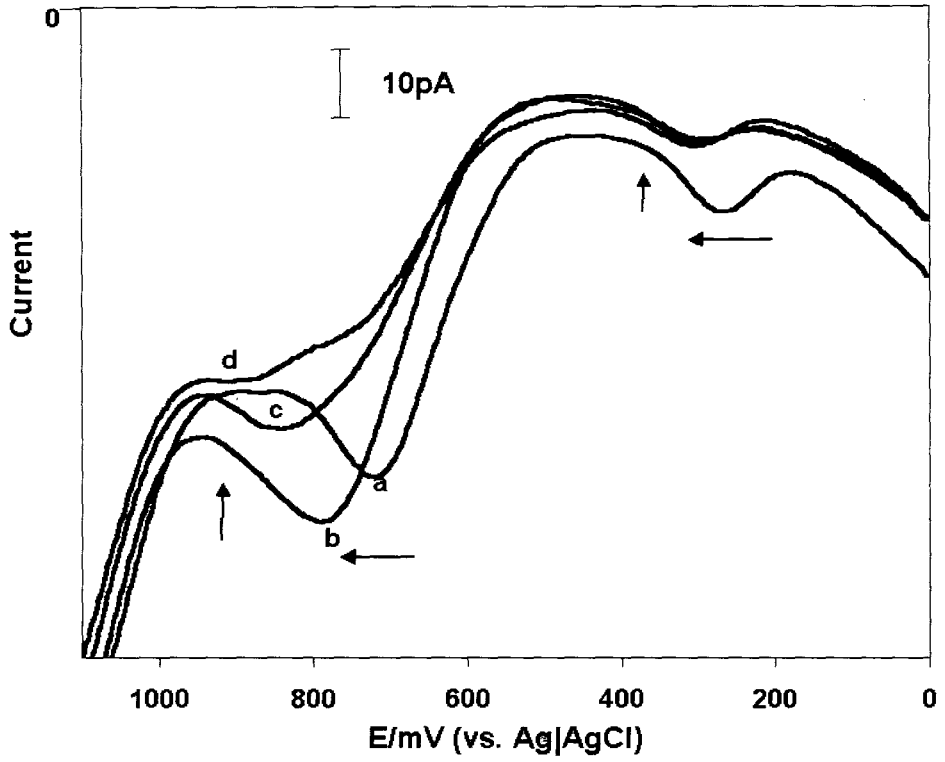

Figure 5. 12 DPV scan of NO oxidation on CoPc-ME (without Nafion® coating) in blood plasma (a) immediately after NO injection (b) 30 sec later (c) 2 min. later (d)5 min. later.

Figures 5.10(i) and 5.11(i) show the DPV of blood serum and whole blood, respectively, in the absence of added NO. DPV peaks were observed at 0.36, 0.24 and 0.34 V for plasma, serum and whole blood, respectively, before the addition of NO. These oxidation peaks are in the range for the oxidation of serotonin, but could also be due to a range of other biological molecules. These peaks shifted to lower potentials for whole blood (0.29 V) and blood serum (0.16 V) on addition of NO, but disappeared immediately in blood plasma using CoPc-ME coated with Nafion®. On CoPc-ME that

was not coated with Nafion®, Figure 5.12, a peak at 0.27 V was observed. The peak shifted to more positive potentials following addition of NO and decreased with time. For blood serum, a large peak was also observed at 0.89 V in the absence of added NO. This peak shifted to more positive potential (0.91 V) with time following injection of NO, without significant decrease in currents. This peak has not yet been identified. It is not due to nitrite since it did not increase on spiking the samples with nitrite.

Stirring of the whole blood or its component following the decrease in NO oxidation currents to the very low levels shown in Figures 5.10 and 5.11, resulted in the regeneration of the current to less than 20% of the original oxidation currents of NO. This suggests that the reaction of NO with blood or its components including oxygen is more important for the disappearance of the NO peak than its diffusion into the bulk solution. It has been reported before that under stirring, NO concentration decreased faster than under static conditions, when porphyrin microsensor was employed.[89]

Figure 5.13 compares the decrease in catalytic currents for NO in whole blood, blood serum and plasma, when determined on CoPc-ME (Nafion® coated). For the same concentration of NO injected, the current decay is much slower in blood serum, when compared to whole blood and blood plasma as observed before for porphyrin microsensors.[89] Red blood cells suspended in blood plasma carry hemoglobin. The rapid disappearance of NO in blood plasma is possibly due to NO oxidation since the heme has a high affinity for oxygen. Blood serum is deprived of the red blood cells hence, NO oxidation is slower and its disappearance is slow, Figure 5.13.

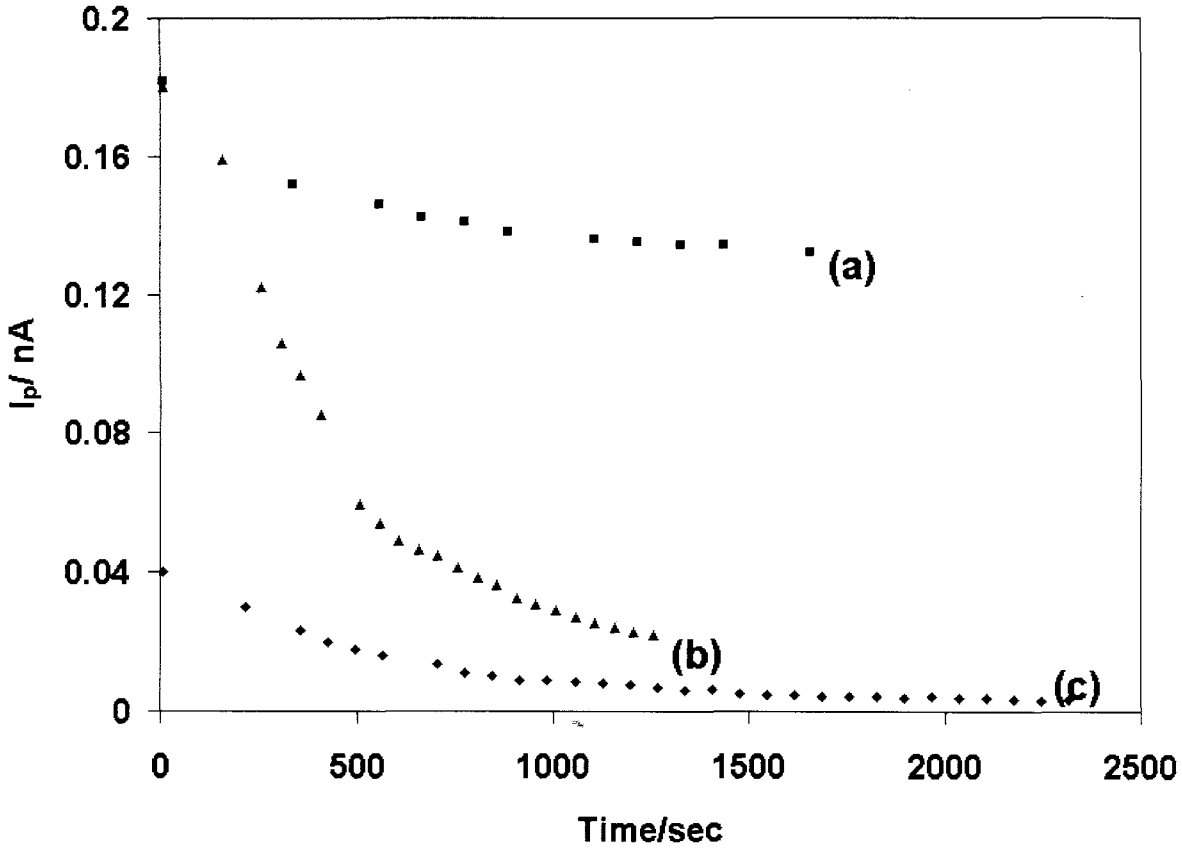

Figure 5. 13 Variation of currents for the oxidation of NO (on CoPc-ME)with time following injection into (a) serum, (b) whole blood and (c) plasma. [NO] = 2.1 x 10^{-4} mol dm^{-3}.

Figure 5.14 shows the effects of increase in the NO concentration on the oxidation currents on CoPc-ME, considering the first scan following the injection of NO into blood plasma. A linear increase was observed suggesting that there is no significant interference from signals originating from other components of the blood plasma.

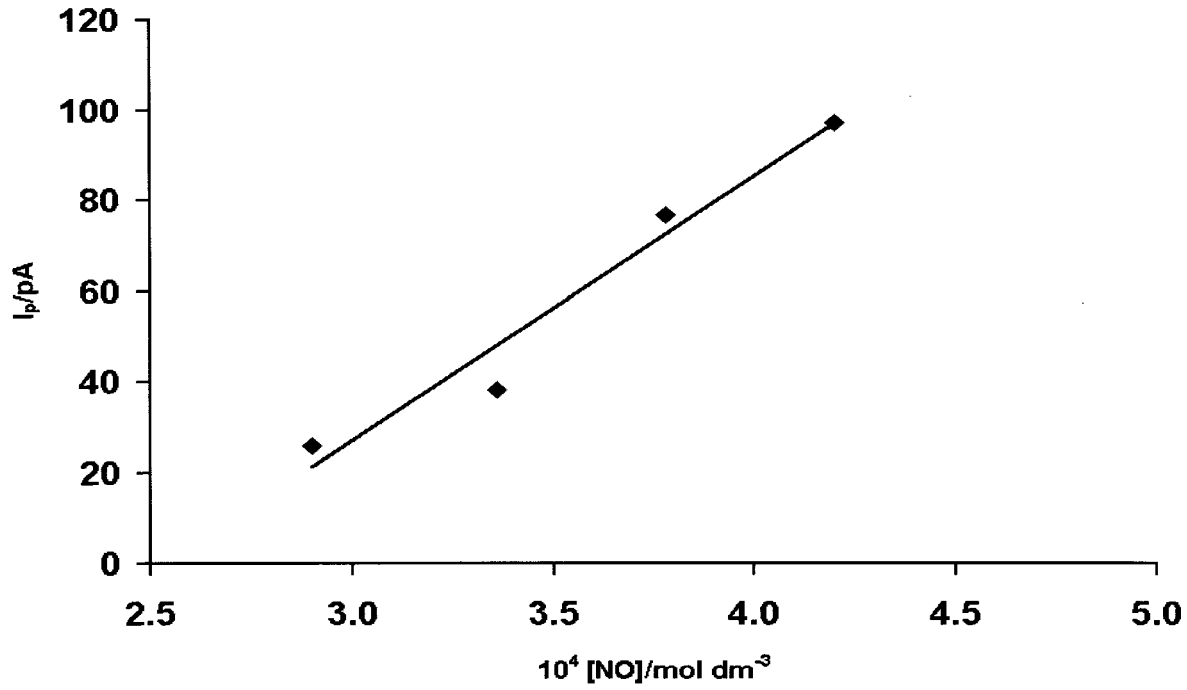

Figure 5. 14 Variation of DPV currents with added NO concentration for the oxidation of NO (on CoPc-ME) in blood plasma. The DPV currents shown are those recorded immediately following addition of NO to blood plasma.

5.4.2 Detection of NO in rat brain slices.

The rat brain was sliced immediately after the rat was sacrificed as described in Section 2.6.2. Measurements of NO were carried out with a CoPc-ME. The CoPc-ME was not coated with Nafion® since Nafion® reduces sensitivity. The microelectrode was modified by electrodeposition as explained above. The CoPc-ME and the Ag|AgCl electrode were placed on the surface of the brain slice and Osteryoung square wave

voltammetry (OSWV) technique was used to measure NO. OSWV was used instead of DPV since the former provides a more rapid response than the latter.

Figure 5.15 shows the OSWV scans of the brain slice 3 minutes after the rat was sacrificed. The first scan, Figure 5.15(a) was recorded immediately after the microelectrode was placed on the surface of the brain slice. Figure 5.15(b) was scanned about 30 seconds later and Figure 5.15(c) was recorded 3 min later. There is an observable shift in potential from 0.75 V, Figure 5.15(a), to more positive potentials, (0.8 V), Figure 5.15(b). It is well known that nitrite is an oxidation product of NO and that it gets oxidized at potentials that are 60 to 80 mV, more positive that those of NO. This could imply that, the first scan records the oxidation of NO but later scans record the oxidation of nitrite. This is more likely since the sensor CoPc-ME was not coated with Nafion®. As explained earlier, coating the electrode with Nafion® decreases the sensitivity of the sensor, and in these studies it was not possible to observe the NO oxidation peak after Nafion® coating. The peak at 0.8 V decreased with time, until no signal was detected after about 5 min.

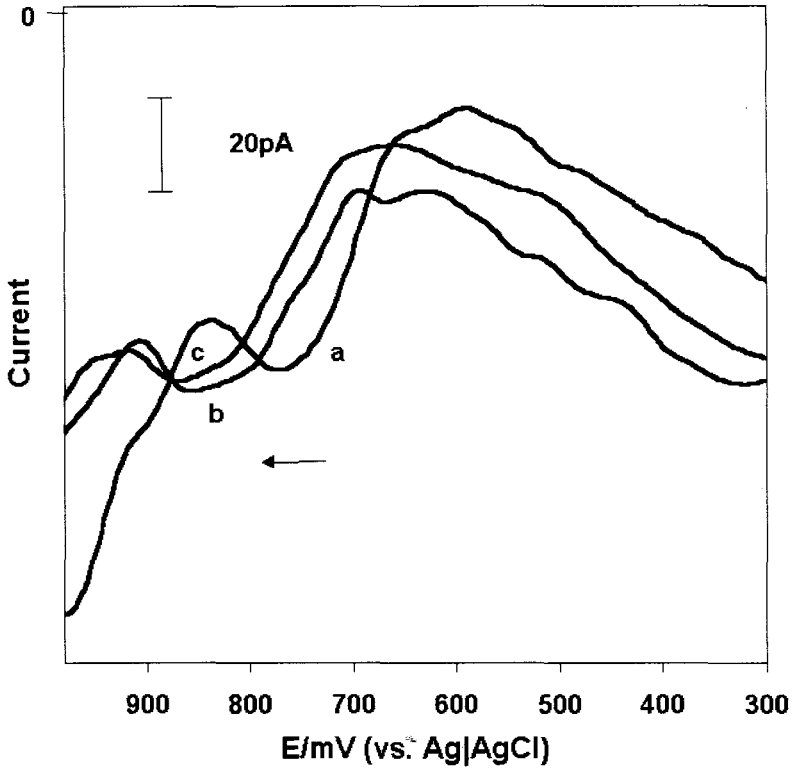

Figure 5. 15 OSWV scan of the brain slice, on CoPc-ME (without a Nafion® coating) (a) 2 min after killing the rat, (b) 30 sec after the first scan, (c) 3 min later.

Bradykinin was then injected into the medium near the brain slice after 3 min. The peak at 0.75V was regenerated. Bradykinin has been used in several studies to induce NO in biological tissue.[80,89] Hence the peak at 0.75 V must be due to NO. This peak also shifted and decreased with time.

CHAPTER SIX : CONCLUSSION

6. CONCLUSION.

In this work it has been shown that nitric oxide coordinates to the cobalt complexes, CoPc and $[CoTSPc]^{4-}$. Spectroscopic evidence for the formation of the Co(III)(NO)Pc species has been given. Hence, the interaction of NO with these cobalt complexes involves an electron transfer from the metal to NO. The rate constants (k_f) for NO coordination to CoPc and $[CoTSPc]^{4-}$ were found to be much smaller than those reported for porphyrin complexes. Coordination of NO to $[CoTSPc]^{4-}$ in water was found to be more favourable than the coordination of NO to CoPc in DMSO.

CoPc, $[CoTSPc]^{4-}$ and $VitB_{12}$ catalysed both reduction and oxidation of NO, however $[ClAlTSPc]^{4-}$ catalysed only the oxidation of NO. $[CoTSPc]^{4-}$ and CoPc displayed ring-based catalysis. It has also been observed in this work that the catalytic reduction potential of NO on a GCE is highly affected by the pH of the solution and the history of the electrode. In pH 4, using NO solution prepared from NO gas, the catalytic reduction peak was observed at –0.6 V, whilst for pH 4, using NO solutions generated from NO_2^- the catalytic reduction peak was observed at –1.2 V on a GCE. When the MPc was immobilized on the electrode, the MPc-GCE electrode showed better catalytic activity for NO reduction than when the MPc complex was in solution. However, for $VitB_{12}$, homogeneous studies showed better catalytic activity than heterogeneous studies. This implies that $VitB_{12}$ is more efficient as a catalyst in solution than when immobilized on the electrode surface. CoPc exhibited better catalytic activity for NO than $[CoTSPc]^{4-}$ and $VitB_{12}$ in terms of current and stability.

A comparison of the catalytic activities of Fe, Co, Ni, Zn and Cu MPc complexes immobilized on a ME, showed that FePc was the most efficient catalyst in terms of NO

reduction potential and current enhancement. During catalysis, nitrosyl complexes are formed, i.e. NO coordinates to the MPc on the surface of the electrode. However, because of the strong bond formed between Fe and NO, regeneration of the electrode is difficult, hence the electrode is poisoned by Fe and its reduction products. Thus in this work, CoPc was the best catalyst since it showed better stability than FePc, though the latter showed higher currents and more favourable potentials. The CoPc-ME exhibited a detection limit of 2×10^{-10}. A substitution of electron donating groups to the CoPc ring enhanced the catalytic activity of the cobalt complex. Cobalt tetraamino phthalocyanine showed better catalytic activity in terms of current than CoPc.

It has also been shown in this work that the CoPc-ME can be used to detect NO in the presence of possible interfering molecules such as dopamine. Its been reported by other researchers that there is interference between dopamine and NO,[88] however, in this work this interference was not observed. It has been shown in this work that there is an interaction between serotonin and NO. Hence, the increase in dopamine currents in the presence of serotonin and on increasing concentrations of NO, is attributed to the summation of the dopamine currents and those of the oxidation products of serotonin.

The CoPc-ME has also been used to monitor NO in biological media; human blood and rat brain. The lifetime of NO in different human blood components was monitored. As has been reported before,[89] the shortest lifetime was observed in blood plasma. The dissipation of NO is attributed mainly to the reactions of NO with blood components including oxygen. The electrode has further been used to detect NO in rat brain slices.

For determination of NO in biological systems, exclusion of nitrite is imperative. Nitrite is oxidized at potentials that are close to NO oxidation but also nitrite is the oxidation product of NO. The use of Nafion® successfully eliminates the interference due to nitrite, however, it compromises the sensitivity of the electrode. Thus, for future work, synthesis of a metallophthalocyanine complex that would both increase the sensitivity of the electrode and simultaneously be able to eliminate interferences due to nitrite is essential. Secondly, there is a need to design microelectrodes that can penetrate tissue and a single cell to allow *in situ* NO detections. There have been reports in literature of such microelectrodes, but they are porphyrin modified.[80,89,102] Since MPc complexes are more stable, it would be important to be able to use them instead of porphyrin complexes.

1. E.Galea, D.J. Reis, H. Xu, D.L. Feinstein, Res. Commun., FASEB J., **9**, 1995, 1632

2. M.A. Dorheim, W.R. Tracey, J.S. Pollock, P. Grammas, Biochem. Biophys. Res. Commun., **205**, 1994, 659.

3. P.L. Feldman, O.W. Griffith, D.J. Stuehr, Special report, C & N 1993, 26.

4. A.R. Butler, D.L.H. Williams, Chem. Soc. Rev., 1993, 233.

5. P. Ascenzi, R. Fruttero, C.I. Ercolan, F. Monacelli, Analusis, **24**, 1996, 316.

6. F.T. Bonner, Stedman G. in: Methods in nitric oxide research (eds: M. Feelisch, J.S. Stamler) Wiley and New York 1996.

7. J.D. Lee, Concise Inorganic Chemistry, Chapman and Hall, 4th edn. 1991.

8. F.T. Bonner, Inorg. Chem., **9**, 1970, 190.

9. N.V. Blough, O.C. Zaffiriou, Inorg. Chem., **24**, 1985, 3504.

10. F.A. Cotton, G. Wilkinson, Advanced Inorganic Chemistry, Weley Interscience, New York, 5th edn, 1988.

11. R.L. Migron in: The colours of life: An introduction to the chemistry of porphyrins and related compounds, Oxford University press 1977.

12. D. Phillips, Pure and Appl. Chem., **67**, 1995, 117.

13. C.E. Dent, R.P. Linstead, A.R. Lowe, J. Chem. Soc., 1934, 1033.

14. M.J. Stillman, T. Nyokong, in Phthalocyanine: Properties and Applications Vol 1 (eds: C.C. Leznoff, A.B.P. Lever) VCH, New York, 1989.

15. D.W. Clack, J.R. Yandle, Inorg. Chem., **11**, 1972, 1738.

16. P.C. Minor, M. Gouterman, A.B.P. Lever, Inorg. Chem., **24**, 1985, 1894.

17. A.B.P. Lever, S. Licoccia, K. Magnell, P.C. Minor, B.S. Ramaswamy, Am. Chem. Soc., **11**, 1982, 237.

18. D.W. Clack, N.S. Hush, I.S. Woolsey, Inorg. Chim. Acta., **19**,1976, 129.

19. J.F. Myers, G.W. Rayner-Canham, A.B.P. Lever, Inorg. Chem.,**14**, 1975, 461

20. C.C. Leznoff, Inorg. Chim. Acta., **89**, 1984, 35.

21. A.B.P. Lever, P.C. Minor, J.P. Wilshire, Inorg. Chem., **20**, 1981, 2550.

22. A.B.P. Lever, P.C. Minor, Inorg. Chem., **22**, 1983, 826.

23. M.K. Ellison, C.E. Schulz, R.W. Scheidt, Inorg. Chem., **38**, 1999, 100.

24. E. Obayashi, K. Tsukamoto, S. Adachi, S. Takahashi, M. Nomura, T. Lizuka, H. Shaun, Y. Shiro, J. Am. Chem. Soc., **119**, 1997, 7807.

25. J.M.C. Ribeiro, J.M.H. Hazzard, R.H. Nussenzveig, D.E. Champagne, F.A. Walker, Science, **260**, 1993, 539.

26. S. Kim, G. Deinum, M.T. Gardner, M.A. Marletta, G.T. Babcock, J. Am. Chem. Soc., **118**, 1996, 8769.

27. J.A. McCleverty, Chem. Rev., **79**, 1979, 53.

28. J.H. Enermark, R.D. Feltham, Coord. Chem. Rev., **13**, 1974, 339.

29. W.R. Scheidt, M.K. Ellison, Acc. Chem. Res., **32**, 1999, 350.

30. P.L. Piciulo, G.W. Rupprecht, W.R. Scheidt, J. Am. Chem., Soc., 1974, 5293.

31. W.R. Scheidt, J.L. Hoard, J. Am. Chem. Soc.,**95**, 1973, 8281.

32. W.R. Scheidt, P.L. Piciulo, J. Am. Chem. Soc., **98**, 1976, 1913.

33. G.B. Richter-Addo, S.J. Hodge, G.B. Yi, M.A. Khan, T. Ma, E.V. Caemelbecke, N. Guo, K.M. Kadish, Inorg.Chem., **35**, 1996, 6530.

34. E. Fujita, C.K. Chang , J. Fajer, J. Am. Chem. Soc., **107**, 1985, 7665.

35. M. Hoshino, L. Laverman, P.C. Ford, Coord. Chem. Rev., **187**, 1999, 75.

36. L.E. Laverman, M. Hoshino, P.C. Ford, J. Am. Chem. Soc., **119**, 1997, 12663.

37. I.J. Ostrich, G. Liu, H.W. Dodgen, J. Hunt, Inorg. Chem., **19**, 1980, 619.

38. L.E. Laverman, P.C. Ford, Chem. Commun., 1999, 1843.

39. M. Hoshino, M. Maeda, R. Konishi, H. Seki, P.C. Ford, J. Am. Chem. Soc., **118**, 1996, 5702.

40. M. Hoshino, K. Ozawa, H. Seki, P.C. Ford, J. Am. Chem. Soc., **115**, 1993, 9568.

41. M. Hoshino, M. kogure. J. Phys. Chem., **93**, 1989, 5478.

42. S.H. Cheng, Y.S. Oliver, Inorg Chem., **33**, 1994, 5847.

43. M. Hoshino, A. Shigeyoshi, M. Yamaji, Y. Hama, J. Phys. Chem., **90**, 1986, 2109.

44. B.B. Wayland and L. Olson, J. Am. Chem. Soc., **96**, 1974, 6037.

45. B.B. Wayland and L. Olson, J. Am. Chem. Soc., **98**, 1976, 94

46. I.M. Lorkovic, P.C. Ford, Inorg. Chem., **38**, 1999, 1467

46. K.M. Kardish, V.A. Adamian, E. Van caemelbecke, Z. Tan, P. Tagliatesta, P. Bianco, T. Boschi, G.B. Yi, M.A. Khan, G.B. Richter-Addo, Inorg. Chem., **35**, 1996, 1343.

48. K. Uchida, S. Mitsuyuki, T. Onishi, K. Tamaru, J. Chem. Soc. Faraday Trans. **75**, 1979, 2839.

49. P. Ascenzi, M. Brunori, G. Pessesi, C. Ercolani, F. Monacelli, J.Chem. Soc. Dalton Trans., 1987, 369.

50. I. Zilbermann, J. Hayon, T. Katchalski, O. Raveh, J. Rishpon, A.I. Shames, A. Bettelheim. J. Electrochem. Soc., **144**, 1997, L228.

51. W.R. Scheidt, K.Hatano, G.A. Rupprecht, P.C. Piciulo, Inorg. Chem., **18**, 1979, 292.

52. W.R. Scheidt, M.E. Frisse, J. Chem. Soc., **97**, 1975, 17.

53. R. Hoffmann, M.M.L. Chen, M. Ellian, A.R. Rossi, P. Mingos, Inorg. Chem., **13**, 1974, 2667.

54. F. Holsboer, W. Beck, H.D. Bartunik, J. Chem. Soc. Dalton Trans., 1973, 1828.

55. W. Hughes, B. Baldwin, Inorg. Chem., **13**, 1974, 1531

56. H. Hori, M. Ikeda-Saito, J.S. Leigh, T. Yonetami, Biochem., **21**, 1982, 1431.

57. N.N. Kundo, N.P. Keier, Russian J. Phys. Chem., **46**, 1968, 707.

58. J.H. Zagal, M. Paez, C. Paez, J. Electroanal. Chem., **237**, 1987, 145.

59. R.A. Firth, H.A.O. Hill, J.M. Pratt, R.G. Thorp, R.J.P. Williams, J. Chem. Soc. (A), 1969, 381.

60. M.Wolak, G. Stochel, M. Hamza, R. van Eldik, Inorg. Chem., **39**, 2000, 2018.

61. H. Kruszyna, J.S. Magyar, L.G. Rochelle, M.A. Russell, R.P. Smith, D.E. Wilcox, J. Pharmacol. Exp. Ther., **285**, 1998, 665.

62. D. Lexa, J.M. Saveant, J. Zickler, J. Am. Chem. Soc., **99**, 1977, 2786.

63. D. Lexa, J.M. Saveant, J. Am. Chem. Soc., **99**, 1976, 2652.

64. N.R. de Tacconi, D. Lexa, J.M. Saveant, J. Am. Chem. Soc., **101**, 1979, 466.

65. D. Faure, D. Lexa, J.M. Saveant, J. Electroanal. Chem., **140**, 1982, 285.

66. D.Lexa, J.M. Saveant, J. Zickler, J. Am. Chem. Soc., **102**, 1980, 2654.

67. S.L. Tackett, J.W. Ide, J. Electroanal. Chem., **30**, 1971, 510.

68. V. Hampl, C.L. Walter, S.L. Archer, Methods in nitric oxide research, chapter 21 (eds: M. Feelisch, J.S. Stamler) Wiley and New York 1996.

69. K.Kikuchi, T. Ngano, J.S. Beckman, Methods in NO research, chapter 32 (eds: M. Feelisch, J.S. Stamler) Wiley and New York 1996.

70. R.M.J. Palmer, A.G. Ferrige, S. Moncada, Nature, **327**, 1987, 524.

71. H. Kosaka, T. Shiga, Methods in NO research, chapter 25 (eds: M. Feelisch, J.S. Stamler) Wiley and New York 1996.

72. D.J. Singel, J.R. Lancester, Methods in NO research, chapter 23 (eds: M. Feelisch, J.S. Stamler) Wiley and New York 1996.

73. Y.A. Henry, D.J. Singel, Methods in NO research, chapter 24 (eds: M. Feelisch, J.S. Stamler) Wiley and New York 1996.

74. W.J. Payne, J. Le Gall, Y. Berlier, Methods in NO research, chapter 27 (eds: M. Feelisch, J.S. Stamler) Wiley and New York 1996.

75. J. Wang, W.S. Caughey, D.L. Roussean, Methods in NO research, chapter 30 (eds: M. Feelisch, J.S. Stamler) Wiley and New York 1996.

76. V. Sampath, D.L. Roussean, Methods in NO research, chapter 29 (eds: M. Feelisch, J.S. Stamler) Wiley and New York 1996.

77. T. Malinski, L.Czuchajowski, Methods in NO research, chapter 22 (eds: M. Feelisch, J.S. Stamler) Wiley and New York 1996.

78. F. Pariente, L.J. Alonso, H.D. Abruna in J. Electroanal. Chem., **379**,1994, 191.

79. L.C. Green, D.A. Wagner, J. Glogowski, P.L. Skipper, J.S. Wishnok, S.R. Tannenbaum, Anal. Biochem., **126**,1982, 131.

80. T. Malinski, Z. Tah, Nature, **358**, 1992, 676.

81. J. Wang, N. Naser, M. Ozsoz, Anal. Chim. Acta., **234**, 1990, 315.

82. K. Ichimori, H. Ishida, M. Fukahori, H. Nakazawa, E. Murakami, Rev. Sci. Instrum., **65**, 1994, 2714.

83. M. Pallini, A. Curulli, A. Amine, G. Palleschi, Electoanalysis, **10**, 1998, 1010.

84. H. Tsukahara, D.V. Gordienko, M.S. Goligorsky, Biochem. Biophys. Res. Commun., **193**, 1993, 722.

85. F. Bedioui, S. Trevin, J. Devynck, J. Electroanal. Chem., **377**, 1994, 295.

86. F. Pariente, J.L. Alonso, H.D. Abruna, J. Electroanal. Chem., **379**, 1994, 191.

87. B. Fabre, S. Burlet, R. Cespuglio, G. Bidan, J. Electroanal. Chem., **426**, 1997, 75.

88. M.M. Iravani, J. Millar, Z.L. Kruk, Journal of Neurochem., **71**, 1998, 1969.

89. T. Malinski, Z. Tah, S. Grunfeld, A. Burewicks, P. Tombolian, Anal. Chim. Acta., **279**, 1993, 135.

90. S. Mesaros, S. Grunfeld, A. Mesarosova, D. Bustin, T. Malinski, Anal. Chim. Acta., **339**, 1997, 265.

91. A. Ciszewski, G. Milczarek, Electroanal., **10**, 1998, 791.

92. K. Shibuki, J. Physiol. (London), **422**, 1990, 321.

93. K. Shibuki, Neurosci. Res., **9**, 1990, 69.

94. J. Hayon, D. Ozer, J. Rishpon, A. Bettelheim, J.Chem. Soc. Chem. Commun., 1994, 619.

95. F. Bedioui, S. Trevin, J. Devynck, Electroanalysis, **8**, 1996, 1085.

96. F. Bedioui, Y. Boulier, C. Sorel, J. Devynck, L. Coche-guerente, A. Deronzier, J.C. Moutet, Electro. Chim. Acta., **38**, 1993, 2485.

97. A. Kitajima, M. Miyake, T. Kobayashi, H. Koyama, O. Ikeda, K. Kijima, T. Komura, A. Uno, A. Yamatodani, Electrochemistry, **67**,1999, 784.

98. F. Bedioui, S. Trevin, V. Albin, M.G.G. Villegas, J. Devynck, Anal. Chim. Acta., **341**, 1997, 177.

99. Y. Liu, C. DeSilva, M.D. Ryan, Inorg. Chim. Acta., **258**, 1997, 247.

100. M. Bayachou, R. Lin, W. Cho, P.J. Farmer, J.Am. Chem. Soc., **120**, 1998, 9888.

101. C. Yu, Y. Su, J. Electroanal. Chem., **368**, 1994, 323.

102. T. Malinski, M.W. Radomski, Z. Tah, S. Moncada, Biochem. Biophys. Res. Comm., **194**, 1993, 960.

103. E. Kubaszewski, A. Peters, S. McClain, D. Bohr, T. malinski, Biochem. Biophys. Res. Comm., **200**, 1994, 213.

104. J.P. Rivot, A. Sousa, J. MontagneClavel, J.M. Besson, Brain Reasèarch, **821**, 1999, 101.

105. A. Escrig, J.L. Gonzalez-Mora, M. Mass, J. Physiol., **516**, 1999, 261.

106. F. Lantoine, S. Trevin, F. Bedioui, J. Devynck, J.Electroanal. Chem., **392**, 1995, 85.

107. M. Pontie, F. Bedioui, J. Devynck, Electroanal., **11**, 1999, 845.

108. S. Trevin, F. Bedioui, J.Devynck, Talanta, **43**, 1996, 303.

109. A. Ciszewski, E. Kubaszewski, M. Lozynski, Electroanalysis, **8**, 1996, 293.

110. J.H. Zagal, Coord.Chem. Rev., **119**, 1992, 89.

111. J.H. Zagal, M. Gulppi, M. Isaacs, G. Cardenas-Jiron, M.J. Aguirre, Electrochim.Acta., **44**, 1998, 1349.

112. T.F. Kang, G.L. Shen, R.Q. Yu, Anal. Chim. Acta., **356**, 1997, 243.

113. K. Hoffman, Acc. Chem. Res., **4**, 1971, 1.

114. J. Ulstrup, J. Electroanal. Chem., **79**, 1977, 526.

115. K. Hanabusa, H. Shirai, Phthalocyanines: Properties and applications, Vol 2, (ed. C.C. Leznoff, A.B.P. Lever) VCH, New York, 1993.

116. M. Kimura, Y. Yamaguchi, T. Koyama, K. Hanabusa, H. Shirai, J. Porphyrin and Phthalocyanine, **1**, 1997, 309.

117. J. Zhang, Y. Tse, A.B.P. Lever, W.J. Pietro, J. Porphyrin and Phthalocyanine, **1**,1997, 323.

118. S. Dong, B. Lui, J.Lui, N. Kobayashi, J. Porphyrin and Phthalocyanine, **1**,1997, 333.

119. F. Zhao, J. Zhang, D. Wohrle, M. Kaneko, J. Porphyrin and Phthalocyanine, **4**, 2000, 158.

120. H. Eichhorn, J of porphyrin and Phthalocyanine, **4**, 2000, 88.

121. M. Kimura, Y. Yamaguchi, T. Koyama, K. Hanabusa, H. Shirai, J. Porphyrin and Phthalocyanine, **4**, 1997, 309.

122. J. Zagal, E. Munoz, S. Ureta-Zanartu, Electrochim. Acta., **27**, 1982, 1373.

123. N. Chebotareva, T. Nyokong, J. Appl. Electrochem., **26**, 1996, 1.

124. M. Dieny, O. Contamin, M. Savy, Electrochim. Acta., **33**, 1988, 121.

125. M.K. Halbert, R.P. Baldwin, J. Chromatogr., **345**, 1985, 43.

126. K. Kofhage, K.Ravichandran, R.P. Baldwin, Anal. Chem., **56**, 1984, 1517.

127. M.K. Halbert, R.P. Baldwin, Anal. Chem., **57**, 1985, 591.

128. M.K. Halbert, R.P. Baldwin, Anal.Chim.Acta., **187**, 1986, 89.

129. K. Ogura, S. Yamasaki, J. Applied Electrochem., **15**, 1985, 279.

130. L. Mao, G. Shi, Y. Tian, H. Liu, L. Jin, K. Yamamoto, S. Tao, J. Jin, Talanta, **46** 1998, 1547.

131 J. Jin, T. Miwa, L. Mao, H. Tu, L. Jin, Talanta, **48**, 1999, 1005.

132. J. Wang, Analytical chemistry, VCH publishers, USA.1994.

133. J. Zagal, R.K. Sen, E. Yeager, J. Electroanal. Chem., **83**, 1977, 207.

134. J. Wang, D.B. Luo, P.A.M. Farias, J.S. Mahmoud, Anal. Chem., **57**, 1985, 158.

135. J.H. Weber, D.H. Busch, Inorg. Chem., **4**, 1965, 469.

136. J.J. Lin, R.T. Holmes, K.M. Smith, J.Porphyrins Phthalocyanines, **2**, 1998, 363-368.

137. N. Kobayashi, H. Lam, W.A. Nevin, C.C. Leznoff, H. Shirai, J. Am. Chem. Soc., **116**, 1994, 879.

138. J. Metz, O. Schneider, M. Hnack, Inorg. Chem., **23**, 1984, 1069.

139. J. Bassett, R.C. Denny, G.H. Jeffery, J. Mendham, Vogel's Textbook of Quantitative Inorganic analysis, Longman, New York, 1981.

140. M.Krejcik, M. Danek, F. Hartl, J. Electroanal. Chem., **317**, 1991, 179.

141. S. Zecevic, B. Simi-Glavaski, E. Yeager, J. Electroanal. Chem., **196**, 1985, 339.

142. L.C. Gruen, R.J. Blagrove, Aust. J. Chem., **26**, 1973, 319.

143. M. Sekota, T. Nyokong, Polyhedron, **16**, 1997, 3279.

144. T. Nyokong, J. Chem. Soc. Dalton Trans., 1993, 3601.

143. P. Ascenzi, M. Brunori, P. Pennesi, C. Ercolani, F. Monacelli, J. Chem. Soc. Dalton Trans., 1990, 105.

146. T. Nyokong, Polyhedron, 1995, **14**, 2325.

147. A.B.P. Lever, E.R. Milaeva, G. Speier, in Phthalocyanines: Properties and applications, Vol 3 (eds. C. C. Leznoff, A.B.P. Lever) VCH, 1993.

148. J. Limson, T. Nyokong, Electroanalysis, **9**, 1997, 255.

149. J. Zhou, E. Wang, Electroanalysis, **4**, 1992, 473.

150. T.F. Connors, J.V. Arena, J.F. Rustling, J. Phys. Chem., **92**, 1988, 2810.

151. J.F. Rustling, T.F. Connors, A. Owlia, Anal. Chem., **59**, 1987, 2123.

152. D. Lexa, J.M. Saveant, J.P. Soufflet, J. Electroanal. Chem., **100**, 1979, 159.

153. C.L. Miaw, N. Hu, J.M. Bobitt, Z. Ma, M.F. Ahmali, J.F. Rusling, Langmuir, **9**, 1993, 315.

154. Q. Qui, S. Dong, Electrochim. Acta., **38**, 1993, 2297.

155. H. Li, T. Li, E. Wang, Talanta, **42**, 1995, 885.

156. R.N. Boos, J.E. Carr, J.B. Conn, Science, **117**, 1953, 603.

157. S. Zecevic, B. Simic-Glavaski, E. Yeager, A.B.P. Lever, P.C. Minor, J. Electroanal. Chem., **196**, 1985, 339.

158. Y.H. Tse, P. Janda, H. Lam, J. Zang, W.J. Pietro, A.B.P. Lever, J. Porphyr. Phthalocyanine, **1**, 1997, 3.

159. H. Li, T.F. Guarr, J. Chem.,Soc., Chem. Commun., 1989, 833

APPENDIX

1. IR spectra of $[CoTSPc]^{4-}$
2. IR spectra of $[ClAlTSPc]^{4-}$
3. IR spectra of CoTMPyP

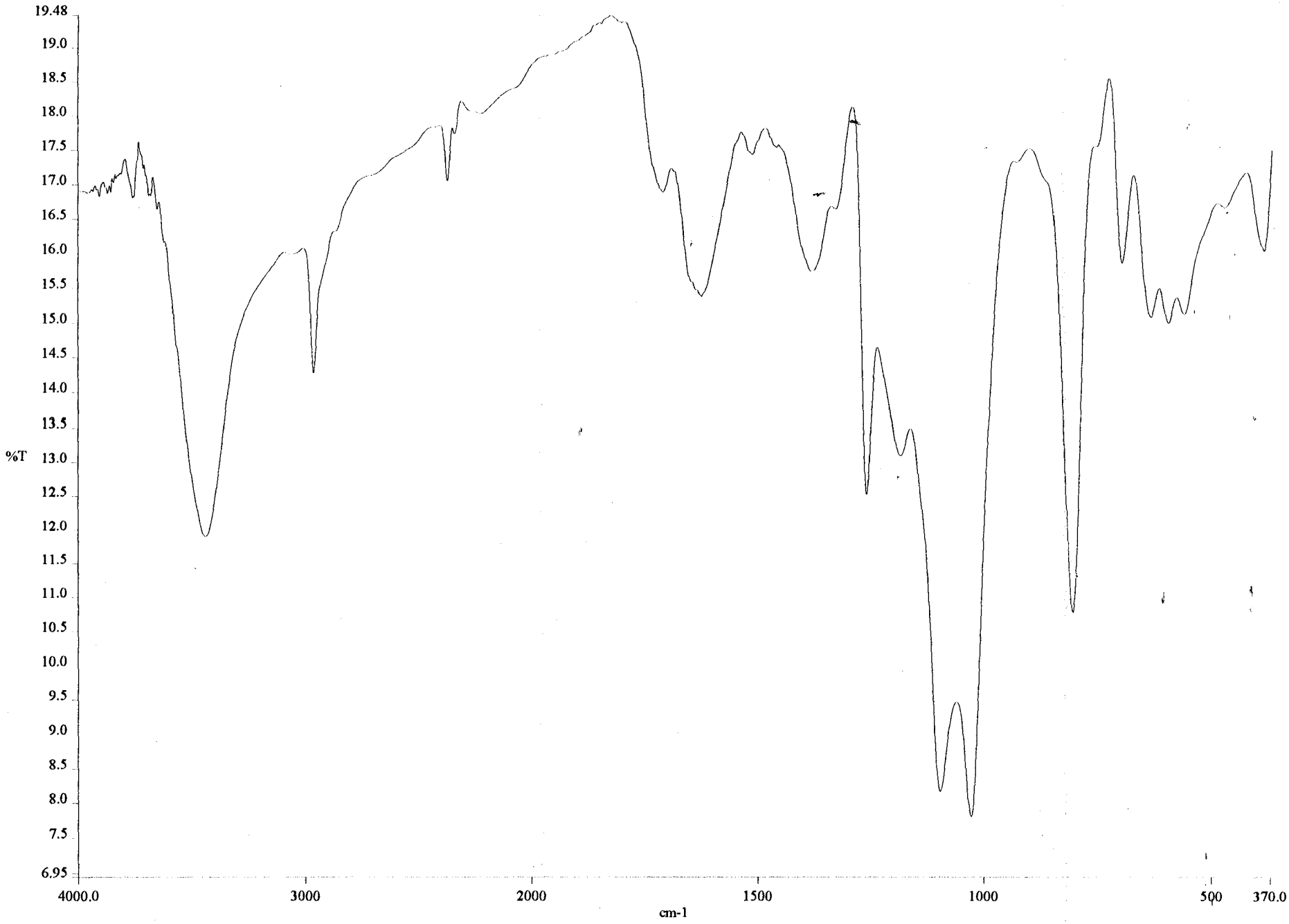
19.48
19.0
18.5
18.0
17.5
17.0
16.5
16.0
15.5
15.0
14.5
14.0
13.5
%T
13.0
12.5
12.0
11.5
11.0
10.5
10.0
9.5
9.0
8.5
8.0
7.5
6.95
4000.0
3000
2000
1500
1000
500
370.0
cm-1

[CoTSPc]$^{4-}$

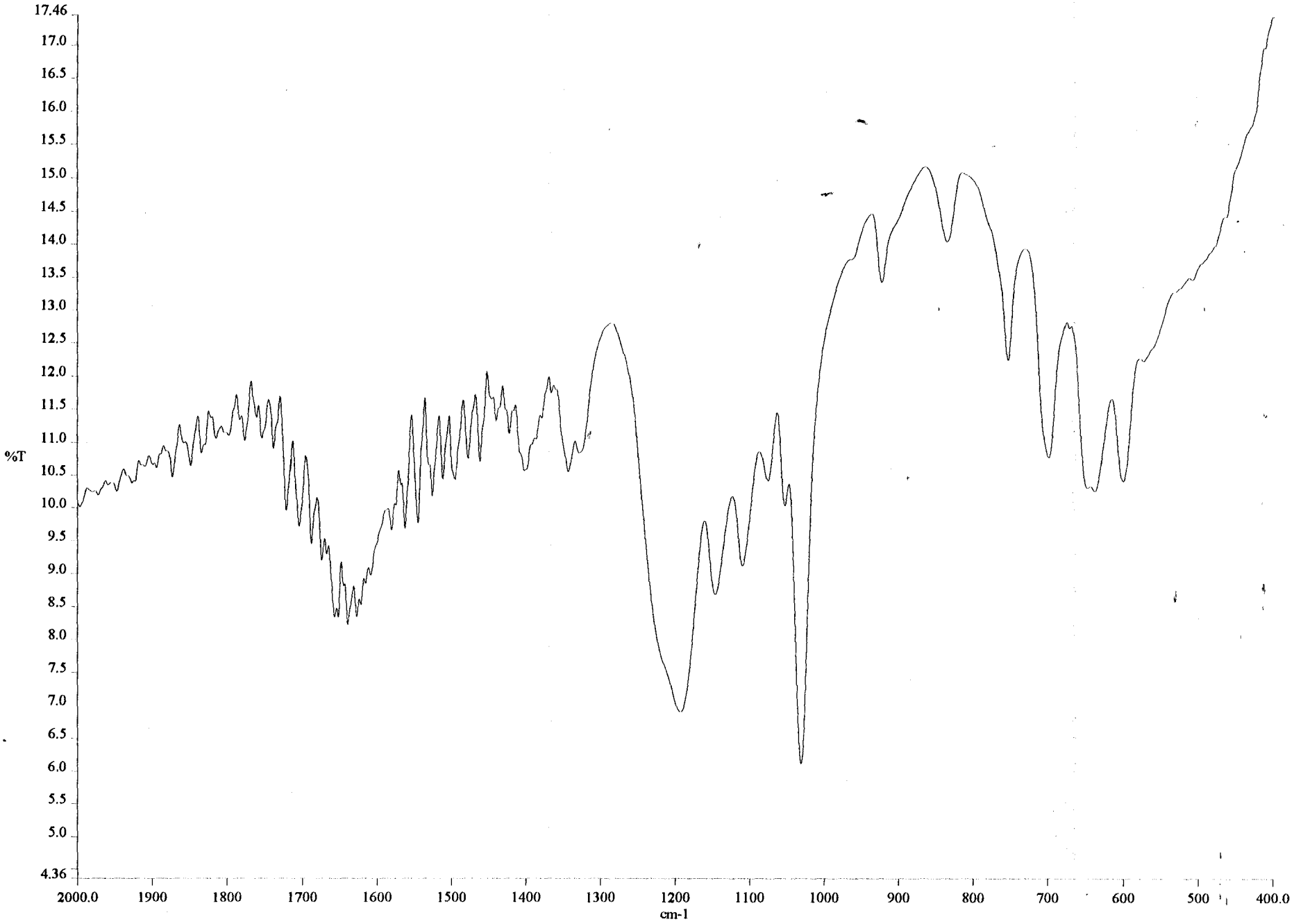
17.46
17.0
16.5
16.0
15.5
15.0
14.5
14.0
13.5
13.0
12.5
12.0
11.5
11.0
10.5
10.0
9.5
9.0
8.5
8.0
7.5
7.0
6.5
6.0
5.5
5.0
4.36
%T
2000.0
1900
1800
1700
1600
1500
1400
1300
1200
1100
1000
900
800
700
600
500
400.0
cm-1

[ClAlTSPc]$^{4-}$

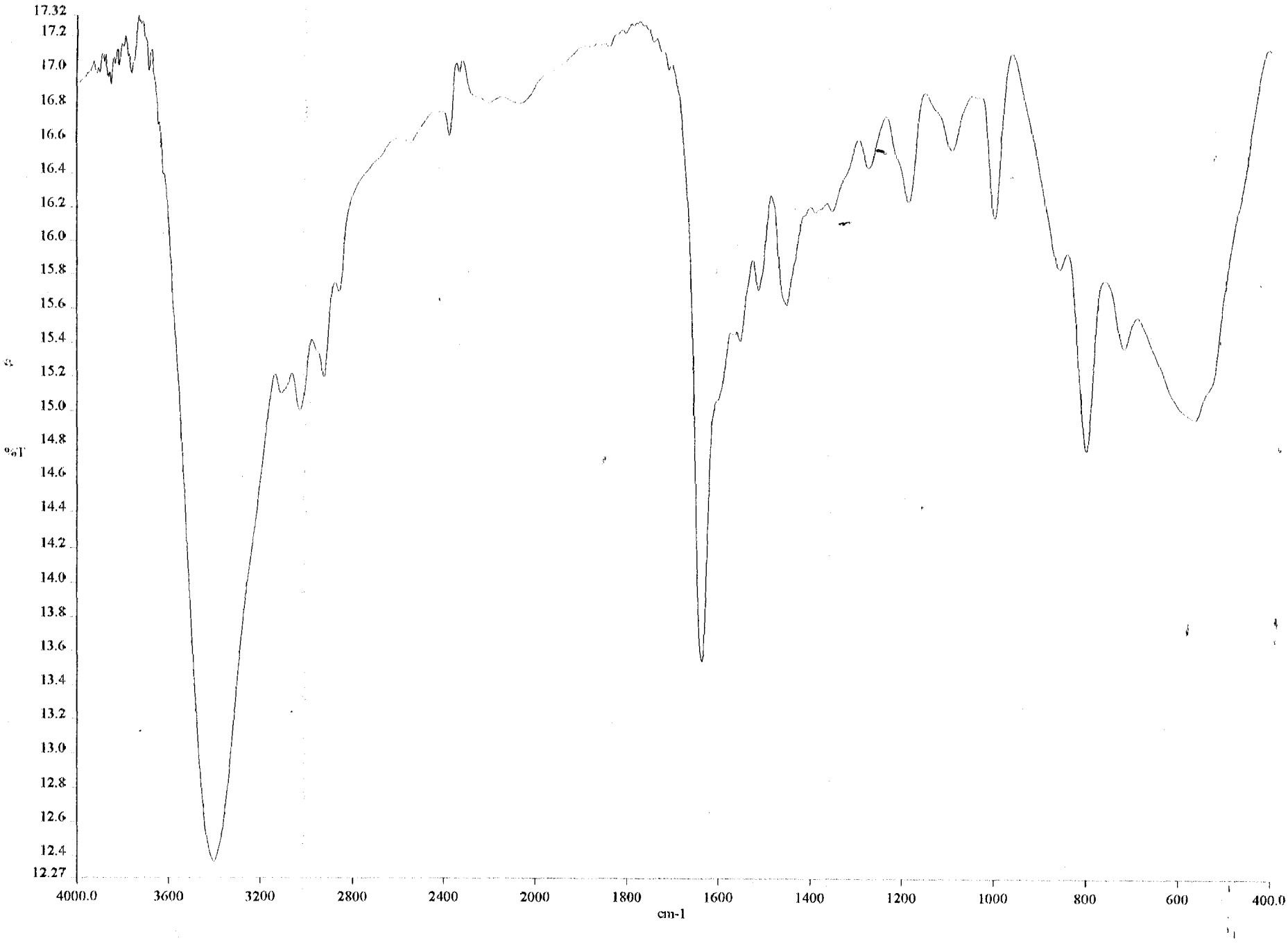
17.32
17.2
17.0
16.8
16.6
16.4
16.2
16.0
15.8
15.6
15.4
15.2
15.0
14.8
14.6
14.4
14.2
14.0
13.8
13.6
13.4
13.2
13.0
12.8
12.6
12.4
12.27
%T
4000.0
3600
3200
2800
2400
2000
1800
1600
1400
1200
1000
800
600
400.0
cm-1

CoTMPyP